THÈSE

En vue de l'obtention du

DOCTORAT DE L'UNIVERSITÉ DE TOULOUSE

Délivré par :

Institut National Polytechnique de Toulouse (INP Toulouse)

Discipline ou spécialité :

Génie des Procédés et de l'Environnement

Présentée et soutenue par :

M. AHMED JARRAY

le mardi 3 novembre 2015

Titre :

MESOSCOPIC MODELING, EXPERIMENTAL AND THERMODYNAMIC
APPROACH FOR THE PREDICTION OF AGGLOMERATES
STRUCTURES IN GRANULATION PROCESSES

Ecole doctorale :
Mécanique, Energétique, Génie civil, Procédés (MEGeP)

Unité de recherche :
Laboratoire de Génie Chimique (L.G.C.)

Directeur(s) de Thèse :
M. VINCENT GERBAUD
M. MEHRDJI HEMATI

Rapporteurs :
M. BERNARD ROUSSEAU, UNIVERSITE PARIS 11
M. KHASHAYAR SALEH, UNIVERSITE DE TECHNOLOGIE DE COMPIEGNE

Membre(s) du jury :
M. KHASHAYAR SALEH, UNIVERSITE DE TECHNOLOGIE DE COMPIEGNE, Président
M. MEHRDJI HEMATI, INP TOULOUSE, Membre
M. MOHAMED BENALI, UNIVERSITE DE TECHNOLOGIE DE COMPIEGNE, Membre
M. VINCENT GERBAUD, INP TOULOUSE, Membre

Résumé de thèse

Le procédé de granulation en voie humide nécessite l'ajout d'un agent d'enrobage ou liant, typiquement composé d'agents tensioactifs, d'eau, de plastifiant et de charge hydrophobe. Cependant, dans les procédés de granulation en voie sèche, l'agent d'enrobage est ajouté sous la forme de fines particules solides. L'objectif de ce travail est double : d'une part, examiner le comportement des particules dans les systèmes secs et aqueux aux échelles microscopique et mésoscopique, et d'autre part, développer des méthodologies prédictives permettant de choisir le liant adéquat et formuler la bonne solution d'enrobage. Dans le cadre de cette étude, nous avons utilisées l'hydroxypropyl-méthylcellulose (HPMC) et la cellulose d'éthyle (EC) comme agents d'enrobage, polyvinylpyrrolidone (PVP) et la cellulose microcristalline (MCC) généralement utilisés comme liants, l'acide stéarique (SA) qui est une charge hydrophobe, et le polyéthylène glycol (PEG) comme plastifiant. Tous ces matériaux sont largement utilisés dans les industries alimentaires et pharmaceutiques.

La réussite d'une granulation dépend de l'affinité entre les particules primaires et le liant. Afin de prédire l'affinité liant-substrat en milieu sec et en milieu aqueux, nous avons comparé deux approches; la première est basée sur le travail de l'adhésion alors que la seconde s'appuie sur le concept de résistance à la traction idéale. L'équation de résistance à la traction idéale a été étendue aux systèmes ternaires dans le but de l'appliquer pour la granulation en milieu aqueux. Les approches développées ont été ensuite confrontées aux données expérimentales sur différent systèmes (composées de PVP, MCC, HPMC, SA, EC, PEG et l'eau). Nous avons ainsi trouvé que l'approche basée sur le travail d'adhésion semble donner de meilleures prédictions des affinités. Les deux approches prédisent que le HPMC est un bon liant pour le MCC. Les résultats indiquent également que le PEG a une bonne affinité avec le HPMC et le SA.

Nous avons ensuite étudié la structure des agglomérats formés dans les formulations colloïdales utilisées dans les procédés d'enrobage. Pour ce faire, nous nous sommes appuyés sur des analyses expérimentales et des simulations mésoscopiques. Ces dernières reposent sur l'utilisation de la méthode de dynamique des particules dissipatives (DPD) dans laquelle les composés sont décrits comme un ensemble de billes souples (approche « coarse-grain ») interagissant selon le modèle de Flory-Huggins. Les interactions répulsives entre les billes ont été évaluées en utilisant le paramètre de solubilité (δ) calculé par simulation moléculaire tout-atome. Les résultats de simulation DPD ont été comparés aux résultats expérimentaux obtenus par plusieurs voies : cryogénique-MEB, analyse de distribution de taille de particule et par la technique DSC. Les résultats de la simulation DPD montrent que le polymère HPMC est un meilleur agent stabilisant pour le SA que le PVP et le MCC.

En outre, HPMC est capable de recouvrir la germe de SA d'une couche épaisse et d'y pénétrer en profondeur, empêchant ainsi l'agglomération et la croissance des cristaux de SA. Néanmoins, HPMC est incapable de stabiliser les particules de SA lorsque celles-ci sont en quantités élevées (supérieurs à 10% (w/w)). Nous constatons également que le PEG se diffuse à l'intérieur des chaînes de HPMC entrainant l'extension de ce dernier, formant ainsi un polymère composite lisse. Les résultats expérimentaux montrent des tendances similaires; l'analyse de la distribution de taille de particule indique qu'en présence de HPMC, pour de faible pourcentages de SA (au-dessous de 10% (w/w)), la majorité des particules de SA sont inférieures à 1 μm de diamètre. Les images MEB révèlent que HPMC entoure les cristaux de SA avec un film texturé et ancre sur leur surface.

Mots clés

Agglomération, liant, simulation moléculaire, DPD, colloïdes, produits pharmaceutiques, enrobage.

Ph.D. Thesis abstract

Wet granulation process requires the addition of a coating agent or binder, typically composed of surfactants, water, plasticizers and fillers. In dry granulation however, the coating agent is added to the system in the form of fine solid particles. Our goals are to investigate the particles behaviour and agglomeration mechanism in dry and aqueous systems at the micro and meso scales, and also, to develop predictive methodologies and theoretical tools of investigation allowing to choose the adequate binder and to formulate the right coating solution. In this study we chose materials widely used in food and pharmaceutical industries, including; coating agents such as Hydroxypropyl-methylcellulose (HPMC) and Ethyl cellulose (EC), binders such as Polyvinylpyrrolidone (PVP) and Microcrystalline cellulose (MCC), hydrophobic filler such as Stearic acid (SA) and plasticizer such as Polyethylene glycol (PEG).

A successful granulation requires good affinity between host and guest particles. In this context, in the first part of this work, two approaches to predict the binder-substrate affinity in dry and in aqueous media were compared; one based on the work of adhesion and the other based on the ideal tensile strength. The concept of ideal tensile strength was extended to ternary systems and applied for granulation in aqueous media. The developed approaches were thereafter tested for various systems (composed of PVP, MCC, HPMC, SA, EC, PEG and water) and compared to experimental observations. Approaches yielded results in good agreement with the experimental observations, but the work of adhesion approach might give more accurate affinity predictions on the particles affinity than the ideal tensile strength approach. Both approaches predicted that HPMC is a good binder for MCC. Results also indicated that PEG has a good affinity with HPMC and SA.

In a second part of our work, we used mesoscale simulations and experimental techniques to investigate the structure of agglomerates formed in aqueous colloidal formulations used in coating and granulation processes. For the simulations, dissipative particle dynamics (DPD) and a coarse-grained approach were used. In the DPD method, the compounds were described as a set of soft beads interacting according to the Flory-Huggins model. The repulsive interactions between the beads were evaluated using the solubility parameter (δ) as input, where, δ was calculated by all-atom molecular simulations. The mesoscale simulation results were compared to experimental results obtained by Cryogenic-SEM, particle size distribution analysis and DSC technique. According to the DPD simulations, HPMC polymer is a better stabilizing agent for SA than PVP and MCC. In addition, HPMC is able to cover the SA germ with a thick layer and to adsorb in depth into its inner

core, preventing further agglomeration and crystal growth of SA. But, for high amounts of SA (above 10% (w/w)), HPMC is unable to fully stabilize SA. We also found that PEG polymer diffuses inside HPMC chains thereby extending and softening the composite polymer. Experimental results presented similar trends; particle size distribution analysis showed that in the presence of HPMC, for low percentages of SA (below 10% (w/w)), the majority of SA particles are below 1 μm in diameter. SEM images revealed that HPMC surrounds SA crystals with a hatching textured film and anchors on their surface.

Keywords

Agglomeration, binder, molecular simulation, DPD, colloid, pharmaceutical products, coating.

Acknowledgments

This work is the result of three years of research efforts during my Ph.D. studentship. Of course, most of such work would have not been possible without the support of many people that I wish to thank.

First of all, I wish to express my deep and sincere gratitude to my supervisors Prof. Gerbaud Vincent and Prof. Hemati Mehrdji for inviting me to this exiting journey into the realm of granulation science and molecular simulation. Without their knowledge, enthusiasm and encouragement, this thesis would not have been possible.

I wish to express my appreciation to Prof. Khashayar Saleh and Prof. Bernard Rousseau, the reviewers of the thesis, for their constructive comments and remarks on the manuscript. My gratitude goes also to Dr. Mohammed Benali for accepting to examine my work, and I am grateful for his achievements during his thesis back in 2006, from which the work described in this thesis followed.

I am most grateful to Dr. Yaocihuatl Medina Gonzalez for her fruitful interaction within my research work. My gratitude goes also to Dr. Fabien Laboulfie for helping me in the experimental part of this thesis.

I thank Bruno Payres and Yves Martinez from CMEAB for their co-operation in the field of cryogenic electron microscopy, and for their helpful advice and suggestions.

Special thanks to Dr. Pierre Yves Pontalier for his support and encouragement.

I also thank Federico Senior Arenas for his positive view on all aspects of life and for his encouragement from the beginning of my thesis.

A warm thanks to my dear Sabrina for being there with me during the most difficult times when writing this thesis; especially during the weekends, she gave me the moral support and she even cooked for me!

I wish especially to thank Alain Philip for his amazing help and encouragement at all time. Thank you for being there for both me and all the others Ph.D. students.

I also thank Ivonne for her friendship. She was a never-ending source of encouragement and motivation.

Content

List of Tables

List of Figures

"Concentrate every minute on doing what's in front of you with precise and genuine seriousness, tenderly, willingly, with justice. And on freeing yourself from all other distractions. Yes, you can— if you do everything as if it were the last thing you were doing in your life, and stop being aimless, stop letting your emotions override what your mind tells you, stop being hypocritical, self-centered , irritable. You see how few things you have to do to live a satisfying and reverent life? If you can manage this, that's all even the gods can ask of you.

-Marcus Aurelius

General Introduction

Granulation is a size-enlargement process during which small particles are formed into larger and physically strong agglomerates (Salaman, 2007). In wet granulation processes, this is performed by spraying a liquid binder onto the particles as they are agitated in tumbling drum, fluidized bed, high shear mixer or similar device (Hemati et al. 2007; Holm, 1997). Coating, on the other hand, is a process which allows to deposit on the surface of particles a thin film layer which can be of different nature: polymers, salts, sugars etc.

These two operations confer on powders new properties for customers, such as hydrophobicity, masking bitterness, reducing the risks of explosion, avoiding the segregation of the constituents, improving the flow properties and the compression characteristics of the mix.

Processes of size enlargement involve the coupling of two classes of parameters. The first class corresponds to the local physico-chemical parameters dependent on the nature of the solutions and powders. The second class corresponds to the parameters of the processes which are the constraints exercised by the process equipment on the bed of powder, such as the temperature and the flow rates. The quality of the end product depends on the control of the coupling between these two families of parameters which exist at different scales. At present, the optimization of these parameters, notably the choice of solvent and binders is based on an empirical, by nature long and expensive approach. In addition, formulating the optimum binder or coating is essential even if suitable operating conditions may bring enough mechanical energy to obtain rigid granules.

Today, important issues in binder formulation and wet granulation process are; a) the assessment of binder-particle interactions in dry and aqueous systems which is experimentally expensive and time consuming, b) the choice of a stabilizing agent which is empirical; an instable dispersion may results in an uncomplet film formation, c) the selection of a suitable plasticizer compatible with the materials that compose the coating film, and d) the structure of agglomerates at the mesoscale level.

In this study we chose materials widely used in food and pharmaceutical industries, including coating agents such as Hydroxypropyl-methylcellulose (HPMC) and Ethyl cellulose (EC), binders such as Polyvinylpyrrolidone (PVP) and Microcrystalline cellulose (MCC), hydrophobic filler such as Stearic acid (SA) and plasticizer such as Polyethylene glycol (PEG).

This thesis is organized in six chapters;

In chapter 1; **Background and motivations**, we present the context of the study; we give an overview of the granulation process and the coating and binder formulation. We also describe briefly

the computational tools used in wet granulation processes. At the end of the chapter, the objectives of the study are listed.

In chapter 2; **Materials and experimental characterization techniques**, experimental techniques and chosen materials used throughout the study are described.

In chapter 3; **Aqueous coating formulation: experimental characterization**, we use experimental characterization technique to analyze the structure of aqueous coating formulations. We use particle size distribution analysis to investigate the stability of coating formulations containing Stearic acid and polymers. Cryogenic-SEM technique is used to observe the structure of the coating formulation. Plasticizer-polymer compatibility is also analyzed via DSC.

In chapter 4; **Solubility Parameter (δ) and COSMO's σ-profiles**, we describe the methods used for the calculation of the solubility parameter δ and we analyse the σ-profiles of the materials. σ-profiles give insights on the solubility of the different materials in water, and the compatibility between certain polymers. The calculated δ values of each material are used in the next chapter for the prediction of solid-binder interactions.

In chapter 5; **Prediction of solid - binder affinity in dry and aqueous systems**, we compare two approaches to predict the binder-substrate affinity in dry and in aqueous media, one based on the work of adhesion and the other based on the ideal tensile strength. The equations used in both approaches are generalized and rewritten as a function of the Hildebrand solubility parameter δ. The concept of ideal tensile strength, originally formalized by Gardon (1967) for binary systems, is extended to ternary systems and applied for granulation in aqueous media.

In chapter 6; **Dissipative particle dynamics simulation of composite coating solutions**, we use dissipative particle dynamics (DPD) to elucidate the structure of aqueous colloidal formulations. The effect of percentage of SA on the structure of the HPMC-SA suspension is investigated. In addition, the stability of SA in the presence of MCC and PVP is examined. Plasticizer-polymer compatibility is also studied. Then, DPD simulation results are compared to the experimental findings obtained in chapter 3.

Several appendixes are presented at the end of the thesis. They provide supplementary details and include the scripts used in molecular and mesoscale simulations.

Chapter 1

Background and Motivations

"One ultimate goal would be to quantify the behaviour at the micro and meso scales in terms of rates laws, apply them in a conservation statement and then produce a description of the macro behaviour."

— *Agba Salman, Granulation, 2007*

1. Introduction

Granulation is a process that transforms crystallized or amorphous powder particles into solid agglomerates more or less strong and more or less porous called granules (Salman, 2007). In wet granulation, a binder (or coating solution) is sprayed on the primary particles to obtain agglomerates or coated particles.

The success of wet granulation process is conditioned by the binder formulation (i.e. the behavior of suspensions when in contact with the primary particles). A good binder (or coating solution) should; (a) be suitable with the primary particles (or granule) onto which they it'll be pulverized, (b) provide the quality requirements and the expected properties in the final products, and (c) be compatible with the equipment used in the granulation process (e.g. sprayable by the designed turbine).

In granulation process, the particles are attached together by adhesion and cohesion forces. These forces arise from interatomic and intermolecular bonds: Van der Waal forces, electrostatic forces, etc. While two particles may attract each other in vacuum, they may repel each other when placed in a medium (e.g water). In this context, it is important to distinguish between the particles agglomeration that occurs; (i) during the granulation process, and (ii) during binder (or coating) preparation.

This chapter is divided into three parts; in the first part, we describe briefly the granulation process, first in the context of agglomeration mechanism and then in the context of coating mechanism. The second concerns colloid agglomeration and stability. Terms such as colloidal stability, plasticizers and

polymer-particle surface adsorption are defined. Finally, we describe briefly the different multi-scale methods and models used for the modeling of granulation and agglomeration mechanisms.

2. Granulation process

The word "granulation" is taken to cover all forms of particle size enlargement processes and not a specific mechanism. "Initial particle" refers to particles charged as raw material in the granulation process before growth takes place, and the word "granule" is used to mean any particle product. Granulation is widely used in the pharmaceutical, agricultural, fertilizer, and mining industries. Granulation includes a number of processes that purposely convert, by a sequence of events, small particles into large permanent masses in which the initial primary units are still identifiable. These granules exhibit better flow characteristics, higher content uniformity and better compressibility in comparison to the ungranulated powder. Granule growth occurs either by the collision and successful adherence of primary feed particles into discrete granules or by growth centered around a nucleus on to witch particles collides and attach themselves to form a layer (Salman, 2007). The obtained granule may, eventually, be made into tablets or a similar compressed compact. Granulation can be categorized into wet granulation and dry granulation.

2.1. Dry granulation

Dry granulation technique does not use a liquid phase and therefore lacks a drying step. Fine particles with sizes of less than several microns are mostly cohesive and are readily agglomerated by exerting pressure on them. This technique utilizes the cohesive characteristics of the particles to form larger granules without using any binders but with pressure by extruding, tumbling and fluidizing powders as shown in Fig. 1.1 (Salman, 2007).
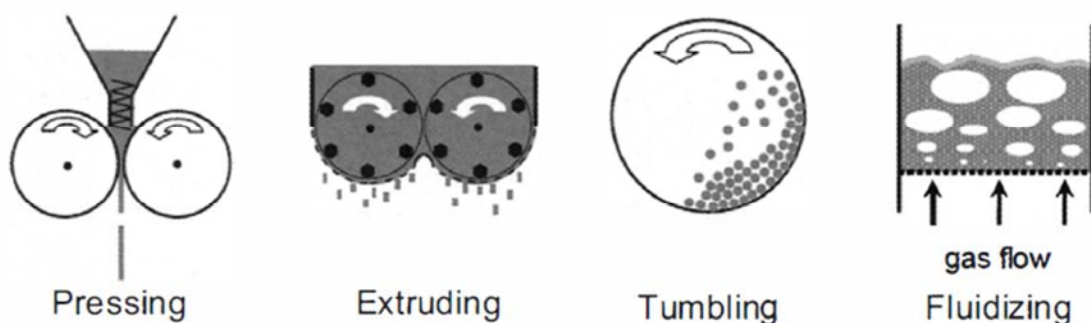
Fig. 1.1 - Typical dry granulation methods (Salman, 2007).

Dry granulation major disadvantages are the generation of dust, uncontrollable granule size and irregular granulate properties and therefore it is not considered to be the preferred granulation method (Kleinebudde, 2004; Miller, 2005). Other than the mechanical forces excreted by the dry granulation equipment, the final product is also influenced by the interactions between the raw primary particles. As we will see later in chapter 5, the organization and the structure of the granule in dry granulation can be predicted by analyzing the affinity between the primary particles.

2.2. Wet granulation

The process of wet granulation is brought about when a bed of solid particles moves, with simultaneous intensive mixing, in the presence of a liquid phase. This motion provides particle collisions and individual particles coalesce and bind together (Salman, 2007). This can be done using fluid bed granulators, tumbling drums, shear mixers, or extruders.

In 1958, Newitt and Conway published a paper describing for the first time the binding mechanism in wet granulation. This was the precursor of wet granulation science that opened the path for many other researchers including Israelachvili (2010) who explained the binding forces between the particles in terms of intermolecular and interface forces, Schubert (1975, 1981) who studied the interparticle contact forces and the agglomerate structure by calculating the tensile strength, and Rumpf (1962) who classified the binding mechanisms according to the forces between the granules and proposed a model for relating the strength of agglomerates to the presence of pores.

2.3. Agglomeration mechanism

"The terms agglomerate and aggregate are qualitative and have been interchanged by most researchers for so long that it probably no longer matters how they are used."

Gary Nichols, 2002.

- **Agglomerate** [from the Latin agglomerare (glomus-meris ball)]. Gathered into a ball or cluster; collected into a mass (Simpson, 1989). Assemblage of particles rigidly joined together, as by partial fusion (sintering) or by growing together (Gregory, 1988)

- **Aggregate** [from the Latin aggregare held together (grex gregis flock)]. A mass formed by the union of individual particles; an assemblage, a collection (Simpson, 1989). Assemblage of particles which are loosely coherent (Gregory, 1988).

Gerstner (1966) defined both names in terms of the granule structure; soft agglomerate (i.e. friable and readily dispersed granule) would be equivalent to an agglomerate and a hard agglomerate (i.e. strong, non-friable, gritty, and not readily dispersed) would be equivalent to an aggregate. However,

as long as there is no way to measure quantitatively the degree of association of particles in an assemblage, it's difficult to choose between both terms. At the end of their article, Gary and coworkers (2002) proposed that when particles assemblages are described, the term agglomerate is used exclusively. For prenucleation structure, obtained upon association of molecules into macromolecules (that may develop into agglomerate), the term aggregate may be used.

Fig 1.2 schematically shows the mechanisms of agglomeration and coating. The initial step of an agglomeration mechanism is the nucleation where wet particles coalesce and the liquid between them dries to form solid bridges between primary particles and thus forms a primary agglomerate (nuclei) (See Fig. 1.2 (a)). Iveson et al. (2001a) demonstrated that the nucleation formation mechanism depends on the relative sizes of the droplets and of the primary particles. In this context, Schæfer and Mathiesen (1996) suggested that the nucleation stage can be divided into two basic mechanisms: Distribution and Immersion.
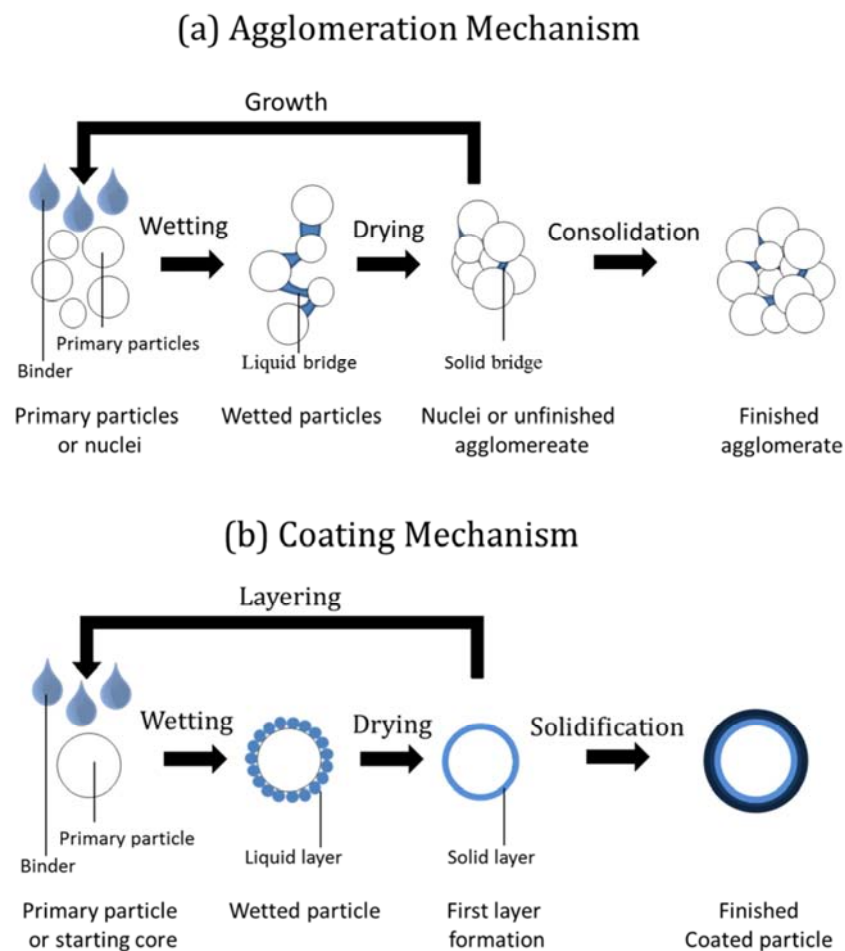
Fig. 1.2 – Agglomeration and coating mechanism.

When the binder droplet is smaller or of comparable size to the primary solid particles, it disperses as a film on the particles surface, and nuclei are formed by successful collision and bridging of particles. This nucleation mechanism is referred to as the distribution mechanism (Fig. 1.3 (a)). In the immersion mechanism, the binder, whose droplet size is larger than the primary particles, represents the core of the agglomerate (Fig. 1.3 (b)). Finally, when the droplet size is identical to that of the particles, the distribution of phenomena and the immersion phenomena may occur concurrently and in balanced manner. It's worth mentioning here that the immersion-distribution hypothesis assumes that the thermodynamics of the wetting process are favorable which means that the binder will always spread over the powder surface. In addition, the possibility of the solid spreading over the liquid must be included (Hapgood et al., 2009). During the consolidation phase, the agglomeration process is dominated by the mechanical characteristics of the mixer. The consolidation step marks the final stage of a successful agglomerate formation and it affects the mechanical properties of the agglomerates by reducing the size and porosity of the granules and by decreasing their possibilities of deformation, thereby reducing their ability to coalescen after contact.
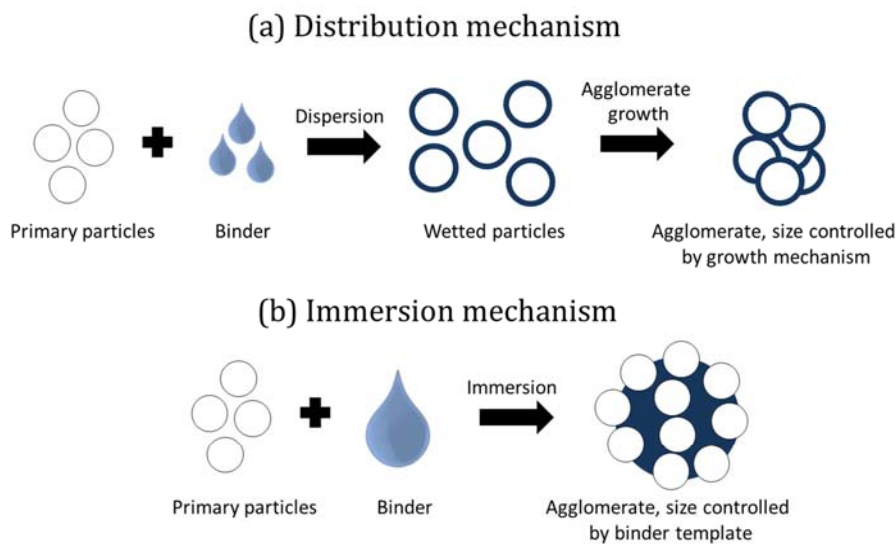
Fig. 1.3 – Distribution and immersion mechanisms.

Binder choice is important in agglomeration mechanism. Liquid binders can be either aqueous or non-aqueous, although aqueous solutions are more commonly used for safety reasons (Salman, 2007). The binder must have sufficient viscosity to promote agglomeration and growth, but also provide sufficient strength to hold dried granules together in order to avoid breakage as the liquid inter-particle bonds dry during the consolidation stage. Schaefer and Mathiesen (1996) analyzed the effect of viscosity on granulation; they found that the initial growth rate decreases for higher molecular weight of Polyethylene glycol but the subsequent growth rate increases. Eliasen et al. (1998) investigated the effect of binder viscosity on the granulation of lactose and found that a low-viscosity

binder reduces the strength of the granules. Similarly, Keningley et al. (1997) found that, depending on the primary particle size, a critical minimum binder viscosity is required to form granules. In another study, it was also found by Johansen and Schaefer (2001) that more spherical granules and an improved binder distribution can be obtained upon reducing the binder viscosity. Overall, increased binder viscosity traduces into an increased average granule size (Salman, 200).

Jaiyeoba and Spring (1980b) studied the effect of wettability of powders, they concluded that granule growth is low if the starting material is poorly wettable. For soluble powder in the binder, Jaiyeoba and Spring (1980a) suggested that the amount of liquid should be reduced accordingly since the amount of powder is lower. Fu et al. (2004) investigated the impact behavior of wet granules; they found that particles restitution decreases upon increasing primary particle size. Simons et al. (2005) studied the effect of binder adhesive strength and the amount of binder captured by the granule and concluded that binder selection should be based on both the dry and wet binder surface energies. Thielmann et al. (2008) investigated the effect of surface properties of primary particles on their agglomeration behaviour in fluidised bed granulation. Hydrophilic particles were found to result into a narrower granule size distribution than hydrophobic ones, however, hydrophobic primary particles grow to larger sizes. Planinšeka et al. (2000) and Zhanga et al. (2002) emphasized on the importance of the wetting kinetics and surface free energy for successful granulation.

Inspired by Ennis' work (1990, 1991), Benali et al. (2009) proposed the modified capillary number Ca' to evaluate the importance of the viscous force in binders with respect to the adhesion work. When the $Ca' > 1$, the cohesion of dynamic liquid bridges during nucleation and growth becomes greater than that of the static liquid bridges. This is attributed to the effect of viscous energy dissipation. When the $Ca' < 1$, the effect of the adhesion force is dominant. Mastering granule processing under the $Ca' > 1$ regime is routine for laboratory and industrial practitioners. Mastering the $Ca' < 1$ regime requires to select binders adequately. The quality of the final solid products is therefore determined by both the parameters of the processes equipment and the physicochemical properties of the raw materials.

2.4.   Coating mechanism

Agglomeration and coating mechanism coexist in wet granulation processes. In the case of coating process, agglomeration mechanism is a parasitic phenomenon which should be minimized in the process. Specific coating equipment and optimal processing conditions are essential to ensure that an equal amount of coating solution is distributed evenly on the surface of the particles; some well-known coating equipment are given in Fig. 1.4. The coating process involves the covering of particulate materials including seeds, agglomerates, pellets and powders with a surrounding layer of a

coating agent (or coating material) (Salman, 2007) (See Fig. 1.2 (b)). Coating occurs when wet particles are dried before a collision with other particles takes place or when the mechanical forces exerted by the wet granulation equipment can break the bonds between the particles. During the film-coating process, formation of an acceptable layer of film on the substrate requires the followings (McGinity and Felton, 2008):

1. Formation of appropriate-size droplets,
2. Contact of these droplets with the substrate,
3. Spreading and coalescence of the droplets,
4. Evaporation of the solvent.

The macroscopic properties of the coated granule depend on the properties of the constituent phases of the coating agent, the coating-granule affinity interactions, and the texture of the coating and surface appearance (Salman, 2007). It's important to avoid sedimentation or coagulation of the coating solution prepared by dispersion; otherwise, uncompleted film formation may occur (Lehmann, 1982). Iley (1991) demonstrated that bigger particles capture more coating than smaller particles during the coating of poly-distributed particles in a fluidized bed. In another study, Smith and Nienow (1982) concluded that the formation of coated particles depends also on the strength of the bond holding the particles. Saleh et al. (2003) Studied the effects of particle size on coating characteristics and showed that both growth rate and efficiency increase with decreasing the particle size. Poor spreading of the coating on the surface of particle can lead poor or incomplete coating film formation. Khoufech et al. (2015) showed that impact speed increases the maximum extent of spreading of the droplet on hydrophobic surfaces and adding CarboxyMethylCellulose sodium salt into water induces splashing and rebound inhibition.
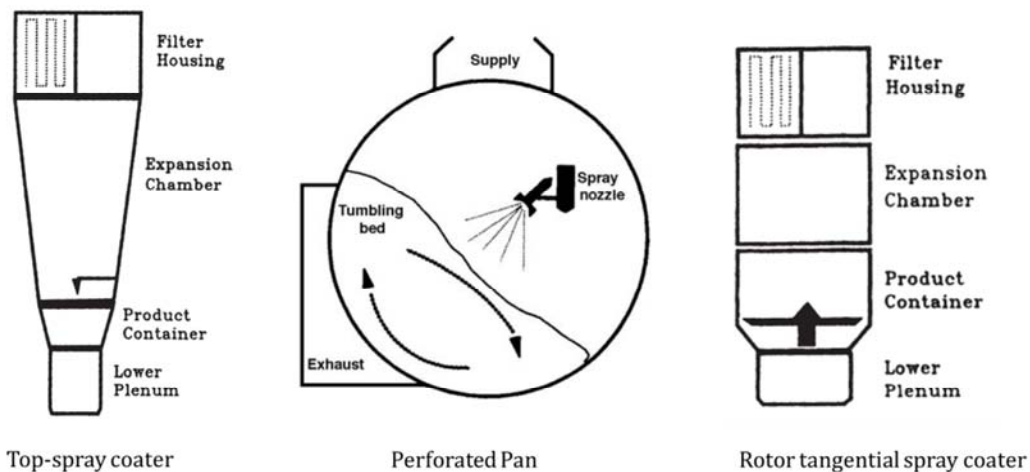
Fig. 1.4 – Examples of equipment used in film coating process, adapted from McGinity and Felton (2008).

2.5 Bonding mechanisms

Whether it is a coating or agglomerate, the bonding mechanisms in wet granulation that determines the structure of the granule can be divided into two categories (Ormos, 1994; Rumpf, 1958) (see Fig. 1.5):

Bonding mechanisms in the presence of a binding material:

- Solid bridges, created by transfer of material (chemical reaction, recrystallization of dissolved substances, partial melting, contact fusion by sintering, solidification of high viscous bond agents),
- Quasi-liquid bridges with low or limited mobility generated by macromolecules or high viscous polymers that form strong bonds equivalent in strength to the solid bridges,
- Bonds due to mobile liquid (liquid bridges) and created by capillary forces or surface tension.

Bonding mechanisms without material bridges:

- Van der Waals, electrostatic forces and magnetic forces.
- Mechanical interlocking due to the shape and roughness of the particle surface.
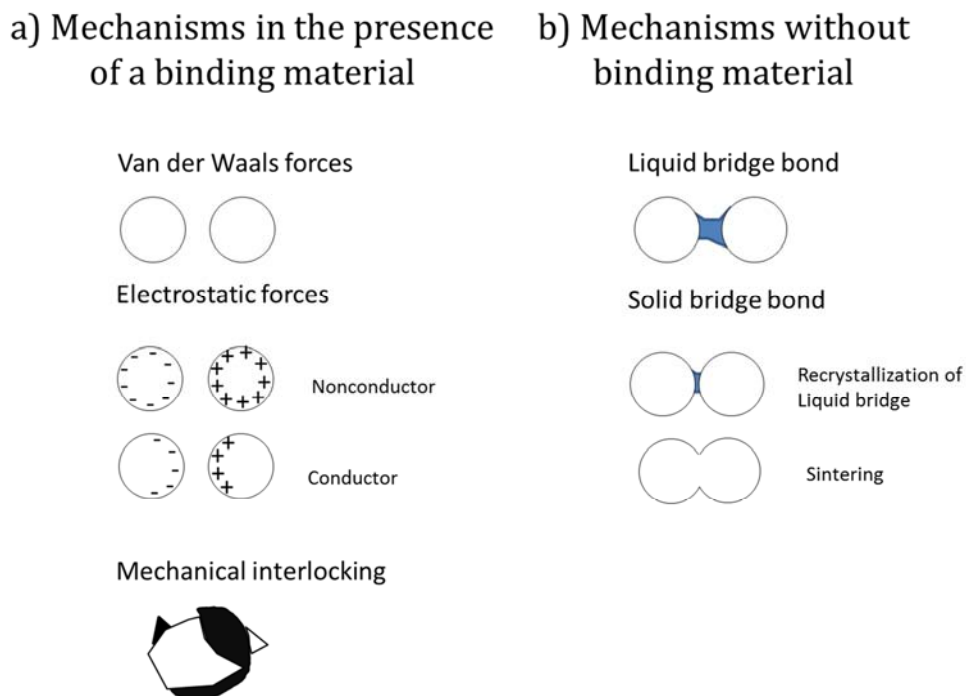
Fig. 1.5 – Bonding mechanisms in granulation process

Bonding mechanisms involves the simultaneous interactions of many molecules (Israelachvili, 2010), and they become particularly severe when dealing with short-range interactions that determine, for example, adhesion and bonding forces. At the beginning of the granulation process, the particles are generally of low size and contain only marginal amounts of water. This small amount of binder does not create liquid bridges between the particles. At this stage of granulation, the forces of Van der Waals or electrostatic origin are dominant.

In every situation involving a substrate and a binder or coating, the combination of adhesion and cohesion determines the overall bonding effectiveness, and thus, governs the agglomerate growth mechanism and the coating efficiency. Adhesion and cohesion forces between a liquid and a solid depend on the liquid surface tension and liquid-solid contact angle.

- Binder selection is empirical and time consuming,
- It's difficult to experimentally asses the affinity between the primary particles, and between the primary particles and the binder,
- Models for solid-binder affinity in aqueous systems are unavailable.

3. Coating formulation

"A product based on organic binders, which when applied to a substrate produces a cohesive, virtually water-impermeable, protective and possibly decorative film, is called a coating material."

Thomas Brock, European Coatings Handbook, 2010.

Coatings generally consist of mixtures of various raw materials that are added to confer or enhance specific properties to the final product. Typically, a coating solution is composed of water, film forming polymer, stabilizing agent, filler and plasticizer.

One of the important issues regarding the aqueous coating process is the stability of the aqueous dispersion. An instable dispersion results in the agglomeration of the colloidal particles as a result of the van der Waals attraction. This attractive energy becomes very large at short distances between the colloidal particles and may lead to coagulation or sedimentation, thereby affecting the film coating properties and eventually the granulation process. For aqueous coating formulation to be successful, stable colloidal suspensions should be obtained.

3.1. Colloids

"Watching and measuring the motion of colloidal particles had made the world of molecules finally tangible"

Jean Baptiste Perrin, Les atomes, 1913.

Historically, it was the theory of Albert Einstein (1926) on Brownian motion and the experiments of Jean Baptiste Perrin (1913) on gum colloids that laid the foundations of modern colloid physics, which in fact opened the path to soft matter science.

A particle suspension in a liquid medium (e.g. water) is called colloidal when the particles are large enough to present a structure and small enough to be submitted to Brownian motion. Their size range is typically between 10 nm and several microns. As an example, glues and gels are colloids that form in solution called colloidal suspensions.

The thermal motion in a liquid is responsible for the constant motion of the mesoscopic particles and the motor of the Brownian motion in a colloidal suspension. Because of it, particles jiggle around randomly by collisions; they bounce and separate again after the shock. As shown in Fig. 1.6, the structure of the dispersed particles changes when a small amount of salt is added to the dispersion. Small particles stick to each other after collision, and agglomerates are formed (Fig. 1.6 (b)), resulting in the reduction of the total number of dispersed particles. This phenomenon is called coagulation, flocculation or destabilization and may lead to phase separation.
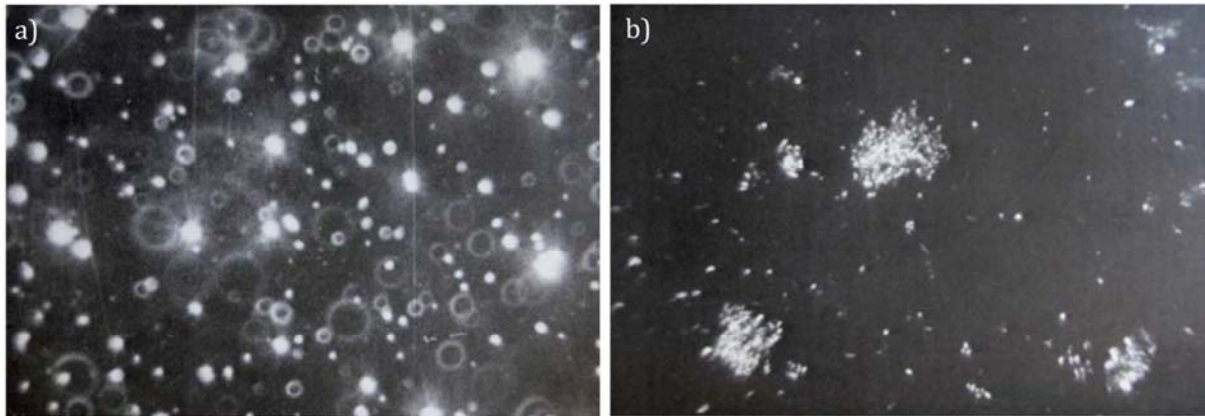
Fig. 1.6 – a) Image of a stable suspension of clay particles observed in dark field optical microscopy, b) A small amount of salt was added. Clays dispersed particles form aggregates. The suspension is destabilized. Images are taken from Van Olphen (1963).

A schematic presentation of colloidal instability and the subsequent mechanisms is shown in Fig. 1.7. Flocculation (or agglomeration in a suspension) is a reversible phenomenon; it is a process of contact and adhesion whereby the particles form larger clusters. The coagulation is a much denser form of

flocculation. Sedimentation is the tendency of particles in the suspension to decant the fluid (see Fig. 1.7).
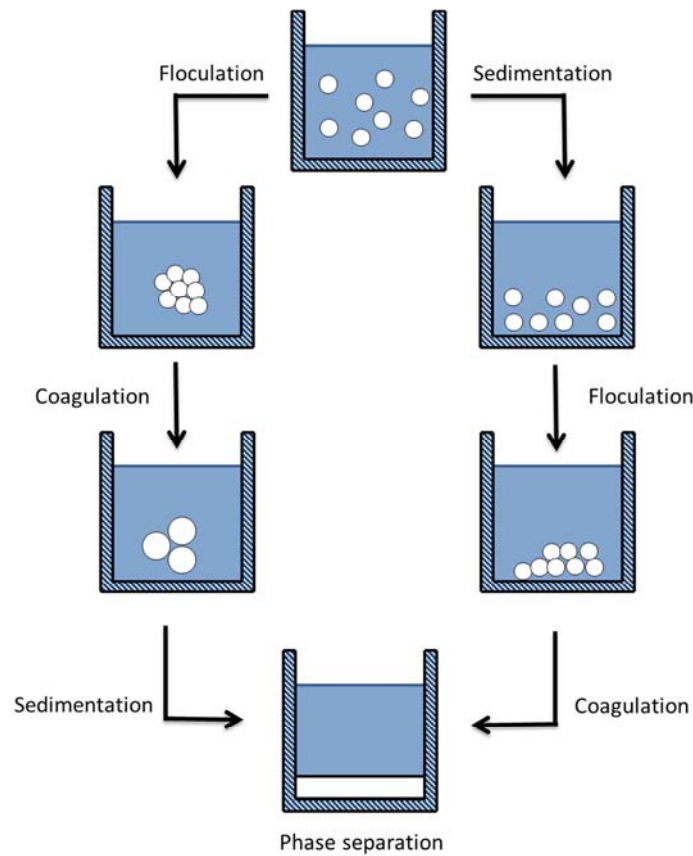
Fig. 1.7 – Colloidal instability; through sedimentation (on the right), and through flocculation (on the left).

3.2.   Colloidal stability

A colloidal dispersion is said to be stable when the colloidal particles remains dispersed over a long time scale (i.e. the total number of particles remains constant over time). Colloidal suspensions behavior is determined by the interactions between the particles. On one hand, we have the attractive interactions of van der Waals and the Brownian movement which are at the origin of the flocculation of the particles. On the other hand, we have the repulsive interactions between particles that ensure kinetically stable suspensions. There are basically two types of repellents colloids. The first type consists of charged colloids in aqueous phase. This repulsion results from electrostatic repulsion forces acting between the surfaces of the particles. The sum of the attractive interaction of van der Waals forces and the repulsive electrostatic interaction is known as the DLVO interaction (Derjaguin, 1941; Verwey, 1948). Fig. 1.8 shows the sum of the two aforementioned interaction potentials

resulting in the Derjaguin-Landau-Verwey-Overbeek (DLVO) potential. It highlights the existence of an energy barrier that will moderate the kinetic energy of the two colliding particles.
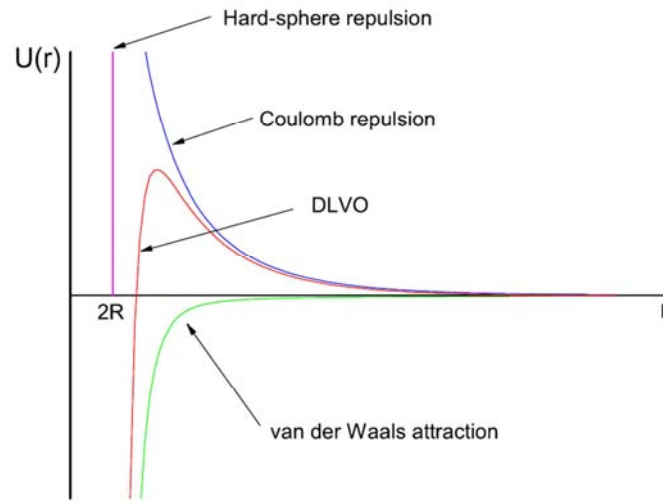
Fig. 1.8 – Illustration of the DLVO potential and all its components (Lucio, 2007)

The second type of repulsion, and most important for us, is encountered between colloids whose surface is covered by non-charged polymers. Under the presence of a good solvent, the adsorbed polymer forms a barrier that keeps the colloidal particle dispersed. As we will see later, the concentration of the adsorbed polymers, which give insights on the effectiveness of the stabilizing polymer agent, can be assessed by a numerical method.

The role of polymers in the stabilization process during coating solution preparation can be classified into two phases; (a) the initial dispersion of the particles in the medium (normally with shear) and (b) the stabilization of that dispersion (without shear) (Vincent, 1974). The protective action by an adsorbed polymer layer is now generally referred to as "steric stabilization", steric stabilization acts essentially by preventing the approach of the particle cores to a separation where their mutual van der Waals attraction would be sufficient for aggregation to occur (Vincent, 1974).

Polymeric steric stabilization against aggregation requires that the solid particle provides an adsorbing substrate for the polymer and that the polymer is irreversibly adsorbed (Gregory, 1978). Much emphasis has been placed on the thickness of the adsorbed layer that confers to the particles a barrier against agglomeration. In this context, Koelmans and Overbeek (1954) suggested that only if the thickness of the adsorbed layer was comparable in size to the diameter of the dispersed particles could a polymeric steric mechanism provide sufficient protection. Albers and Overbeek (1960) later modified this suggestion. As a result of their work on water/oil emulsions, it was shown that the van der Waals inter-particle attraction forces had been greatly over-estimated in the earlier work. In the

same context, Walbridge and Waters (1966) showed that the minimum steric barrier thickness required for the largest particles was of the order of 5 nm. Finally, some recent experiments by Crow and Malati (1966) indicated the importance of good anchoring of the polymer on the surface of the colloid particles in the stabilizing process.

Another type of colloid Stabilization is called the electro-steric stabilization which, as its name indicates, combines electrostatic and steric effects to avoid re-agglomeration of the particles where a charged organic compound is adsorbed to the particle surface (Fritz, 2002).

> - Coating formulation is a complex issue and selection of suitable stabilizing agents is expensive and time consuming,
> - Mesoscale models for particle agglomeration and polymer adsorption in aqueous dispersions are unavailable,
> - Microscopic SEM observation of agglomerate structure and colloids in a polymeric dispersion are unavailable.

3.3. Film formers

In general, film formers are organo-chemical macromolecule-forming substances which polymerize and form crystalline or amorphous continuous structure as the coating dries. The role of the film former is to form a cohesive coating film on a given substrate and – where relevant – to hold together the components of the coating (Brock et al., 2010). Film formation is the result of the increase in polymer concentration in the colloidal dispersion, leading to the formation of a three dimensional network.

The formation of a polymeric film arises from the 'coalescence', i.e. deformation, cohesion and polymer chain interdiffusion, of the individual colloidal particles normally held apart by stabilizing forces (Steward et al., 2000). Evaporation of the interstitial water upon drying leads to the deformation of the particles of polymer until complete coalescence (Fig. 1.9). This mechanism requires sufficient colloidal stability to form close packing upon coalescence; otherwise, poor film may be obtained. Film formation process also requires the spreading of the solution into a thin-layer. Keddie et al. (1995, 1996) demonstrated that voids could remain in the film during film formation even after water evaporation. According to Spitael and Kinget (1980), the formation of a gel was the most important stage of solvent-cast film formation.
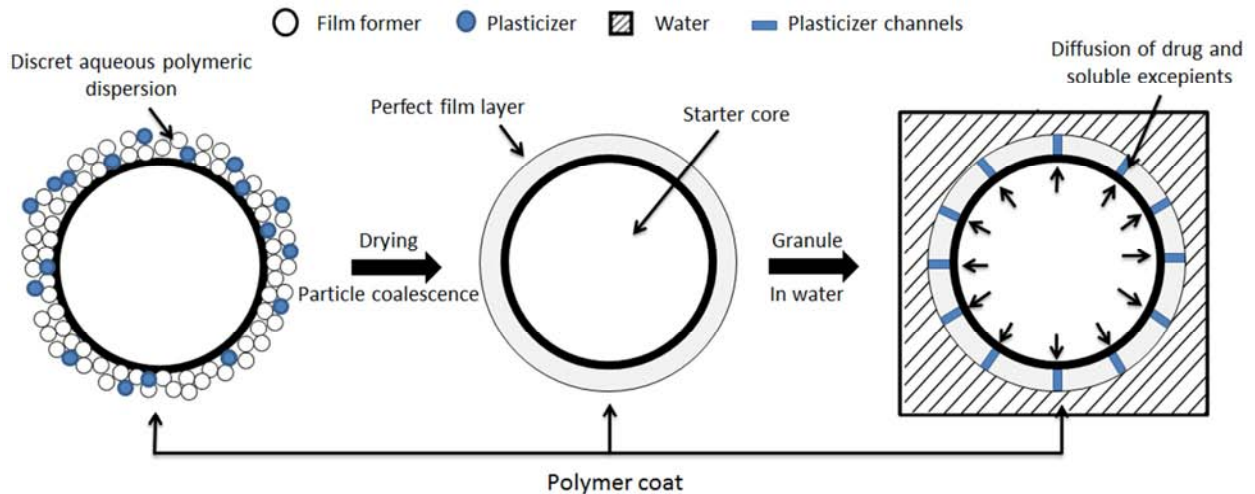
Fig. 1.9 – Schematic representation of typical film formation mechanism from aqueous polymer dispersions, and plasticizer effect on release mechanism.

The obtained film must be smooth and uniform, or, typically, film coating prepared from pure polymer tends to be brittle and crack upon drying. To overcome this problem, one way is to add a plasticizer to the coating solution.

3.4.   Plasticizers

For polymers with limited film-formation ability, a plasticizer may be added to ease the deformation and to favor colloidal particles coalescence. The plasticizer partially eliminates the interactions responsible of the mechanical cohesion between the chains, and therefore increases their mobility. As a consequence, the rigid material is transformed into soft and flexible material (Cole, 1995). Plasticizers reduce the glass transition temperature Tg and the minimum polymer film forming temperature (MFT) at levels that depends on the coating process. Plasticizers also create channels through which drug diffuses for pellets coated with insoluble films (Ozturk et al., 1990) (Fig. 1.9).

A good choice of a plasticizer depends on its compatibility with the polymer and on the permanence of the plasticizer in the film during coating. High compatibility between a polymer and a plasticizer produces stable and homogeneous coating. It's characterized by a high miscibility between the plasticizer and the polymer. However, polymer-plasticizer incompatibility influences not only the mechanical properties, but also drug release (Amighi and Moes, 1996; Arwidssonet al., 1991). Permanence of a plasticizer means its tendency to remain in the plasticized material; i.e. long term compatibility, it depends on the size of the molecule and on its rate of diffusion.

Bodmeier and Paeratakul (1994, 1997) studied the distribution of plasticizers between the aqueous phase and colloidal polymeric dispersions. They also studied the factors influencing the rate of diffusion of plasticizer through the polymer. For optimal mixing between the plasticizer and the

16

polymeric dispersion, Bodmeier and Paeratakul recommended the introduction of insoluble plasticizer to aqueous polymer dispersion before dilution of the latter. They also recommended a longer plasticization time for insoluble plasticizers than for soluble plasticizers. In his work on the coating of large Alumina particles, Ould-chikh (2008) found that adding a plasticizer (Polyvinyl Alcohol (PVA)) in aqueous suspension reduces dramatically the segmentation or the cracking of the coating films upon drying. Laboulfie et al. (2013) also studied the effect of plasticizer on the mechanical resistance and thermal behavior of composite coating films. They found that adding a plasticizer (Polyethylene glycol (PEG)) enhanced the plastic behavior of the coting films and improved its mechanical properties.

> ⚠ ▪ The selection of suitable plasticizers during coating formulation is time consuming and empirical.

3.5. Fillers

Fillers generally refer to cheap and inert materials that are included in a coating composition in order to take up space and diminish the cost of the product. Typically, fillers (such as stearic acid) are added to the coting dispersion to enhance some desired properties such increasing the viscosity or the hydrophobicity of the final product.

4. Computational methods in granulation process

In this work, we will use different numerical methods to investigate the structure of agglomerates and the interactions between the particles in the coating solution. Simulation and properties prediction of agglomerates and granular systems is subject to the constraint of computational performances and thus require a hierarchic division: microscopic, mesoscopic and macroscopic. Fig. 1.10 schematically shows these different lengths and relates them to a number of different multi-scale methods and models based on levels of molecular details they are able to resolve. At the bottom left of the time and length scale there is the quantum mechanics methods. This method takes into consideration electronic configurations, and therefore is located at a time and space range typically of the order of Å and ps. At slightly larger scale, there is the all-atom simulation that allows, within the framework of molecular mechanics, the description of the non-covalent interactions responsible for the formation of agglomerates and self-assembled systems.
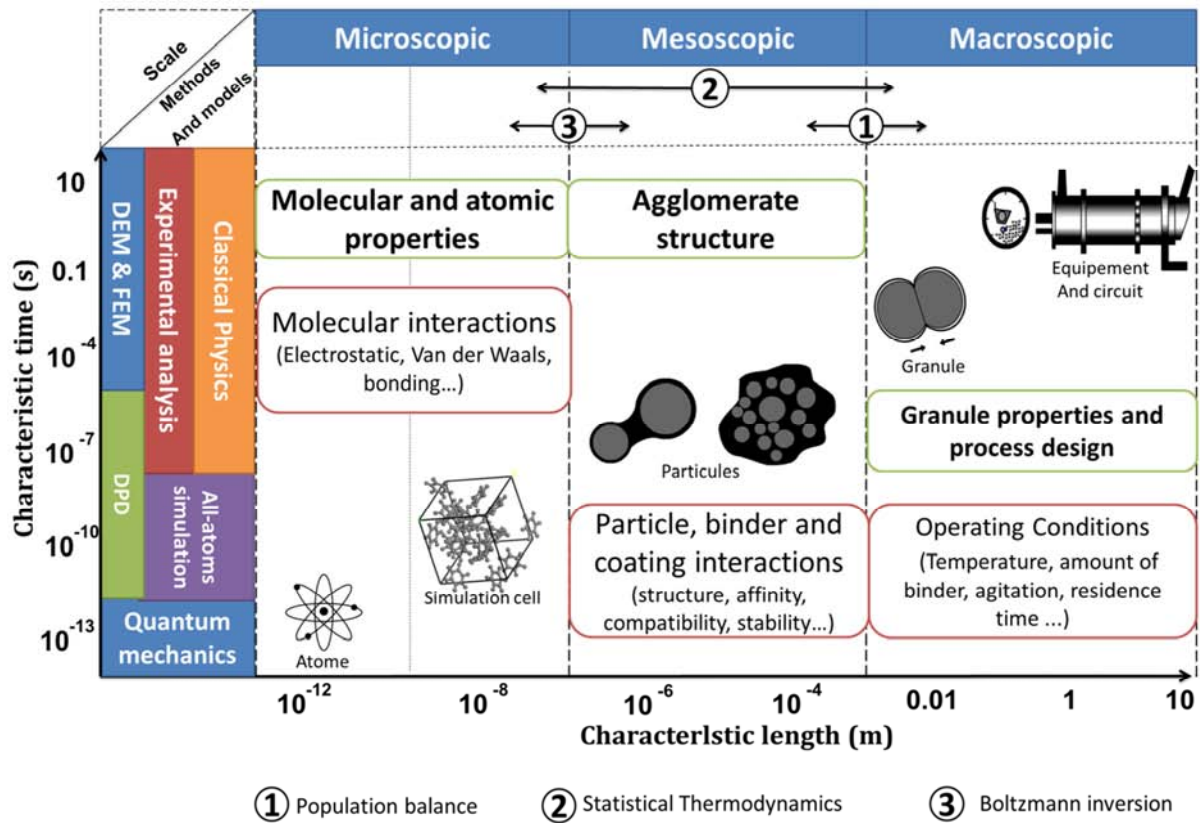
Fig. 1.10 – Multiscale modeling in granulation process. Figure adapted from Cameron (2005), Chipot (2003) and Sutmann (2009).

However, all-atom simulations are computationally heavy, and the computing capabilities sets a limit for the system size and simulation time to 10-100 Å and several ns respectively. All-atom simulation are therefore valuable for simple systems and cannot give access to several mesoscale phenomena including the structure of agglomerate, polymer-surface adsorption and self-assembly of large polymers. This led to the development of mesoscopic simulation methods such as DPD, with an intermediate level of detail and intermediate computational cost, and which opens the accessibility to a larger length between nm and micrometer, and time scale between nanoseconds and microseconds. It also shares a time-space range with the experimental study which makes the validation of DPD simulation results possible.

Finally, macroscopic simulation methods can be used for larger spatio-temporal scales; methods such as the distinct elements method (DEM) and the finite element methods (FEM). DEM is a simulation technique where the particles are considered individually rather than as a continuum and interact only at contact points. FEM is a simulation method based on the division of space on a mesh. An equation is obtained for each point of FEM discretization and the resolution of these equations allows the definition of a coupling between the particle and its surrounded fluid.

Several methods are used to link the different scales such as Boltzman inversion, population balance method and statistical thermodynamics. Boltzmann inversion is a mapping method used to derive potentials for coarse-grained systems. The general idea of this method is to generate the pair correlation function for the center-of-mass of molecules or molecule fragments corresponding to coarse-grained beads for each interaction in the trajectory of an atomistic simulation. Then, convert this pair function to a potential of mean force. In a second step, calculations of the distribution function in the coarse-grained system are performed, and if the results corresponds to the all-atom distribution function, then the derived potential is good, if not, more iterations are performed to improve the potential. Population balance method is used to relate the particulate level (i.e. mesoscale level) to the macroscopic and process scale. It's a mathematical tool that describes how particle size distribution changes as a function of time. This method is used for keeping track of the number of particles and their properties. Statistical thermodynamic describes the thermodynamic behavior of macroscopic systems on basis of its microscopic properties. The macroscopic system behavior is a result of statistical average of an ensemble of states, starting from a description of the motion of the atoms or particles (more details are given in chapter 4).

5. Conclusion and general objectives

Through chapter 1, we have described briefly the granulation mechanism and process, as well as the coating mechanism and components. We are aware that this short chapter does not cover all the work and study done in granulation, but we wanted to emphasize on the importance of the choice and formulation of the binder (or coating) which, at present, remains empirical and time consuming, and therefore, require more investment and study. In this work, we seek to understand the agglomeration mechanism in dry and aqueous systems by considering the interactions between the particles at the molecular and the mesoscopic scale. We will propose approaches allowing to choose the adequate binder and to formulate the right coating solution to produce good coated particles or agglomerates. Also, we will present numerical methodologies to assist scientists during binder formulation. The general objectives of this study can be summarized, as follows:

- Binder and coating solution characterization via experiments (Chapter 2 and 3),
- Understand the mechanism by which polymer stabilizes colloidal particles (Chapters 3 and 6),
- Prediction of the interactions between solid particles, and between solid particles and binders that control the agglomeration mechanism (Chapter 5 and 4),
- Developing a model for affinity prediction between solid particles in aqueous systems (Chapter 5),

- Building a mesoscale model for colloidal agglomeration in polymeric aqueous dispersions used in coating and granulation processes (Chapter 6),

- Assessment of polymer-plasticizer compatibility using experiments (Chapter 3), molecular simulation methods (Chapter 4) and mesoscale simulations (Chapters 6),

- Validation of the developed model through experimental observation and analysis (Chapter 3 and 6).

Chapter 2

Materials and experimental characterization techniques

"It doesn't matter how beautiful your theory is, it doesn't matter how smart you are. If it doesn't agree with experiment, it's wrong."

— *Richard P. Feynman, The Character of Physical Law lecture, 1965.*

1. Introduction

Our experimental study is elaborated with different model suspensions widely used in the form of excipient in food and pharmaceutical industries. The suspensions are composed of PVP: Polyvinylpyrrolidone (K10), MCC: Microcrystalline cellulose (Avicel PH-101), HPMC: Hydroxypropyl-methylcellulose (E19), EC: Ethyl cellulose (10P, N14), NA: Niflumic acid, SA: Steric acid, PEG: Polyethylene glycol.

In this chapter; we begin with a presentation of the materials used throughout this thesis. The relevant functional categories and properties of the materials are presented. Then, we present the various experimental characterization techniques used in the analysis of the coating and binder formulation along with the instruments used for the suspensions and coating films preparation are also described. Coating and films preparation protocol is described at the end of the chapter as well as the composition of the different suspensions studied throughout this thesis.

2. Materials

The characteristics of the compounds that we have used in this study and their essential characteristics will be covered in this subsection. Table 2.1 gives a summary of the functional category of these materials. The properties of the different compounds are displayed in Table 2.2. For the prediction of the surface free energy, the molar Parachor of the polymers was calculated using correlation (E.2) in appendix E. For acids and water we used the structural contribution method of Sugden (2002). Our interest in these compounds stems from their widespread application in the pharmaceutical and food industries (more information can be obtained from appendix J).

Table 2.1 – Relevant functional category of the material studied throughout this study. Data collected from Rowe (2009) and other literatures presented under this table.

	Filler	Coating agent	Binder	Plasticizer	Emulsifying agent	Solubility in water	Toxicity
PVP			X			Soluble (95% w/w)	Nontoxic
MCC					X	Practically Insoluble	Relatively nontoxic
HPMC		X	X		X	Soluble in cold water	Nontoxic
SA	X					Practically Insoluble (0.03% w/w at 25°C)[a]	Nontoxic
PEG				X		Soluble	Nontoxic
EC		X				Insoluble	Nontoxic
NA						Slightly soluble (1.9% w/w) [b]	Toxic

PVP: Polyvinylpyrrolidone, MCC: Microcrystalline cellulose, HPMC: Hydroxypropyl-methylcellulose, EC: Ethyl cellulose, NA: Niflumic acid, SA: Steric acid, PEG : Polyethylene glycol.

a: Green and Perry (2008), b: Yalkowsky and Dannenfelser (1992).

Table 2.2 – Solubility parameter, surface free energy and density found in the literature.

Compounds	Density (g.cm^{-3})	Surface free energy (mJ.m^{-2}). Experiments		Surface free energy (mJ.m^{-2}). Parachor	Solubility parameter (J.cm^{-3})$^{1/2}$	Molar volume v^* (cm^3.mol^{-1})
		γ	γ_d	γ	δ	
PVP	1.25[a]	53.6[h]	28.4[h]	47.65	-	90.56
MCC	1.59[b]	53.1[c]	42.4[c]	50.48	29.3[i]	204.02
HPMC	1.26[c]	34[f]	17[f]	36.05	22.8[h]	338.49
EC	1.27[d]	35.8[f]	25[f]	31.75	19-21[j]	387.87
NA	1.56[d]	45.9[f]	26.2[f]	52.83	23.8[k]	180.90
SA	0.847[b]	-	-	26.94	17.6[h]	335.87
PEG200	1.127[e]	46.7[g]	43.5[g]	44.95	24[j]	172.32
PEG400	1.127[e]	-	-	-	-	353.59
CA	1.31[b]	45.9[a]	-	42.64	24[j]	375.87
NC	1.6[a]	38[a]	-	48.13	21.7[j]	371.41
Water	0.997[b]	72[c]	21.8[c]	81.29	47.9[j]	18.05

PVP: Polyvinylpyrrolidone, MCC: Microcrystalline cellulose, HPMC: Hydroxypropyl-methylcellulose, EC: Ethyl cellulose, NA: Niflumic acid, SA: Stearic acid, PEG : Polyethylene glycol, CA : Cellulose acetate, NC : Nitrocellulose

* The molar volume of each monomer is calculated from the ratio of the molecular weight to the density.

a: Mark 1998, b: Rowe 2009, c: Benali 2006, d: Barra 1999, e: Ash 1998, f: Barra 1998, g: Demajo 2000, h: Rowe 1989a, i: Rowe 1989b, j: Barton 1991, k: Bustamante 1993.

From Table 2.2, we can see that the agreement is reasonable between the values of the total surface free energy obtained by the Parachor (See appendix E) method and those estimated experimentally from the contact angle method.

2.1   Polyvinylpyrrolidone (PVP)

Polyvinylpyrrolidone or Povidone (PVP) occurs as a fine, white to creamy-white colored, odorless or almost odorless, it's also described as a synthetic polymer consisting essentially of linear 1-vinyl-2-pyrrolidinone groups (see Fig. 2.1), the differing degree of polymerization of which results in polymers of various molecular weights (Rowe, 2009).
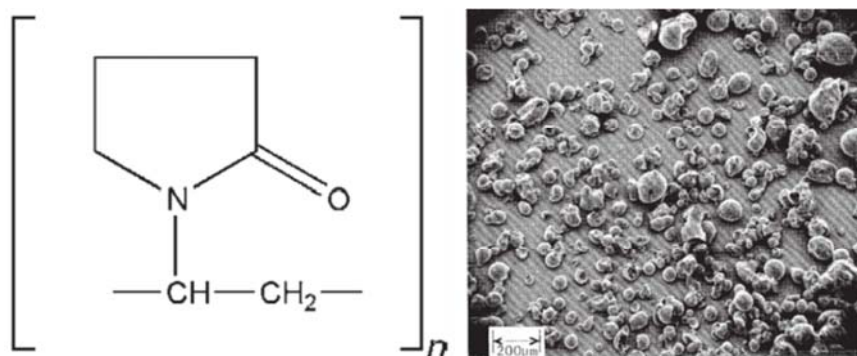
Fig. 2.1 – Structural formula of Polyvinylpyrrolidone (PVP) and SEM image of PVP's (Povidone K-30) dry powder (Rowe, 2009).

Although PVP is used in a variety of pharmaceutical formulations, it is primarily used in solid-dosage forms. PVP solutions are used as binders in wet-granulation processes (Becker, 1997, Stubberud, 1996) and as a solubilizer in oral and parenteral formulations. PVP solutions may also be used as coating agents or as binders when coating active pharmaceutical ingredients on a support such as sugar beads (Rowe, 2009). PVP is additionally used as a suspending, stabilizing, or viscosity-increasing agent in a number of oral suspensions and solutions. When consumed orally, PVP may be regarded as essentially nontoxic.

2.2   Microcrystalline cellulose (MCC)

Microcrystalline cellulose (MCC) is purified cellulose, practically insoluble in water and in most organic solvents, produced by converting fibrous-cellulose to a redispersible gel or aggregate of crystalline cellulose using acid hydrolysis (Milani, 2012). MCC is highly cohesive cellulose (Chitu, 2009). It is widely used in pharmaceuticals, primarily as a binder/diluent in oral tablet and capsule formulations where it is used in both wet-granulation and direct-compression processes (Enézian, 1972). In addition to its use as a binder/diluent, MCC also has some lubricant (Lerk, 1973) and

disintegrant properties that makes it useful in tableting. MCC is generally regarded as a relatively nontoxic and nonirritant material (Rowe, 2009).
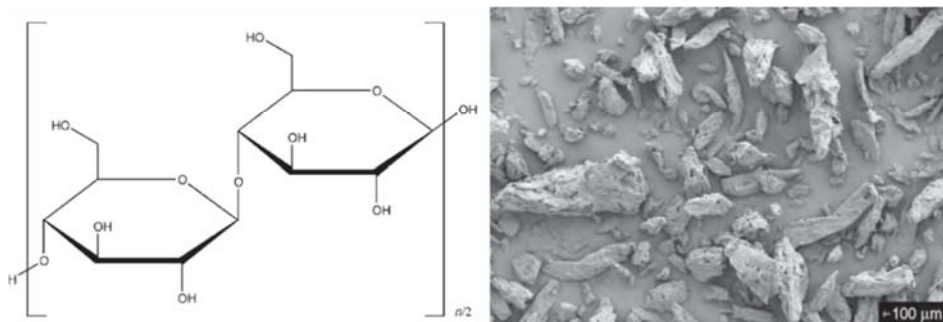
Fig. 2.2 – Structural formula of Microcrystalline cellulose (MCC) and SEM image of MCC's (Avicel PH-102) dry powder (Rowe, 2009).

2.3   Hydroxypropyl methylcellulose (HPMC)

Hydroxypropyl-methylcellulose or Hypromellose (HPMC) is an odorless and tasteless, white or creamy-white fibrous or granular powder. It's available in several grades that vary in viscosity and extent of substitution (Rowe, 2009). It's soluble in cold water, forming a viscous colloidal solution; practically insoluble in hot water. HPMC is widely used in oral, ophthalmic, nasal, and topical pharmaceutical formulations. In granulation, HPMC is used as a protective colloid by coating hydrophobic particles with multimolecular layer and promote wetting (Mahato and Narang, 2011). In oral products, HPMC is mainly used as a tablet binder (Chowhan, 1980), in film-coating, as a film former and as a matrix for use in extended release tablet formulations (Rowe, 1977). High-viscosity grades of HPMC may be used to retard the release of drugs from a matrix at levels of 10–80% (w/w) in tablets and capsules (Rowe, 2009). Depending upon the viscosity grade, concentrations of 2–20% (w/w) are used for film-forming solutions to film-coat tablets. Lower viscosity grades are used in aqueous film-coating solutions.

Compared with Methylcellulose, HPMC produces aqueous solutions of greater clarity, with fewer undissolved fibers present, and is therefore preferred in formulations for ophthalmic use (Rowe, 2009). In addition, HPMC is used as an emulsifier, suspending agent, and stabilizing agent in topical gels and ointments. As a protective colloid, it can prevent droplets and particles from coalescing or agglomerating, thus inhibiting the formation of sediments. HPMC is generally regarded as a nontoxic and nonirritating material. For the preparation of an aqueous solution, it is recommended that HPMC is dispersed and thoroughly hydrated in about 20–30% (w/w) of the required amount of water. The water should be heated to 80–90°C, and then the HPMC should be added (Rowe, 2009).
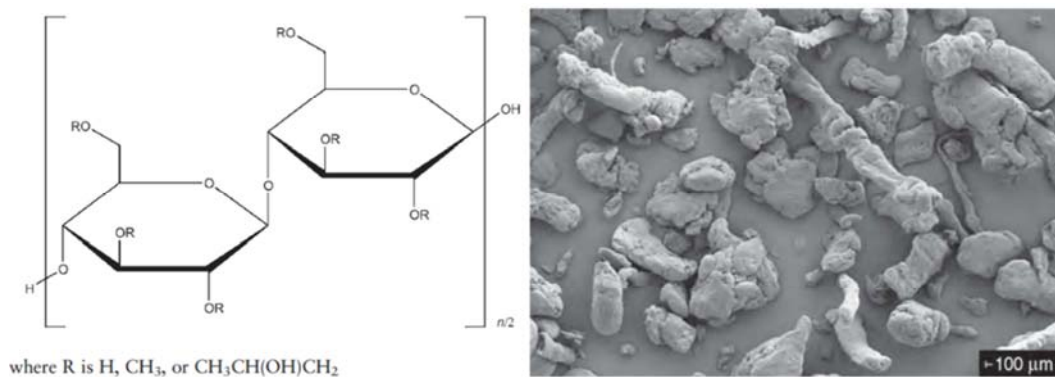
Fig. 2.3 – Structural formula of Hydroxypropyl methylcellulose (HPMC) and SEM image of HPMC's (Methocel E5) dry powder (Rowe, 2009).

2.4   Stearic acid (SA)

Stearic acid is a fatty acid, and a hard, white or faintly yellow-colored, somewhat glossy, crystalline solid or a white or yellowish white powder (Rowe, 2009), and practically insoluble in water (Yalkowsky; 2003, Green and Perry, 2008).
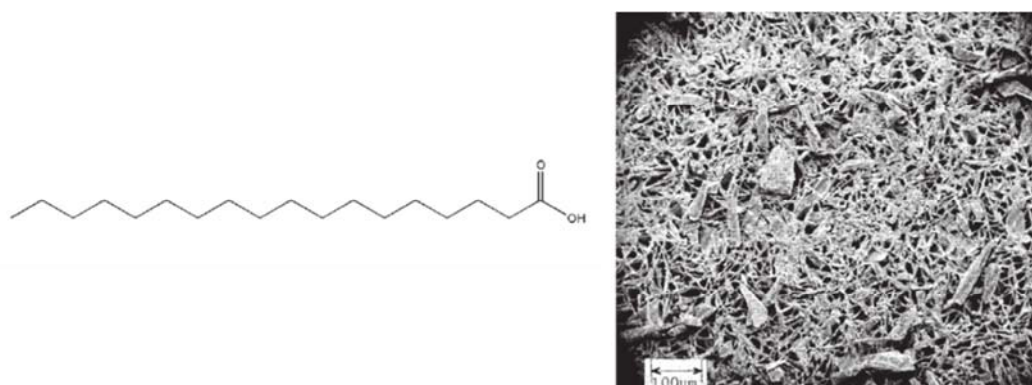
Fig. 2.4 – Structural formula of Stearic acid (SA) and SEM image of SA's dry powder (Rowe, 2009).

Stearic acid (SA) is often added to the cellulose derivatives to enhance specific properties. For example, adding SA to HPMC leads to a decrease in the water affinity due to SA hydrophobic properties caused by its content of long-chains (Jiménez et al., 2010). Stearic acid is widely used in oral and pharmaceutical formulations as a tablet and capsule lubricant (Iranloye and Parrott, 1978; Mitrevej and Augsburger, 1982), although, it can also be used as a binder and for formulating sustained-release preparations. Stearic acid is also used in cosmetics and food products. Stearic acid is generally regarded as a nontoxic and nonirritant material (Rowe, 2009).

2.5 Polyethylene glycol (PEG)

Polyethylene glycols (PEG's) or macrogols are described as an addition of ethylene oxide and water. Polyethylene glycol grades 200–600 are liquids; grades 1000 and above are solids at ambient temperatures. All grades of polyethylene glycol are soluble in water and miscible with other polyethylene glycols (after melting, if necessary).

PEGs are widely used in a variety of pharmaceutical formulations and can be used to enhance the aqueous solubility or dissolution characteristics of poorly soluble compounds (Miralles et al., 1982). They are also useful as plasticizers in microencapsulated products to avoid rupture of the coating film when the microcapsules are compressed into tablets. When added to mixtures of HPMC, they improve the mechanical properties of the final coating product (Laboulfie, 2013; Heinämäki et al., 1994; Kundu et al., 2008). Their main advantage over fatty acids is their physical and thermal stability on storage. However, they are chemically more reactive than fats (Rowe, 20009) and have only limited binding action when used alone. Aqueous polyethylene glycol solutions can be used either as suspending agents or to adjust the viscosity and consistency of other suspending vehicles. Generally, they are regarded as nontoxic and nonirritant materials (Rowe, 2009).
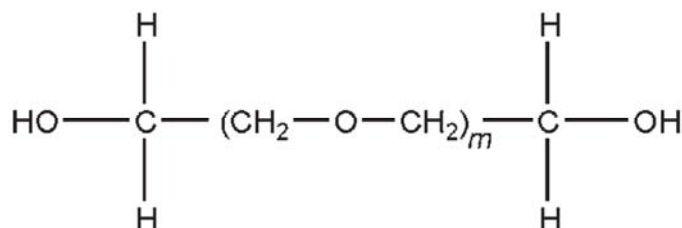
Fig. 2.5 – Structural formula of Polyethylene glycol (PEG).

2.6 Ethylcellulose (EC)

Ethylcellulose (EC), an ethyl ether of cellulose, is a long-chain polymer of b-anhydroglucose units joined together by acetal linkages, it's is a tasteless, free-flowing, white to light tan-colored powder produced by the reaction of ethyl chloride with the appropriate alkaline solution of cellulose. EC is practically insoluble in water and it is widely used in oral and topical pharmaceutical formulations. The main use of EC in oral formulations is as a hydrophobic coating agent for tablets and granules (Ozturk et al., 1990; Sadeghi et al., 2001).

EC coatings are used to modify the release of a drug, to mask an unpleasant taste or to improve the stability of a formulation; for example, granules are coated with EC to inhibit oxidation (Rowe, 2009). In tablet formulations, EC may additionally be employed as a binder. EC is generally regarded as a

nontoxic, nonallergenic, and nonirritating material. Drug release through EC-coated dosage forms can be controlled by diffusion through the film coating (Rowe, 2009).
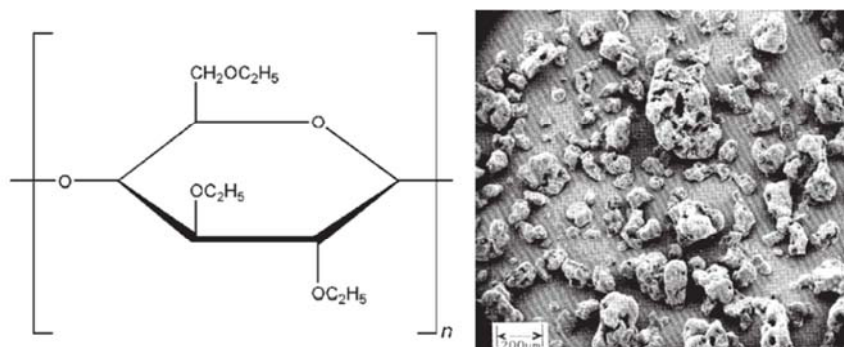
Fig. 2.6 – Structural formula of Ethylcellulose (EC) and SEM image of EC's dry powder (Rowe, 2009).

2.7 Niflumic acid (NA)

Niflumic acid is a strong acid that has the form of a crystalline solid. Its structural formula is shown in Fig. 2.7. NA is a drug used in the treatment of rheumatoid arthritis, and, more generally, muscle and joint pain and it is regarded as a toxic material. NA is prepared by dissolving the crystalline solid in an organic solvent such as ethanol, methanol, acetone, DMSO, or acetonitrile. The solubility of NA in these solvents is approximately 50 mg.ml^{-1} (Barnett et al., 1994; Johnson et al., 1995). It's also slightly soluble in water.
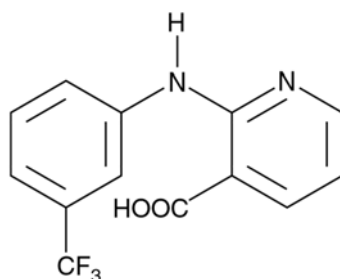
Fig. 2.7 – Structural formula of Niflumic acid (NA).

3. Equipment and analysis instruments

3.1 Ultra-Turrax disperser for coating preparation

The Ultra-Turrax® T 25 (JANKE& KUNKEL, IKA) is a dispersion unit which, in connection with a dispersion tool, manufactures emulsions and dispersions. The apparatus is equipped with a motor (Fig. 2.8 (a)) for the movement of the rotor at different speeds: 500 to 10 000 rpm.

The axis of the dispersion tool comprises two parts; a stator and a rotor (Fig. 2.8 (b)), which are two cylinders separated by a gap. The contact end of these two parts has square indentations allowing the circulation of the fluid (Fig. 2.8 (c)). In principle, the solution is sucked axially into the head of the disperser to be ejected through the slots of the rotor / stator. The speed is very high and the air gap between the rotor and the stator is low, the fluid is subjected to a high shear field, which allows obtaining smaller dispersions (Renouf, 2000).
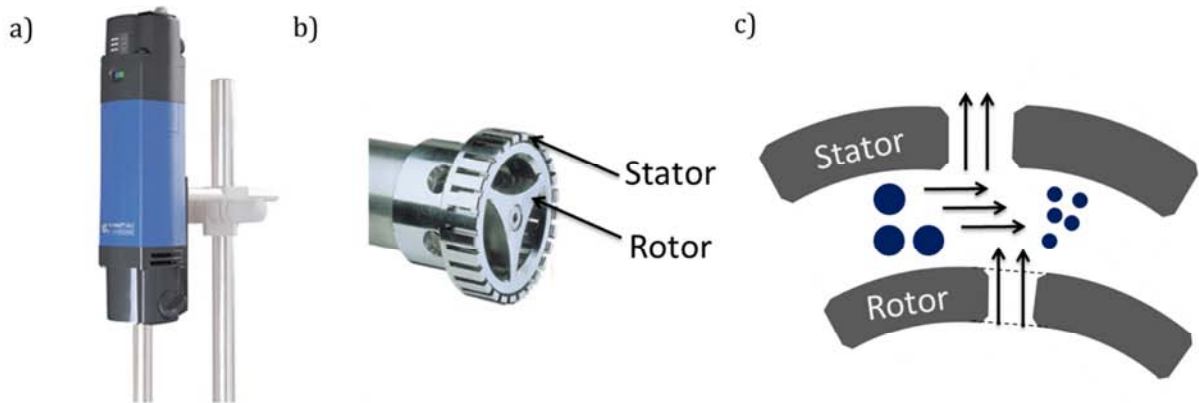
Fig. 2.8 – Ultra-Turrax disperser; a) Ultra-Turrax motor, b) Ultra-Turrax axe composed of rotor and stator, c) dispersion of particles in between the rotor and the stator, adapted from Renouf (2000).

3.2   CAMAG handcoater

CAMAG handcoater (Fig. 2.9) is an instrument mainly used in paint industries to produce thin liquid films by spreading the solution on a glass plate. This allows the production of uniform film with a thickness of 500 µm. The films are afterward dried in an oven at 40°C.

Fig. 2.9 – CAMAG handcoater.

3.3 Cryogenic-SEM instruments

Cryogenic-SEM is a technique that allows visual checking of the structure of dispersions (separated or agglomerated particles) in two dimensions by freezing the sample by ultra-rapid freezing not allowing time for ice crystals to grow. This technique is widely used by biologists or chemists (Glicksman, 2000) or in the food industry (Moor and Riehle, 1968).

To observe the structure of our samples we used Cryogenic-SEM technique following several steps; first, in order to fix the structure and the morphology of the samples, rapid freezing of the sample in pasty nitrogen (-210°C) or in liquid ethane (-172°C) or by high pressure freezing was used. The frozen samples were then transferred to the cool preparation chamber (PP3000T Quorum Technologies) and they were fractured by striking them with a cold scalpel. Afterward, the revealed fractured surface was metal-coated with a beam of electrons and introduced in the analysis chamber to be examined in a scanning electron microscope (SEM) (Hitachi MEB ESEM Quanta 250 FEG FEI) (Fig. 2.10 (a)) while being maintained at -135 °C. Various detectors are used to analyze these particles and to reconstruct an image of the surface.

In a second phase of the analysis, the fractured samples were sublimated at -90 °C for 20 to 40 minutes in a vacuum SEM cool chamber (PP3000T cryochamber) before examination in the cryo-stage SEM. The sublimation step was performed to remove water from frozen samples and therefore expose the first layer of particles inside the dispersion.

The freezing step is a critical step, because the sample may be damaged by the growth of ice crystals when using pasty nitrogen as a freezing medium. To avoid this problem, amorphous ice must be produced. To do so, one technique is the high pressure freezing which can create amorphous ice with a thickness of 200 microns. This technique was first suggested by Moor and Riehle (1968). This is made possible by combining an extremely high cooling rate to a high pressure. Another technique for rapid freezing is by using liquid ethane as a freezing medium.

For freezing using pasty nitrogen, the sample was plunged into pasty nitrogen slusher pot of workstation, trademarked PrepDek. Slusher pot evacuated by primary pom transformed the liquid nitrogen (-196°C) to pasty nitrogen (-210°C approximately). To provide the best conditions for pre-freezing using liquid ethane, we used Leica EM GP automatic plunge freezer (Fig. 2.10 (b)).

For the high pressure freezing, the samples were inserted between two "planchettes" dedicated for cryofracture to create a sandwich, and it was loaded in a HPM100 high-pressure freezing machine (Leica microsystems, Vienna, Austria) and the sample was fixed and froze within 5 ms at 2100 bar.
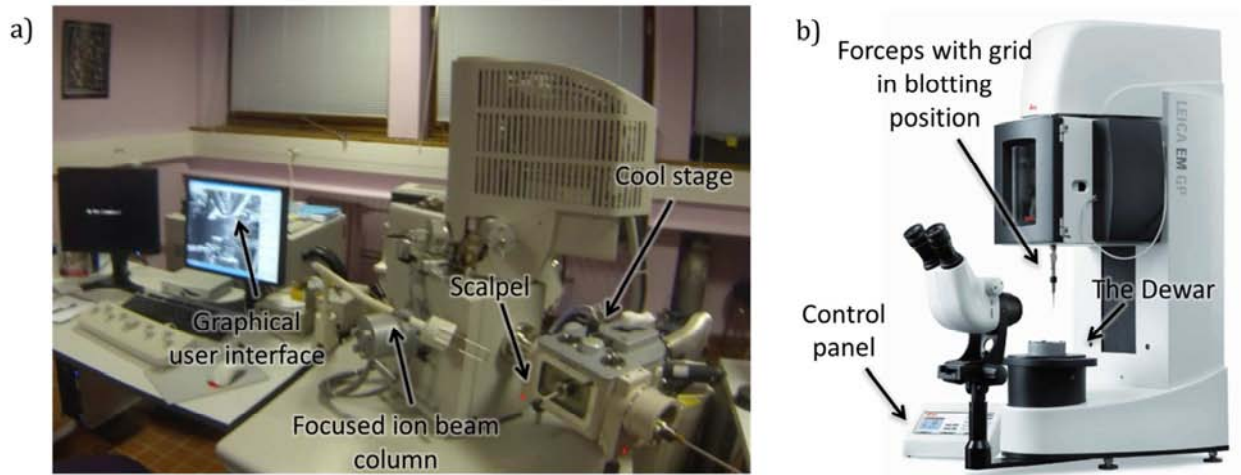
Fig. 2.10 – Cryogenic-SEM instruments; a) Hitachi MEB ESEM Quanta 250 FEG FEI, b) Leica EM GP.

High-pressure freezing was performed in BIC (Bordeaux Imaging center, Université de Bordeaux, Bordeaux). Pasty nitrogen and liquid ethane freezing, as well as SEM analysis took place within the CMEAB (Centre de Microscopie Électronique Appliquée à la Biologie, Faculté de Médecine Rangueil, Toulouse).

SA particles counting in HPMC blends images obtained by Cryogenic-SEM through high pressure freezing was carried out with the image software ImageJ (Rasband, 1997). ImageJ is a Java based public domain image processing and analysis program, which is freely available and open source. This qualitative image analysis software was used by several scientists including Hermana and Walz (2015) who used ImageJ to determine the size distribution of adsorbed latex nanoparticles in colloid dispersion. Ellison et al. (2014) also used it for the calculation of the mean particle diameter of coated silver nanoparticles, and Baghbanzadeh et al. (2015) used ImajeJ to measure the surface roughness of membranes.

In imageJ, in order to remove smooth continuous backgrounds from SEM images of HPMC-SA dispersions, we applied a "rolling ball" of 30 pixels. To improve the counting and the selection of high intensity objects; filters median (radius 2 pixels) and highpass (radius 0.7 pixel) were applied to remove the noise of the images (background) and to increase the high intensities of the particles in the dispersions. On the images, a threshold was realized to select the objects to be counted between 90 and 255 in grey levels (8 bits images) with a save of the count mask of the outlines of the counted objects. A second count mask is applied to select multiple ROI (region of interest) when the images are not flat.

3.4 Particle size distribution

Most of the materials used in this study are stearic acid (SA) suspensions dispersed in a polymeric solution. The properties of dispersed material are strongly related to their particle size. Measuring of the particle size distribution was done using laser particle size analyzer MALVERN Mastersizer 2000 available at Analysis and Process Service (SAP) in the chemical engineering laboratory (LGC, Toulouse). This instrument is equipped with a wet dispersion module type HYDRO that allows the characterization of particle size between 0.1 and 1000 micrometer. The particle size analyses reported throughout this study are the average of three successive laser diffraction runs.

The particle size distribution is well representative of the stirring conditions and formulation in which the suspension has been developed. The shape of the particle size distribution curve is an important information because it gives insights on the effect of several properties such as the viscosity and the stability of the formulations. Laser diffraction instrument measure distributions generally by volume, that is to say, it represents the proportion by volume of a set of particles in a diameter class relative to the total volume of the dispersed phase.

With this technique, we were able to access different diameters d_{10}, d_{50}, d_{90}, d_{32} which are representative of an average of the entire population of particles. We can also calculate the coefficient of variation of the distribution C_V. d_{50} is the median value of the distribution, that is to say, the value where half of the particles population resides above this value, and the other half resides below it. Similarly, d_{10} and d_{90} represent the particle sizes below which are 10% and 90% of the particles respectively. The surface diameter d_{32} (called the Sauter diameter) is obtained by the ratio of the moment of order 3 to the moment of order 2. The coefficient of variation Cv of the distribution provides access to the spread of the distribution, it is given by:

$$C_v = \frac{d_{90} - d_{10}}{d_{50}} \tag{2.1}$$

In Fig. 2.11 are shown some typical particle size distributions whose width is associated with the polydispersity of the suspension. Polydispersity is used to describe the non-uniformity of a particle size in a dispersion.
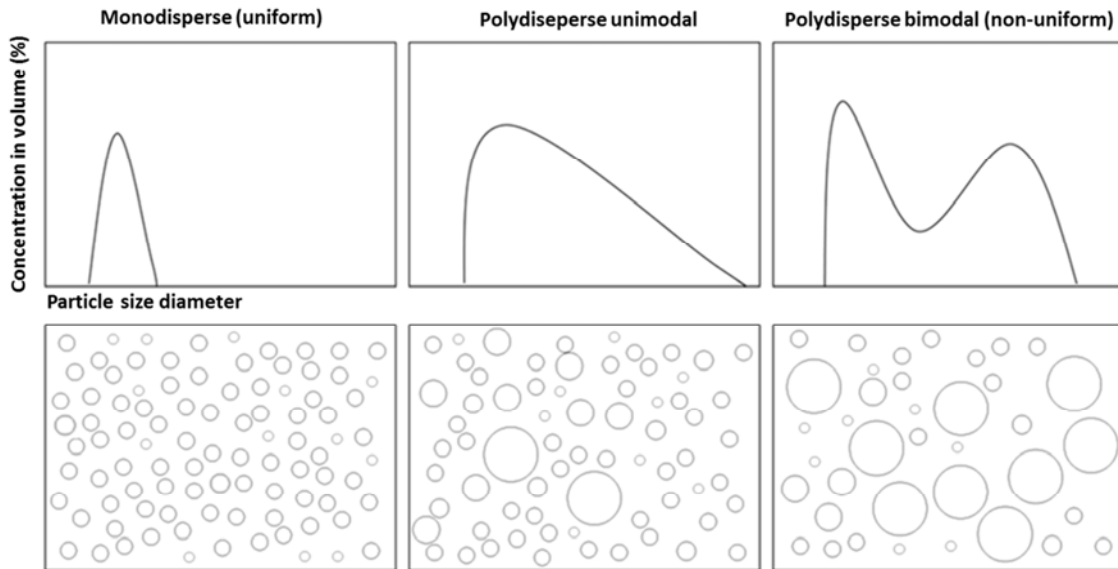
Fig. 2.11 – Typical examples of particle size distributions.

3.5 Differential scanning calorimetry (DSC)

Differential scanning calorimetry (DSC) performs measurements of heat flow by varying the thermal energy supplied to the sample. This technique is particularly useful for determining the glass transition temperature Tg and the melting temperature Tm. Tg is defined as the temperature below which the polymer is in a glassy state and above which it's in a rubbery state. For example the glass transition temperature of EC is 120 °C, thus, an unplasticized EC film would be in the glassy state at room temperature, and therefore needs a plasticizer to improve its flexibility and reduce brittleness (McGinity and Felton, 2008). On the macromolecular level, glass transition is associated with a change in the degree of freedom of movement of the polymer chain segments. Above Tg, the free volume increases, allowing the movement of the chains and the deformation of the polymer. In the other hand, melting is a phase transition, characterized by the melting temperature Tm, that occur when the polymer chains fall out of their crystal structures and become a disordered liquid.

In this work, the DSC tests were carried out with a differential scanning calorimetry analyzer DSC Q 2000 (Fig. 2. 12 (a)). The software used for analysis of DSC data was Universal Analysis 2000 software analysis.

In the DSC instrument, the samples were sealed in DSC aluminum pan and scanned between 25 to 300 °C with heating rate of 20°C.mn⁻¹. An empty aluminum pan served as reference. Each pan is in contact with a thermocouple connected to a computer (Fig. 2.12 (b)). The registration of a signal proportional to the difference in the heat flow between these two pans is used to determine glass transition temperature Tg, melting temperature Tm and the melting enthalpy ΔH. Tg is detected in the DSC thermogram by a sudden curve change, and is measured either at the "onset", at "mid-point" or

at the "End-point" (Fig. 2.13 (a)). Throughout this study, Tg values corresponds to the "Mid-point". The peak temperature of the melting endotherm in the DSC curves was taken to be the melting temperature Tm of the polymer. ΔH was calculated by integrating the melting peak's area for each sample (Fig. 2.13 (b)).

In our DSC analysis, we studied more precisely the crystalline melting points of the films associated with the appearance of endothermic peak in the DSC curves. This melting peak provides access to the melting temperature T_m, and to the energy required for melting different morphologies crystals.
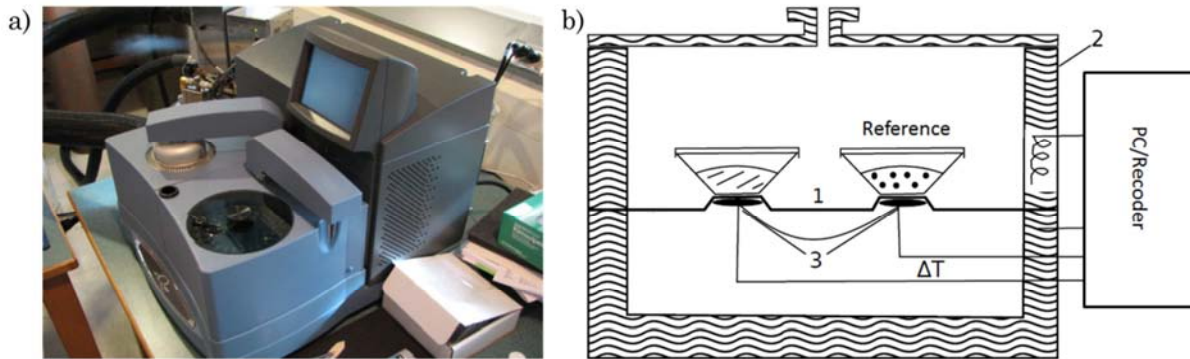
Fig. 2.12 – a) DSC Q2000, b) Schematic of DSC Sample Chamber, 1) discs, 2) oven/lid, 3) thermocouples (adapted from Bouillot (2011)).
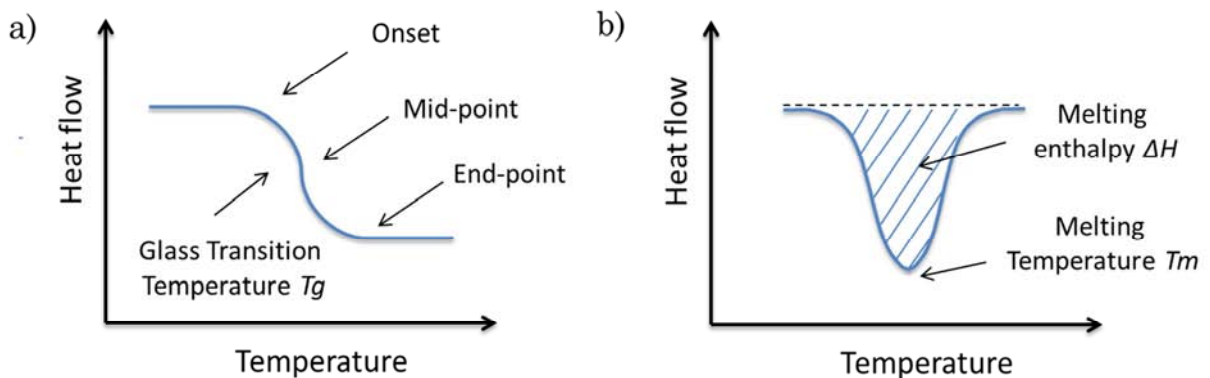
Fig. 2.13 – Schematic DSC curves; a) Determination of glass transition temperature Tg, b) Determination of melting temperature Tm.

4.   Preparation protocol of the suspensions

HPMC-SA mixtures were prepared by adding the cellulose polymer in deionized water previously heated to 80°C. The mixture was then homogenized by moderate agitation for 30 to 60 minutes using a rotor-stator homogenizer (Ultraturrax T25, Janke and Kunkel, Germany) at 85°C. Stearic acid was then added to the HPMC solution progressively under agitation until it was evenly dispersed. The

mixture was then cooled using an ice bath under agitation for 30 minutes. Solutions were thereafter degassed at 50 mbar for 2 hours. To attain maximum stabilization, the readily prepared solutions were stored immediately at 5°C for at least 24 hours.

The same protocol was used for the preparation of PVP-SA and MCC-SA mixtures.

Polymer-plasticizer-water samples (PVP-PEG, HPMC-PEG and MCC-PEG in water) and polymer-water samples (PVP, HPMC, MCC and PEG in water)were firstly prepared following the same previous protocol. They were thereafter spread on a glass plate using the Camag handcoater to produce a thin film. The liquid films are then placed for 24 hours at ambient temperatures. Table 2.3 presents the different formulations used throughout this study.

Table 2.3 – Composition of the different formulation studied throughout this thesis.

Formulation name	Binder/coating composition (w/w)			
	Polymer	Filler	Plasticizer	Solvent
SA 10%	-	10% SA	-	90% water
HPMC 10%	10% HPMC	-	-	90% water
PVP 10%	10% PVP	-	-	90% water
MCC 10%	10% MCC	-	-	90% water
PEG 10%	-		10% PEG	90% water
HPMC-SA 10%-2%	10% HPMC	2% SA	-	88% water
HPMC-SA 10%-10%	10% HPMC	10% SA	-	80% water
HPMC-SA 10%-20%	10% HPMC	20% SA	-	70% water
PVP-SA 10%-10%	10% PVP	10% SA	-	80% water
MCC-SA 10%-10%	10% MCC	10% SA	-	80% water
MCC-SA 10%-20%	10% MCC	20% SA	-	70% water
HPMC-PEG 10%-10%	10% HPMC	-	10% PEG	80% water
PVP-PEG 10%-10%	10% PVP	-	10% PEG	80% water
MCC-PEG 10%-10%	10% MCC	-	10% PEG	80% water

SA: Stearic acid, HPMC: Hydroxypropyl-methylcellulose, PVP: Polyvinylpyrrolidone, MCC: Microcrystalline cellulose, PEG : Polyethylene glycol.

5. Conclusion

In this chapter, we presented the different material studied in this work, as well as the instruments used to characterize the coating and binder formulations which are:

- Cryogenic-SEM instruments for visual observation of the structure of dispersions,

- Malvern Mastersizer 2000 for particle size distribution analysis,
- Differential scanning calorimetry (DSC) for thermal analysis.

The instruments used for the suspension preparation were also presented including the Ultra-Turrax disperser and the CAMAG manual handcoater.

Chapter 3

Aqueous coating formulation: experimental characterization

Results in this chapter have been submitted to Powder Technology journal:

Jarray A., Gerbaud V. and Hemati M., Structure of aqueous colloidal formulations used in coating and agglomeration processes: mesoscale model and experiments, Powder. Technol..

1. Introduction

Particle growth process relies on the addition of a solution or suspension that will adhere on particles to produce agglomerate or coated particles. The former is governed by agglomeration mechanisms where the particles agglomerate by virtue of a binder. The latter is obtained through coating or layering process where the particles are entirely covered by the coating solution. Whether it is a coated particle or agglomerate, the coating solution or the binder is usually prepared through aqueous polymer dispersion.

Hydrophilic stabilizing polymers (such as hydroxypropyl-methylcellulose, HPMC), plasticizers (such as polyethylene glycol, PEG) or hydrophobic filler (such as stearic acid, SA) are added during the preparation of the polymer dispersion. These additives are present in the final binder or coating solution, therefore, they affect various properties of the final product. The film forming dispersions should be physically stable and the hydrophobic particles should be uniformly dispersed in the medium. This can be achieved by formulating the adequate coating or binder solution and by obtaining stable colloids with good affinity and sufficient interactions between its components.

This chapter is organized as follows: we first give an overview of material interactions during binders and coatings preparations and we discuss colloidal stability. Second, the suspension preparation

protocol is described. Third, we present the experimental results; the structure of HPMC-SA, PVP-SA and MCC-SA blends are analyzed using particle size distribution analysis, and then observed using Cryogenic-SEM. The effect of the percentage of SA on the HPMC-SA structure is investigated. Thermal analysis of the pure materials and the blends is also performed using DSC.

2. Behavior of HPMC, PEG and SA during coating preparation

The aqueous solution used in coating and agglomeration processes is a multicomposite polymer dispersion. This includes the film forming polymer, insoluble or instable film additives or surfactants to promote spreading, and plasticizers to impart flexibility, improve flow and reduce brittleness. Thus, one of the major issues in the particle size enlargement process is the selection of suitable compounds and the elaboration of a stabilized colloidal dispersion. The stability of these solutions strongly depends on the interactions between the constituents of the mixture in the presence of a solvent which is often water.

Once the coating or binder solution is sprayed onto the powders through the various unit processes, it will result in the formation of a continuous film on the surface of particles during the coating, or in the formation of solid bridges between the grains during agglomeration (see Fig. 3.1). The particles get closer during the drying process and the interparticle forces makes the particles eventually coalesce with each other, and cause the spheres to fuse, resulting in a coated film or solid bridges between the primary particles (see Fig. 3.2).
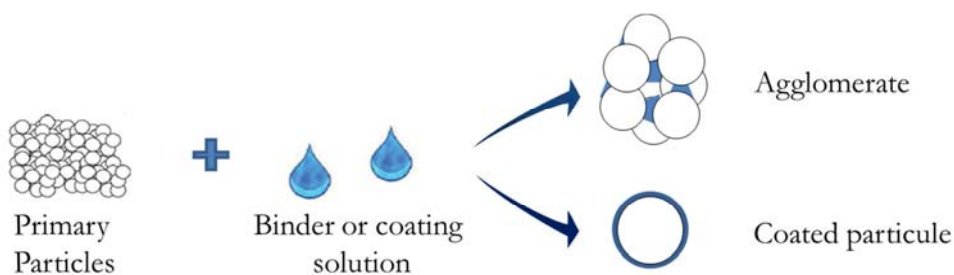
Fig. 3.1 – Wet particle growth mechanisms.

The properties of the final product depend on the affinity between the surface of the powder and the pulverized solution. It also depends on the interactions between the different components (polymers, fatty acids, solvent…) involved in the formulation of the composite coating agent.
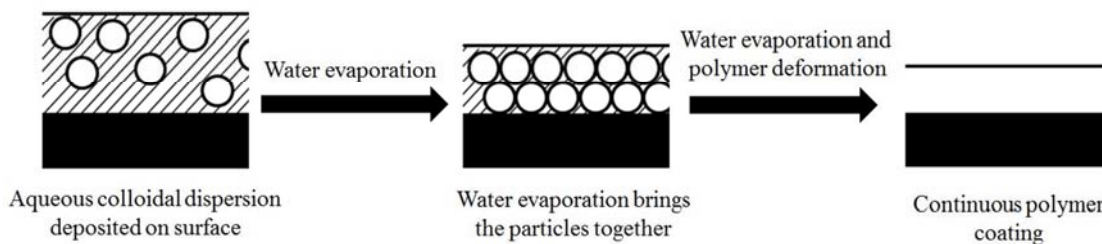
Fig. 3.2 – Film formation during the evaporation phase. Figure adapted from Onions (1986).

In this chapter, we are interested in the coating of solid particles by an aqueous solution containing HPMC as a matrix for film formation (10% w/w), micronised SA as a hydrophobic filler (2% to 20% w/w) and polyethylene glycol as a plasticizer (2% w/w).

During polymeric solution preparation (see Fig. 3.3), the hot aqueous solution of HPMC is mixed with the PEG plasticizer and the SA hydrophobic filler. Then nucleation occurs as the particles gather together by affinity. Typically, hydrophobic SA particlesagglomerate, whereas HPMC and PEG can dissolve in water. After cooling, the fine colloidal SA particles will be stabilized by HPMC. HPMC polymer is able to form a gel network. This gel will entrap SA particles and prevent them from getting close in the range of attractive forces.
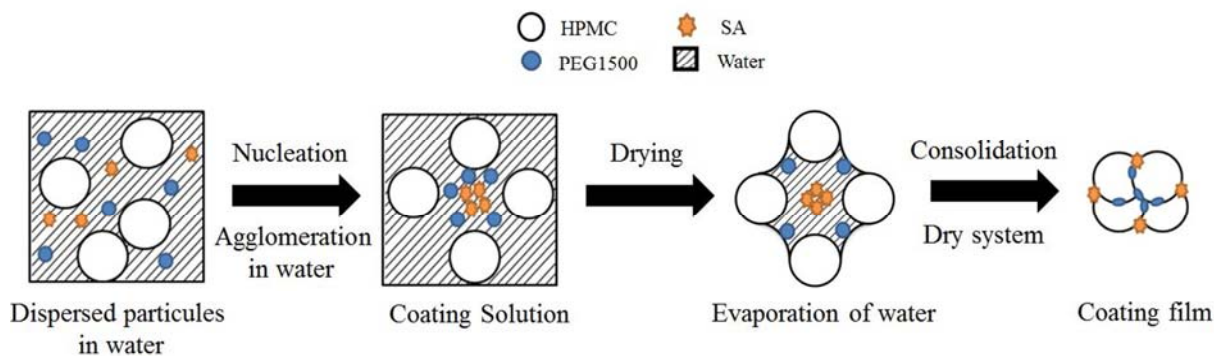
Fig. 3.3 – Coating preparation steps of HPMC-SA-PEG1500 mixture placed in water, HPMC: Hydroxypropyl-methylcellulose, SA: Stearic acid, PEG1500: Polyethylene glycol 1500.

During film formation by drying, the evaporation of the interstitial water leads to the formation of liquid bridges between the HPMC polymer chains. The final composite film of HPMC and PEG incorporates crystal inclusions of PEG and SA (Laboulfie et al., 2013) (see Fig. 3.3). According to these authors, the presence of crystals of SA in the interstitial space between the molecules of HPMC reduces the interactions between the polymer chains and, therefore, prevents their coalescence. An increase in the drying temperature leads to the formation of smaller crystals of PEG in the liquid bridges. Thus, the lack of contact between the polymer chains due to the presence of SA crystals is replaced by the contact between HPMC and PEG molecules. This will improve the plastic properties of the dry coating film.

3. Colloid stability

Colloidal systems are dispersed phases finely subdivided in a dispersion medium (Napper, 1983). Particles are said to be colloidal in character if they possess at least one dimension in the size range 1–100 nm. The dispersion of larger particles whose size is greater than 1 μm is usually referred to as a suspension. A colloidal dispersion is said to be stable when the dispersed phase remains so over a long time scale (e.g. months or years) (Napper, 1983). Colloidal particles always undergo Brownian motion and are attracted to each other with long range attractive forces. Consequently, in order to favor colloid stability, it's necessary to create long range repulsion between the colloidal particles. This can be obtained by entrapping colloidal particles with a polymer (steric stabilization). The polymer will generate a layer at the particles surface and prevent their aggregation (see Fig. 3.4). An increase in the layer thickness of the formed polymer has been found to improve the colloidal stability (Napper, 1983). The layer thickness should be at least several nanometers to provide effective stabilization (Phillips, 2009). Koelmans and Overbeek (1954) suggested that only if the thickness of the adsorbed layer was comparable in size to the diameter of the dispersed particles could a polymeric steric mechanism provide sufficient protection. Walbridge and Waters (1966) showed that the minimum steric barrier thickness required for the largest particles was of the order of 5 nm. To attach themselves on the particles, the polymer chains adsorb by affinity on the surface to give full coverage. The attachment between the polymer chains and the colloidal particles should be strong enough to prevent the polymer desorption when the particles undergoes Brownian collisions. When the polymer content in the aqueous phase is sufficiently high, the particles may be immobilized in a polymer gel network.
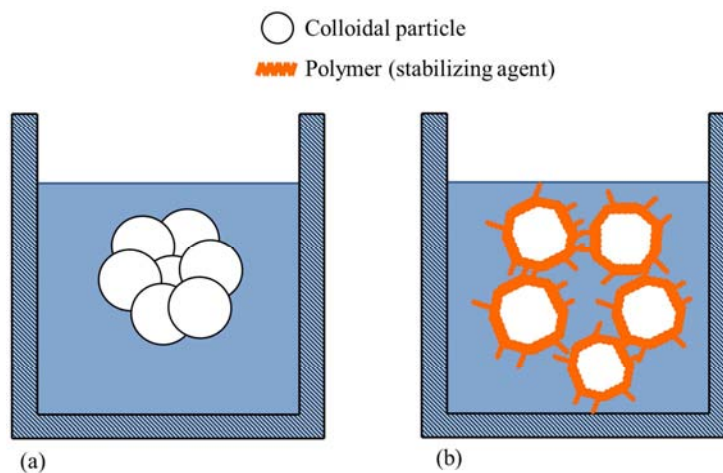
Fig. 3.4 – Schematic representation of the stabilization of colloidal particles. a) Colloidal particles agglomerate in water, b) Colloidal particles stabilized in water by a polymer.

4. Experimental results

One of the important issues when preparing coating solutions and binders containing HPMC and SA, is the stability of the SA colloidal particles since any colloidal particle agglomeration could negatively impact the performance of the final coating solution. Another concern during coating formulation is the compatibility between the polymer (HPMC, MCC and PVP) and the plasticizer (PEG). This compatibility can be assessed by the miscibility between the polymer and the plasticizer. Colloid agglomeration or phase separation indicates low compatibility.

Fig. 3.5 shows photographs of the appearances of the samples used in this study and prepared using the protocol described at the end of chapter 2. Pure SA in water shows phase separation (Fig. 3.5 (a)) due to SA agglomeration. HPMC is soluble in water and forms a homogenous transparent solution (Fig. 3.5 (b)). Pure MCC in water forms a white solution (Fig. 3.5 (c)). PVP in water forms a transparent yellowish mixture (Fig. 3.5 (d)).
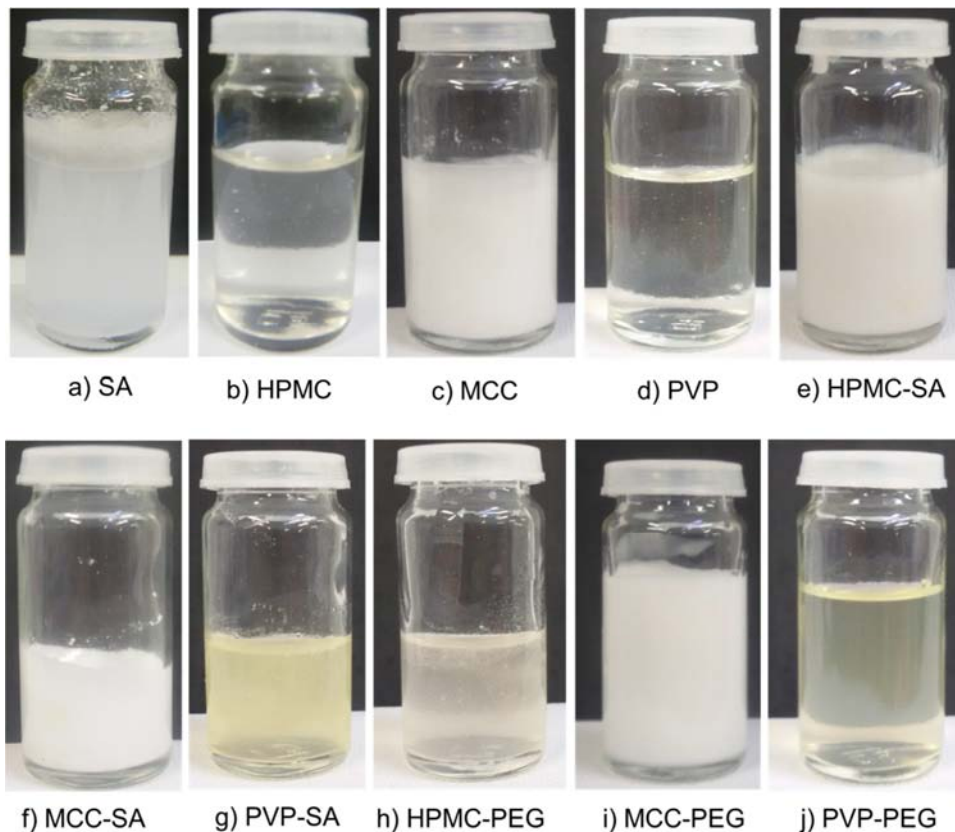
Fig. 3.5 – Appearances of a) Pure SA 10%, b) Pure HPMC 10%, c) Pure MCC 10%, d) Pure PVP 10%, e) HPMC-SA 10%-10%, f) MCC-SA 10%-10%, g) PVP-SA 10%-10%, h) HPMC-PEG 10%-10%, i) MCC-PEG 10%-10%, j) PVP-PEG 10%-10%, all the mixtures weight percentages.

When mixing SA and HPMC in water, following the preparation protocol described above, a white homogenous solution is obtained and no phase separation can be observed by the naked eye (Fig. 3.5 (e)). When mixing SA with MCC, we also obtain a white solution and it's difficult to tell if there is phase separation (Fig. 3.5 (f)). PVP-SA forms a yellow-transparent solution and we cans distinguish a phase separation (Fig. 3.5 (g)). HPMC-PEG (Fig. 3.5 (h)), MCC-PEG (Fig. 3.5 (i)) and PVP-PEG (Fig. 3.5 (j)) blends form homogenous phase. PVP-PEG and HPMC-PEG are transparent and MCC-PEG is white and no phase separation can be observed by the naked eye.

To monitor the stability of the prepared dispersions we used particle size distribution. Cryogenic-SEM was used to microscopically observe the prepared coating solutions. Different freezing techniques were used to preserve the structure of the suspensions.

4.1 Particle size distribution

Prepared samples were subjected to laser diffraction particle size analyzer with a Master Sizer (MALVERN). The particle size analyses reported throughout this study are the average of three successive laser diffraction runs. Particle size analysis of aqueous solutions of PVP-SA and HPMC-SA show only the particle size distribution of SA in the mixtures. Particle size distribution in number is calculated using the particle size distribution in volume results, on the assumption that the particles are spherical.

4.1.1 HPMC-SA mixtures: effect of SA content

Particles size distribution in number and in volume of aqueous solution of pure SA (10% (w/w)), HPMC-SA under different amount of SA are shown in Fig. 3.6 and Fig. 3.7 respectively. Table 3.1 and Table 3.2 show the granular properties of each suspension in volume and in number respectively.

The SA (10% (w/w)) curve shows that the majority of SA agglomerates have a size above 5 μm with a mean diameter of d_{50} = 387.269 μm. SA is insoluble in water and its hydrophobic character favors the aggregation of SA molecules, thus, forming large cluster.

The curves in Fig. 3.6 show that the control of SA aggregation by HPMC is limited to SA percentages below 20%. At 2% (w/w) of SA, the curve is narrowand the agglomerates are monodisperse. HPMC fully stabilizes SA giving rise to the smallest particles. Regarding the HPMC-SA (10%-10%) mixture, the distribution is multimodal and wider (Cv = 3.99) with fine particles around 0.3 μm, and the mean diameter in volume is d_{50} = 1.369 μm. This means that the SA crystals are stabilized by the HPMC polymer with formation of some small agglomerate with a size between 1 and 20 μm. As the percentage of SA increases, the median particle size in volume increases significantly from 0.26 μm to 246.65 μm, and the size distribution curve shifts to higher distribution sizes (Fig. 3.6). This traduces

the formation of big SA agglomerates especially at 20% (w/w) of SA where the solution shows narrower distribution curve at higher particles sizes (Cv = 1.47). At this point, any other addition of SA particles will not have a noticeable effect on the particle size distribution.
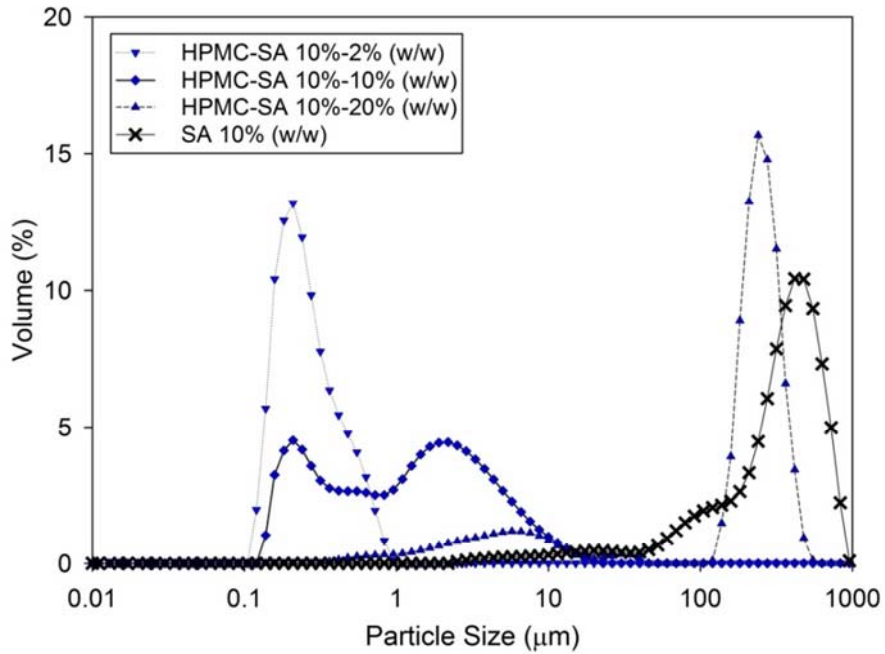
Fig. 3.6 – Particle size distribution in volume of HPMC-SA under different percentages of SA. HPMC: Hydroxypropyl-methylcellulose, SA: Stearic acid.
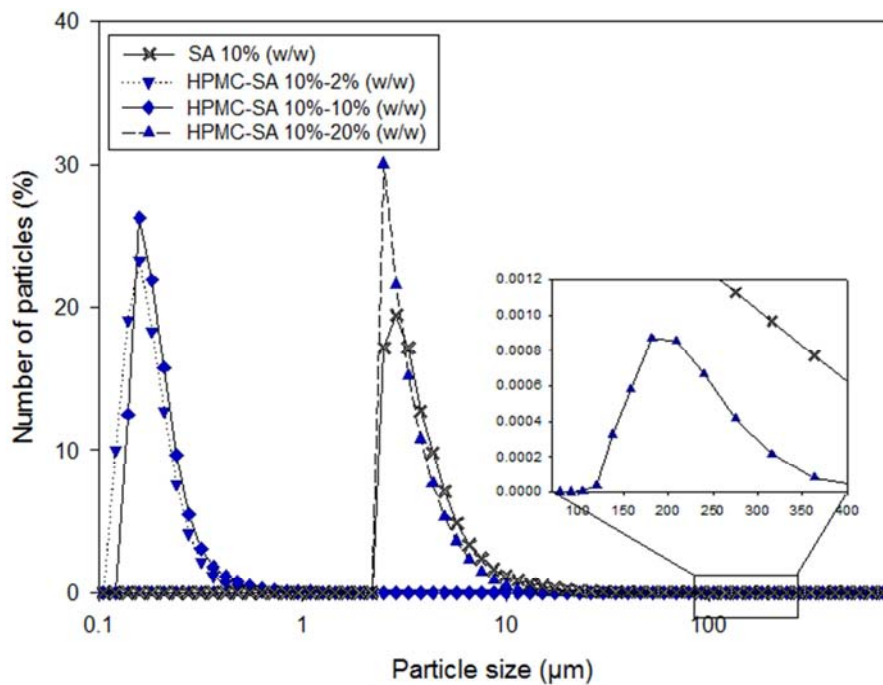
Fig. 3.7 – Particle size distribution in number of HPMC-SA under different percentages of SA. HPMC: Hydroxypropyl-methylcellulose, SA: Stearic acid.

Table 3.1 – Granular properties in volume of the dispersions.

Sample	d_{10} (µm)	d_{50} (µm)	d_{90} (µm)	d_{32} (µm)	Cv
SA 10% (w/w)	81.32	387.27	684.62	105.93	1.56
HPMC-SA 10%-2% (w/w)	0.16	0.26	0.55	0.25	1.50
HPMC-SA 10%-10% (w/w)	0.22	1.37	5.69	0.62	3.99
HPMC-SA 10%-20% (w/w)	5.14	246.65	369.45	13.70	1.47

Table 3.2 – Granular properties in number of the dispersions.

Sample	d_{10} (µm)	d_{50} (µm)	d_{90} (µm)	Cv
SA 10% (w/w)	2.33	3.19	4.9	0.81
HPMC-SA 10%-2% (w/w)	0.12	0.15	0.24	0.8
HPMC-SA 10%-10% (w/w)	0.13	0.16	0.27	0.87
HPMC-SA 10%-20% (w/w)	2.31	2.84	4.7	0.85

4.1.2   PVP-SA and MCC-SA mixtures

Particles size distribution in volume and in number of aqueous solution of pure SA (10% (w/w)), HPMC-SA 10%-20% (w/w), pure MCC 10% (w/w), MCC-SA (10%-10% (w/w)), PVP-SA (10%-10% (w/w)) and MCC-SA (10%-20% (w/w)) are shown in Fig. 3.8 and Fig. 3.9 respectively. Granular properties of the dispersions in number and in volume are also shown in Table 3.3 and Table 3.4 respectively.

Pure MCC has a wide particle size distribution (Fig. 3.8) and a median particle size d_{50} = 12.10 µm. This is because MCC has a very low solubility in water. After adding 10% (w/w) of SA to MCC, the curve shifts a little to higher values of particle sizes and the median particle size is equal to 18.73 µm, which is notably lower than that of pure SA 10% (w/w). This indicates that MCC may be able to stabilize SA, but it's not as good as HPMC. At 20% (w/w) of SA, we notice that MCC-SA particle distribution curve shifts slightly to higher values with a median size equal to 23.53 µm, but still, its particle size range is below that of HPMC-SA 10%-20% (w/w), indicating that, for high values of SA (above 10%), MCC interacts better than HPMC with SA particles and thus prevent the formation of big SA agglomerates. This also suggests that MCC is a better stabilizing agent for higher SA contents than HPMC.
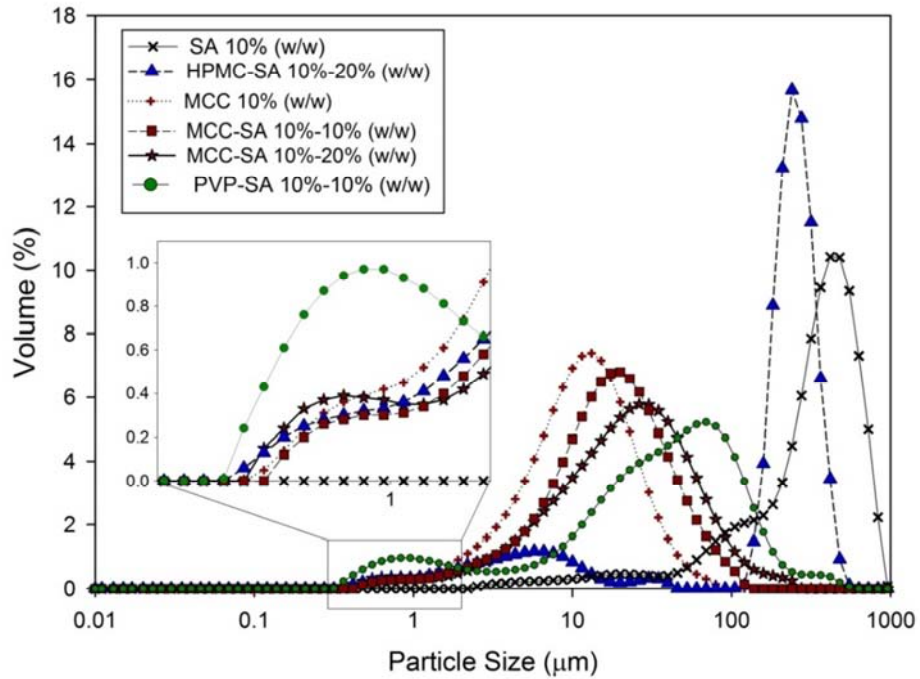
Fig. 3.8 – Particle size distribution in volume of pure SA, pure MCC, HPMC-SA, PVP-SA and MCC-SA in water. HPMC: Hydroxypropyl-methylcellulose, PVP: Polyvinylpyrrolidone, MCC: Microcrystalline cellulose, SA: Stearic acid.
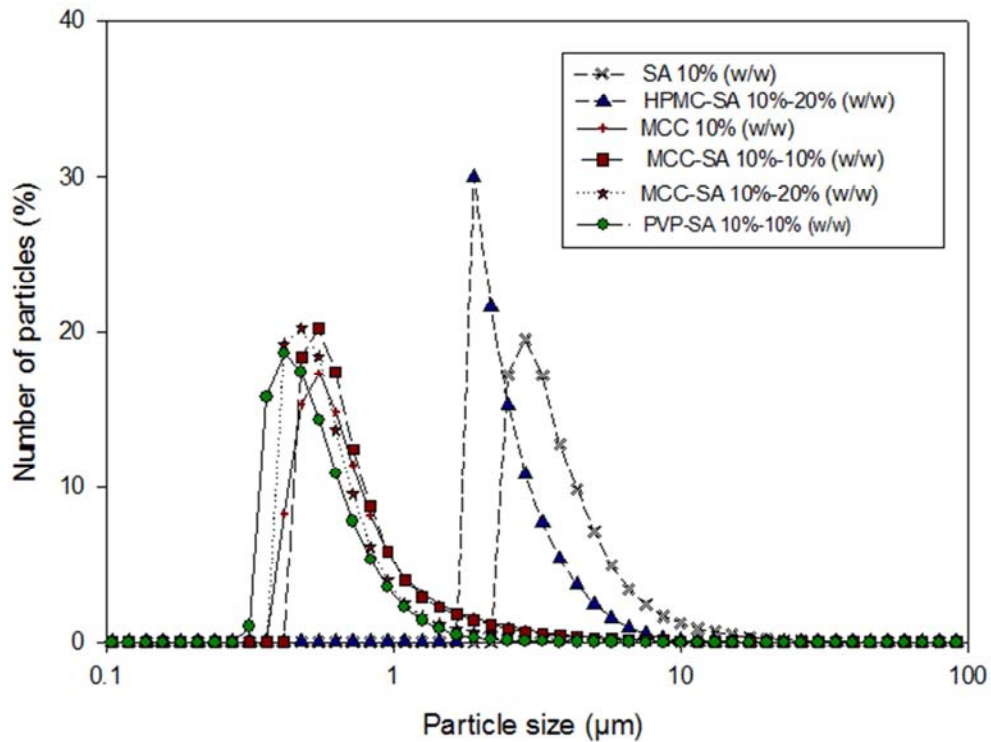
Fig. 3.9 – Particle size distribution in number of pure SA, pure MCC, HPMC-SA, PVP-SA and MCC-SA in water. HPMC: Hydroxypropyl-methylcellulose, PVP: Polyvinylpyrrolidone, MCC: Microcrystalline cellulose, SA: Stearic acid.

45

The previous findings are also confirmed by the particle size distribution in number shown in Fig. 3.9, where mixtures containing MCC have a lower distribution range than the pure SA and the HPMC-SA 10-20% (w/w) mixtures. Also, we notice that, at lower particles sizes range (below 1 μm), MCC-SA 10%-20% (w/w) has a higher percentage than MCC-SA 10%-10% (w/w) and MCC 10% (w/w) curves (Fig. 3.8 and Fig. 3.9), indicating an increase of the number of small particles at high SA contents. We infer that this is due to the small particles of SA; smaller than the MCC particles, which surround the big MCC particles.

In the case of the PVP-SA mixture, the mean diameter is higher (d_{50} = 41.78 μm) compared to the HPMC-SA 10%-10% (w/w) case and the curve is in a higher particle diameter range (between 0.5 μm and 900 μm). In comparison with MCC-SA, PVP-SA curve peak is at higher particle size, indicating the formation of bigger SA agglomerates. Also, in the particle size range below 1.5 μm, PVP-SA shows higher percentages of small particles than MCC.

According to Fig. 3.9 showing the particle size distribution in number, the majority of SA particles for PVP are below 1 μm. This means that PVP is able to partially stabilize SA, but, for lower SA percentage (below 10%), it is not as effective as HPMC.

Table 3.3 – Granular properties in volume of the dispersions.

Sample	d_{10} (μm)	d_{50} (μm)	d_{90} (μm)	d_{32} (μm)	Cv
SA 10% (w/w)	81.32	387.27	684.62	105.93	1.56
PVP-SA 10%-10% (w/w)	2.42	41.78	135.42	6.72	3.18
MCC 10% (w/w)	3.524	12.10	29.65	6.89	2.16
MCC-SA 10%-10% (w/w)	5.08	18.73	50.91	9.54	2.45
MCC-SA 10%-20% (w/w)	4.96	23.53	71.53	9.24	2.83

Table 3.4 – Granular properties in number of the dispersions.

Sample	d_{10} (μm)	d_{50} (μm)	d_{90} (μm)	Cv
SA 10% (w/w)	2.33	3.19	4.9	0.81
PVP-SA 10%-10% (w/w)	0.33	0.47	0.82	1.04
MCC 10% (w/w)	0.42	0.59	1.44	1.72
MCC-SA 10%-10% (w/w)	0.44	0.59	1.29	1.44
MCC-SA 10%-20% (w/w)	0.39	0.52	0.94	1.06

4.2 Cryogenic-SEM results

4.2.1 Pure HPMC and Pure SA dispersed in water.

In order to assess the structure of stearic acid (SA) particles dispersed in HPMC-water blend, HPMC-water, MCC-SA-water and HPMC-SA-water mixtures were subjected to cryo-fixation first using pasty nitrogen, then, liquid ethane, and finally using high pressure freezing (Leica HPM100). Samples were thereafter examined in a scanning electron microscope (SEM) (Hitachi MEB ESEM Quanta 250 FEG FEI).

To distinguish between HPMC and SA structure, two cryofixated samples were observed using transmission electron microscopy (SEM), the first sample contains 10% (w/w) of HPMC in water and the second one contains 10% (w/w) of SA in water.

From a glance at the SEM images presented in Fig. 3.10, we can distinguish between SA and HPMC. SA has the form of crystalline needles that form large agglomerate in water and their size is around 50 μm (Fig. 3.10 (c)), while HPMC becomes amorphous and forms transparent solution (Fig. 3.10 (a)) which makes it difficult to distinguish between HPMC and water.
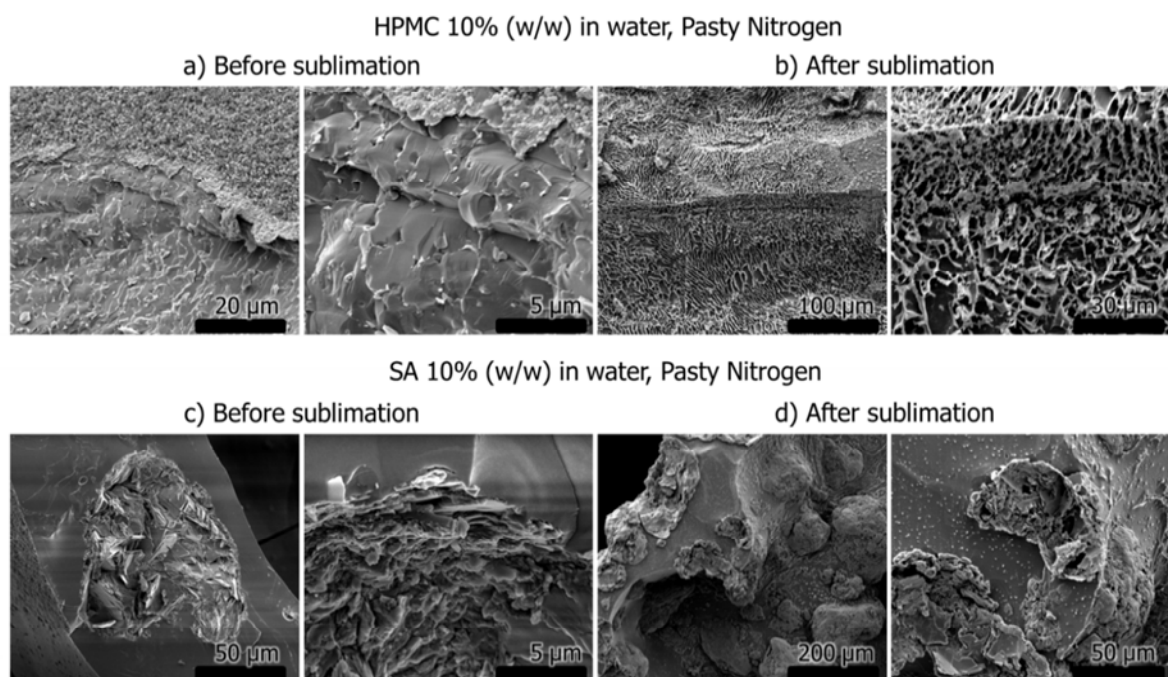
Fig. 3.10 – SEM micrographs of HPMC (top) and SA (bottom) in water before and after sublimation, cryofixated using pasty nitrogen. HPMC: Hydroxypropyl-methylcellulose, SA: Stearic acid.

When the samples are sublimated (Fig. 3.10 (b) and (d)), we notice that HPMC-water architecture shows a perforated structure designed by the sublimated ice crystals templates. Cryofixation using pasty nitrogen is a relatively slow freezing process that generates ice crystals inside the samples, consequently, inner parts of HPMC-water mixture freeze slower than the outer parts, and therefore, exhibit larger pores after sublimation.

To avoid the formation of crystals, we also used cryo-fixation using high pressure freezing. From Fig. 3.11 (a) and (b), taken after sublimation, we notice the absence of perforations. We can see that pure HPMC becomes amorphous and forms transparent solution. After dispersing SA particles in the HPMC-water mixture, SA white crystals and their distribution in the HPMC-water blend can be visually assessed (Fig. 3.11 (c) and (d)), hence, the stabilization effect of SA crystals by HPMC can be characterized using the Cryo-SEM with high pressure freezing (HPM100).
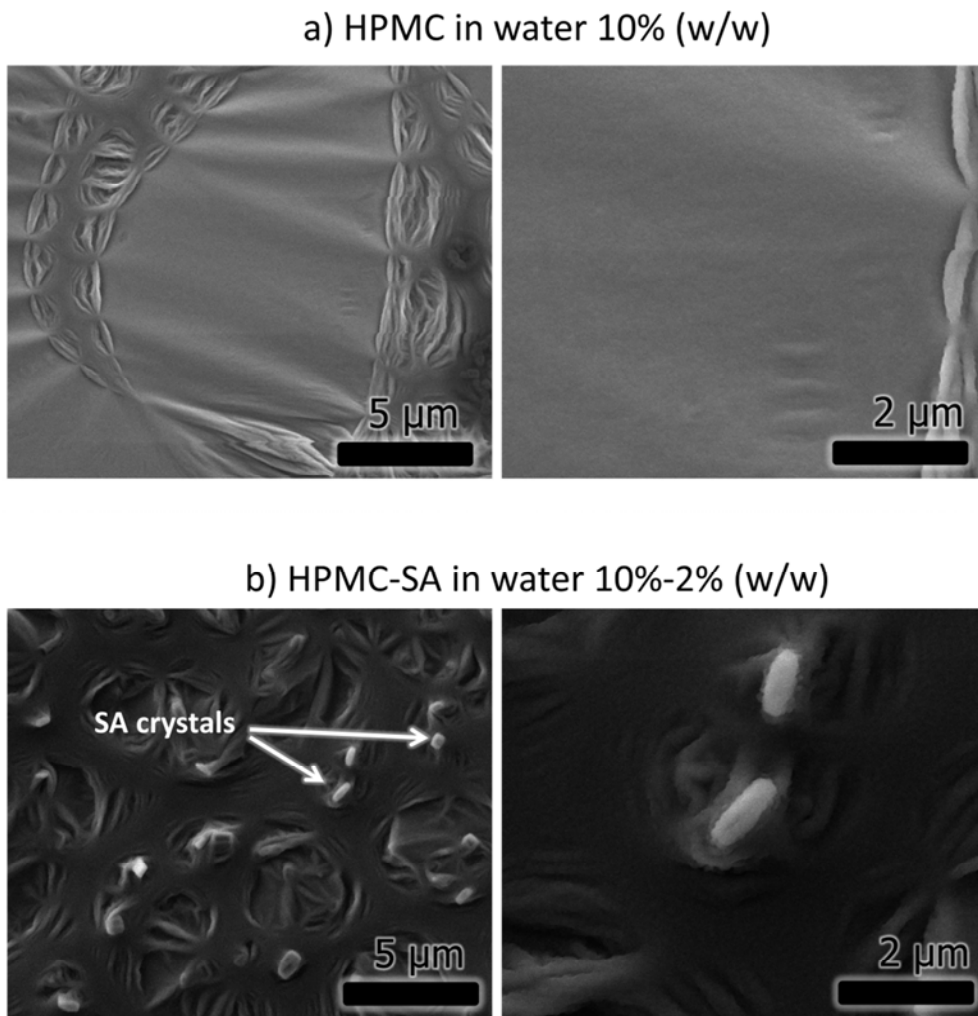
Fig. 3.11 – SEM micrographs of HPMC-SA in water (10%-10% (w/w)). HPMC: Hydroxypropyl-methylcellulose, SA: Stearic acid.

4.2.2 HPMC-SA mixtures: effect of SA content

HPMC-SA mixed in aqueous system under different amounts of SA was subjected to cryo-fixation first using pasty (Fig. 3.12) then using liquid ethane (Fig. 3.13) and finally using high pressure freezing (Fig. 3.14).

When HPMC-SA sample is frozen using pasty nitrogen (Fig. 3.12), HPMC shows pores in the micrometer scale, patterned by the ice crystals. The ice crystals are formed due to the slow freezing process. We notice that the pores size also depends on the SA contents. An increase in the SA content in the mixture increases the pore size. In addition, SA crystals can be seen inside the HPMC pores and they are covered by the HPMC.

Alternatively, when using liquid ethane as a freezing medium (Fig. 3.13), the pore size becomes significantly small. SA white crystals are more distinguishable than in the previous case, and their distribution in the HPMC-water blend is more noticeable. The best observation of SA crystals is obtained in Fig. 3.14 when using high pressure freezing where no perforations were observed to the high freezing speed.

As shown in Fig. 3.14, the size and distribution of SA particles within the suspension varies under different amounts of SA. When the SA weight percentage is 2%, SA crystals are evenly dispersed in the HPMC suspension and their size is below 1 µm in diameter (Fig. 3.14 (a) and (b)). HPMC is very well anchored on the surface of the SA agglomerate and covers it with a hatching textured film that resembles dried soil (Fig. 3.14 (a) and (b)). SA crystals are therefore trapped in the HPMC network. This allows the stabilization of SA agglomerates whose size is near 1 µm in diameter. At 10% (w/w) of stearic acid (Fig. 3.14 (c) and (d)), we can see that white SA crystals are distributed in the HPMC-water amorphous phase and have a size below 1 µm. Some of them are outside (or partially outside) the amorphous phase, other are covered with the HPMC-water phase, but they are still distinguishable from the bulginess of the HPMC-water surface. There are no big agglomerates and the only difference compared to the case of 2% (w/w) SA (Fig. 3.14 (a) and (b)) is that the number of stearic acid crystals increases significantly. On the other hand, when the SA weight percentage is up to 20%, SA agglomerates become notably large and seems more polydisperse; which destabilizes the dispersion (Fig. 3.14 (e) and (f)). The likely reason for the re-arrangement of the structure of SA agglomerate is that the amount of HPMC is insufficient to reduce the free energy associated with the SA crystallites. Therefore HPMC becomes unable to prevent SA aggregation, causing the small SA aggregates to adhere on the surface of large SA agglomerate and thus, their growth. This also corresponds to the Malvern particle distribution analysis shown in Fig. 3.6 where samples with lower SA contents have the lowest mean particle diameter.

HPMC-SA in Water 10%-2% (w/w)

a) 5 µm   b) 2 µm

HPMC-SA in Water 10%-10% (w/w)

c) 5 µm   d) 2 µm

HPMC-SA in Water 10%-20% (w/w)

e) 5 µm   f) 2 µm
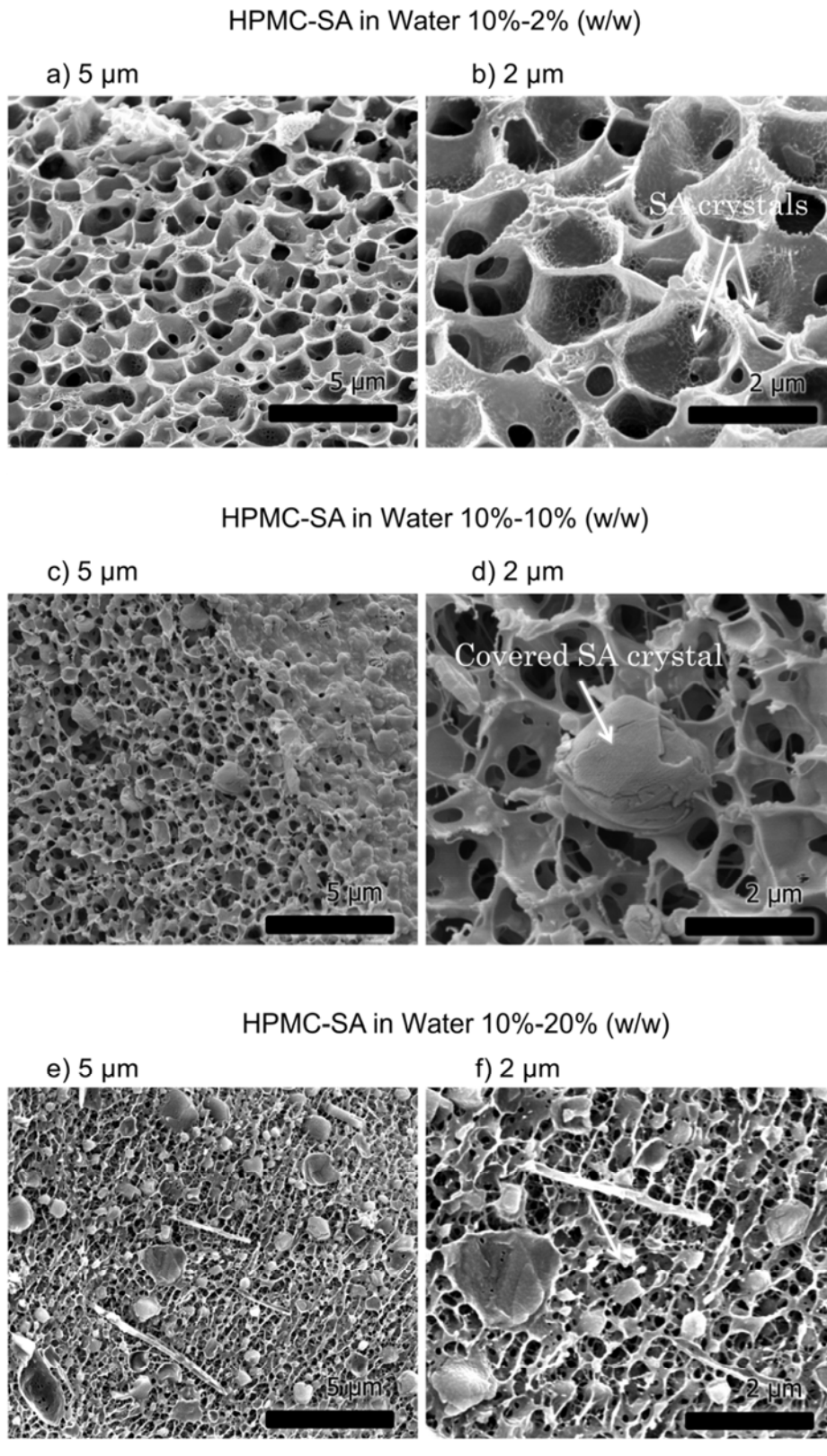
Fig. 3.12 – Observations using pasty nitrogen freezing, SEM micrographs of HPMC-SA in water under different percentages of SA and taken after sublimation. HPMC: Hydroxypropyl-methylcellulose, SA: Stearic acid.
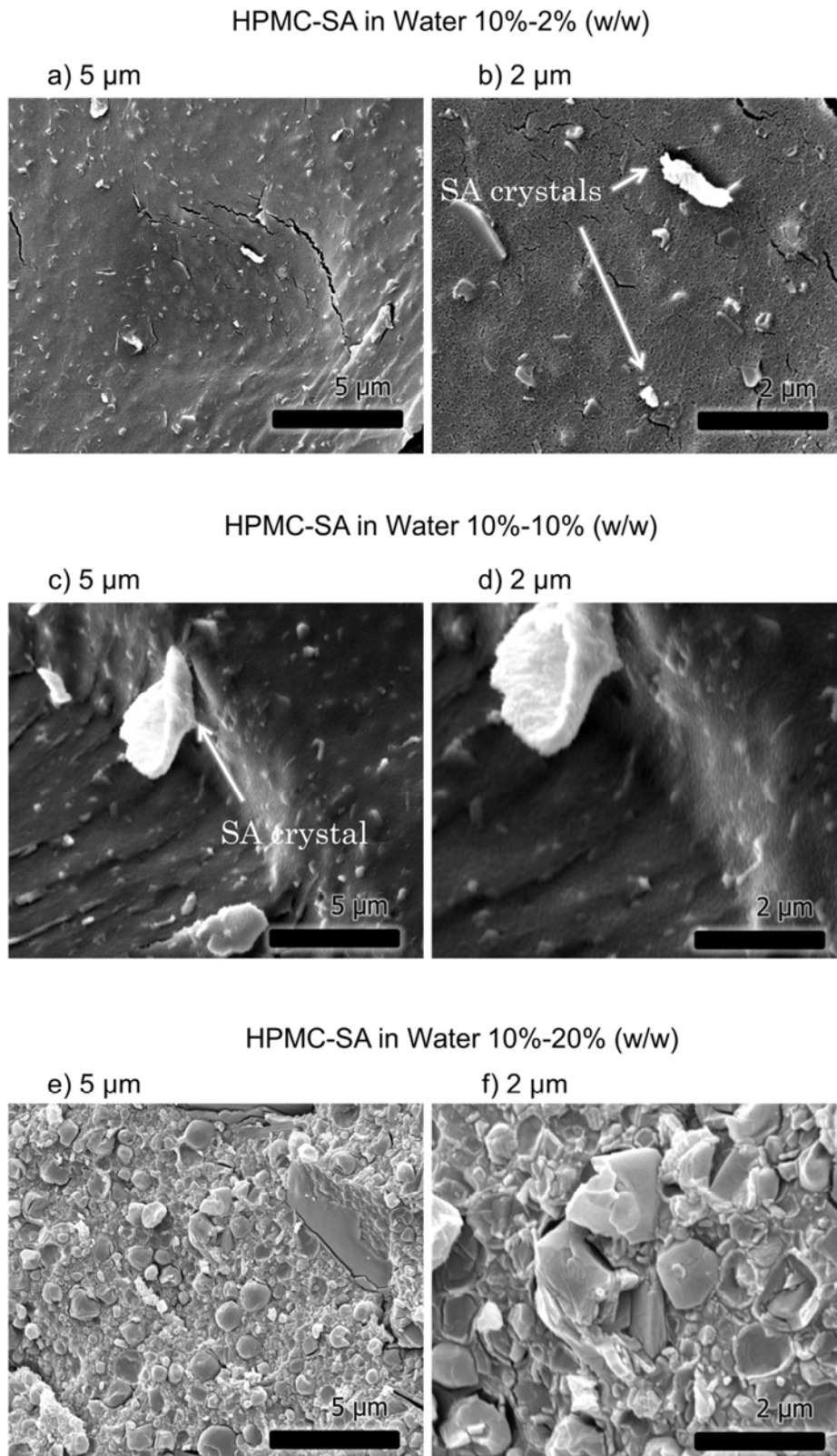
Fig. 3.13 – Observations using liquid ethane as a freezing medium, SEM micrographs of HPMC-SA in water under different percentages of SA and taken after sublimation. HPMC: Hydroxypropyl-methylcellulose, SA: Stearic acid.
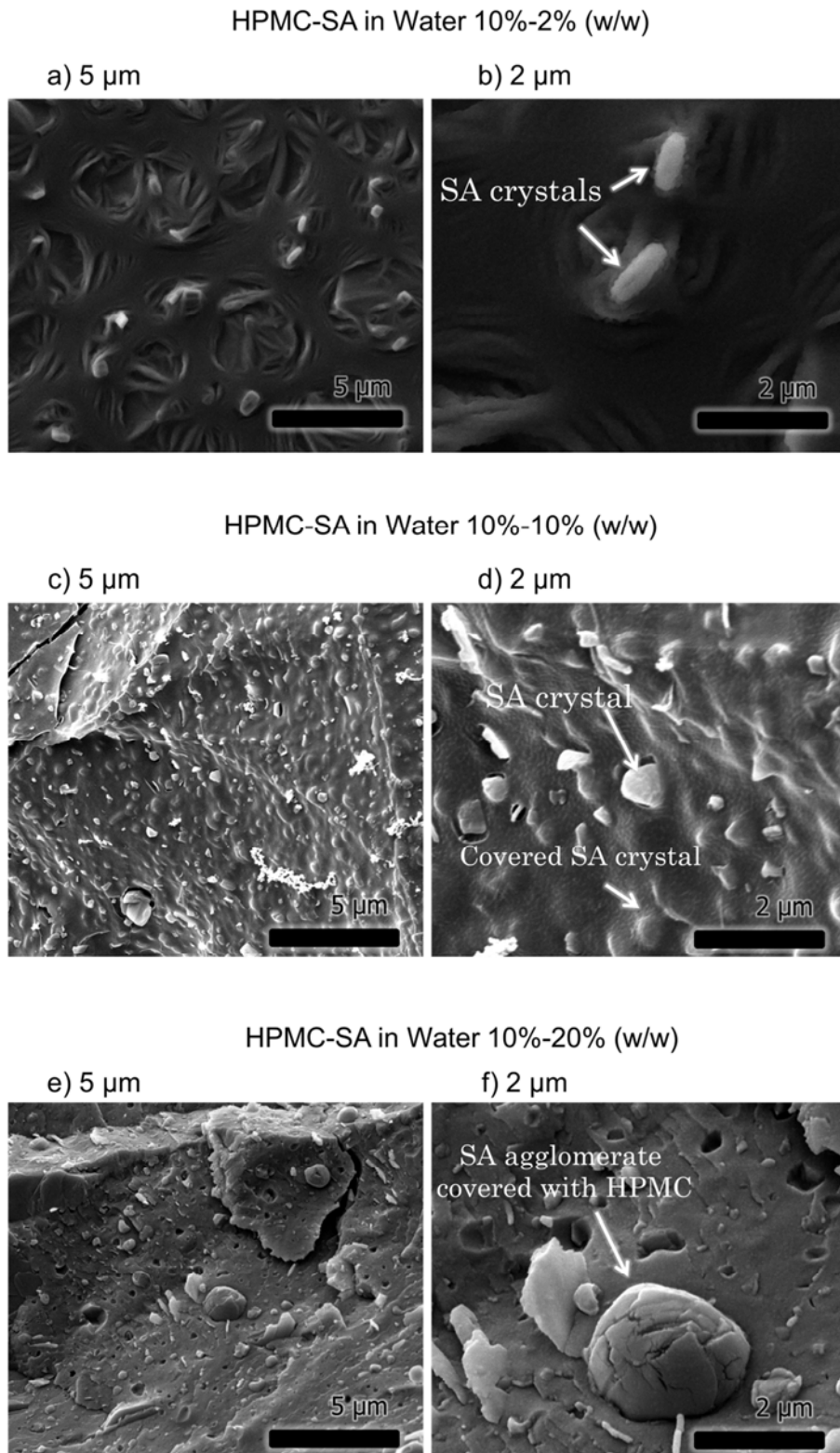
Fig. 3.14 – Observations using high pressure freezing, SEM micrographs of HPMC-SA in water under different percentages of SA and taken after sublimation. HPMC: Hydroxypropyl-methylcellulose, SA: Stearic acid.

Fig. 3.15 presents the counting of SA crystals obtained using scientific image analysis program ImageJ (Rasband, 1997) software. We used only the images obtained using high pressure freezing. For each SA percentages (2%, 10% and 20% (w/w)) several images were analyzed and the results were averaged. The counting is based on the percentage of white intense SA surface present in the images. At 2% (w/w) of SA in HPMC, we have 2.43% of white SA that covers the image. At 10% (w/w) of SA, we found 9.91% of SA in the analyzed images. These results indicate that SA crystals are well dispersed in HPMC-water mixture. They also show that high pressure freezing technique is able to preserves the structure of dispersed particles.

At 20% (w/w) of SA, we obtain 15.65%. This low value, lower than the actual percentage of SA in HPMC-SA (i.e. 20% (w/w)), can be explained by a polydispersity in the mixture, because at high polydispersity, the chosen images to be treated by ImageJ become less representative of the distribution of the particles and high calculated error may be obtained.
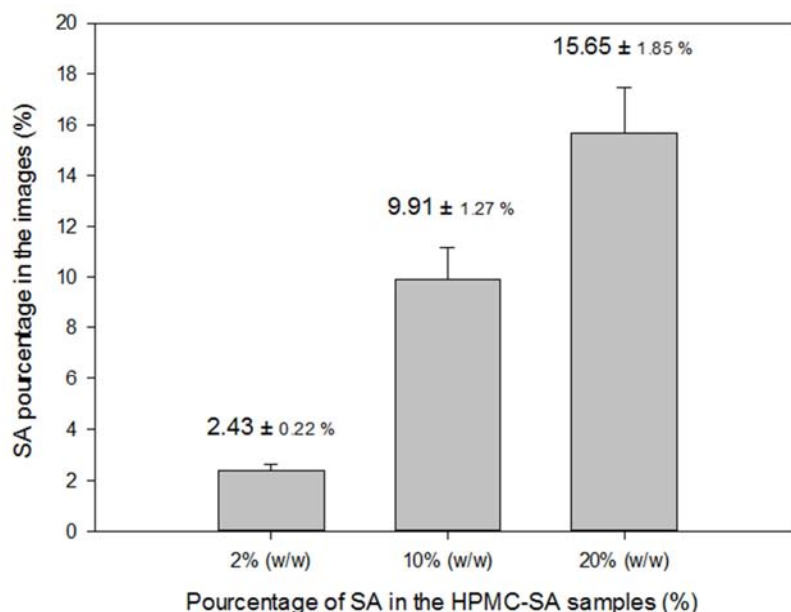
Fig. 3.15 – Counting of stearic acid in HPMC by image analysis.

4.2.3   PVP-SA and MCC-SA mixtures

Fig. 3.16 presents the SEM images of PVP-SA (10%-10%) sample.

In the inner part of the sample (Fig. 3.16 (a)), large SA agglomerates as well as some small SA crystals (in white) can be seen. This means that some of the small primary SA particles are stabilized by PVP. This is confirmed by the particle size distribution shown in Fig. 3.8 and Fig. 3.9 where there are SA particles below 1 μm in size. We also noticed that in the surface of the PVP-SA sample, SA crystals form bigger agglomerates with irregular shape (Fig. 3.16 (b)). Non-stabilized SA agglomerates migrate

to the surface of the sample and form larger agglomerates. We may deduce that PVP is not as effective stabilizer as HPMC but it is able to partially stabilize SA.
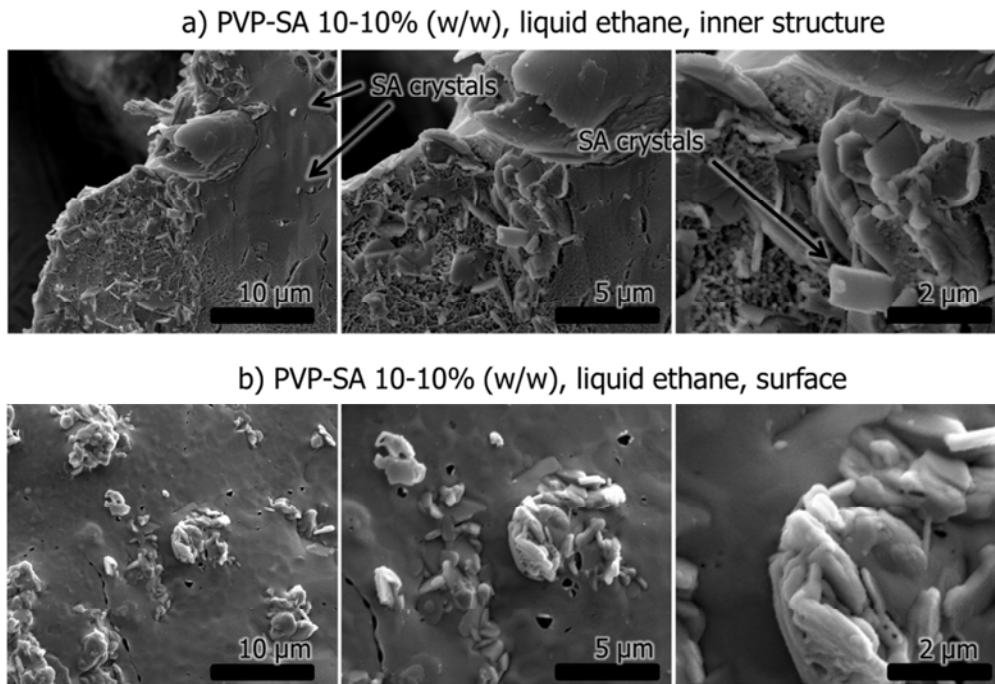
Fig. 3.16 – SEM micrographs of PVP-SA in water taken after sublimation. PVP: Polyvinylpyrrolidone, SA: Stearic acid.

Fig. 3.17 shows the SEM images of MCC-SA (10%-10%) mixture. When using pasty nitrogen (Fig. 3.17 (a)), we can see SA crystals with different sizes trapped in a network of MCC. This latter has a different structure than the matrix formed in the HPMC-SA mixture (Fig. 3.12 (c) and (d)); it has different shapes; there is no perforations, and the MCC network is like a crossing net. It seems also that MCC surrounds SA crystals without adsorbing on their surface since we can see some small SA white crystal needles in the SA agglomerate surface.
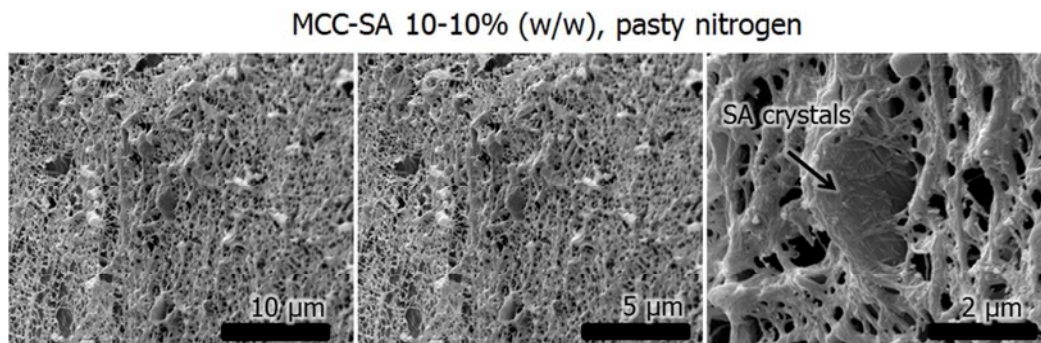
Fig. 3.17 – SEM micrographs of MCC-SA in water taken after sublimation. MCC: Microcrystalline cellulose, SA: Stearic acid.

54

4.3 DSC results

DSC thermograms of the dried polymers (HPMC, PVP, MCC and PEG400) and the dry films (HPMC-PEG, MCC-PEG and PVP-PEG) were recorded using Differential Scanning Calorimeter.

To estimate the interaction between the materials in the blend, we used the Flory-huggins theory (Flory, 1949). The Flory-Huggins theory has provided a good empirical description of the mixing behavior of polymer-diluent systems and polymer-polymer systems (Martinez-Salazar, 1996; Scott et al., 1949, Lyngaae-Jorgensen 1976). Cao et al. (2005) and Marsac et al. (2006, 2009) used the Flory-Huggins theory for the estimation of polymer-solvent interaction using the melting point depression data obtained from DSC thermograms. Melting point depression is the reduction of the melting point of a polymer when mixed with another material and occurs when the two components are miscible or partially miscible (Marsac, 2009). Also, Nishi and Wang (1975) used the Flory-Huggins theory for drug–polymer interaction. For the estimation of the Flory-Huggins interaction parameter χ between the plasticizer and a polymer, we have decided to use the same concept and we calculated χ using the following equation:

$$\frac{1}{T_m} - \frac{1}{T_m^0} = -\frac{R}{\Delta Hm}(\ln x_{plast} + (1 - \frac{1}{m_r})(1 - x_{plast}) + \chi(1 - x_{plast})^2) \tag{3.1}$$

where ΔHm is the melting heat of the pure plasticizer, T_m and T_m^0 are the melting temperatures of the plasticizer in the plasticizer-polymer mixtures and in the pure plasticizer respectively, R is the gas constant, x_{plast} is the volume fraction of the plasticizer and m_r is the ratio of the volume of the polymer repeating unit to that of the pure plasticizer.

A negative χ means that the attraction between a polymer–plasticizer pair is stronger than the average attraction between a polymer–polymer pair and a plasticizer–plasticizer pair (i.e., plasticizer–polymer > 1/2(plasticizer–plasticizer + polymer–polymer)). In this case, plasticizer molecules prefer to be in contact with polymer segments than with the plasticizer molecules. The more negative the value of χ, the stronger the attraction between the plasticizer and the polymer, and vice versa; a positive value of χ indicates that the polymer and plasticizer molecules tend to be in contact with their own kind, leading to repulsion between the plasticizer and the polymer.

The DSC curves presented in Fig. 3.18, Fig. 3.19 and Fig. 3.20 show the effects of the addition of PEG on thermal properties of HPMC, MCC and PVP films respectively. HPMC and MCC exhibits melting peaks at 129°C and 130°C respectively. However, the lowest melting point is observed for PVP at $Tm = 102$°C. The melting peak of MCC is wider than that of HPMC. A wide melting peak is attributed to crystallite size or imperfections through the polymer because small crystal tends to melt

at lower temperature, whereas, a sharp symmetric melting endotherm can indicate relative purity (Cheremisinoff, 1989). This implies that HPMC form more ordered crystal structure with fewer impurities than MCC. The wideness of the DSC curve also depends on the heating rate.
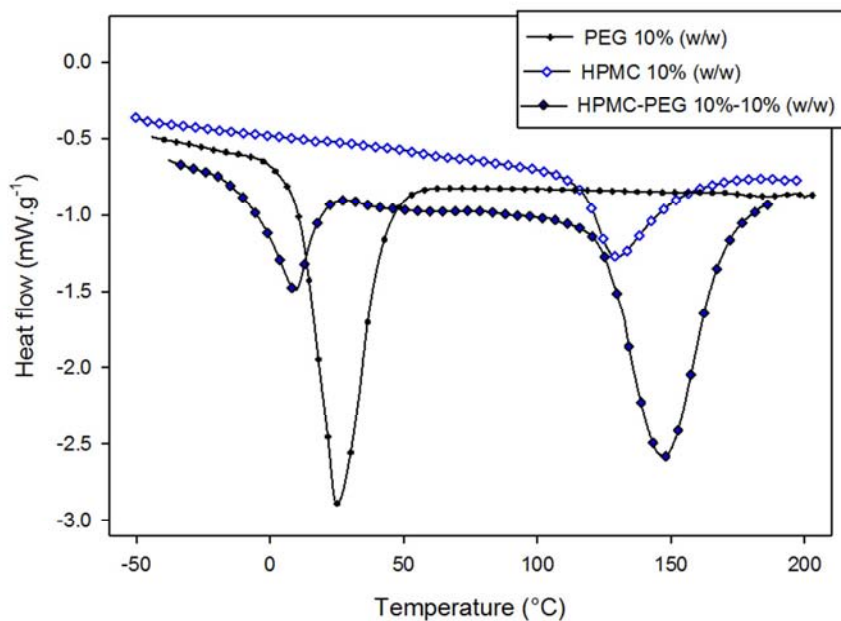
Fig. 3.18 – DSC curves of PEG 10% (w/w), HPMC 10% (w/w) and HPMC-PEG 10%-10% (w/w).

Multiple melting peaks can be observed in blends where the mixed polymers retain their individual thermal characteristics (Cheremisinoff, 1989). Both HPMC-PEG and MCC-PEG present a double-melting behavior confirmed by the double endothermic peaks in the DSC curves. The first melting peak indicates partial melting of the blend until complete melting which occurs at the end of the second peak; around 147°C for HPMC-PEG and 132°C for MCC-PEG. Parcella and coworkers (1986) studied the blends of a liquid crystalline polyester (HTH10) with poly (buty1eneterephthalate (PBT) and encountered the same behaviour of a distinct double melting curve, they inferred that this is reminiscent of an absence of interactions between the polymers. Duris et al. (2012) attributed the absence of a second melting peak in a blend to a good miscibility between the materials. Patel et al. (2012) explained the presence of two distinct melting peaks by saying that one of the materials lacks sufficient time to incorporate into the growing lattice accurately to form perfect crystal.

The thermal behavior of HPMC-PEG blend presents a high-temperature peak at 147°C and a low-temperature peak at 6.36°C (Fig. 3.18). HPMC and PEG within HPMC-PEG blend exhibit their own melting behavior at the range of temperatures when they are alone (i.e. note mixed with PEG), indicating that the two crystalline phases are not cocrystallizable; and both types of crystallites remained in the blends. Nevertheless, from Fig. 3.18, there is melting point depression between PEG and HPMC-PEG, suggesting a substantial degree of mixing and miscibility. Mixing HPMC with PEG

56

reduced the melting temperature of PEG from 24.7 to 6.3. Adding PEG to HPMC enhances the chain mobility in the amorphous phase of HPMC, and HPMC-PEG blend crystallizes with more ease at lower temperatures.
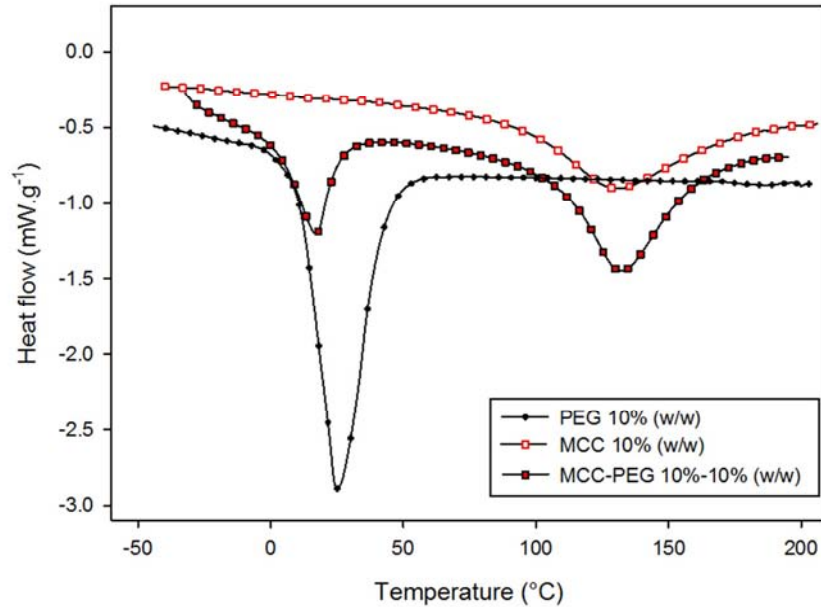
Fig. 3.19 – DSC curves of PEG 10% (w/w), HPMC 10% (w/w) and HPMC-PEG 10%-10% (w/w).
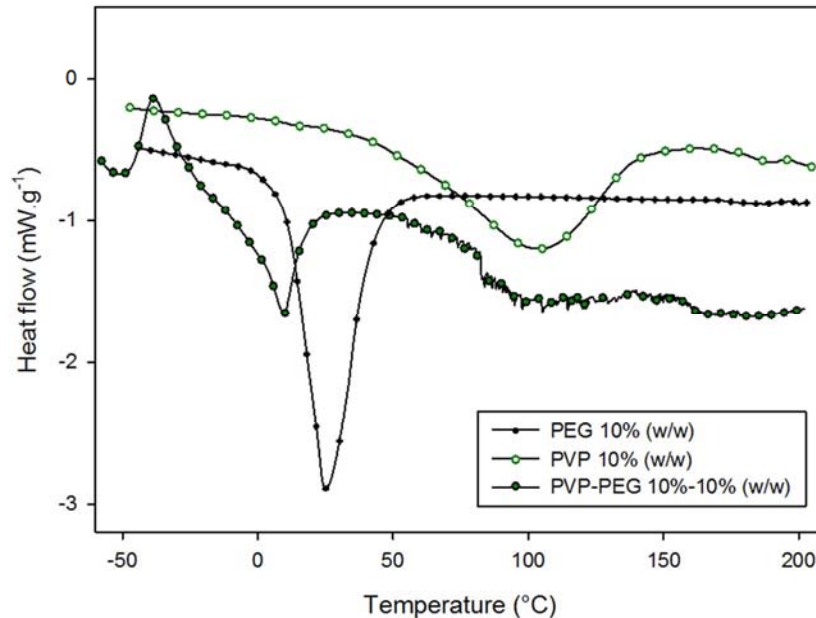
Fig. 3.20 – DSC curves of PEG 10% (w/w), PVP 10% (w/w) and PVP-PEG 10%-10% (w/w).

Similarly to the HPMC-PEG case, MCC-PEG presented two enthalpy events, one at 16.8 °C associated to the melting of PEG in the blends, and the second at 132.1 °C attributed to the melting

of MCC. The melting peak temperature of PEG generated in the MCC-PEG blend is higher than the one generated in the HPMC-PEG blend, indicating better interactions between HPMC and PEG than between MCC and PEG.

We also note that HPMC-PEG and MCC-PEG does not show a glass transition shape in the curve. Borsacchi et al. (2011) encountered the same problem in their analysis of blends composed of PEG and polymers. They inferred that the lack of observable glass transition is either due to the formation of an amorphous blend with a high PEG content, or possibly masked by the Polymer and PEG melting. Halász and Csóka (2013) associated the absence of Tg in PEG composites to the presence of the plasticizer which provided more flexibility to the polymer chains.

Table 3.5 – Melting temperature (Tm) and melting enthalpy (ΔHm)

	Tm (°C)	ΔHm J.g^{-1}
HPMC	129.25	48.83
MCC	130.1	106.5
PVP	102.5	133.5
PEG	24.7	140.6
HPMC in HPMC-PEG	147.4	133.0
MCC in MCC-PEG	132.1	98.2
PVP in PVP-PEG	-	-
PEG in HPMC-PEG	6.3	32.5
PEG in MCC-PEG	16.8	38.1
PEG in PVP-PEG	9.61	37.2

PVP-PEG sample DSC curve (Fig. 3.20) shows an exothermic peak at -46 °C which is attributed to the cold crystallization, followed by an endothermic peak at 9.61 °C. Above 90°C, the curve of PVP-PEG becomes very noisy. This may be explained by foaming or condensation of the sample due to high temperature. The presence of an exothermic peak indicates crystallization and show that PEG and PVP are able to form an ordered structure when mixed together. In addition, the melting temperature of PEG is reduced from 24.7 to 9.61 °C. This indicates that there is miscibility between the components. This was confirmed by calculating the interactions parameter between the materials using Flory-huggins theory based on equation (3.1).

In the case of MCC-PEG, the positive value of $\chi = 1.07$ indicates repulsion between the PEG and MCC molecules. The negative value of $\chi = -1.79$ in the HPMC-PEG blend indicates attraction between HPMC and PEG molecules. Regarding PVP-PEG blend, large negative value of $\chi = -3$ is obtained suggesting high attraction between PEG and PVP molecules, and consequently high miscibility.

5. Conclusion

In this chapter, we have examined the structure of blends composed of hydroxypropyl-methylcellulose (HPMC), polyvinylpyrrolidone (PVP), microcrystalline cellulose (MCC), polyethylene glycol (PEG) and stearic acid (SA).

At low SA percentages, HPMC fully stabilize SA which gave rise to the smallest SA particles. Increasing SA percentage led to bigger SA agglomerates and instable polymeric suspension. When using PVP as a stabilizing agent, the median size increases but some of the SA particles are below 1 μm in diameter, meaning that PVP is able to partially stabilize SA. Particle size distribution curves also showed that the small particles of SA surround the big particles of MCC. Also, MCC is able to prevent the formation of big SA agglomeration.

Cryogenic-SEM images revealed that HPMC surrounds SA agglomerates with a hatching textured film and anchors on their surface, thus preventing their agglomeration. Upon increasing the SA percentage, larger SA agglomerates were seen in the SEM images. In addition, High pressure freezing with HPM100 provided better observation of the mixtures and SA white crystals and their distribution in the water-HPMC blend were more distinguishable. In the inner part of PVP-SA mixture, big SA agglomerates as well as some small SA crystals were observed. This confirmed the particle size distribution results concerning the partial stability of SA crystal in the presence of PVP. Regarding MCC-SA mixture, SEM images showed that MCC network is like a crossing net around the SA crystals.

DSC analysis showed that there is a better interaction between HPMC and PEG than between MCC and PEG, and that HPMC shows higher degree of miscibility and more attraction to PEG molecules than MCC. In addition, PEG is a good plasticizer for PVP.

Chapter 4

Solubility Parameter (δ) and COSMO's σ-profiles

"[Quantum mechanics] describes nature as absurd from the point of view of common sense. And yet it fully agrees with experiment. So I hope you can accept nature as She is - absurd."

— Richard P. Feynman

1. Introduction

In the previous chapter, the binder materials and the interactions between them were analyzed experimentally. In this chapter, we will study the properties of these materials at the molecular level using different computational methods. Our work will be based on the solubility parameter δ and the sigma profile. This will allow establishing predictive models for solid-binder interactions later on.

The solubility parameter, δ (i.e. the square root of the cohesive energy density), describes the intramolecular and intermolecular forces of a substance. It is a measure of the tendency of a molecule to interact with the surrounding molecules. Solubility parameter has been proved useful for several pharmaceutical applications and has been correlated to a variety of properties (Barton, 1991) such as the surface tension, refractive index, work of adhesion and tensile strength. Solubility parameter was also used in the coating industry for selecting compatible solvents for coatings solvents

for coatings materials, and in surface characterization of fillers (Hansen, 2007).

For the prediction of the solubility parameter, predictive group contribution models have been proposed including Van krevelen (1965), Hansen (1967) and Hoy (1970). These models use the concept of addition of the contributions of chemical groups that composes the molecule to predict its properties. Then, molecular simulation techniques have emerged as a complementary tool able to predict the solubility parameter.

In another register, σ-profiles present a map of the charge density over the surface of the molecule and provide information about the molecule and an understanding of the mutual solubilities of solvents Klamt (2005). COSMO computations are performed to obtain the charge density distribution and to construct the sigma profile.

In this chapter, we give a description of the COSMO model that allows the construction of the σ-profiles. Also, methods for the calculation of the solubility parameter are presented including molecular simulation and group contribution methods. In the result section, σ-profiles curves are presented and discussed. Then, solubility parameters of the different materials used in this thesis are calculated and the results are compared to experimental values obtained from the literature. Also, we discuss polymer-plasticizer compatibility prediction based on solubility parameter values.

2. COSMO, DFT and σ-profiles

COSMO (Conductor-like Screening Model) (Klamt and Schüürmann, 1993) is a predictive model for the thermodynamic properties of fluids and solutions that combines quantum chemistry and statistical thermodynamics. In this model, the solvent is regarded as a homogeneous conducting medium, but affected by a finite dielectric constant arising from a large number of electrostatic charges enveloping the surface of the solute molecule. The surface of this molecule bears a polarization charge density. To determine this density, quantum mechanics calculation based on the density functional theory (DFT) are launched in order to optimize the geometry of the molecule and to establish its electronic structure. Then, calculations based on the COSMO model are used to construct the charge density curve called sigma-profile.

DFT is a method for solving the nonrelativistic, time-independent Schrodinger equation:

$$H\Psi = E\Psi \tag{4.1}$$

Where, H is the Hamiltonian which includes all the energy terms, both those provided by the atom nucleus (kinetic and potential energy) and by electrons. $\Psi = \Psi(r_1,...,r_N)$, with r the position of the

particles and N the total number of particles, is a wave function describing the state of a system of energy E.

The DFT method formalism was established from the work of Hohenberg and Kohn (1964) and Kohn and Sham (1965). This method proposes to bring the intractable problem of interaction with the electrons in the presence of atomic nuclei to a problem based on a single variable: the electron density. The structure and charge distribution of a molecule are optimized in order to find the minimum energy of the system by DFT quantum chemistry calculations. DFT uses numerical orbitals for the basis functions. Basis sets are a set of functions used to build molecular orbitals. Greater accuracy of the electronic surface potential and charge density is obtained by using larger basis sets because this will consider the electrons at large distance from the nucleus (some basis sets are provided in Appendix A). Hence, if the basis set is small then, the results may be off-target. Then, using COSMO calculations, a list of charges on surface segments are generated and we obtain a histogram (or curve) of the distribution of charges on the molecules surface called profile sigma (σ). This profile is the probability $p(\sigma)$ of finding surface segment with the charge density σ (Klamt, 2005):

$$p(\sigma) = A_i(\sigma) / A_i \tag{4.2}$$

with $A_i(\sigma)$ the surface area with a charge density of value σ and Ai the total surface of the material i

For the generation of the σ-profile, methods known as GGA (generalized gradient approximation), also called non-local methods have been developed. COSMO employs molecular shaped cavities that represent the electrostatic potential by partial atomic charges. The results depend mainly on the van der Waals radii used to evaluate the cavity surface. The cavity surface is obtained as a superimposition of spheres centered at the atoms, discarding all parts lying on the interior part of the surface (Klamt and Schüürmann, 1993). The points of the grid of the cavity surface are then collected into segments and the screening charges are located at the segment points.

Fig. 4.1 shows the sigma profile of water as well as its COSMO surface. Water can act either as H-bond donor or H-bond acceptor. The σ-profile of water spans in the range of ± 0.02 e.Å⁻². It is dominated by two major peaks arising from the strongly polar regions; the positive region (H-bond acceptor region) is due to the polar oxygen and the negative one (H-bond donor region) is due to the polar hydrogen atoms. The negatively charged surfaces of the water molecules appear blue and the positively charged ones appear red. Non-polar part of surface of the molecule is green. The peak arising from the positively polar hydrogens is located on the left side, at about -0.015 e.Å⁻². Most parts of the surface of water molecules are able to form more or less strong hydrogen bond. Hydrogen bonding is considered as weak up to ± 0.01 e.Å⁻². Outside this limit, molecules can be regarded as strongly polar (Klamt, 2005).
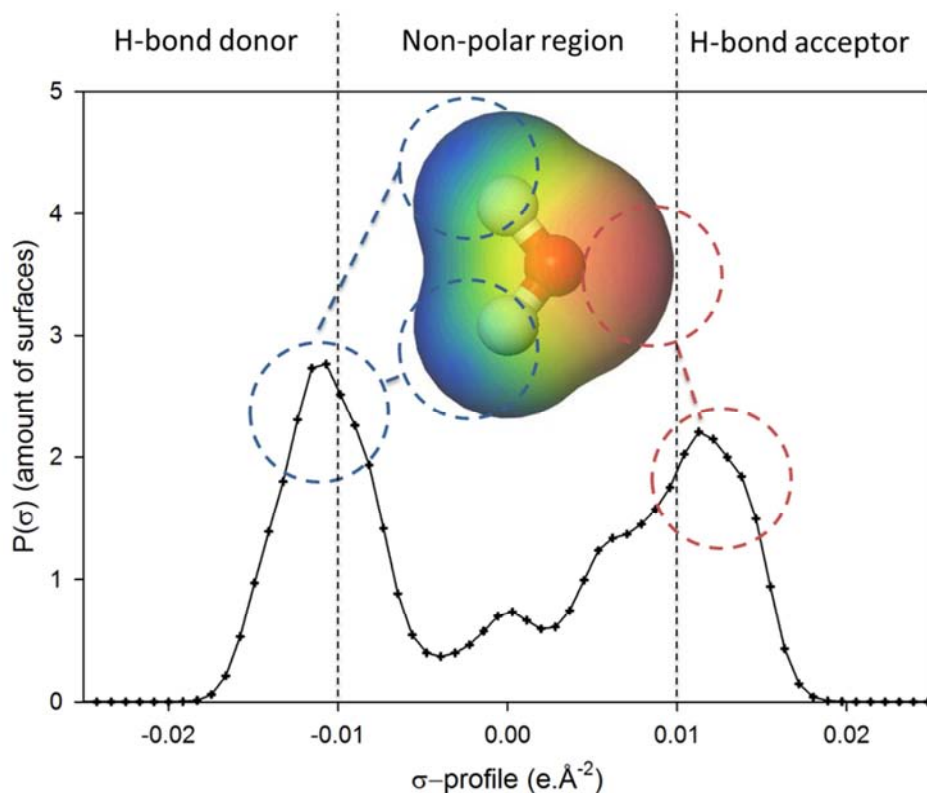
Fig. 4.1 – σ-profile of water

3. The Solubility parameter δ

The solubility parameter δ is based on thermodynamic considerations, and can be defined using the molar energy of vaporization (Hildebrand, 1950):

$$\delta = \sqrt{\frac{\Delta H_{vap} - RT}{V}} \qquad (4.3)$$

where ΔH_{vap} is the molar enthalpy of vaporization, R is the gas constant, V the molar volume and T the temperature.

To overcome deficiencies of the Hildebrand's approach that was built for hydrocarbon solvent and did not include hydrogen bonding and polar solvent, Hansen proposed in 1967 to split this parameter δ into three components (equation (4.4)): the first component δ_d is relative to the forces called "dispersion" of London (nonpolar interactions), the second component, δ_p, is related to the polarity between permanent dipoles, and the last one, δ_h, represents hydrogen bonding forces and more generally interactions involving electronic exchanges.

$$\delta = \sqrt{\delta_d^2 + \delta_p^2 + \delta_h^2} \qquad\qquad (4.4)$$

Following this scheme, Hansen (1967) obtained a three-dimensional space (Fig. 4.2) wherein all the solid or liquid substances may be localized on the assumption that the total cohesive energy of the substances is the geometric sum of the Hansen solubility parameter components defined above (equation (4.4)) and δ is the vector from the origin to this point.
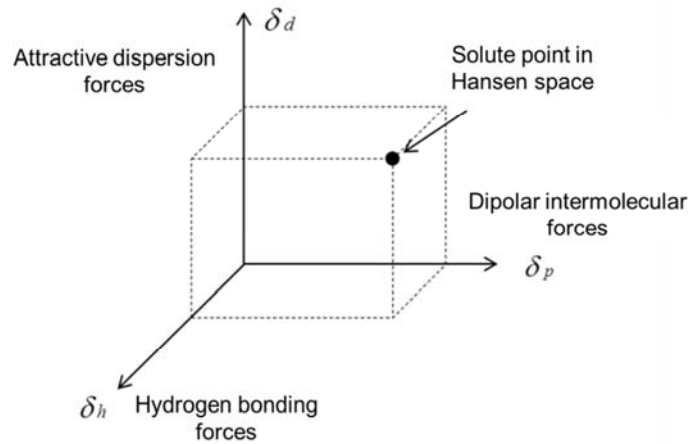
Fig. 4.2 – 3D representation of the Hansen solubility parameters (1967).

For a solid substance to be soluble in a liquid, or two liquids to be miscible, it is necessary that their position in the Hansen space is close, that is to say that their solubility parameters are similar. To characterize the solubility between materials, Skaarup (Hansen, 2007) developed in 1967 the solubility parameter distance, Ra, from plots of experimental data:

$$Ra = \sqrt{4(\delta_{d2} - \delta_{d1})^2 + (\delta_{p2} - \delta_{p1})^2 + (\delta_{h2} - \delta_{h1})^2} \qquad\qquad (4.5)$$

Where the factor "4" was suggested by Hansen based on empirical testing because it was found convenient and correctly represented the solubility data as a sphere encompassing the good solvents (Hansen, 2007). Solubility requires that Ra be less than the radius of a solubility sphere determined experimentally.

Hildebrand solubility parameter δ can also be expressed in terms of the individual Hildebrand parameters describing two contributions to the cohesive energy, namely, the non-polar Van der Waals dispersion forces δ_d, and the polar interactions (electrostatic) δ_p. Hydrogen bonding interactions δ_h are included here in the polar contribution (Hildebrand, 1950):

$$\delta = \sqrt{\delta_d + \delta_p}$$

(4.6)

Once the Hildebrand solubility parameter is determined, a set of properties could be correlated. For the surface tension γ calculation, Beerbower (1971) proposed the following formula:

$$\gamma = 0.0715\, v_m^{1/3} \delta^2$$

(4.7)

with v_m is the molar volume. Koenhen and Smolders (1975) found the following relationship after analysis of solvent data:

$$\delta_d^2 + \delta_p^2 = 13.8 (\frac{1}{v_m})^{1/3} \gamma$$

(4.8)

As shown in the work of Hildebrand and Scott (1950), the compatibility between a plasticizer and a polymer can be determined by miscibility based on solubility parameter. The enthalpy of the polymer (1) -plasticizer (2) mixture can be determined by:

$$\Delta H = v_{mix} ((\frac{\Delta E_2}{v_1})^{1/2} - (\frac{\Delta E_1}{v_2})^{1/2})^2 x_1 x_2 - v_{mix} (\delta_1 - \delta_2) x_1 x_2$$

(4.9)

Where v_{mix} is the molar volume of the mixture, v_1 and v_2 are molar volume of the polymer and the plasticizer respectively, ΔE_1 and ΔE_2 are molar energies of vaporization, x_1 and x_2 are volume fractions.

A plasticizer (1) and a polymer (2) are miscible in all proportion when $\delta_1 = \delta_2$ (McGinity, 2008), which gives a positive value of the enthalpy of the mixture. This assumes that the Gibbs free energy of mixing ΔG is negative ($\Delta G = \Delta H - T\Delta S$) to allow solution formation. In this case, all the interactions between the molecules of the plasticizer and the polymer are of the same order of magnitude. The degree of miscibility between a plasticizer (1) and a polymer (2) increases as the difference between the solubility parameters $\Delta \delta = (\delta_1 - \delta_2)^2$ decreases.

4. Calculation methods of the Solubility parameter δ

4.1. Experimental methods

Experimentaly, there are numerous methods for Hildebrand solubility parameter determination such as the homomorph method (Barton, 1991), the maximum-in-swelling method often used for the

determination of solubility parameters of crosslinked polymers by immersing the sample in a series of liquids of varying δ (Gee, 1946) and the inverse gas chromatography by measuring the infinite dillution weight fraction activity coefficient in a gas chromathography column which can be related to the Hildebrand solubility parameter (Choi, 1996; King, 1995). Other experimental methods and their results have been reported by Grulke (1998).

4.2   Group Contribution methods and HSPiP

In 1932, Parks and Huffman have shown that some thermodynamic properties of organic compounds could be reasonably calculated from parameters related to molecular structures. Since then, several authors developed predictive models and methods based on this finding, those are called group contribution methods. Group contribution methods are predictive methods allowing assessing any properties by summing the number frequency of each fragment occurring in the molecule, times its contribution, on the assumption that these contributions are independent of the rest of the molecule. These methods do not require substantial computational resources and thus have the advantage, over molecular simulation, of faster properties estimation. However, many of these methods are of questionable accuracy and have limited applicability when they are built with a limited set of data.

Hansen's partial solubility parameters of compounds can be calculated theoretically from their chemical structure, from the contributions of the various constituent groups by the method proposed by Hoftyzer and van Krevelen (Grulke, 1999):

$$. \delta_d = \frac{\sum F_{di}}{V_m} \quad , \quad \delta_p = \frac{\sqrt{\sum F_{pi}^{\,2}}}{V_m} \text{ and } \delta_h = \frac{\sqrt{\sum E_{hi}}}{V_m} \tag{4.10}$$

F_{di} and F_{pi} are called molar attraction constants; they are characteristics of different groups within the chemical constitution of the compound. E_{hi} is the hydrogen-bonding functional group value

Many scientists have proposed correlations and lists of contributions for various chemical groups, including Hansen (1967), Van Krevelen (1965), Hoy (1970), Small (1953) and recently Yamamoto (HSPiP, 2010). HSPiP (Hansen Solubility Parameters in Practice) is a software product for the prediction and calculation of solubility parameters using group contribution methods. Being built over a data set covering more than 10 000 molecules, Yamamoto's molecular breaking method is the most predictive in the group contribution method cited. It also allows the prediction of other properties such as boiling point, melting point, density or the saturated vapor pressure (Pirika, 2010).

4.3. Molecular Simulation

For the calculation of the solubility parameter, molecular simulation has proven a convenient tool by many authors. By averaging the cohesive energy from the molecular dynamic trajectories, Benali (2007) calculated the solubility parameters of several pharmaceutical products and found results in good agreement with experimental values. Belmares (2004) calculated the cohesive energy density for 64 solvent using molecular simulations the results were also close to the experimental values, Choi (1992) also used molecular simulation to estimate the Hansen solubility parameters for nonionic surfactant, and Sistla (2012) used it for ionic liquids and found good agreement with experimental values.

Molecular simulation uses relationships from statistical thermodynamics to determine macroscopic properties of a system from the knowledge of intermolecular interactions and other molecular properties. The quality of the predicted properties in molecular simulations depends on the choice of the thermodynamic ensemble and on the ability of the adopted forcefield to describe the interactions between the molecules and atoms through molecular dynamics.

4.3.1 Statistical Thermodynamics

The purpose of statistical thermodynamic is to calculate the macroscopic properties of a system from its microscopic properties. Consider a cup of water, in the macroscopic scale; we have a fluid at rest, fully described by four macroscopic properties (Pressure, temperature, volume and masse). In the microscopic scale however, we have millions of particles rotating, vibrating and shaking in all directions making incessant collisions. In this scheme, properties such as temperature and pressure are always fluctuating. In the macroscopic scale, properties measurement time is so large (of the order of 1 ms to 10 s) compared with the time scale of the fluctuations, thus, the property value seems constant. Thus, the macroscopic system behavior is a result of statistical average of an ensemble of states. Macroscopic properties value X is the average over time t_{total} of the fluctuations measured at the micro scale level (Prausnitz et al., 1999; Diu et al., 1989):

$$<X>_{ensemble} = \frac{1}{t_{total}} \sum_{t=1}^{t_{total}} X(t) \tag{4.11}$$

Many other values can be calculated from the variance that expresses fluctuations around the mean value:

$$\Omega_X^2 = \frac{1}{t_{total}} \sum_{t=1}^{t_{total}} ((X(t) - <X>_{enemble})^2) = <X^2> - <X>^2 \tag{4.12}$$

All systems studied within the framework of statistical thermodynamics should be in a statistical ensemble. The four most common are:

- NVE ("microcanonical"),
- NVT ("canonical"),
- NPT ("isobaric - isothermal"),
- μVT ("grand canonical"),

Fluctuations depend on the ensemble in which they are calculated. Each ensemble is characterized by constant values. For example, there is no fluctuation of volume or energy in the NVE ensemble and the system is closed. In this ensemble N, V and E are controlled by the user, the remaining variables being known only by an average value on the ensemble.

For static fluctuating quantities calculated using molecular simulation at several steps in time, if the time between two simulation frames is too short, consecutive values of theses quantities may be correlated over time, and the correlation has to be taken into account (Frenkel and Smit, 1996). To estimate the error on average properties over uncorrelated frames and to compute the time correlation-function, we may use the block average method. Block average is essentially a real space renormalization group technique applied in the one-dimensional, discrete space of simulation time (Flyvbjerg and Petersen, 1989). More details about the block average method are given in Appendix B.

4.3.2   Molecular Dynamics (MD)

Molecular dynamics (MD) is one of the two usual methods with Monte Carlo (MC) to sample systems configuration. The principle of molecular dynamics is to generate trajectories of a finite set of particles by numerically integrating the classical equation of motion of Newton. For a particle of mass m_i moving with a velocity v_i and subjected to a force f_i, the simplified equation is given by:

$$\sum \vec{f}_i = m_i \frac{d\vec{v}_i}{dt}, \quad i = 1..N \tag{4.13}$$
$$f_i = -\frac{dU}{dx}$$

N is the number of particles in the simulation. The forces f_i acting on the particle are determined by the gradient of the inter-atomic potential energy function U in the x direction (Becker & Watanabe, 2001). The quality of these potentials determine the accuracy of molecular dynamic simulation, which all together form the forcefield to be applied on the constructed molecules placed in the simulation cell. The force field depends on the nature of the simulated material, as it contains all the physical data characterizing the atoms and possibly their chemistry.

According to Becker & Watanabe (2001), a molecular dynamics simulation can be outlined by four steps. The steps 2, 3 and 4 are repeated as many times as possible:

1) Definition of the initial state of atoms: atomic coordinates, interatomic connectivities, and accelerations of atoms,

2) Calculation of the forces exerted on each particles from their intermolecular interactions (requires a force field (see next section)),

3) Solving the equations of motion of particles subjected to forces (Newton's law), is done with various algorithm such as Verlet's (Frenkel and Smit, 1996)),

4) Taking another step forward in time and the particles are moved. If required, writing the state of the system.

Each simulation step in MD is usually in the order of femtoseconds (i.e. 10^{-15}s). The trajectories determined by MD are used to evaluate the static and dynamic properties by time averaging.

Periodic boundary conditions are used to avoid wall effects while having a system with a finite number of particles. Thus, the molecules near the edges of the central box are surrounded by molecules in the same way that a molecule in the center of the box (see Fig. 4.3). Launching molecular simulation involves the optimization of the simulation cell box to minimize strain, and then starting the molecular dynamic simulation.

Original simulation box   3 periodic Images
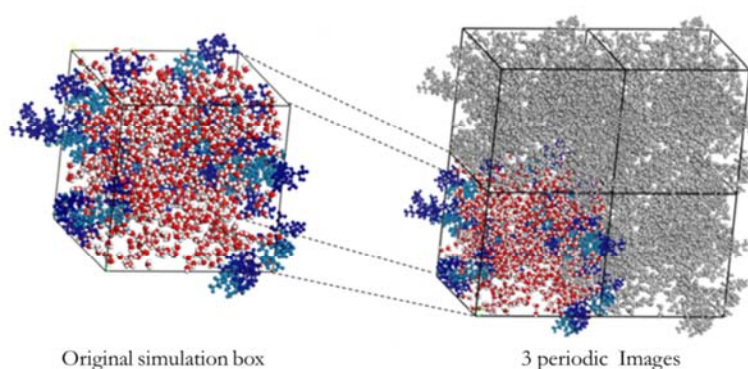
Fig. 4.3 – A molecular dynamics system setup. The coloured simulation box is filled with 10 Hydroxypropyl methylcellulose molecules (in blue) surrounded by 1000 water molecules (in red). This box is is surrounded by 3 images of itself (in grey).

70

Molecular dynamic simulation runs consists of an equilibration phase and a production phase. The equilibration phase is intended to bring the system from an initial configuration where, usually, the molecules are randomly dispersed in the simulation cell, to a representative configuration of the system from which material properties can be calculated from the positions, velocities and forces by performing overall statistical thermodynamic calculations. The large computational effort in molecular simulation is due to the large number of pair interactions which need to be evaluated at each integration step. Molecular simulation results are critically dependent on how the forcefield describes the atomic interactions.

4.3.3   Forcefields

Force fields are a set of mathematical functions and parameters related to the potential energy of a molecular system configuration. A forcefield uses an empirical representation of the potential energy where the interaction between atoms can be divided into contributions from the intramolecular and intermolecular interactions; therefore any potential energy calculated using a force field has the following general form:

$$U = U_{intermoléculàre} + U_{intramoléculàre} \qquad (4.14)$$

This form can be expanded to the following form which is used in the COMPASS II forcefield (Sun, 1998):
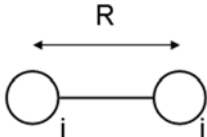
$$U = \sum_{stretch} k_b (b - b_0)^2 + \sum_{angle} k_\theta (\theta - \theta_0)^2 + \sum_{dihedral} k_\chi (1 - \cos(n\chi - \Psi)) + ... $$

$$... + \sum_{nonbond} D_0 \left((\frac{R_0}{R})^{12} - 2(\frac{R_0}{R})^{6} \right) + \sum_{nonbond} C \frac{q_i q_j}{\xi R} \qquad (4.15)$$

The range of intermolecular interaction which mainly concerns non-bonding interactions is determined by the exponent of the distance between the particles concerned. For example, the Coulomb ones have a long range interaction which means that the occurrence of interactions between atoms will be felt much further. **Bonded pair interactions**
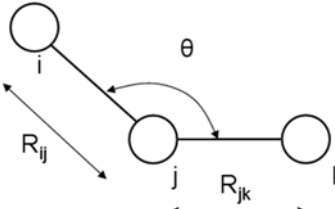
In molecular simulation, atoms (represented by the spheres), are connected by springs. Bonded terms involve three or four body interactions and correspond to bond stretching, angles and torsion energies:

Bond Stretching Potential (Harmonic):

$$U_{stretch} = \sum_{stretch} k_b (b - b_0)^2 \qquad (4.16)$$
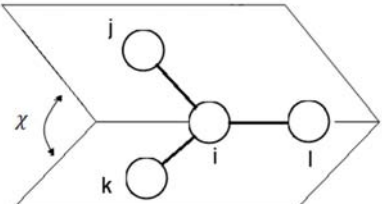
Where, k_b is bond force constant (in kcal.mol^{-1}.Å^{-1}), b is the bond length (in Å), b_0 is the equilibrium bond distance (in Å).

Angle bend (Harmonic):

$$U_{angle} = \sum_{angle} k_\theta (\theta - \theta_0)^2 \qquad (4.17)$$

Where, k_θ is the valence angle force constant (in kcal.mol^{-1}), θ is the valence angle, θ is the equilibrium angle.

Dihedral angle:

$$U_{dihedral} = \sum_{dihedral} k_\chi (1 - \cos(n\chi - \Psi)) \qquad (4.18)$$

Where, k_χ the dihedral force constant (in kcal.mol^{-1}), χ is the dihedral or torsion angle between bonding atoms, Ψ is phase angle and n is a multiplicity constant.

- **Non Bonded pair interactions**

These interactions are usually described by two terms: Van der Waals potential and an electrostatic potential.

The best known function of Van der Waals potential is the Lennard-Jones function 12-6. The 6-term approximates the attraction and the 12-term approximates the short distance repulsion.

$$U_{vdw} = \sum_{nonbond} D_0 \left(\left(\frac{R_0}{R}\right)^{12} - 2\left(\frac{R_0}{R}\right)^6 \right) \qquad (4.19)$$

Where R is the distance between particle i and j. This equation contains two adjustable parameters: the equilibrium distance R_0 which is the minimum approach distance between the two atoms i and j for which the energy is the lowest, and thee D_0 which represents the minimum of potential energy, which corresponds to the most stable interaction.

The electrostatic interaction between different atoms of the same molecule or two molecules can be calculated using Coulomb's law as the sum of interactions between pairs of point charges q:

$$U_{Coulomb} = \sum_{nonbond} C \frac{q_i q_j}{\xi R} \tag{4.20}$$

Where, q_i and q_j are the charges on the atoms i and j (in e-), C = 332.0647 (in kcal.Å.mol^{-1}.e^{-2}) is a unit conversion factor, and ξ is the dielectric constant. Typically, ξ is equal to 1, corresponding to the permittivity of the vacuum. Point charge values are fitted or approximated from quantum mechanics calculations.

Other function forms can also be found depending on the molecules and atoms placed in the cell.

4.3.4   Pair distribution function

The structure of a simple monoatomic fluid is characterized by a set of radial distribution function describing the atomic positions, the simplest of which is the pair distribution function *g(r)*. *g(r)* represents the probability of finding an atom at a distance *r* from another atom taken as the origin, and therefore characterizes the distance between the atoms. It's given by the following equation:

$$g(r) = \frac{V}{N^2} < \sum_i \sum_{i \neq j} \Delta(\vec{r} - \vec{r}_{ij}) > \tag{4.21}$$

Where N is the total number of atoms, V is the volume of the system and Δ is the Dirac function.

Fig. 4.4 shows a typical pair distribution function *g(r)* for monoatomic fluid. The first peak displays the position of the closest neighboring atoms and corresponds to the first spherical Layer. Oscillation peak decreases for larger distances and refers to the successive spherical layers. Below r_v, *g(r)* is equal to zero, r_v then corresponds to the minimum distance between two particles.
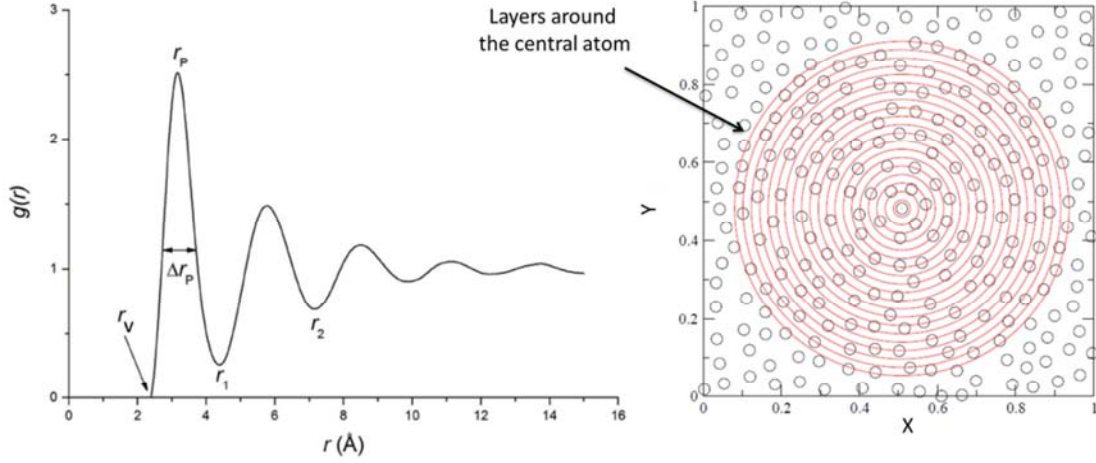
Fig. 4.4 – Pair distribution function of liquid Zirconium, adapted from Hennet et al. (2007)

The pair distribution function is useful, first, because it provides insight into the material structure, and secondly, because the ensemble average of any pair functions Z may be expressed in the following form (Allen and Tildesley, 1987):

$$< Z(r_i, r_j) > = \frac{1}{V^2} \int dr_i dr_j \, g(r_i, r_j) a(r_i, r_j) \tag{4.22}$$

For example, the energy E:

$$E = (3/2) N K_B T + 2\pi N \varrho \int_0^\infty r^2 v(r) g(r) dr \tag{4.23}$$

Or the pressure:

$$PV = N K_B T - (2/3)\pi N \varrho \int_0^\infty r^2 w(r) g(r) dr \tag{4.24}$$

The structure factor $S(Q)$ is also derived from the radial distribution function:

$$S(Q) = 1 + \varrho \int_v e^{iQr} g(r) dr \tag{4.25}$$

4.3.5.   Calculation of δ by molecular simulation

In molecular simulation, the Hildebrand solubility parameter can be calculated from the pair potential by summing the pairwise interactions (Belmares et al., 2004). The cohesive energy density is equal to minus the intermolecular energy, i.e. the intramolecular energy minus the total energy:

$$\delta_k^2 = \frac{< \sum_{i=1}^{n} E_i^k - E_c^k >}{N_{av} < V_{cell} >}$$
(4.26)

With n the number of molecules in the simulation cell, N_{av} the Avogadro number, $k = 1, 2$, are the van der Waals energy (dispersion) and the coulombian energy (polar) respectively. "< >" denotes a time average over the duration of the dynamics in the canonical ensemble NVT, V_{cell} the cell volume, the index "i" refers to the intramolecular energy of the molecule i, and the index "c" represents the total energy of the cell. Appendix G presents a developed script for the solubility parameter calculations based on equation (4.26).

5. Computational details and methods

5.1 COSMO and DFT

Conductor-like Screening Model (COSMO) implemented in Dmol3 module as a part of Material Studio 7.0 package of Accelrys was used to generate the sigma-profiles of the molecules. Water is chosen as the solvent environment (relative dielectric constant = 78.54). A global orbital cutoff radius of 3.7 Å was used throughout the calculations. We have used the gradient-corrected functionals (GGA) of Perdew and Becke (Perdew and Wang, 1992; Becke, 1988) for the geometry optimization and the COSMO calculations. It has been demonstrated by Perdew and Wang that this technique produces more reliable predictions than the Vosko-Wilk-Nusair (VWN) technique (Voskoet al., 1980). For best accuracy, we used the triple-numerical polarization (TNP) basis set (Delley, 2006). In Dmol3-CSOMO (Biovia, 2013), the radii of the spheres that make up the cavity surface are determined as the sum of the van der Waals radii of the atoms of the molecule and of the probe radius. First, geometry optimization was performed to bring the energy to obtain the most stable conformation and to adjust the coordinates of the atoms. The sigma profiles were thereafter generated.

We noticed that the Dmol3 module produces sigma profile curves similar to those in the literature but they seem to be strongly "squeezed" vertically, i.e. the values at the local maxima are much less than found in literature (see Appendix C for more details). We adjusted the sigma-profile curves by multiplying the values by a corrective values equal to 2.817 for the charge density σ and by 0.080 for the probability $p(\sigma)$, The corrective values were chosen so that the boundaries of the water sigma profiles correspond to the real ones obtained from literature. The sigma profiles of all the materials were multiplied by the same corrective values.

5.2 Molecular simulations

For the computation of the solubility parameters, we run molecular simulations in the canonical ensemble NVT with the Forcite® module of the Material Studio Suite release 7 (Biovia, 2013). Simulations are run over 500 ps with a time step of 1 fs. The temperature is set at $T = 298K$ and controlled by a Nose Hoover thermostat with a Q ratio equal to 0.01. The experimental densities listed in Table 2.2 are used to set the simulation box volume. Energy and pressure stability was checked. The last 50 ps are used for averaging potential energy components. The average cohesive energy is computed to derive the solubility parameter by using equation (4.26). The standard deviation method can be evaluated from the block averages method (Flyvbjerg and Petersen, 1989).

Depending on the components, COMPASSII (Condensed-phase Optimized Molecular Potentials for Atomistic Simulation Studies II) (Sun, 1998) and PCFF forcefields (Polymer-Consistent Force Field) (Sun and Rigby, 1997) were used with their predefined atom type parameters. Both molecular dynamic forcefields describe the energy of interaction by adding an intramolecular contribution accounting for bond stretching, bending and torsion, and an intermolecular contribution term accounting for Van der walls and coulombian interactions. Van der Waals interaction was truncated by a spline function after 15.5 angströms. For the Coulombian interaction, partial charges were assigned by the predefined forcefield equilibration method, while the Ewald summation was used to account for the long range interactions.

6. Results and discussion

6.1 σ-profiles

Fig. 4.5 shows the σ-profile of PVP, HPMC and PEG400, and compares them to that of the water molecule. Fig. 4.6 shows the COSMO surface of PVP, HPMC and PEG400.

HPMC has an asymmetric profile. An asymmetric profile means the material does not feel comfortable in its pure state (Klamt, 2005), i.e. there is an amount of electrostatic misfit. HPMC has a dominant peak in the non-polar region at -0.0029 e.Å^{-2} and a small peak around 0.011 e.Å^{-2} arising in the positive polar region, and another smaller shoulder extending from -0.01 to about 0.015 e.Å^{-2} corresponding to the positively charged atoms. This suggests that HPMC molecule may prefer to be in contact with a solvent showing hydrogen bond donor characteristic. The small shoulder of HPMC is very close to the water negative peak. This similarity may indicate that HPMC can mix with water

since HPMC is able to break the strong bond between water molecules and pair up with the negative region of the water molecule.
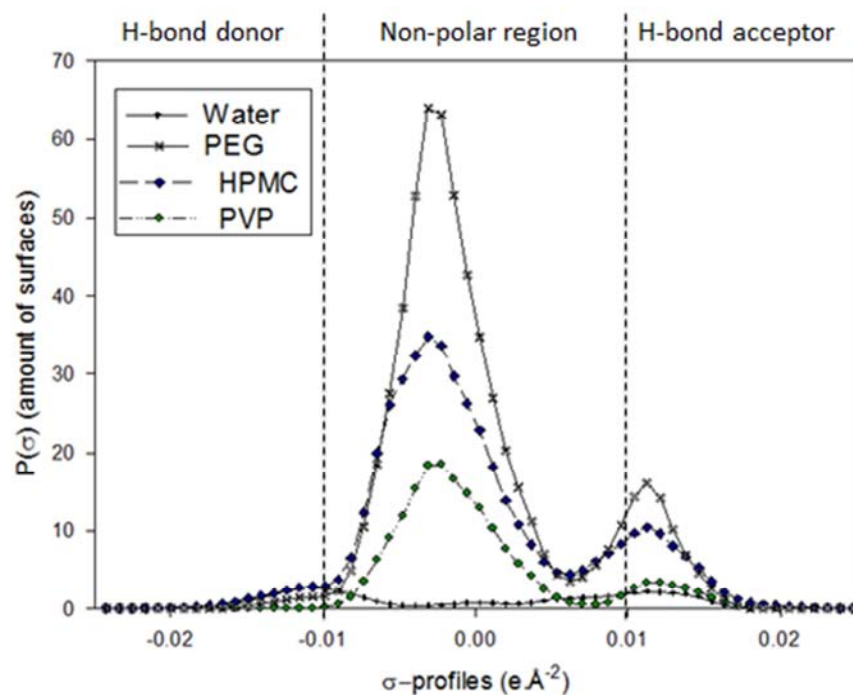
Fig. 4.5 – σ-profile of Water, PVP, HPMC, PEG400
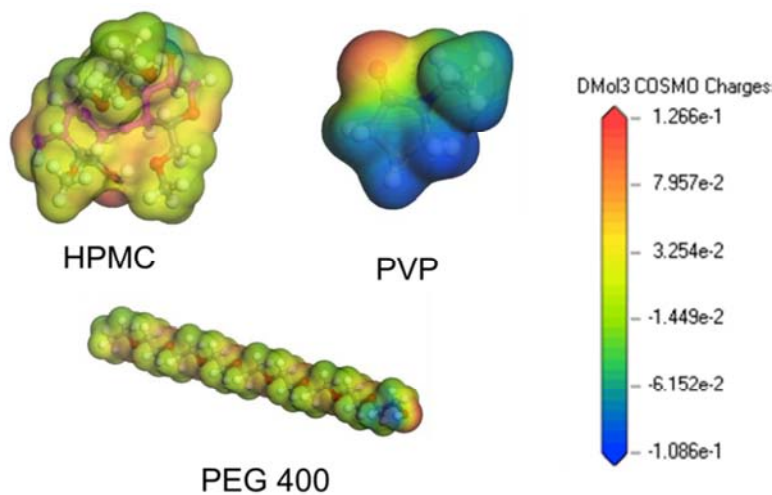
Fig. 4.6 – Dmol3-COSMO surfaces of HPMC, PVP and PEG400.

PVP σ-profile shown in Fig. 4.5 is also asymmetric, it has a major non-polar peak at -0.0028 e.Å^{-2} and a smaller peak in the positive region of σ-profile, meaning that PVP can only act as H-bond acceptor and is looking for a H-bond donor. The polar oxygen in PVP does not find a partner with a reasonably negative σ; hence, when mixing with water, this misfit can be adjusted, and the polar

oxygen may pair up with the polar hydrogen of water. PEG has a very similar curve shape to HPMC, suggesting solubility in water. From Fig. 4.5, we also notice that HPMC, PVP and PEG have similar σ-profile, this indicates a similar behavior in water and, considering that they are all look for a H-bond donor, may suggest that they are miscible in each other if we consider the old chemical aphorism "similia similibus solvuntur" or "like dissolves like".

Fig. 4.7 presents the σ-profile of NA, SA and MCC, and compares them to that of the water molecule. Fig. 4.8 shows the COSMO surface NA, SA and MCC.
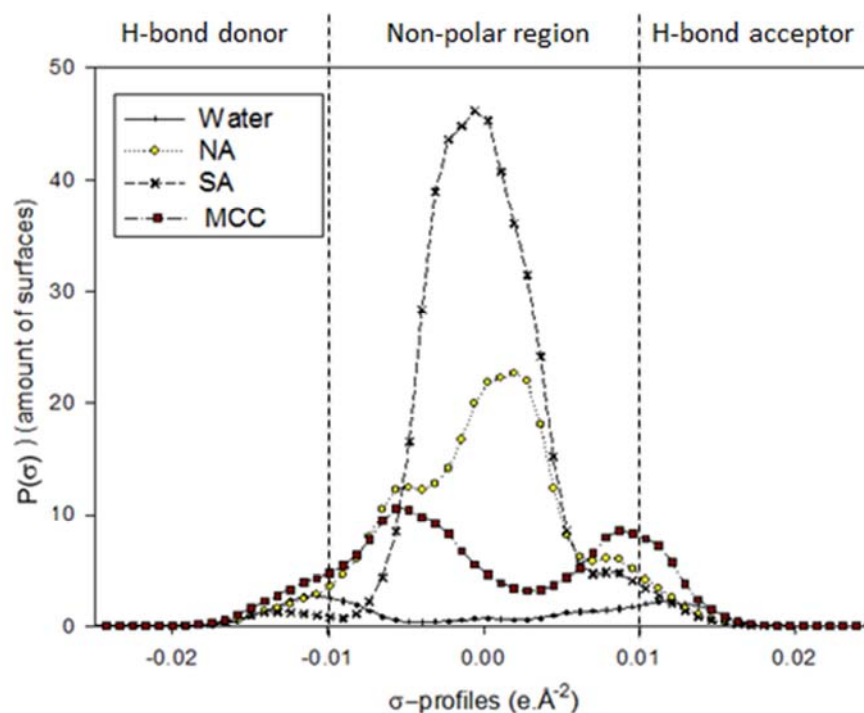
Fig. 4.7 – σ-profile of Water, NA, SA and MCC.

SA is mostly non-polar since it has a narrow σ- profile around σ = 0, this can also be seen in the COSMO surface in Fig. 4.5 where we have a mostly green surface, with a tendency to blue-green on the hydrogen at the end of the molecule and to red-green on the oxygen, whereas water has broad symmetric σ-profile and a higher polar peak in the positive and negative σ-profile curve. A non-polar surface hates to be in water and likes to escape into any other solvent (Klamt, 2005), so, if we try to put a SA molecule into water, the non-polar surface pieces of SA cannot break the strong bond between the water molecules due to its strong positive and negative σ. This indicates insolubility between water and SA. MCC molecule is polar and has two pronounced peaks at -0.005 e.Å^{-2} and 0.009 e.Å^{-2}. In the negative σ-profile region, the position of the peak is clearly shifted to the non-polar σ-profile range and both peaks are stronger than those exhibited by the water molecules. Both

MCC and water have similar σ-profile but a symmetrical one, which means they feel comfortable in their pure state (Klamt, 2005). NA has a different curve shape than the other materials with a non-polar peak around -0.0017 e.Å^{-2}, and a shoulder in the negative σ-profile region around -0.005 e.Å^{-2}. Beyond ± 0.01 e.Å^{-2}, NA is symmetrical suggesting that it would be comfortable in its pure state.
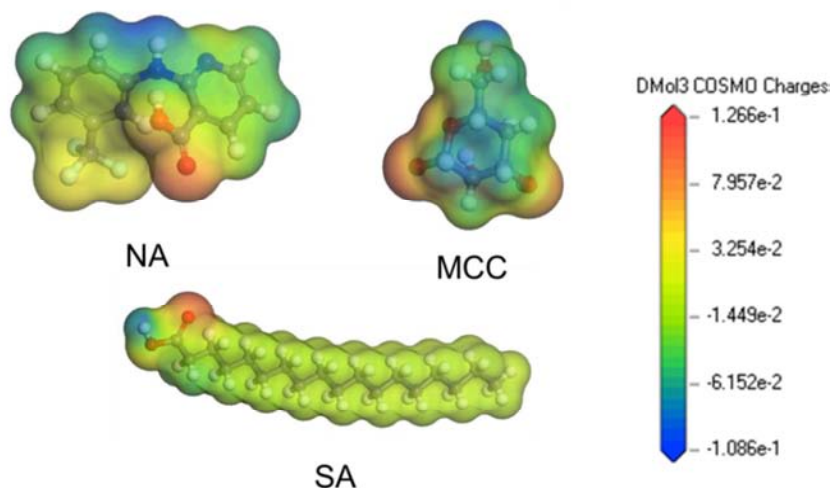
Fig. 4.8 – Dmol3-COSMO surfaces of NA, MCC and SA.

6.2 Solubility parameter calculated by different methods

Table 1 compares experimental solubility parameters with those predicted by the Yamamoto method (HSPiP, 2010) and by molecular simulation.

The average value of the cohesive energy density is obtained for all compounds from the last 50 picoseconds (ps) of the 500 ps dynamic simulation, spanning 500 000 time steps. However, getting a good estimation of the average standard deviation in molecular dynamics simulation requires typically over several millions of time steps, which are practically difficult to obtain in a reasonable lapse of time. Indeed, the average standard deviation must be computed over uncorrelated frames. This can be achieved by using the block average variance method (Flyvbjerg and Petersen, 1989). Its application to simple system, like Lennard-Jones fluids (Frenkel and Smit, 1996) shows that the average standard deviation over uncorrelated frames is at least one order of magnitude greater that the standard deviation computed directly from the molecular dynamics frame trajectory. Its application to the real systems we studied was not possible in a reasonable lapse of time (see Appendix B for more details); therefore we estimated the average standard deviation as ten times the standard error given by Forcite (Biovia, 2013).

Table 4.1 – Solubility parameters calculated by different methods.

Solubility parameter (J.cm⁻³)¹/²	Group contribution		Molecular simulation forcefields				Exp.
	HSPiP		COMPASSII		PCFF		
Compounds	δ	δ_d	δ	δ_d	δ	δ_d	δ
PVP	21.2	18.5	21.12 ± 0.16	19.45 ± 0.18	19.77 ± 0.11	17.60 ± 0.10	-
MCC	29.2	18.8	29.98 ± 0.24	17.04 ± 0.32	28.12 ± 0.13	20.71 ± 0.16	29.3[a]
HPMC	20.2	17.1	20.68 ± 0.13	17.03 ± 0.14	20.98 ± 0.10	18.39 ± 0.09	22.8[b]
EC	18.8	16.7	19.61 ± 0.15	18.73 ± 0.15	16.08 ± 0.08	15.46 ± 0.07	19-21[c]
NA	21.9	19.3	25.40 ± 0.19	21.97 ± 0.23	23.73 ± 0.56	20.23 ± 0.43	23.8[d]
SA	17.5	16.3	18.61 ± 0.22	16.75 ± 0.26	19.89 ± 0.26	17.72 ± 0.28	17.6[b]
PEG200	24.4	16.4	26.54 ± 0.22	19.27 ± 0.24	26.18 ± 0.39	20.91 ± 0.32	24[c]
PEG400	19.0	14.6	22.88 ± 0.24	20.17 ± 0.24	24.07 ± 0.16	22.51 ± 0.17	-
CA	24.4	18.0	20.98 ± 0.22	17.74 ± 0.21	23.17 ± 0.19	21.54 ± 0.18	24[c]
NC	25.0	17.9	22.34 ± 0.41	17.00 ± 0.28	110.13 ± 0.13	26.88 ± 0.17	21.7[c]
Water	47.8	15.5	47.78 ± 0.59	-	47.33 ± 0.20	5.89 ± 1.98	47.9[c]

PVP: Polyvinylpyrrolidone, MCC: Microcrystalline cellulose, HPMC: Hydroxypropyl-methylcellulose, EC: Ethyl cellulose, NA: Niflumic acid, SA: Stearic acid, PEG : Polyethylene glycol. CA: Cellulose acetate, NC: Nitrocellulose
a: Rowe 1989b, b: Rowe 1989a, c: Barton 1991, d: Bustamante 1993.

For the molecular simulation of polymers, the number of repeating unit was chosen so that the solubility parameter remains constant in case of further increasing of the repeating unit. Results are displayed in Fig. 4.9. The number of repetition unit was fixed to 8 for MCC, PVP and EC, and 5 for HPMC.
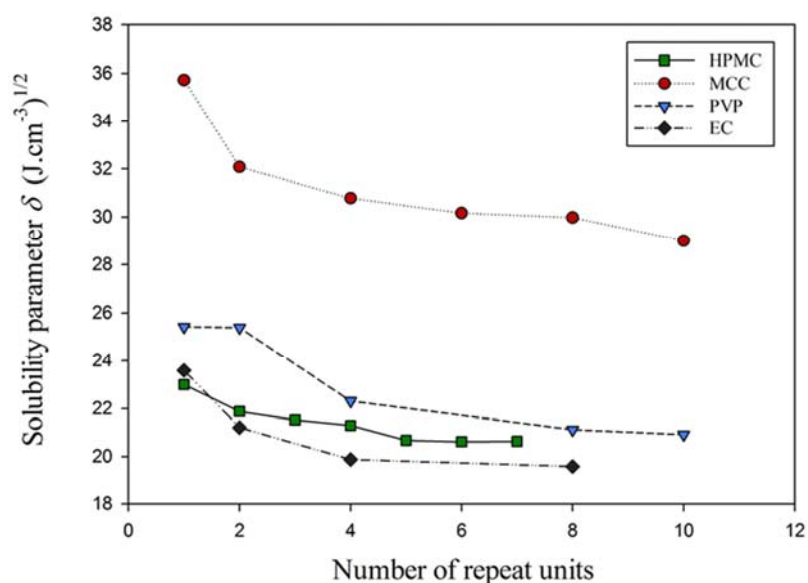
Fig. 4.9 – Variation of Hildebrand solubility parameter versus number of repetition unit of polymers.

In previous work, the number of molecules distributed initially in the simulation cell was shown to have very little effect on the values of the solubility parameters (Benali, 2006). Generally, four polymer chains are sufficient, although for very high molecular weights even one chain can be adequate (Belmares et al., 2004). In our calculations, we placed 10 molecules per cell for PVP, MCC, PEG400 and SA, 8 molecules per cell for HPMC, 6 molecules per cell for CA and NC, 30 molecules per cell for NA, 40 molecules per cell for PEG200 and 100 molecules per cell for water. Larger number will increase the computational effort.

Table 4.1 shows that experimental Hildbrand solubility parameters are close to the COMPASSII forcefield and HSPiP results. Concerning water, only the PCFF forcefield gives a dispersive contribution to the solubility parameter, consequently, throughout this thesis, we will use the solubility parameter predictions obtained from HSPiP and COMPASSII forcefield, except for water where we will use PCFF forcefield values.

Calculation of $\Delta\delta$ for PVP, MCC and HPMC with a plasticizer (PEG400) indicates the likelihood of miscibility between them. PEG gives $\Delta\delta$ (PEG400-PVP) $= 10.7 < \Delta\delta$ (PEG400-HPMC) $= 17.5 < \Delta\delta$ (PEG400-MCC) $= 22.4$ J.cm^{-3}, showing that the miscibility decreases in the following order: PEG400-PVP > PEG400-HPMC > PEG400-MCC. This suggests that PVP and HPMC are more compatible with PEG400 as a plasticizer than MCC.

The Hansen components of the solubility parameter are given in Table 4.2.

Table 4.2 – Hansen solubility parameter components calculated by HSPiP.

Compounds	Hansen solubility parameter components $(J.cm^{-3})^{1/2}$		
	δ_d	δ_p	δ_h
PVP	18.5	8.3	5.9
MCC	18.8	10.7	19.5
HPMC	17.1	7.1	8.3
EC	16.7	5.9	6.2
NA	19.3	7.3	7.4
SA	16.3	3.0	5.5
PEG200	16.4	9.6	15.3
PEG400	14.6	7.8	9.4
CA	18.0	8.5	14.1
NC	17.9	14.2	9.8
Water	15.5	16.0	42.3

7. Conclusion

In this chapter, we described the computational methods and techniques used for solubility parameter calculations (Molecular simulation and group contribution methods). We also have used Dmol3 and COSMO model to generate σ-profiles of the compounds. We have seen that σ-profiles give valuable information regarding polarities, hb-donors and hb-acceptors, wich allow to guess the solubility of compounds. HPMC, PVP and PEG have similar σ-profile, indicating similar behavior in water. This also may suggest that they are miscible in each other. MCC has a different σ-profile shape than the other polymer (HPMC, PVP and PEG) and the curve suggest a low solubility in water. NA has a symmetrical σ-profile suggesting that it would be comfortable in its pure state.

For the calculation of the solubility parameter, we used HSPiP and also molecular simulation. Results were compared to experimental values from the literature. Both methods gave solubility parameter values close to the experimental values. Calculation of $\varDelta\delta$ for PVP, MCC, HPMC and PEG, suggests that PVP and HPMC are more compatible with PEG400 as a plasticizer than MCC.

Hildebrand solubility parameter values will permit us to estimate the work of adhesion and the ideal tensile strength in the next chapter. These quantities enable the predictions of the affinity between solids and solid-binder in aqueous and dry systems.

Chapter 5

Prediction of solid - binder affinity in dry and aqueous systems

Results in this chapter have been published in Powder Technology journal:

Jarray A., Gerbaud V. and Hemati M., Prediction of solid - binder affinity in dry and aqueous systems: Work of adhesion approach vs. ideal tensile strength approach, Powder. Technol. 271 (2015) 61–75.

1. Introduction

A successful granulation requires good affinity between host and guest particles. In addition, when preparing coating or binder solutions, the affinity between the particles in the aqueous systems controls the agglomeration mechanism and the stability of the particles in the coating formulations.

In this chapter, we develop predictive methodologies and theoretical tools of investigation allowing to choose the adequate binder or to formulate the right coating solution to ensure the customer's requested properties of the end product. As such, we explore two theoretical approaches for predicting substrate-binder interactions, one based on the work of adhesion, and the other based on the ideal tensile strength. We extend the approaches to ternary systems so as to study the interactions between compounds mixed in a solvent such as hydroxypropyl-methylcellulose (HPMC) and stearic acid (SA) mixed in water. The first section reviews some theoretical models for binary mixtures interactions. Then, we derive the tensile strength model for ternary mixtures. The last section concerns the model testing. First, we discuss the selection of the model core data, either coming from group contribution method or from molecular simulations, and we compare them with experimental data. Second, a relationship between the surface free energy and solubility parameter is proposed for cellulose derivatives. Third, it is used next for the prediction of the interactions in binary and ternary mixtures. The predictions obtained through the tensile strength approach and the work of adhesion approach are compared and discussed.

2. Theoretical models and equations

In order to predict the affinity between the different compounds, we need to calculate the work of adhesion and the ideal tensile strength. These quantities can be obtained using the Hildebrand (1950) solubility parameter δ. Adhesion and cohesion depend on the liquid surface tension and liquid-solid contact angle and falls under the category of surface free energy.

2.1. Contact angle and surface free energy

One of the fundamental properties of liquids molecules is their spontaneous tendency to gather in order to minimize the surface area. A molecule localized near the gas-liquid interface has fewer neighbors, as consequence, the molecules will tend to surround themselves with as many molecules as possible so as to minimize the area occupied by the gas-liquid interface, therefore, surface tension (i.e. surface free energy in liquid-gas interface) of the liquid changes its geometry to minimize this energy defect, forming a spherical shape. We then define the surface tension γ as the free energy F needed to increase the surface area S by one unit:

$$\gamma = \frac{dF}{dS} \tag{5.1}$$

Surface tension can also be defined as the reversible work required to extend a surface or to bring atoms from the interior to the surface region. For liquid-solid and solid-gas interfaces the surface free energy is called interfacial energy.

Capes and Danckwerts (1965) found that there is a minimum surface tension necessary to granulate particles of a certain size. Knight (1998) showed that in a high-shear mixer, domination of the surface tension over the viscosity in the consolidation process depends on a critical viscosity. Iveson et al. (1998) showed that low surface tension of the binder decreased the dynamic-yield strength of the granules. Zajic and Buckton (1990) used values for the surface energy of binders to predict the spreading over powder and vice versa. The prediction proved that Hydroxypropyl-methylcellulose (HPMC) is a better binding agent than Polyvinylpyrrolidone (PVP). Similarly, Planinšeka et al. (2000) found that HPMC is a better binding agent than PVP, for that, they also used the surface free energy. They concluded that water wets HPMC much faster than PVP. Oh and Luner (1999) used the surface free energy to study the influence of plasticizers on Ethylcelluose (EC), at the end of their article, they concluded on the importance of relating the surface free energy to the adhesion terms.

Surface tension quantifies the wetting characteristics between the binder (or the coating) and the substrate. Wetting is the ability of a liquid to spread on the surface of a solid surface. The purpose of the wetting is to distribute evenly the liquid binder on the particles forming the powder which will cause the formation of small nuclei (Iveson et al., 2001a). The wettability degree can be studied by measuring contact angle θ of the substrate with a given liquid.

Let's consider three phases, S, L and V, notations in reference to solid, liquid and vapor phase respectively. When we put a drop of phase L (in coexistence with Phase V) on a substrate S, two different wetting conditions can be encountered. The liquid may spread on the substrate surface to form a film, or may form a bead. This depends on the substrate-liquid affinity. If the liquid have good affinity with the substrate, it will tend to maximize its contact area and spread to form a film, it's called complete (or good) wetting. However, bad affinity between the liquid and the substrate favors the formation of bead (or spherical) shape of the liquid on the substrate surface, it is called partial wetting since the substrate is only partially covered by the liquid phase.

In the state of partial wetting, the droplet which resists the spreading form an angle θ on three-phase contact line between the solid/liquid interface and liquid/vapor interface known as the contact angle, as shown in Fig. 5.1. This contact angle is determined by the three interfacial energy of the system, via the famous Young's equation (1805):

$$\gamma_{SV} = \gamma_{SL} - \gamma_{LV} \cos(\theta) \quad \text{(in mJ.m}^{-2}\text{)}. \tag{5.2}$$

γ_{SV} = Interfacial energy associated with the air/solid interface (mJ.m^{-2}).

γ_{SL} = Interfacial energy associated with the liquid/solid interface (mJ.m^{-2}).

γ_{LV} = Surface tension associated with the liquid/air interface (mN.m^{-1}).
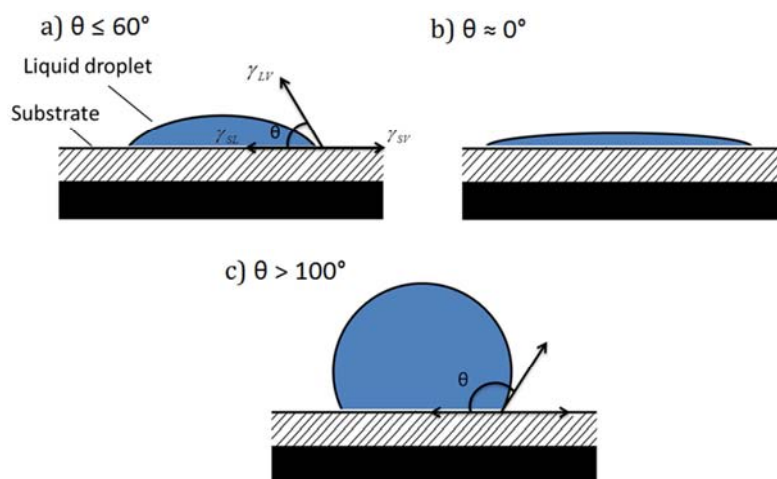
Fig. 5.1 – Representation of the shape of a liquid droplet placed on a substrate for different contact angles.

Interfacial energy causes a spontaneous tendency for the liquid present a minimal surface. Thus when a liquid is non-wetting, it will take a spherical shape. In this context, wetting can be classified into four states:

- Liquid spread on the substrate surface and the wetting is perfect : $\theta = 0°$;
- Good wetting : $0° < \theta \leq 90°$;
- Poor wetting: $90° < \theta < 180°$;
- No wetting: $\theta = 180°$.

During agglomeration, the nucleation phase depends on the thermodynamic parameters relating to the wettability such as the angle of solid-liquid contact and the coefficient of the solid-liquid spreading. The agglomeration is promoted when the binder is capable of wetting the solid namely when the contact angle formed between the two phases is between 0° and 90°. As an example, the effect of contact angle in $\cos(\theta)$ on the lactose/salicylic acid mixtures nuclei size formed in fluid-bed granulation is illustrated in Fig. 5.2. Nuclei size is seen to improve with contact angle (Ennis et al., 1990).
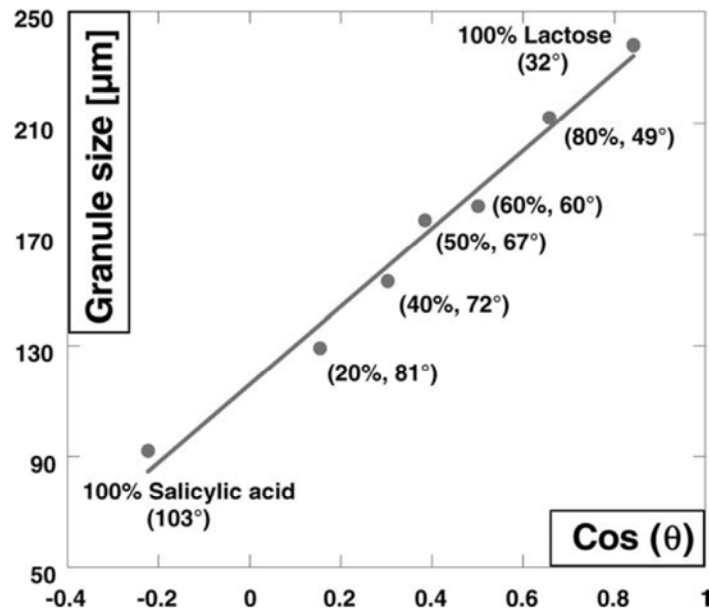
Fig. 5.2 – The influence of contact angle θ on nuclei size formed in fluid-bed granulation of lactose/salicylic acid mixtures. Powder contact angle determined by goniometry and percent of lactose of each formulation are given in parentheses (Ennis et al., 1990).

Fowkes (1964) proposed another interesting relationship for determining the interfacial energies which considers the polar and dispersive contributions for both solid and liquid:

$$\gamma_{LV}(1 + \cos(\theta)) = 2(\gamma_{LV}^{d}\gamma_{SV}^{d})^{1/2} + 2(\gamma_{LV}^{p}\gamma_{SV}^{p})^{1/2} \tag{5.3}$$

Here, the superscripts "d" and "p" refers to the dispersive and polar contribution, respectively. The polar component is due to hydrogen bonding and electrostatic interactions, and the dispersion component due to van der Waals interactions. However, in some cases, it is difficult to determine the contact angle especially between polymers. To solve this problem, Owen and Wendt (1969) proposed an alternative equation that uses the geometric mean:

$$\gamma_{SL} = \gamma_L + \gamma_S - 2(\gamma_{LV}^d \gamma_{SV}^d)^{1/2} + 2(\gamma_{LV}^p \gamma_{SV}^p)^{1/2} \tag{5.4}$$

Another expression was also derived from Fowkes relationship by Wu (1973) but, rather than using the geometric mean, he used the harmonic mean:

$$\gamma_{SL} = \gamma_L + \gamma_S - 4\frac{\gamma_{LV}^d \gamma_{SV}^d}{\gamma_{LV}^d + \gamma_{SV}^d} - 4\frac{\gamma_{LV}^P \gamma_{SV}^P}{\gamma_{LV}^P + \gamma_{SV}^d} \tag{5.5}$$

2.2. The work of adhesion and cohesion

The cohesion of the pulverized liquid in wet granulation process is a key factor in controlling the agglomeration or the coating forces between solid particles. Particle interactions can be broadly classified into two classes, namely cohesive and adhesive (Zimon, 1982). The energy required to separate unit areas of two surfaces A and B from contact is referred to as the work of adhesion (W_{AB}), and for surfaces of the same material, this is called the work of cohesion (W_{AA}). Either cohesion or adhesion becomes significant when gravitational forces acting upon these particles become negligible; that is, when the dimensions of the particulate materials become smaller than $10\mu m$ (Visser, 1995). For two identical surfaces in contact (Fig. 5.3 (b) and (c)), the work of cohesion can be related to the surface tension by the following formula:

$$\gamma_1 = \frac{1}{2}W_{11} \tag{5.6}$$

For solids, γ_1 is often denoted by γ_S (or γ_{SV}), and for liquids, γ_1 is often denoted by γ_L (or γ_{LV}).

The work of adhesion W_{12} can also be described as the energy difference between the initial and the final state of separation. Dupree (1869) simplified Young's equation and combined the work of adhesion at the solid-liquid interface with interfacial energies, he obtained the following equation (Fig. 5.3 (d) and (e)):

$$\gamma_{12} = \frac{1}{2}W_{11} + \frac{1}{2}W_{22} - W_{12} = \gamma_1 + \gamma_2 - W_{12} \tag{5.7}$$

Note that since all media attract each other in a vacuum, W_{11} and W_{12} are always positive. According to Israelachvili (2010), the work of adhesion between two products A and B in a medium C is related to the process of building A-B agglomerates (adhesion of A and B alone) in a medium C (cohesion of C alone) against the solubilisation of A and B in C (work of adhesion of A and C, and B and C respectively). It has the following form:

$$W_{ACB} = W_{AB} + W_{CC} - W_{AC} - W_{BC} = \gamma_{AC} + \gamma_{BC} - \gamma_{AB} \tag{5.8}$$

Similarly, the work of cohesion of A in a medium C is given by:

$$W_{ACA} = W_{AA} + W_{CC} - 2W_{AC} \tag{5.9}$$

If $W_{ABC} < 0$, we have full spreading of medium 2 on medium 1, both separated in a medium 3.
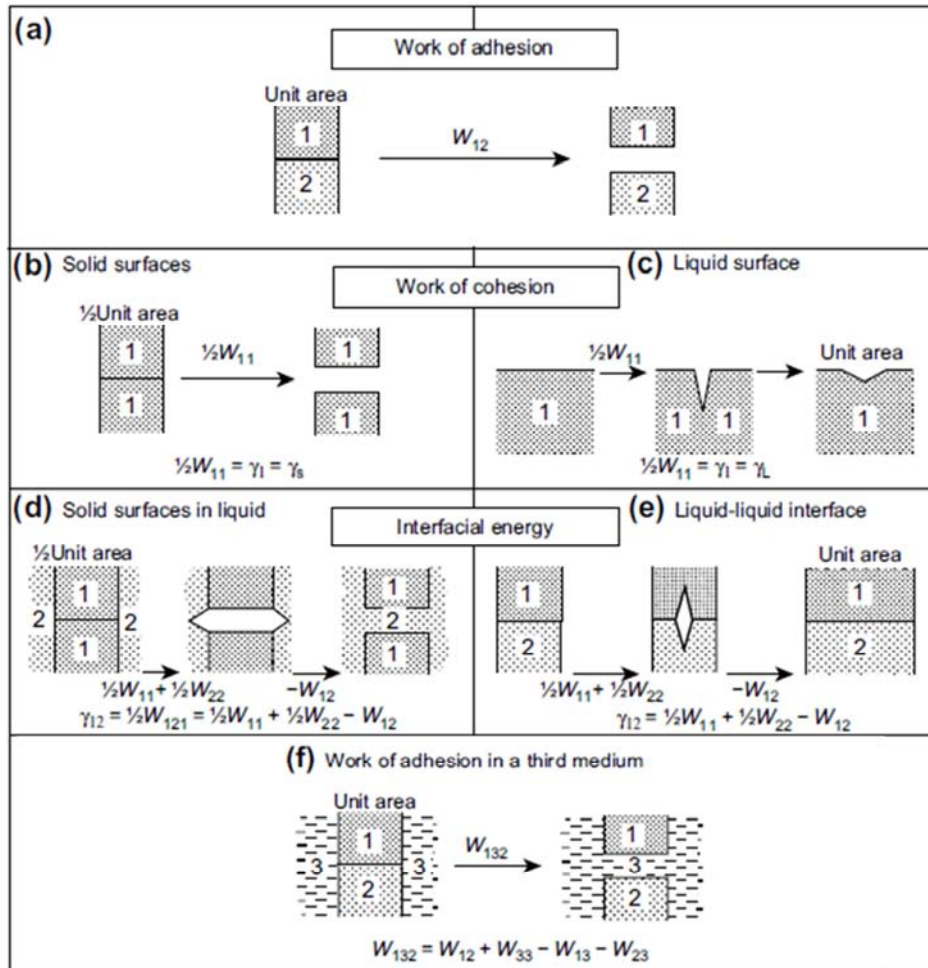
Fig. 5.3 – Definition of the work of adhesion and cohesion for solid and liquid surfaces in vaccum and in a third medium, Figure adapted from Israelachvili (2010).

As discussed in the article of Kinloch (1994), in most systems involving adhesion and cohesion, intimate molecular contact and active interactions are present. Van der Waals interactions for instance, lead not only to phenomena such as the cohesion of condensed phases, but also to universal forces of attraction between macroscopic bodies. In fact, phenomena such as surface tension, friction, viscosity, adhesion and cohesion, are related to vdW forces (Bhushan et al., 1995; Kim et al., 2008).

Girifalco and Good (1957) have expressed the work of adhesion in terms of the surface free energy of the pure phases by:

$$W_{AB} = 2\Phi_I \Phi_V (\gamma_A \gamma_B)^{1/2} \tag{5.10}$$

Here, Φ_I is a parameter that depends on the repulsive potential constants, γ_A and γ_B are the surface free energy of material A and material B respectively, Φ_V is a parameter that depends on the molar volume of the compounds. The full expression of this equation is given in Appendix D.

As stated by Wu (1973), the utility of this equation is limited, because Φ_I is an empirical parameter and its calculation remains questionable especially for polymers. A similar expression of the work of adhesion was then proposed by Wu (1973):

$$W_{AB} = 2\varphi_{AB} (\gamma_A \gamma_B)^{1/2} \tag{5.11}$$

where, φ_{AB} is a parameter that depends on the surface free energy and the molar volume of each compound. The full expression of Wu's equation is given in Appendix D.

However, this equation depends on the surface free energy which is obtained by time consuming experimental methods.

In this context, a relationship between solubility parameter and surface free energy was presented by Hildebrand in 1950:

$$\frac{\delta^2 v^{1/3}}{\gamma} = k \tag{5.12}$$

with v the molar volume.

In 1967, Gardon asserted in his treatise that this equation reasonably holds for a variety of materials for which he assumed that $k = 16$. This constant k varies only between certain limits according to the type of molecules (Barton, 1991) and should be constant for a variety of materials (Gardon, 1977).

We will use this relationship in section 3 to develop equations of the work of adhesion as a function of the Hildebrand solubility parameter which we can estimate using molecular simulation.

2.3. The ideal tensile strength

The work of adhesion and the ideal tensile strength involve the same force by which two materials attract each other when an attempt is made to separate them. Whereas the tensile strength divides this force by the cross section of the materials, the work of adhesion integrates this force through the distance between the materials. Gardon (1967) defined the tensile strength $\sigma_{AB}^{\max}$ as the maximum stress that can support the interface between two materials A and B. He related it to the work of adhesion between two materials (A and B) separated by a potential equilibrium distance d_{AB}^{0}:

$$\sigma_{AB}^{\max} = \frac{1.03 W_{AB}}{d_{AB}^{0}}$$

(5.13)

Gardon used the equation (5.10) proposed by Girifalco and Good (1957) into equation (5.12) and, by expressing the equilibrium distance d_{AB}^{0} as the distance between the neighboring spherical sites of material A and material B, he ended up with the ideal tensile strength equation in terms of the solubility parameter:

$$\sigma_{AB}^{\max} = 0.2452 \Phi_{I} \Phi_{V}^{3/2} \delta_{A} \delta_{B}$$

(5.14)

Here, $\sigma_{AB}^{\max}$ is in J.cm^{-3} and δ in (J.cm^{-3})$^{1/2}$. These equations take into consideration the parameter Φ_{V} which takes into account the different sizes of the interacting spherical sites.

Rowe (1988) aimed at finding an expression for the ideal tensile strength in terms of the solubility parameter. He started with Gardon's expression (equation (5.13)) to obtain the ideal tensile strength using the work of adhesion. Then, he used Hildebrand's equation (5.12) with a k value $k = 16$ to substitute the surface free energy by the Hildebrand solubility parameter in Wu's equation (5.11). He ended up with the following expression:

$$\sigma_{AA}^{\max} = 0.25 \delta_{A}^{2}, \ \sigma_{BB}^{\max} = 0.25 \delta_{B}^{2} \text{ and } \sigma_{AB}^{\max} = 0.25 \varphi_{AB} \delta_{A} \delta_{B} \quad \text{(J.cm}^{-3}\text{)}$$

(5.15)

where $\sigma_{AA}^{\max}$ and $\sigma_{BB}^{\max}$ are the ideal tensile strength for compound A and compound B respectively, $\sigma_{AB}^{\max}$ is the maximum adhesive tensile strength between A and B.

The application of Rowe's model to real systems was partially conclusive at first because of the inaccuracy of the solubility parameter calculation approach that mixed Hoy and Van Krevelen group contribution methods (Barra, 1998). Benali (2006) adopted the same model but, instead of the group contribution methods, he used molecular simulation to calculate the solubility parameter. This approach provided better prediction of binary systems affinity in accordance with experiments.

Furthermore, a closer examination of Rowe and Gardon's derivation shows two differences: the constant multiplier was approximated by Rowe from 0.2452 to 0.25. Furthermore, if we follow Rowe's derivation method from Gardon's (1967) expression, we should obtain the following formula for the ideal tensile strength which differ from Rowe's equation (5.15) by the factor Φ_V:

$$\sigma_{AB}^{\max} = 0.2452 \varphi_{AB} \delta_A \delta_B \Phi_V^{1/2} \qquad \text{(J.cm}^{-3}\text{)} \tag{5.16}$$

The two equations (5.14) and (5.16) are still based on the use of the constant $k = 16$ proposed by Gardon (1967). We will propose a more general expression in subsection 3.1.

3.   Affinity prediction model for binary and ternary mixtures

The previous equations of the work of adhesion and the ideal tensile strength are only relevant to binary systems. In, this section, we will generalize these equations to our selected materials, and we will extend the ideal tensile strength to ternary systems. The resulting equations are then used to predict the affinity between granulation materials in binary and ternary systems.

3.1. Generalization of the work of adhesion and tensile strength formula

Rowe recognized that his model (equation (5.15)) was oversimplified and did not have a general validity (Rowe, 1988). We have already mentioned that Rowe's derivation should lead to equation (5.16) where a factor $\Phi_V^{1/2}$ was omitted by Rowe. We can further generalize Rowe's equation by removing the assumption that $k = 16$: The appropriate choice of the factor k should depend on the compound of interest. Hence, if we consider the general form of Hildebrand relationship:

$$\delta = k'(\frac{\gamma}{v^{1/3}})^m \quad \text{or} \quad \delta^2 = k(\frac{\gamma}{v^{1/3}})^{2m}$$

(5.17)

where $k' = k^{1/2}$ and m are constants that depend on the type of material, γ in dynes.cm^{-1}, δ in (cal.cm^{-3})$^{0.5}$, v in cm^3.mol^{-1}. We obtain the general expressions of the ideal tensile strength:

$$\sigma_{AA}^{max} = 16.42(\frac{\delta_A}{k'_A})^{1/m_A}$$

(5.18)

$$\sigma_{BB}^{max} = 16.42(\frac{\delta_B}{k'_B})^{1/m_B}$$

(5.19)

$$\sigma_{AB}^{max} = 16.42 \varphi_{AB} \Phi_V^{1/2} (\frac{\delta_B}{k'_B})^{1/2m_B} (\frac{\delta_A}{k'_A})^{1/2m_A}$$

(5.20)

$$\varphi_{AB} = 2 \ \frac{x_A^d x_B^d}{g_A x_A^d + g_B x_B^d} + \frac{x_A^p x_B^p}{g_A x_A^p + g_B x_B^p}$$

(5.21)

with $x_i^d = (\frac{\delta_d}{\delta})^{1/m}$, $x_i^p = 1 - x_i^d$

(5.22)

$$g_A = \frac{\delta_A^{1/m_A} k_B'^{1/m_B} v_A^{1/3}}{\delta_B^{1/m_B} k_A'^{1/m_A} v_B^{1/3}} \text{ and } g_B = \frac{1}{g_A}$$

(5.23)

where σ_{AB}^{max} is in J.cm^{-3} and δ in cal$^{1/2}$.cm$^{-3/2}$, x_i^p and x_i^d are the polar and the nonpolar fraction of material i $(i = A \text{ or } B)$. We use equation (5.20) to calculate the adhesive tensile strength for binary mixtures. For the same material, we use equation (5.18) describing mutual cohesion. Here k' and m have to be determined for each type of material.

Following the same route of computation, the work of adhesion described by equation (5.11) becomes:

$$W_{AB} = 2\varphi_{AB} (\frac{\delta_A}{k'_A})^{1/2m_A} (\frac{\delta_B}{k'_B})^{1/2m_B} (v_A v_B)^{1/6}$$

(5.24)

where W_{AB} is in mJ.m^{-2}, δ in cal$^{1/2}$·cm$^{-3/2}$ and v in cm^{-3}·mol^{-1}.

3.2. Extension of the ideal tensile strength model to ternary systems

In this section, we extend the relationship (5.16) proposed by Gardon for the ideal tensile strength for a binary mixture in vacuum to ternary mixtures where the substrates are dispersed in a third medium.

By implementing the equation of work of adhesion in a third medium given by Israelachvili (2010) in the process of resolution followed by Gardon (1967), we derive the relationship between the total work of adhesion W_{ACB} and the ideal tensile strength σ_{ACB}^{max} in third medium, along with an expression of the equilibrium distance at zero potential energy d_{ACB}^0:

$$\sigma_{ACB}^{max} = \frac{1.0263\,W_{ACB}}{d_{ACB}^0} \quad (\text{J.cm}^{-3}) \tag{5.25}$$

$$d_{ACB}^0 = 0.629 * 10^{-8} \left(\frac{\sigma_{AB}^{max}(v_A^{1/3}+v_B^{1/3})^9 + \sigma_{CC}^{max}(2v_C^{1/3})^9 - \sigma_{AC}^{max}(v_A^{1/3}+v_C^{1/3})^9 - \sigma_{BC}^{max}(v_A^{1/3}+v_C^{1/3})^9}{\sigma_{AB}^{max}(v_A^{1/3}+v_B^{1/3})^3 + \sigma_{CC}^{max}(2v_C^{1/3})^3 - \sigma_{AC}^{max}(v_A^{1/3}+v_C^{1/3})^3 - \sigma_{BC}^{max}(v_B^{1/3}+v_C^{1/3})^3} \right)^{(1/6)} \tag{5.26}$$

The detailed demonstration is given in Appendix F.

Using equation (5.8), equation (5.25) can be rewritten as:

$$\sigma_{ACB}^{max} = \frac{1.0263(W_{AB}+W_{CC}-W_{AC}-W_{BC})}{d_{ACB}^0} = \frac{(d_{AB}^0\sigma_{AB}^{max}+d_{CC}^0\sigma_{CC}^{max}-d_{AC}^0\sigma_{AC}^{max}-d_{BC}^0\sigma_{BC}^{max})}{d_{ACB}^0} \tag{5.27}$$

Combining equation (5.26) and (5.27), we obtain:

$$\sigma_{ACB}^{max} = \frac{(\sigma_{AB}^{max}(v_A^{1/3}+v_B^{1/3})+2\sigma_{CC}^{max}(v_C^{1/3})-\sigma_{AC}^{max}(v_A^{1/3}+v_C^{1/3})-\sigma_{BC}^{max}(v_B^{1/3}+v_C^{1/3}))}{\left(\frac{\sigma_{AB}^{max}(v_A^{1/3}+v_B^{1/3})^9+\sigma_{CC}^{max}(2v_C^{1/3})^9-\sigma_{AC}^{max}(v_A^{1/3}+v_C^{1/3})^9-\sigma_{BC}^{max}(v_A^{1/3}+v_C^{1/3})^9}{\sigma_{AB}^{max}(v_A^{1/3}+v_B^{1/3})^3+\sigma_{CC}^{max}(2v_C^{1/3})^3-\sigma_{AC}^{max}(v_A^{1/3}+v_C^{1/3})^3-\sigma_{BC}^{max}(v_B^{1/3}+v_C^{1/3})^3}\right)^{(1/6)}} \tag{5.28}$$

According to equation (5.25), the ideal tensile strength σ_{ACB}^{max} is proportional to the work of adhesion W_{ACB}, thus, by analogy with the conclusions of Barra (1998) and Benali (2006), we can state that in a ternary system (see also Fig. 5.4):

- If $\sigma_{ACB}^{max} > 0$: one of the compounds is partially spread over the other, and C (water for example) does not spread between A and B,

- If $\sigma_{ACB}^{max} < 0$: Medium C will displace compound B and "spread on " or "totally wet" the surface of A,

- If $\sigma_{ACB}^{max} < \sigma_{ACA}^{max} < \sigma_{BCB}^{max}$: both compounds tend to mix,

- If $\sigma_{ACA}^{max} < \sigma_{ACB}^{max} < \sigma_{BCB}^{max}$: compound A will surround compound B in solvent C,

- If $\sigma_{BCB}^{max} < \sigma_{ACB}^{max} < \sigma_{ACA}^{max}$: compound B will surround compound A in solvent C.
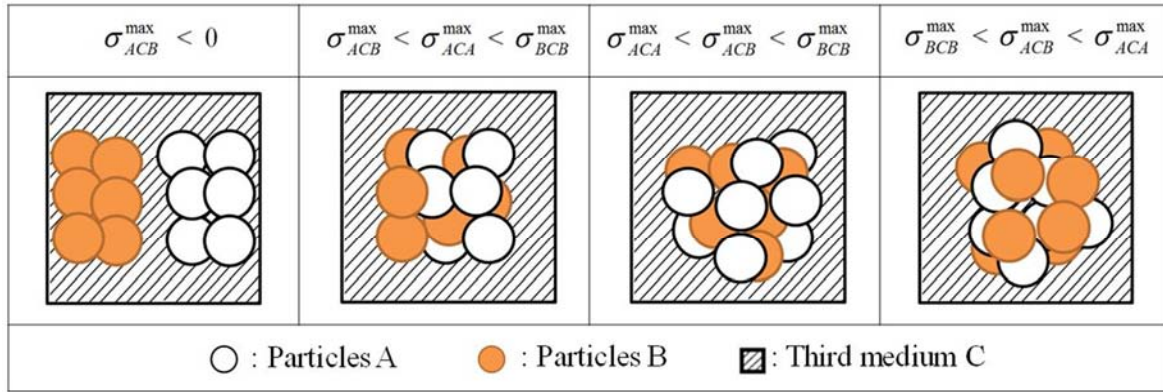
Fig. 5.4 – Interactions predicted between particles A and particles B in a third medium C based on the tensile strength approach.

The same predictions were stated by Israelachvili (2010) but in terms of the work of adhesion of two compounds placed in a third medium.

4. Model application and discussion

Before applying the above equations to predict the affinity in binary and ternary systems, we establish a correlation between δ and the experimental surface tension γ for cellulose derivative (such as HPMC and Ethyl cellulose). The solubility parameters are calculated using molecular simulation with the COMPASSII forcefield (see chapter 4).

4.1. Relationship between solubility parameter and surface free energy for cellulose derivatives

For computing the work of adhesion (equation (5.24)), we need to select constants k' and m that come from equation (5.17). Hildebrand (1950) used $k' = 4.1$ and $m = 0.43$ when δ is in $cal^{1/2}cm^{-3/2}$. Gardon (1967) proposed $k = 16$ ($k' = 4$) and $m = 0.5$ for organic acids and molten metals, which gave an error on the ideal tensile strength usually below 25% for the systems he studied. For water he proposed ($k' = 4.376$) and $m = 0.5$. From simple statistical thermodynamic considerations, Bonn and van Aartsen (1972) related the solubility of polymers to the surface tension and obtained $k = 11.5$ ($k' = 3.39$) by regression analysis. For compounds which do not contain OH, COOH and a COH groups, Sheldon et al. (2005) proposed $k = 14.0$ ($k' = 3.74$) with $m = 1$, and $k = 35.13$ ($k' = 5.927$) with $m = 0.45$ otherwise:

$$\delta^2 = \begin{cases} 14\gamma / v^{1/3} & if \quad nOH + nCOOH + nCOH = 0 \\ \\ 35.13\gamma / v^{0.45} & otherwise \end{cases}$$

(5.29)

For cellulose polymers, we regress an expression by using the Hildebrand solubility parameter values over the data of 5 compounds; MCC, HPMC, EC, CA and NC. The theoretical best fit line is shown in Fig. 5.5.

The following expression was obtained:

$$\delta = 4.00 \left(\gamma / v^{1/3}\right)^{0.59} \qquad\qquad (\text{cal.cm}^{-3})^{1/2}$$

(5.30)
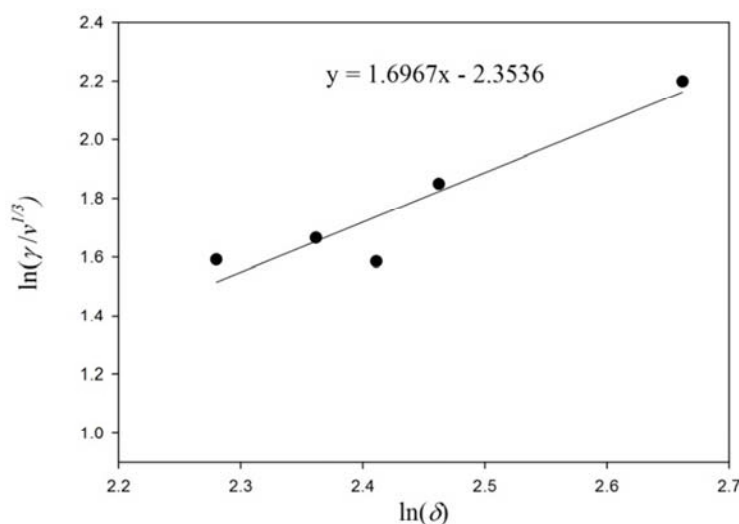
Fig. 5.5 – Logarithm of the ratio $\gamma/v^{1/3}$ plotted against the logarithm of the Hildebrand solubility parameters δ. δ in $(\text{cal.cm}^{-3})^{1/2}$ and surface tension γ in mJ.m^{-2}. γ and δ of celluloses derivatives are obtained from literature

Table 5.1 collects the prediction of the work of cohesion calculated using the various correlations cited above and compares them with the experimental values of the work of cohesion $W_{AA} = 2\gamma$ (for when A = B). The solubility parameter in the correlations is obtained by molecular simulation using the COMPASSII forcefield (see chapter 4).

In Table 5.1, the results obtained using equation (5.30) are close to the experimental values for MCC, HPMC, EC and PEG. Gardon's (1977, 1967) correlation is close to the experimental values for acids and water. For PVP, Bonn's (1972) correlation is the closest. Therefore, we select the corresponding best fit values: $k' = 4$ for acids, $k' = 3.39$ for PVP, $k' = 4.376$ for water, and equation (5.30) for the celluloses derivatives and PEG.

Table 5.1 – Work of cohesion in mJ.m^{-2} calculated using different correlations

	Solubility parameter (J.cm^{-3})$^{1/2}$		Cohesion work W_{AA} (mJ.m^{-2})					
	COMPASSII		Gardon[1977, 1967] $k'=4$ $m=0.5$ $k'=4.38$ *	Hildebrand[1950] $k'=4.1$ $m=0.43$	Sheldon[2005] Eq. (5.29) $k'=5.93$ $m=0.45$	Bonn[1972] $k'=3.39$ $m=0.5$	This work Eq. (5.30) $k'=4$ $m=0.59$	$W_{AA}= 2\gamma$ Exp.**
	δ	δ_d						
PVP	21.12	19.45	59.75	76.82	30.75	83.19	44.86	107.2
MCC	29.98	17.04	158.01	227.69	87.90	219.99	106.73	106.2
HPMC	20.68	17.03	89.01	113.65	45.59	123.92	67.26	68.0
EC	19.61	18.73	83.75	105.10	42.40	116.60	64.31	71.6
NA	25.40	21.97	108.96	148.76	58.42	151.70	77.38	91.8
SA	18.61	16.75	71.89	88.70	35.97	100.09	56.09	-
PEG200	26.54	19.27	117.05	162.10	63.38	162.97	82.03	93.4
PEG400	22.88	20.17	110.55	145.87	57.91	153.91	81.02	-
Water	47.33$	5.89$	175.48	293.39	108.05	244.32	103.25	144.0

PVP: Polyvinylpyrrolidone, MCC: Microcrystalline cellulose, HPMC: Hydroxypropyl-methylcellulose, EC: Ethyl cellulose, NA: Niflumic acid, SA: Stearic acid, PEG : Polyethylene glycol.

*Only for water, ** Calculated using the experimental interfacial tension γ given in Table 2.2, $ PCFF forcefield

4.2. Prediction of the interactions in binary mixture

By using the k' and m values in equation (5.24) where the solubility parameter δ occurs, we calculate the work of adhesion and cohesion in a binary system. The results obtained by molecular simulations and by Yamamoto's molecular breaking method (HSPiP, 2010) are presented in Table 5.2 and Table 5.3 respectively.

Table 5.2 – Cohesion work (diagonal) and adhesion work in mJ.m^{-2} in the binary mixture calculated using the solubility parameter obtained from COMPASSII forcefiled.

Compounds	PVP	MCC	HPMC	EC	NA	SA	PEG200	PEG400
PVP	83.19							
MCC	72.85	106.73						
HPMC	66.87	69.40	67.26					
EC	64.95	56.39	61.05	64.31				
NA	90.58	91.02	68.21	63.14	108.96			
SA	76.32	70.78	66.11	63.00	81.00	71.89		
PEG200	73.29	87.10	71.39	60.92	81.62	71.71	82.03	
PEG400	79.51	74.53	71.79	68.46	82.52	75.96	76.60	81.02

PVP: Polyvinylpyrrolidone, MCC: Microcrystalline cellulose, HPMC: Hydroxypropyl-methylcellulose, EC: Ethyl cellulose, NA: Niflumic acid, SA: Stearic acid, PEG: Polyethylene glycol.

Table 5.3 – Cohesion work (diagonal) and adhesion work in mJ.m^{-2} in the binary mixture calculated using the solubility parameter obtained from HSPiP method.

Compounds	PVP	MCC	HPMC	EC	NA	SA	PEG200	PEG400
PVP	83.82							
MCC	84.33	102.06						
HPMC	65.97	68.66	64.63					
EC	61.03	61.97	61.65	59.87				
NA	82.32	82.02	65.77	61.10	81.00			
SA	69.15	65.91	61.50	59.14	68.82	63.57		
PEG200	67.36	79.83	63.25	57.87	66.27	56.63	71.12	
PEG400	59.60	65.96	60.61	57.08	59.31	54.63	62.68	59.10

PVP: Polyvinylpyrrolidone, MCC: Microcrystalline cellulose, HPMC: Hydroxypropyl-methylcellulose, EC: Ethyl cellulose, NA: Niflumic acid, SA: Stearic acid, PEG: Polyethylene glycol.

We can also calculate the ideal tensile strength in binary mixtures by using equation (5.20). The ideal tensile strength values obtained with δ computed by molecular simulation are shown in Table 5.6, and those obtained using the Yamamoto's molecular breaking method (HSPiP, 2010) are presented in Table 5.7.

By comparing the adhesion and cohesion work values (Tables 5.2 and 5.3) and the ideal tensile strength results (Tables 5.4 and 5.5), we predict the affinity between the different compounds (Tables 5.6,5.7, 5.8 and 5.9). The adhesive and the tensile approach being derived from the same core show similar predictions.

Table 5.4 – The ideal tensile strength in binary mixtures in J.cm^{-3} calculated using the solubility parameter obtained from COMPASSII forcefiled

Compounds	PVP	MCC	HPMC	EC	NA	SA	PEG200	PEG400
PVP	152.07							
MCC	115.18	148.66						
HPMC	95.73	88.53	79.14					
EC	90.44	70.17	70.20	72.31				
NA	146.48	129.32	88.60	79.97	157.98			
SA	109.45	90.42	77.88	72.54	105.37	84.81		
PEG200	119.59	124.73	93.41	77.71	119.30	93.97	120.87	
PEG400	112.84	94.33	83.85	78.16	106.34	88.84	99.42	93.96

PVP: Polyvinylpyrrolidone, MCC: Microcrystalline cellulose, HPMC: Hydroxypropyl-methylcellulose, EC: Ethyl cellulose, NA: Niflumic acid, SA: Stearic acid, PEG: Polyethylene glycol.

Table 5.5 – The ideal tensile strength in binary mixtures in J.cm^{-3} calculated using the solubility parameter obtained from HSPiP method.

Compounds	PVP	MCC	HPMC	EC	NA	SA	PEG200	PEG400
PVP	153.23							
MCC	133.34	142.16						
HPMC	94.45	87.58	76.04					
EC	84.98	77.11	70.89	67.31				
NA	133.13	116.54	85.44	77.38	117.45			
SA	99.15	84.20	72.46	68.09	89.52	74.99		
PEG200	109.92	114.33	82.77	73.82	96.87	74.21	104.80	
PEG400	84.58	83.48	70.79	65.17	76.43	63.90	81.35	68.53

PVP: Polyvinylpyrrolidone, MCC: Microcrystalline cellulose, HPMC: Hydroxypropyl-methylcellulose, EC: Ethyl cellulose, NA: Niflumic acid, SA: Stearic acid, PEG: Polyethylene glycol.

Table 5.6 – Interactions predicted for PVP and MCC

B / A	PVP						MCC				
	exp. obs.	W_{AB} exp.	W_{AB} HSPiP	σ_{AB} HSPiP	W_{AB} compassII	σ_{AB} compassII	exp. obs.	W_{AB} exp.	W_{AB} HSPiP	σ_{AB} HSPiP	W_{AB} compassII	σ_{AB} compassII
PVP	-	-	-	-	-	-		M	O	M	M	M
MCC		M	X	M	M	M	-	-	-	-	-	-
HPMC		O	O	O	M	O	O[a]	O	O	O	O	O
EC		O	O	O	O	O		O	O	O	M	M
NA		O	O	O	X	M		M	O	M	M	M
SA			O	O	O	O			O	O	M	O
PEG200		M	M	O	M	M		O	O	O	O	O
PEG400			O	O	M	O			O	O	M	O

PVP: Polyvinylpyrrolidone, MCC: Microcrystalline cellulose, HPMC: Hydroxypropyl-methylcellulose, EC: Ethyl cellulose, NA: Niflumic acid, SA: Stearic acid, PEG: Polyethylene glycol.

O: A surrounds B, X: B surrounds A, M: Bad affinity.

a: Benali, 2006.

Table 5.7 – Interactions predicted for HPMC and EC

B / A	HPMC						EC				
	exp. obs.	W_{AB} exp.	W_{AB} HSPiP	σ_{AB} HSPiP	W_{AB} compassII	σ_{AB} compassII	exp. obs.	W_{AB} exp.	W_{AB} HSPiP	σ_{AB} HSPiP	W_{AB} compassII	σ_{AB} compassII
PVP		X	X	X	M	X		X	X	X	X	X
MCC	X[a]	X	X	X	X	X		X	X	X	M	M
HPMC	-	-	-	-	-	-	M[b]	M	X	X	M	M
EC	M[b]	M	O	O	M	M	-	-	-	-	-	-
NA	X[b]	X	X	X	X	X	M[b]	X	X	X	M	X
SA			M	M	M	M		M	X	M	X
PEG200	X[c]	M	M	X	X	X		M	M	X	M	X
PEG400			O	O	X	X		M	M	X	X

PVP: Polyvinylpyrrolidone, MCC: Microcrystalline cellulose, HPMC: Hydroxypropyl-methylcellulose, EC: Ethyl cellulose, NA: Niflumic acid, SA: Stearic acid, PEG: Polyethylene glycol.

O: A surrounds B, X: B surrounds A, M: Bad affinity.

a: Benali 2006, b: Barra 1998, c: Laboulfie 2013.

Table 5.8 – Interactions predicted for NA and SA

A \ B	NA						SA					
	exp. obs.	W_{AB} exp.	W_{AB} HSPiP	σ_{AB} HSPiP	W_{AB} compassII	σ_{AB} compassII	exp. obs.	W_{AB} exp.	W_{AB} HSPiP	σ_{AB} HSPiP	W_{AB} compassII	σ_{AB} compassII
PVP		X	X	X	O	M			X	X	X	X
MCC		M	X	M	M	M			X	X	M	X
HPMC	O[a]	O	O	O	O	O			M	M	M	M
EC	M[a]	O	O	O	M	O			M	O	M	O
NA	-	-	-	-	-	-			X	X	X	X
SA			O	O	O	O	-	-	-	-	-	-
PEG200		M	M	M	M	M	M[b]		M	M	M	X
PEG400			O	O	O	O			M	M	X	X

PVP: Polyvinylpyrrolidone, MCC: Microcrystalline cellulose, HPMC: Hydroxypropyl-methylcellulose, EC: Ethyl cellulose, NA: Niflumic acid, SA: Stearic acid, PEG: Polyethylene glycol.
O: A surrounds B, X: B surrounds A, M: Bad affinity.
a: Barra 1998, b: Laboulfie 2013.

Table 5.9 – Interactions predicted for PEG200 and PEG400

A \ B	PEG200						PEG400					
	exp. obs.	W_{AB} exp.	W_{AB} HSPiP	σ_{AB} HSPiP	W_{AB} compassII	σ_{AB} compassII	exp. obs.	W_{AB} exp.	W_{AB} HSPiP	σ_{AB} HSPiP	W_{AB} compassII	σ_{AB} compassII
PVP		M	M	X	M	M			X	X	M	X
MCC		X	X	X	X	X			X	X	M	X
HPMC	O[a]	M	M	O	O	O			X	X	O	O
EC		M	M	O	M	O			M	M	O	O
NA		M	M	M	M	M			X	X	X	X
SA	M[a]		M	M	M	O			M	M	O	O
PEG200	-	-	-	-	-	-			X	X	M	X
PEG400			O	O	M	O	-	-	-	-	-	-

PVP: Polyvinylpyrrolidone, MCC: Microcrystalline cellulose, HPMC: Hydroxypropyl-methylcellulose, EC: Ethyl cellulose, NA: Niflumic acid, SA: Stearic acid, PEG: Polyethylene glycol.
O: A surrounds B, X: B surrounds A, M: Bad affinity.
a: Laboulfie 2013.

In all cases, we have $W_{HPMC-HPMC} < W_{HPMC-NA} < W_{NA-NA}$, this means that HPMC will adhere over the particles of NA. Moreover, as first observed experimentally by Barra (1998), and recently reviewed by Benali (2006), HPMC particles surround NA particles.

According to the work of adhesion predictions obtained on the basis of molecular simulation, the particles of EC interact neither with NA nor with HPMC (Table 5.7). This was also observed by Barra (1998). However, the tensile approach predicts that the particles of EC tend to adhere over the particles of NA (Table 5.7). This suggests that the adhesion approach gives more accurate predictions than the tensile approach. It's worth mentioning here that Barra observed also a low interaction between NA and EC for medium sized particles, where EC tends to adhere over the particle of NA, which may explain the disagreement between the predictions obtained with the adhesion approach and those obtained with the tensile strength approach in the case of the couple EC-NA.

Moreover, the predictive results based upon both approach (tensile strength and work of adhesion approach) indicate that HPMC would be a good binder for MCC substrate (Table 5.7) and consequently will produce rigid agglomerates. In their work on the interactions between HPMC and MCC, Benali (2006) and Lovorka and Graham (1990) arrived to the same conclusion.

However, no interactions are observed in the case of HPMC-SA mixture which may results in friable agglomerate or coating film. To improve the properties of this mixture, one way is to add another compound compatible with SA and HPMC. Predictions obtained using molecular simulation show good affinity between PEG400 and both HPMC and SA (see Table 5.9). One could suspect that the addition of PEG400 to the SA-HPMC mixture should indirectly improve the consistency of the resulting agglomerate. This actually corresponds to the conclusions of Laboulfie et al. (2013) where they stated that adding PEG to the HPMC-SA mixture will enhance the mechanical properties of the resulting composite coating.

In the light of the previous analyses, we conclude that the predictions obtained on the basis of molecular simulation calculations reproduce the available experimental observations, especially in the case of the adhesion work approach.

4.3. Prediction of the interactions in aqueous system: dispersion of substrate in a third medium

The work of adhesion and cohesion of different polymers and acids placed in water are calculated using the Israelachivili's relationships (5.8) and (5.9). The results based upon molecular simulation are presented in Table 5.10, and those obtained using the Yamamoto's molecular breaking method (HSPiP, 2010) are presented in Table 5.11.

Table 5.10 – Cohesion work (diagonal) and adhesion work in mJ.m^{-2} of the compounds dispersed in water, calculated using the solubility parameter obtained from COMPASSII and PCFF forcefileds.

Compounds	PVP	MCC	HPMC	EC	NA	SA	PEG200	PEG400
PVP	181.54							
MCC	114.68	92.04						
HPMC	162.00	108.01	159.17					
EC	174.51	109.43	167.39	185.08				
NA	166.24	110.16	140.65	150.01	161.93			
SA	174.22	112.16	160.79	172.11	156.21	169.34		
PEG200	150.65	107.94	145.53	149.49	136.29	148.62	138.40	
PEG400	176.76	115.26	165.82	176.92	157.08	172.76	152.86	177.17

PVP: Polyvinylpyrrolidone, MCC: Microcrystalline cellulose, HPMC: Hydroxypropyl-methylcellulose, EC: Ethyl cellulose, NA: Niflumic acid, SA: Stearic acid, PEG : Polyethylene glycol.

Table 5.11 – Cohesion work (diagonal) and adhesion work in mJ.m^{-2} of the compounds dispersed in water, calculated using the solubility parameter obtained from HSPiP.

Compounds	PVP	MCC	HPMC	EC	NA	SA	PEG200	PEG400
PVP	119.55							
MCC	88.89	75.45						
HPMC	114.55	86.07	126.06					
EC	115.06	84.83	128.53	132.20				
NA	120.80	89.33	117.10	117.88	122.23			
SA	122.11	87.70	127.31	130.40	124.53	133.76		
PEG200	100.45	81.75	109.19	109.26	102.11	106.95	101.57	
PEG400	107.68	82.87	121.54	123.46	110.14	119.94	108.12	119.53

PVP: Polyvinylpyrrolidone, MCC: Microcrystalline cellulose, HPMC: Hydroxypropyl-methylcellulose, EC: Ethyl cellulose, NA: Niflumic acid, SA: Stearic acid, PEG : Polyethylene glycol.

Table 5.12 – The ideal tensile strength in ternary mixtures in J.cm^{-3} of the compounds dispersed in water, calculated using the solubility parameter obtained from COMPASSII and PCFF forcefileds.

Compounds	PVP	MCC	HPMC	EC	NA	SA	PEG200	PEG400
PVP	347.85							
MCC	174.82	115.83						
HPMC	237.51	129.15	186.14					
EC	251.79	129.36	194.13	212.39				
NA	272.13	146.06	179.71	190.08	230.28			
SA	255.73	135.19	188.86	200.41	201.09	199.8		
PEG200	250.37	144.06	188.00	191.34	194.47	192.97	199.70	
PEG400	256.15	138.00	192.88	203.80	200.10	201.82	196.44	204.99

PVP: Polyvinylpyrrolidone, MCC: Microcrystalline cellulose, HPMC: Hydroxypropyl-methylcellulose, EC: Ethyl cellulose, NA: Niflumic acid, SA: Stearic acid, PEG : Polyethylene glycol.

Table 5.13 – The ideal tensile strength in ternary mixtures in J.cm^{-3} of the compounds dispersed in water, calculated using the solubility parameter obtained from HSPiP method

Compounds	PVP	MCC	HPMC	EC	NA	SA	PEG200	PEG400
PVP	216.01							
MCC	128.03	91.87						
HPMC	158.70	97.75	140.85					
EC	155.78	93.73	140.93	142.42				
NA	189.93	114.04	144.22	142.08	169.4			
SA	171.04	100.22	143.06	143.87	155.25	151.84		
PEG200	156.50	103.41	134.05	131.13	139.39	131.57	139.40	
PEG400	146.84	92.52	133.99	133.52	133.24	132.52	131.31	130.34

PVP: Polyvinylpyrrolidone, MCC: Microcrystalline cellulose, HPMC: Hydroxypropyl-methylcellulose, EC: Ethyl cellulose, NA: Niflumic acid, SA: Stearic acid, PEG : Polyethylene glycol.

We notice that the work of adhesion is positive for all the materials. Following Israelachvili's (2010) conclusions, all the compounds should agglomerate in water; furthermore, the water doesn't

penetrate between the compounds, which means that there is a spreading of one of the compounds over the other, or that the two compounds will self-associate in water without interacting. This can be explained by the high cohesive energy between water molecules, i.e. the interactions between them are much more attractive than their attraction with the other molecules.

The ideal tensile strength in ternary mixtures is calculated by using equation (5.28). The results based upon molecular simulation are presented in Table 5.12 and those obtained using the Yamamoto's molecular breaking method (HSPiP, 2010) are presented in Table 5.13.

First, we notice that the cohesion and adhesion work in water obtained using the HSPiP data are much smaller than those obtained with COMPASSII and PCFF forcefield data. We state that this happens because the PCFF forcefield underestimates the dispersive contribution of the solubility parameter of water compared to HSPiP (see Table 4.1 in chapter 4).

Regarding the prediction of affinity, for all methods, MCC has the lowest work of adhesion and cohesion in water, this imply that, for all the mixtures, MCC will most likely adhere on the surface of the other compounds when they are dispersed in water.

The magnitude of interaction and therefore the affinity between compound A and compound B in a medium C is proportional to minus W_{BAC} ($W_{BAC} = W_{ACA} - W_{ACB}$). This also means that, in the presence of water, if minus W_{BAC} is high, the film formed in the surface of the stronger cohesive material will be thicker; this is identified in the case of the couple MCC-EC where minus $W_{MCC-EC-Water}$ is the highest (Table 5.10).

On the basis of the previous Tables (Table 5.10, 5.11, 5.12 and 5.13), we can predict the affinity of our ternary systems (Table 5.14, 5.15, 5.16 and 5.17).

Table 5.14 – Interactions predicted for PVP and MCC

A \ B	PVP				MCC			
	W_{ACB} CompassII	σ_{ACB} CompassII	W_{ACB} HSPiP	σ_{ACB} HSPiP	W_{ACB} CompassII	σ_{ACB} CompassII	W_{ACB} HSPiP	σ_{ACB} HSPiP
PVP	-	-	-	-	X	X	X	X
MCC	O	O	O	O	-	-	-	-
HPMC	O	O	M	O	X	X	X	X
EC	M	O	M	O	X	X	X	X
NA	O	O	X	O	X	X	X	X
SA	O	O	X	O	X	X	X	X
PEG200	O	O	M	O	X	X	X	X
PEG400	M	X	M	O	X	X	X	X

PVP: Polyvinylpyrrolidone, MCC: Microcrystalline cellulose, HPMC: Hydroxypropyl-methylcellulose, EC: Ethyl cellulose, NA: Niflumic acid, SA: Stearic acid, PEG : Polyethylene glycol.
O: A surrounds B, X: B surrounds A, M: A and B tend to mix.

Table 5.15 – Interactions predicted for HPMC and EC

A \ B	HPMC				EC			
	W_{ACB} CompassII	σ_{ACB} CompassII	W_{ACB} HSPiP	σ_{ACB} HSPiP	W_{ACB} CompassII	σ_{ACB} CompassII	W_{ACB} HSPiP	σ_{ACB} HSPiP
PVP	X	X	M	X	M	X	M	X
MCC	O	O	O	O	O	O	O	O
HPMC	-	-	-	-	O	O	O	O
EC	X	X	X	X	-	-	-	-
NA	M	M	M	X	M	M	M	M
SA	X	X	X	X	O	O	M	X
PEG200	O	X	O	M	O	M	O	M
PEG400	X	X	O	O	M	M	O	O

PVP: Polyvinylpyrrolidone, MCC: Microcrystalline cellulose, HPMC: Hydroxypropyl-methylcellulose, EC: Ethyl cellulose, NA: Niflumic acid, SA: Stearic acid, PEG : Polyethylene glycol.

O: A surrounds B, X: B surrounds A, M: A and B tend to mix.

Table 5.16 – Interactions predicted for NA and SA

A \ B	NA				SA			
	W_{ACB} CompassII	σ_{ACB} CompassII	W_{ACB} HSPiP	σ_{ACB} HSPiP	W_{ACB} CompassII	σ_{ACB} CompassII	W_{ACB} HSPiP	σ_{ACB} HSPiP
PVP	X	X	O	X	X	X	O	X
MCC	O	O	O	O	O	O	O	O
HPMC	M	M	M	O	O	O	O	O
EC	M	M	M	M	X	X	M	O
NA	-	-	-	-	M	X	O	X
SA	M	O	X	O	-	-	-	-
PEG200	M	M	O	M	O	M	O	M
PEG400	M	M	M	O	X	X	O	O

PVP: Polyvinylpyrrolidone, MCC: Microcrystalline cellulose, HPMC: Hydroxypropyl-methylcellulose, EC: Ethyl cellulose, NA: Niflumic acid, SA: Stearic acid, PEG : Polyethylene glycol.

O: A surrounds B, X: B surrounds A, M: A and B tend to mix.

Table 5.17 – Interactions predicted for PEG200 and PEG400

A \ B	PEG200				PEG400			
	W_{ACB} CompassII	σ_{ACB} CompassII	W_{ACB} HSPiP	σ_{ACB} HSPiP	W_{ACB} CompassII	σ_{ACB} CompassII	W_{ACB} HSPiP	σ_{ACB} HSPiP
PVP	X	X	M	X	M	O	M	X
MCC	O	O	O	O	O	O	O	O
HPMC	X	O	X	M	O	O	X	X
EC	X	M	X	M	M	M	X	X
NA	M	M	X	M	M	M	M	X
SA	X	M	X	M	O	O	X	X
PEG200	-	-	-	-	O	M	O	X
PEG400	X	M	X	O	-	-	-	-

PVP: Polyvinylpyrrolidone, MCC: Microcrystalline cellulose, HPMC: Hydroxypropyl-methylcellulose, EC: Ethyl cellulose, NA: Niflumic acid, SA: Stearic acid, PEG : Polyethylene glycol.

O: A surrounds B, X: B surrounds A, M: A and B tend to mix.

Although they differ from the type of input data that they use (HSPiP vs COMPASSII/PCFF forcefield), both solubility parameter calculation methods tend to give similar affinity predictions.

Overall, the affinities, obtained through the ideal tensile strength and the work of adhesion based upon molecular simulation, are similar in 75% of the systems.

As expected, because of their low cohesion strength in water, MCC molecules surround the other compounds (Table 5.14). This also can be explained by the high hydrophilic character of the MCC.

Also, in the case of HPMC-SA, whereas no interactions are observed between SA and HPMC in absence of water (Table 5.7), HPMC will adhere on the surface of SA (Table 5.15) when they are placed in water. It's a rather foreseeable result, since HPMC is a hydrophilic polymer and SA is a hydrophobic acid. In practice, a clear solution is obtained by dispersing HPMC in water, whereas, a white colored solution is obtained for HPMC-SA mixture in water. As explained by Laboulfie (2013), HPMC will generate a repulsive force on the surface of SA which will stabilize the mixture and prevent the agglomeration of SA particles, thus explaining the behavior that we sketched in Fig. 3.3 of chapter 3 and the experimental SEM observation of chapter 3.

The same conclusions are obtained for the couple HPMC-EC: HPMC will surround the hydrophobic particles of EC.

According to the tensile approach calculated using molecular simulation, there is no interactions between SA and PEG200 nor between EC and PEG200 (Table 5.17). In the other hand, the adhesion approach predicts that PEG200 will adhere over SA and over EC when placed in water which is in accordance with the fact that PEG200 is a hydrophilic polymer and SA and EC are both hydrophobic.

These conclusions lead to the suggestion that the work of adhesion approach may give better predictions than the tensile strength approach. Furthermore, the polarity of PEG400 is lower than that of PEG200, which means that PEG400 is less hydrophobic than PEG200. This was actually observed by Oelmeier et al. (2012) who stated that PEG with higher molecular weight have lower polarity and hence are less hydrophilic. This implies that, as we shift from PEG200 to PEG400, HPMC particles should surround PEG, and, as shown in Table 5.15, this is predicted by the work of adhesion approach. This was also observed experimentally by Laboulfie (2013) for PEG1500. Additionally, the adhesion work approach predicts that PEG200 surrounds PEG400 which is in adequacy with the previous statements.

5. Conclusion

In this chapter, two approaches to predict the affinity between polymers and acid in binary mixture were analyzed and compared; the tensile strength approach and the work of adhesion approach. To extend the study to any compounds used in coating and granulation processes, the work of adhesion and the tensile strength formula were generalized with the inclusion of Hildebrand's solubility parameter. A correlation between surface free energy and solubility parameter for cellulose derivative was proposed. It yielded values for the work of cohesion in good agreement with those measured.

In the case of a ternary mixture, we derived an equation for the ideal tensile strength. This equation hints at which compound would predominantly surround the other in ternary mixtures.

The two models were applied to binary and ternary systems. The binary mixtures included a film forming polymer (HPMC), a hydrophobic filler (SA), a plasticizer (PEG), a binder/diluant (EC and MCC) and a pharmaceutical drug (NA). In ternary systems, water was added as a solvent to the previous mixtures. The two models gave similar results in good agreement with the available experimental observations overall, but the work of adhesion approach might give more accurate predictions than the ideal tensile strength approach. The prediction obtained using the work of adhesion confirmed the experimental observations of Laboulfie et al. (2013): SA particles are stabilized by HPMC particles in water. Also, the addition of PEG400 to the mixture holds the SA and HPMC particles together and consequently enhance the consistency of the formed hydrophobic film. The affinity between particles in aqueous systems is better when their interfacial nature is the opposite (i.e. hydrophobicity and hydrophilicity).

The work of adhesion model in dry systems does not take into consideration the effect of particle size which influences the affinity and organization of the agglomerate; hence, in chapter 7, we will develop affinity predictive approaches that take into account the particle size of the interacting particles. But before that, in the next chapter, we will further investigate the interaction of particles in a medium and the structure of colloidal particles that composes the coating (or binder) using DPD simulations.

In Appendix M, we further study the affinity between the materials by using the Hamaker constant and the work of adhesion equations, and we present approaches that we have developed to predict the affinity, in dry system, between particles of different sizes.

Chapter 6

Dissipative particle dynamics simulation of composite coating solutions

1. Introduction

In this chapter, we used mesoscale simulations to investigate the structure of agglomerates formed in aqueous colloidal formulations used in coating and granulation processes. The formulations include water, a film forming polymer (Hydroxypropyl-methylcellulose, HPMC), a hydrophobic filler (Stearic acid, SA) and a plasticizer (Polyethylene glycol, PEG). A good coating solution should, a) be stable, i.e. the particle of hydrophobic filler remain dispersed and small in size b) contain plasticizers compatible with the film forming polymer.

Typically, factors that can be used to determine the stability of the coating solutions are the diffusivity coefficient, the structure factor, adsorption strength and the surface coverage between the stabilizing agent and the dispersed particles. Some of this information can be brought by molecular simulations. Considering that the agglomerate materials we are studying have a size between 0.1 and 100 μm, it is relevant to perform the simulation at the mesocale level where molecules are represented as polyatomic beads. As the number of degrees of freedom is reduced compared to all-atom simulations, the computational effort is decreased.

In this chapter, we perform mesoscale simulations using the dissipative particle dynamics (DPD) method to investigate the structure of colloidal polymeric dispersions and the affinity between polymers in aqueous systems. We begin by reviewing the principles of the DPD method and of the coarse-grain modeling. Then, we build a coarse grain-model and we describe the DPD approach applied to systems made of polymers (HPMC, polyvinylpyrrolidone (PVP) and microcrystalline cellulose (MCC)) in the presence of a plasticizer (PEG) or a hydrophobic filler (SA) in aqueous

systems. Finally, we present the results. Interfacial energy of each compound is calculated via DPD simulation and compared with experimental values. The effect of percentage of SA on the structure of the HPMC-SA suspension is investigated by DPD. Structure factor and polymer end-to-end distance which give insights about the agglomerate structure is analyzed. DPD predictions are compared to those obtained using our former predictive models (tensile approach and work of adhesion approach) (see chapter 5). Simulation results are also compared to experimental results previously presented in chapter 3.

2. Theory and simulation methods

In order to study the colloidal particles structure and stability in aqueous polymeric dispersions, we will use the mesoscale "coarse-grain" approach combined with the dissipative particle dynamics (DPD) simulation method which is described below.

2.1. The dissipative particle dynamics (DPD) method

The dissipative particle dynamics method (DPD) is a particle mesoscopic simulation method which can be used for the simulation of systems involving colloidal suspensions, emulsions, polymer solutions, Newtonian fluids and polymer melts. This method enables accessing larger spatio-temporal scales than those in the molecular dynamics.

Recently, a number of workers have used DPD to study several phenomena. Groot (2003) used the DPD method to study the aggregation of surfactant. Rekvig et al (2004) adopted the DPD method for the simulation of interacting oil-water-surfactant interfaces. DPD was also used by Hoogerbrugge and Koelman (1993) and by Boek et al. (1996, 1997) for the simulation of colloidal suspensions. Novik and Coveney (1997, 1998) used DPD to study phase separation in binary immiscible fluids. To run simulations of polymer systems, Schlijper et al. (1995), Schulz et al., (2004, 2005), Tomasini and Tomassone (2012), and Cao et al. (2005) also used DPD simulations. Gama Goicochea (2007) used it to study polymer adsorption. Mayoral and Nahmad-Achar (2012) studied the interfacial tension between an organic solvent and aqueous electrolyte solutions and found good agreement with experimental data. The DPD method has also been used for the simulation of number of other physical systems and material interactions which are not considered in this thesis, including the behavior of lipid bilayer membranes (Venturoli and Smit, 1999), nanoparticles in brush polymer (Guskova et al., 2009) and flow in pores (Liu et al, 2007).

In the DPD method, the compounds are composed of molecules described as a set of soft beads that interact dynamically in a continuous space and move along the Newton momentum equation

(equation 6.1). These interactions between the soft beads govern the affinity between the compounds and therefore, control the final structure built by the beads in the DPD simulation.

$$\frac{d\vec{r}_i}{dt} = \vec{v}_i \quad \text{and} \quad \frac{d\vec{v}_i}{dt} = \vec{f}_i \tag{6.1}$$

where r_i and v_i are the position and velocity of the bead i, f_i represents the sum of the forces acting on the bead:

$$\vec{f}_i = \sum_{j \neq i} (\vec{F}_{ij}^C + \vec{F}_{ij}^D + \vec{F}_{ij}^R + \vec{F}_{ij}^S) \tag{6.2}$$

F_{ij} represent the force exerted by a bead i on the bead j. Each bead is subjected to three non-bonded forces; a conservative repulsive force F^C that determines the thermodynamic behavior of the system, a dissipative force F^D which includes the friction forces, and a random term F^R accounting for the omitted degrees of freedom (Español, 1997), and a bonded force F^S. The non-bonded forces are given in equation (6.5).

$$\vec{F}_{ij}^C = a_{ij}\omega(r_{ij})\hat{r}_{ij}$$

$$\vec{F}_{ij}^D = -\partial \omega^2(r_{ij})(\vec{r}_{ij}\vec{v}_{ij})\hat{r}_{ij} \tag{6.3}$$

$$\vec{F}_{ij}^R = \sigma(\Delta t)^{-1/2}\omega(r_{ij})\xi_{ij}\hat{r}_{ij}$$

with $\vec{r}_{ij} = r_i - r_j$, $r_{ij} = |\vec{r}_{ij}|$, $v_{ij} = v_i - v_j$, $\hat{r}_{ij} = \vec{r}_{ij}/r_{ij}$ and $a_{ij} = a_{ji}$.

This last term a_{ij} represents the maximum repulsion between two beads; it encompasses all the physical information of the system. ξ_{ij} is a random parameter which describe the noise with a zero mean and one unit variance, σ is the noise strength and ∂ is the dissipation parameter. $\omega(r_{ij})$ is a weight function which determines the radial dependence of the repulsive force:

$$\omega(r_{ij}) = \begin{cases} 1 - r_{ij}/r_c & r_{ij} \leq r_c \\ 0 & r_{ij} \geq r_c \end{cases} \tag{6.4}$$

with r_c is a cut-off distance. Non-bonded forces act within a sphere of radius r_c. Outside this sphere, interaction forces are ignored. $\omega(r_{ij})$ is qualified as a soft repulsion in opposition to a hard sphere repulsion potential. The soft repulsion fits well the mesoscale nature of the system and allows longer time steps simulations (Español, 1997).

The connected beads undergo spring bonding force:

$$\vec{F}_{ij}^{S} = C_r \vec{r}_{ij} \qquad (6.5)$$

with C_r the harmonic spring constant. The behavior of a single polymer chain is deducted by means of interactions generated by its neighbors. DPD method is then applied on soft cluster of molecules called "beads" obtained through "coarse-grain" modeling.

The original velocity-Verlet algorithm is used for the integration of all the equations (Groot and Warren, 1997). More details about the DPD method are given by Trofimov (2003).

2.2. The "coarse-grain" modeling

In order to reduce the computation cost in molecular simulation for many body systems, we perform simulations at the mesoscopic scale. The molecules or segments of polymer chains are converted into so-called beads through the coarse-grain approach which consists in aggregating several atoms into a single bead.

Simulations in the DPD system are performed in reduced units. The reduced number density $\overline{\rho}$ in the DPD system is related to the real number density ρ of the compound by the following relationship:

$$\overline{\varrho} = \varrho r_c^3 \qquad (6.6)$$

where $\overline{\varrho}$ is the number of beads in one cubic simulation cell of volume r_c^3 (see Fig. 6.1), the cut-off radius r_c represents the unit length in the DPD system and also used to establish the reference scale.
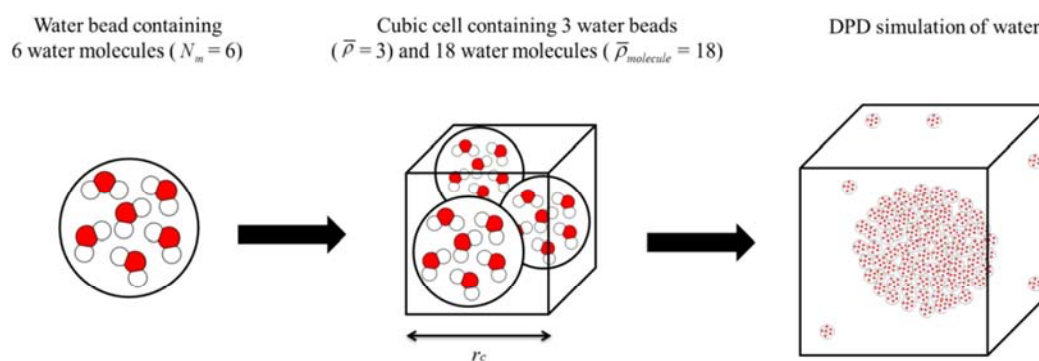
Fig. 6.1 – Schematic representation of the coarse-graining of a water molecule. In this case, $\overline{\rho}$ = 3 and N_m = 6, the cut-off distance r_c is therefore equal to the length of one side of the cubic cell.

Arguments have been raised regarding the difference in the size of beads. The bead volume and mass has no influence on the structure or on the morphology of the simulated system. However, considering that the mass, as well as the volume, is the same for all beads in the DPD system, unit

conversion from DPD units to real physical units requires a coarse-grained system with close beads volume and mass (Groot and Rabone, 2001), especially for cases where the simulation is intended to mimic the real physical quantities and to predict properties such as interfacial energy.

The coarse-graining degree N_m represents the number of molecules of water placed in a single bead (See Fig. 6.1). Grouping several molecules of water in one bead is used to match the volume of the different beads in the DPD simulations. N_m can be evaluated using the following formula:

$$N_m = \frac{\bar{\varrho}_{molecule}}{\bar{\varrho}}$$ (6.7)

with $\bar{\varrho}_{molecule}$ is the number of molecules in one cubic unit cell of volume r_c^3. Through this paper, the upper script "−" denotes the property in the DPD system.

Using equation (6.7) and (6.6), the cut-off radius can be obtained by using the following relationship:

$$r_c = (\frac{\bar{\varrho}}{\varrho})^{1/3} = (N_m V_{molecule} \bar{\varrho})^{1/3}$$ (6.8)

For a water molecule, we find the same relation proposed by Groot and Rabone (2001):

$$r_c = 3.1072 (N_m \bar{\varrho})^{1/3} \text{ in Å}$$ (6.9)

The reference mass is that of a bead containing N_m water molecules, it can be obtained by the following equation:

$$m_{ref} = m_{bead} = N_m m_{H2O}$$ (6.10)

There have been discussions regarding the scalability of the DPD scheme in relation to the upper limit N_m^{max} of the level of coarse-graining. According to Flekkoy et al. (2000) and Español et al. (1997), grouping many molecules of the same compound into one bead does not change the average kinetic energy of the system. On the other hand, Trofimov (2003) stated that the limit of coarse-graining N_m^{max} should not exceed ten molecules of water in a single bead, otherwise, the DPD system will confront the Hansen-Verlet(-Schiff) freezing criterion (Hansen and L. Verlet, 1969; Hansen and Schiff, 1973). This criterion states that a system congeals when the height of the main peak of the

structure factor of the mixture surpasses the quasi-universal value of 2.85. Such situation must be avoided in DPD simulations. This effect was also observed by Pivkin and Karniadakis (2006).

2.3.   DPD parameters calculations

The forces parameters (in equation (6.3) and (6.6)) required to perform the DPD simulations are: the repulsion parameter a_{ij}, the parameter of dissipation ∂, the random parameter ξ_{ij} and the harmonic spring constant C_r. There is also the DPD number n_{DPD} which represents the number of similar beads by which a polymer chain can be described.

DPD repulsion parameter a_{ij} can be calculated using Hildebrand solubility parameter δ (1950), the number density ρ, and the coarse-graining number N_m. According to Groot and Warren (1997), the repulsion parameter a_{ii} that governs the interaction between the beads in the DPD simulation has the following expression:

$$a_{ii} = (16N_m - 1)\frac{k_B T}{2\varsigma\rho r_c^4} \tag{6.11}$$

where ς is an adjustment parameter equal to 0.101 ($\pm$ 0.001). The detailed demonstration is given in Appendix L. The dimensionless equation takes the following form:

$$\bar{a}_{ii} = \frac{(16N_m - 1)}{2\varsigma\bar{\varrho}} \tag{6.12}$$

The repulsive parameters for unlike-beads $\bar{a}_{ij}$ can be determined according to a linear relationship with the Flory-Huggins parameter χ_{ij} (Groot and Warren, 1997; Flory, 1942):

$$\bar{a}_{ij}(\bar{\varrho} = 3) = \bar{a}_{ii} + \frac{\chi_{ij}}{0.286} \tag{6.13}$$

The number density $\bar{\rho}$ is equal to 3 DPD units, for which the repulsion parameter/Flory-Huggins parameter relationship has been defined (Groot and Warren, 1997).

The Flory-Huggins values can be calculated from the Hildebrand solubility parameter (Hildebrand, 1950) using the formula:

$$\chi_{ij} = \frac{(\delta_i - \delta_j)^2 (V_i + V_j)}{2k_B T}$$

(6.14)

with V the volume of the beads, δ_j and δ_i are the solubility parameters of bead i and j respectively. We notice that the parameter $\bar{a}_{ij}$ is always positive which means that the conservative force F^C is always repulsive.

The previous model of Groot and Warren was built based on the isothermal compressibility of water (See appendix L) and on the assumption of equal repulsive interactions between similar beads at the interface in binary mixtures ($a_{ii} = a_{jj}$). This hypothesis was defended by Groot and Warren (1997), and by Maiti and McGrother (2004) by saying that all beads have the same cutoff radius and the same volume. In an attempt to eliminate the restriction of having the same repulsive interaction parameters between like beads ($a_{ii} = a_{jj}$), Travis et al. (2007) recently proposed an alternative relation between conservative interaction parameters a_{ij} and the solubility parameter:

$$(\delta_i - \delta_j)^2 = -r_c^4 \varsigma(\varrho_i^2 a_{ii} + \varrho_j^2 a_{jj} - 2\varrho_i \varrho_j a_{ij})$$

(6.15)

Using the dimensionless parameters: $\bar{a}_{ii} = a_{ii} r_c / k_B T$, $\bar{\delta}_i = \delta_i (r_c^3 / k_B T)^{1/2}$ and $\bar{\varrho} = \varrho r_c^3$, we obtain the final form of the dimensionless equation:

$$(\bar{\delta}_i - \bar{\delta}_j)^2 = -\bar{\varrho}^2 \varsigma(\bar{a}_{ii} + \bar{a}_{jj} - 2\bar{a}_{ij})$$

(6.16)

Regarding the conservative interaction parameter between the same beads a_{ii}, Travis et al. (2007) proposed the following expression:

$$a_{ii} = \frac{\delta_i^2}{\varsigma \varrho_i^2 r_c^4}$$

(6.17)

In terms of reduced units, equation (6.17) has the following form:

$$\bar{a}_{ii} = \frac{\bar{\delta}_i^2}{\varsigma \bar{\varrho}_i^2}$$

(6.18)

The fluctuation-dissipation theorem states that the noise parameter σ and the dissipation parameter ∂ are connected by the following relation:

$$\sigma^2 = 2\partial k_B T$$

(6.19)

with k_B the Boltzmann constant. Regarding the parameters of dissipation ∂ here, studies have shown that the simulations are not really sensitive to this parameter if it is between 2 and 32 DPD reduced units (i.e. between 0.04019 and 0.64308 g.mol^{-1}.fs^{-1}) (Groot and Warren, 1997). If this value exceeds 32 DPD units, the force friction between the beads becomes very high and the integration time becomes insufficient to correctly simulate the system. To avoid this problem, an alternative is to decrease the time step.

According to the literature, the harmonic spring constant C_r gives good results for values between 2 and 4 DPD units (i.e. between 75 and 150 J.mol^{-1}.Å^{-2}) (Groot and Warren, 1997), which is sufficient to maintain the adjacent beads well-connected in the polymer chain. The spring constant C_r is chosen such that the mean distance between connected particles coincides with the peak of the radial distribution function of our material (Groot and Warren, 1997).

For polymers, the number of beads that composes one polymer chain can be estimated with the DPD number n_{DPD}:

$$n_{DPD} = \frac{M_w}{M_m C_n} \tag{6.20}$$

M_w is the molecular weight of the polymer, M_m the molecular weight of the monomer and C_n the characteristic ratio of the polymer.

3.   Computational simulation details

3.1. The mesoscale "coarse-grain" model

As stated earlier, all beads in the DPD simulation should have the same volume; hence, the task of finding the adequate coarse-grained model comprises two concomitant parts: a) estimating the most suited volume common to all beads, and b) avoiding the solidification of the system. In this context, we select the reference volume of a single bead equal to 180 Å^3, because, as we will see later, it allows assimilating each molecule or monomer to a bead whose volume is close to that value. Then, a water bead must represent $N_m = 6$ water molecules (volume of a water molecule $\approx$ 30 Å^3), which roughly corresponds to a single monomer of PVP, and to a half monomer of MCC (C×2). SA is thus composed of 3 beads; one bead containing the fragment SA1 and two beads of the fragments SA2 (see Fig. 6.2). PEG is composed of three similar beads; each one contains the same fragment which we called PEG1. In the same way, HPMC repeating unit is coarse-grained into 4 beads (one HL, two

HO and one HC) (see Fig. 6.2). Irisa and Yokomine (2010) and Hongyu Guo et al. (2013) also used $N_m = 6$ water molecules in their DPD simulations.
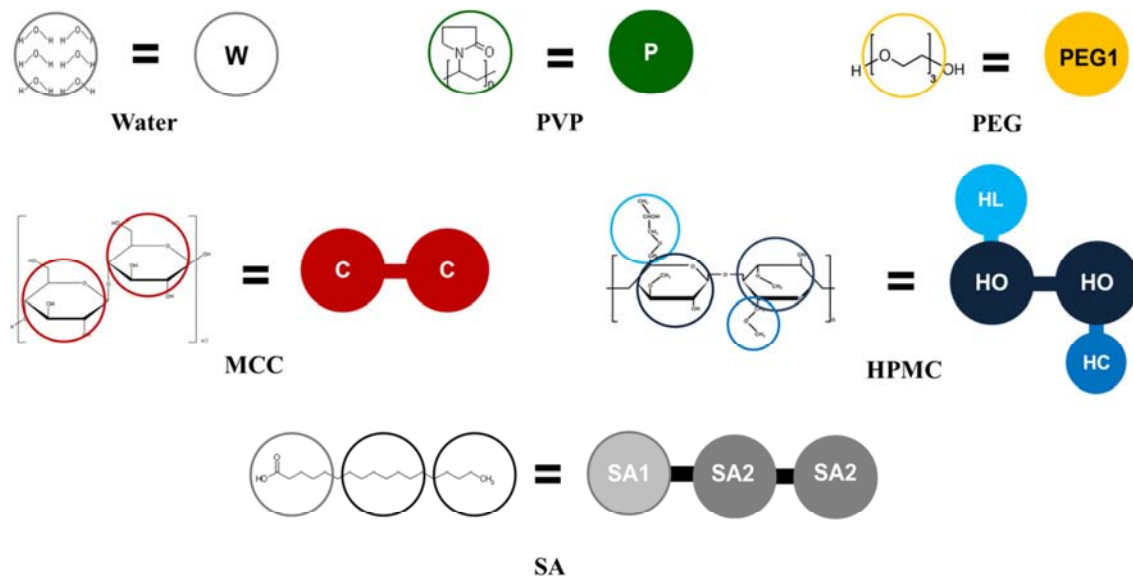
Fig. 6.2 – "Coarse-grain" method; molecules and monomer conversion into beads for water (W), Polyvinylpyrrolidone (PVP), Polyethylene glycol400 (PEG), Microcrystalline cellulose (MCC), Hydroxypropyl-methylcellulose (HPMC) and Stearic acid (SA).

Since the number density $\overline{\rho}$ is equal to 3 DPD units, a cubic simulation cell, with an edge length equal to r_o, contains three beads with 6 molecules of water each and corresponds to a volume of 540 Å^3. Notice that the coarse-graining number $N_m = 6$ is below the limit specified by Trofimov (2003).

3.2. Molecular dynamic simulation and solubility parameter calculation

Following our previous work (Jarray, 2015), the solubility parameters needed to compute the Flory Huggins parameter χ are calculated using either molecular simulations (in Biovia's Material Studio software product (Biovia, 2013) or Yamamoto's molecular breaking method (HSPiP, 2010). The obtained values are presented in Table 6.1. All-atom molecular dynamics simulations are performed with an integration step of 1 femtosecond (fs = 10^{-15}s). The interatomic interactions are described by the COMPASSII (Condensed-phase Optimized Molecular Potentials for Atomistic Simulation Studies) forcefield (Sun, 1998) along with Ewald summation for the long range electrostatics. NPT dynamics is performed first to equilibrate the density of the system for 500 picoseconds (ps = 10^{-12}s) at room temperature ($T = 298$ K) and atmospheric pressure ($P = 1$ atm). Then, another all-atom simulation is launched in the canonical ensemble NVT at a temperature T = 298 K for 500 ps in order to track the convergence of the cohesive energy density. The last 50 ps are used for computing

the averaged Hildebrand solubility parameters for each repeating unit and molecules, as well as their standard deviations (see Table 6.1).

Table 6.1 – Solubility parameter and density of repeating units and molecules.

Compounds		Solubility parameter δ of the repeating unit and molecule $(J.cm^{-3})^{1/2}$		Density e of the repeating unit and molecule $(g.cm^{-3})$	
		COMPASSII	HSPiP	COMPASSII	HSPiP
PVP		22.2 ± 0.3	20.8	0.994 ±0.02	0.986
MCC	C (×2)	31.5 ± 0.6	32.0	1.347 ±0.02	1.434
HPMC	HL	22.1 ± 0.6	22.4	0.893 ±0.02	0.918
	HO(×2)	27.3 ± 0.3	25.5	1.233 ±0.01	1.204
	HC	18.0 ± 0.5	17.5	0.768 ±0.02	0.700
SA	SA1	23.4 ± 0.3	20.4	0.963 ±0.01	0.924
	SA2(×2)	14.5 ± 0.2	15.0	0.648 ±0.01	0.676
PEG1	PEG1 (×3)	23.7 ± 0.3	21.4	0.992 ±0.01	0.993
Water		47.5 ± 0.4	47.8*	0.962 ±0.01	0.997*

PVP: Polyvinylpyrrolidone, MCC: Microcrystalline cellulose, HPMC: Hydroxypropyl-methylcellulose, SA: Stearic acid, PEG: Polyethylene glycol.
*HSPiP literature (HSPiP, 2010)

Table 6.2 – Conversion of monomer and molecules into beads, and properties of the beads.

Compounds		M_w of the repeating unit and molecule $(g.mol^{-1})$	Bead volume $(Å^3)$		Bead radius $(Å)$	
			COMPASSII	HSPiP	COMPASSII	HSPiP
PVP		113.2	185.7	187.3	3.54	3.54
MCC	(×2)	162.2	199.9	187.8	3.55	3.55
HPMC	HL	89.1	165.7	161.2	3.37	3.37
	HO (×2)	144.2	194.2	198.8	3.62	3.62
	HC	45.1	97.5	106.9	2.94	2.95
SA	SA1	115.2	198.6	207.1	3.66	3.67
	SA2 (×2)	85.2	218.3	209.3	3.68	3.68
PEG400	PEG1 (×3)	132.2	221.3	221.1	3.75	3.75
Water		18.0	186.4	179.9*	3.54	3.50

PVP: Polyvinylpyrrolidone, MCC: Microcrystalline cellulose, HPMC: Hydroxypropyl-methylcellulose, SA: Stearic acid, PEG: Polyethylene glycol.
*HSPiP database (HSPiP, 2010)

In Table 6.1, results obtained by molecular simulation are close to HSPiP predictions. Molecular simulation results will be used next as input parameters in the DPD simulations. Table 6.2 shows the beads volume calculated by dividing the molecular weight M_w by the density e. As anticipated, the beads volume and radius are close.

3.3. DPD simulation details

3.3.1. DPD parameters

The number of beads used to describe each polymer in the simulations is determined by the DPD number n_{DPD} which is calculated using equation (6.20). The ratio characteristic is computed using Material Studio's (Biovia, 2013) Synthia module (Bicerano, 2002). The results are shown in Table 6.3.

Table 6.3 – DPD number n_{DPD} of PVP, MCC and HPMC, calculated using equation (6.20)

Composants	Characteristic ratio C_n	Average molecular weight M_w (g.mol^{-1})	Monomer molecular weight M_m (AMU)	n_{DPD}(Number of beads)
PVP	9.90	10 000	111.2	9
MCC	5.09	36 000	162.2	44
HPMC	4.78	20 000	424.5	10

PVP: Polyvinylpyrrolidone, MCC: Microcrystalline cellulose, HPMC: Hydroxypropyl-methylcellulose.

Following Groot and Warren's (1997) approach, the individual self-repulsive interaction parameters a_{ii} determined using equation (6.12) is equal to 157 when $N_m = 6$, according to the authors (Groot and Warren, 1997), it's the same for all beads. The conservative force parameters a_{ij} between every couple of beads is then calculated using the relationship (6.13). The results are summarized in Table 6.4. We also calculate a_{ij} and a_{ii} using equations (6.16) and (6.18) respectively, proposed by Travis et al. (2007), the results are summarized in Table 6.5.

The harmonic spring constant of the polymer chain was set equal to 4.0 DPD reduced units (i.e. 150 J.mol^{-1}.Å^{-2}), which is enough to keep the adjacent beads connected together along the polymer backbone (Groot and Warren, 1997. Having set the coarse-graining number N_m to 6 and the DPD number density $\overline{\rho}$ to 3, the cut-off radius r_c is computed from equation (6.9). We obtain $r_c = 8.14$ Å.

The noise strength σ is equal to 3 DPD units (i.e. 2.723 (J.g.mol^{-1}.fs^{-1})$^{1/2}$) which is the recommended value proposed by Groot and Warren (1997) to ensure a stable simulation. Using equation (6.19), the dissipation parameter ∂ is equal to 4.5 DPD units (i.e. 0.09043 g.mol^{-1}.fs^{-1}).

Table 6.4 – The conservative force parameters a_{ij} and a_{ii} obtained by using Groot and Warren's (1997) equations (6.12) and (6.13).

a_{ij}		PVP	MCC	HL	HO	HC	SA1	SA2	PEG1	Water
PVP		157.00								
MCC		170.85	157.00							
HPMC	HL	157.00	170.5	157.00						
	HO	161.14	159.85	161.12	157.00					
	HC	159.09	179.56	158.82	167.56	157.00				
SA	SA1	157.22	167.92	157.26	159.54	160.58	157.00			
	SA2	167.15	207.65	166.33	185.51	158.66	170.89	157.00		
PEG1		157.38	167.64	157.43	159.26	161.33	157.02	172.71	157.00	
Water		256.78	198.64	252.37	222.05	260.48	250.89	342.12	253.79	157.00

PVP: Polyvinylpyrrolidone, MCC: Microcrystalline cellulose, HPMC: Hydroxypropyl-methylcellulose, SA: Stearic acid, PEG: Polyethylene glycol.

Table 6.5 – The conservative force parameters a_{ij} and a_{ii} obtained by using Travis et al. (2007) equations (6.16) and (6.18).

a_{ij}		PVP	MCC	HL	HO	HC	SA1	SA2	PEG1	Water
PVP		35.56								
MCC		59.88	71.59							
HPMC	HL	35.40	59.85	35.24						
	HO	46.56	63.97	46.47	53.77					
	HC	30.75	60.77	30.53	44.88	23.37				
SA	SA1	37.63	60.33	37.49	47.75	33.56	39.50			
	SA2	29.68	64.45	29.41	46.41	20.16	33.11	15.17		
PEG1		38.20	60.49	38.07	48.09	34.32	40.02	34.02	40.52	
Water		145.84	135.8	146.05	138.03	156.53	143.49	168.38	142.96	162.79

PVP: Polyvinylpyrrolidone, MCC: Microcrystalline cellulose, HPMC: Hydroxypropyl-methylcellulose, SA: Stearic acid, PEG: Polyethylene glycol.

3.3.2. DPD computational details

All DPD simulations were performed within Materials Studio 7 software package (Biovia, 2013). A $30 \times 30 \times 30$ r_c^3 (i.e. $24.4 \times 24.4 \times 24.4$ nm) simulation cell box was adopted where periodic boundary conditions was applied in all three directions. Initially the beads were randomly dispersed in the simulation cell. Each DPD simulation ran for 1000 DPD units (i.e. 5374.17 ps) which was sufficient to get a steady phase. The integration time was taken as t = 0.02 DPD units (i.e. 107.48 fs). DPD simulations were run in the canonical thermodynamic NVT ensemble at a temperature of T = 298 K.

We evaluated the interfacial energy γ by dividing a 30x6x6 r_c^3 simulation box into a number of x-normal slabs. This way, the tensor elements will be a function of the distance in the x direction (Biovia, 2013). An equilibration period of 1400 DPD units (i.e. 7526.59 ps) steps was used and followed by a production run of 600 DPD units (i.e. 3225.69 ps). In the DPD method, the masses of all particles are normally chosen to be the same and equal to108 amu for 6 water molecules in one bead. Therefore, for the interfacial energy calculations, we matched the mass of the beads of each compound to that value (108 amu). This was done by multiplying the simulation target number density $\bar{\rho}$ by the relative density e obtained by averaging the weight density of the beads (see Table 6.1) that compose each compound. Interfacial energy γ in the DPD simulations can then be calculated using the Irving-Kirkwood (Irving and Kirkwood, 1950) equation by integrating the difference between normal and tangential stresses across the interface.

$$\bar{\gamma} = \int \ (< \overline{P}_{xx} > - 0.5(< \overline{P}_{yy} > + < \overline{P}_{zz} >) \ d\bar{x}$$

(6.21)

$$\gamma = \bar{\gamma} \frac{k_B T}{r_c^2}$$

(6.22)

where $\bar{x} = x / r_c$, P is the pressure tensor that consists of three diagonal components P_{xx}, P_{yy}, and P_{zz}.

4. Results and discussion

When preparing a binder or coating solution, the challenge is to fabricate a polymeric solution with a high hydrophobic SA content while maintaining the stability of the suspension. To this end, we used our DPD model for the simulation of the coarse-grained HPMC-SA structure in water under different amounts of SA. Then, we investigate the influence of polymer nature (HPMC, PVP, MCC) on the SA based coating.

Compatibility between the polymer and the plasticizer is also fundamental in coating formualtion. In this context, we also used DPD for the simulation of the interaction between PEG (plasticizer) and HPMC, MCC, PVP (polymer).

4.1. Interfacial energy of polymers

Before using the DPD method on ternary aqueous systems, we calculate interfacial energies of the compounds. We used the DPD method proposed by Groot and Warren (1997) and the DPD method proposed by Travis et al. (2007). Then, we compared the results with experimental values from literature. Computed interfacial energy values are presented in Table 6.6.

Interfacial energy values obtained following Groot and Warren's (1997) method are calculated using the conservative force parameters presented in Table 6.4. Interfacial energy values obtained following Travis et al. (2007) method are calculated using the conservative force parameters presented in Table 6.5.

Interfacial energy values obtained by DPD simulations following Groot and Warren (1997) and Travis et al. (2007) are close to the experimental values, but Groot and warren's approach gives closer values. Henceforth, we will adopt the DPD equations of Groot and Warren.

Table 6.6 – Interfacial energy results obtained by DPD simulations and compared with experimental values.

Compounds	Number density $\bar{\varrho}$	Interfacial energy γ (mJ.m^{-2})		
		DPD Groot and Warren (1997)	DPD Travis et al. (2007)	Exp. from literature
PVP	2.98	48.96 ± 0.36	47.88 ± 0.82	46.7[a]
MCC	4.04	53.19 ± 0.49	42.53 ± 0.54	53.1[a]
HPMC	3.09	43.40 ± 1.16	33.76 ± 0.22	34[b], 38.4[a], 43.1[c], 48.4[d]
SA	2.26	31.38 ± 0.67	19.75 ± 0.28	28.9[e]
PEG400	2.98	54.14 ± 0.37	43.52 ± 0.52	46.7[f]

PVP: Polyvinylpyrrolidone, MCC: Microcrystalline cellulose, HPMC: Hydroxypropyl-methylcellulose, SA: Stearic acid, PEG: Polyethylene glycol.

a: Benali, b: Barra 1998, c: Brogly 2011, d: Rowe 1989b, e: Wypych 2014, f: Demajo 2000.

4.2. Influence of SA concentration on HPMC-SA agglomerate in water

Fig. 6.3 shows three snapshots of configurations of HPMC-SA (10%-10% (w/w)) in water (transparent) after 537.41 ps (Fig. 6.3 (a)), 1074.83 ps (Fig. 6.3 (b)) and 5374.17 ps (Fig. 6.3 (c)) of simulation time. Initially HPMC and SA beads are randomly dispersed in water (Fig. 6.3 (a)).

Hydrophobic SA molecules progressively agglomerate under the action of the repulsion forces of the water beads (Fig. 6.3 (b)). At the same time, HPMC beads gradually diffuse through water and redistribute on the outer surface of the SA agglomerate. As the simulation progresses, the HPMC-SA agglomerate increases in size until the HPMC matrix completely surrounds SA through polymer entanglement and form a thick layer between SA and water (Fig. 6.3 (c)).

(a) Time: 537 ps   (b) Time: 1074.83 ps   (c) Time: 5374.17 ps
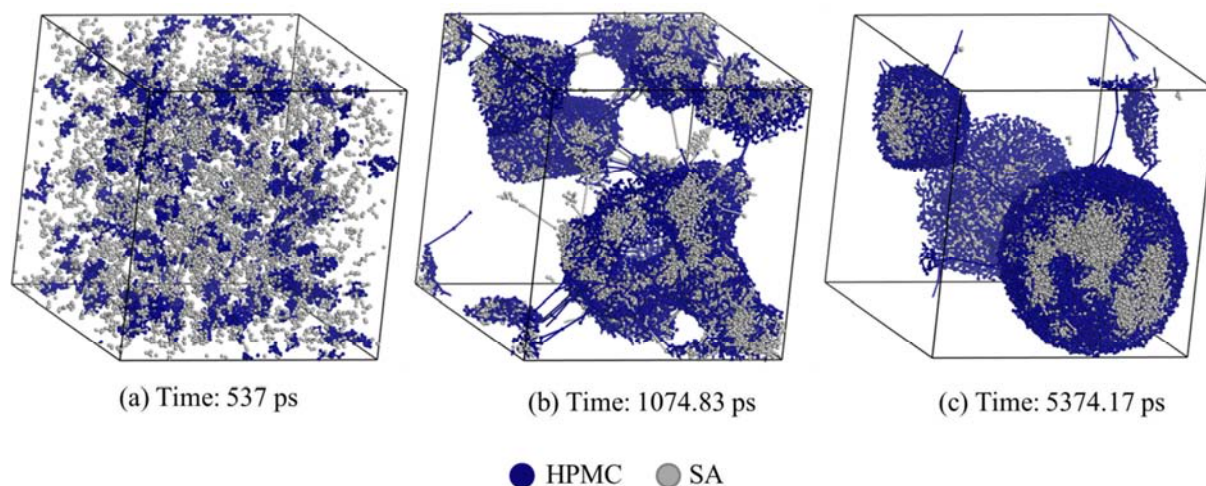
● HPMC   ○ SA

Fig. 6.3 – DPD simulation of HPMC (Hydroxypropyl-methylcellulose, blue, 10%)-SA (Stearic acid, grey, 10%) mixture in water (transparent, 80%)

In Fig. 6.4, we present structures of HPMC-SA mixture under different fractions of SA. All the images show the last step of the DPD simulation when the equilibrium state is reached. When SA fraction is 2% (w/w) (Fig. 6.4 (a)), HPMC polymer completely covers a large SA agglomerate. We notice that some small SA agglomerates swim freely in the simulation cell. Upon increasing the SA percentage we observe a growth of SA agglomerates and a decrease of the number of loosen SA agglomerates. When the SA weight percentage is up to 20% (w/w), the aggregating structure of HPMC-SA is not spherical anymore and a tubular structure is formed (Fig. 6.4 (c)). To waive a possible artifact due to the box size, we display a simulation with an 8 times larger box in Fig. 6.4 (d). Again, a tubular structure is obtained, with a bigger radius. Moreover, there is no loose SA agglomerate in the water (Fig. 6.4 (c) and (d)). We also notice that some HPMC penetrate the inner core of the SA agglomerate to various extend depending on the amount of SA.

(a) HPMC-SA 10%-2% (w/w)
30x30x30 r_c^3 box size

(b) HPMC-SA 10%-10% (w/w)
30x30x30 r_c^3 box size

(c) HPMC-SA 10%-20% (w/w)
30x30x30 r_c^3 box size

(d) HPMC-SA 10%-20% (w/w)
60x60x60 r_c^3 box size
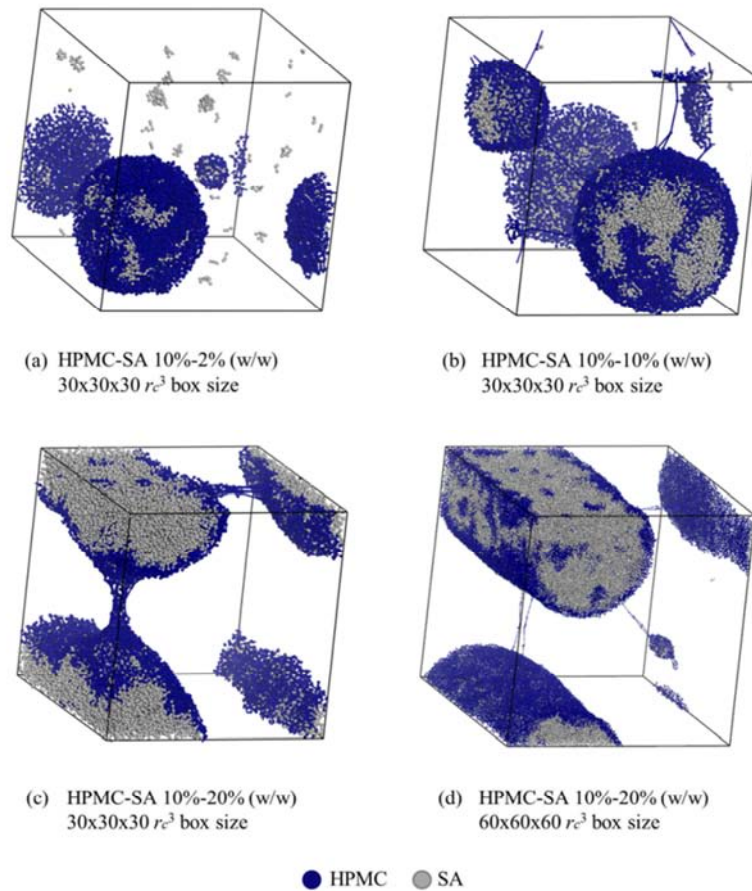
● HPMC ● SA

Fig. 6.4 – Snapshots of DPD simulation at equilibrium state of HPMC-SA (10%-10% (w/w)) mixture in water under different amounts of SA, HPMC: Hydroxypropyl-methylcellulose, SA: Stearic acid.

An important requirement to prevent agglomeration is that the stabilizing agent has to be adsorbed strongly enough on the surface of the particle. If a polymer is only weakly adsorbed, then, it is possible that desorption can take place even during Brownian collisions (without deliberately shearing the system). Thus, agglomeration may take place within the system on standing (Vincent, 1974). Spontaneous, weak, slow agglomeration can also occur in systems where the adsorption is strong, but where the adsorbed layer is thin (Vincent, 1974). The strength of the adsorption in our DPD simulations can be assessed by the amount of stabilizing agent beads which are inside the agglomerate.

Fig. 6.5 shows the distribution of HPMC around and through SA agglomerate as the percentage of SA increases. The percentage of beads of polymer that cover SA agglomerate $N_{beads,polymer}^{outside}$ can be calculated by using the following equation:

$$N_{beads,polymer}^{outside} = \frac{100}{N_{Beads,polymer}} \left(N_{Beads,polymer} - \sum_i \Delta \left(\prod_j 1 - \Delta \left(\left| r_o - r_i \right| + \left| r_i - r_j \right| - \left| r_o - r_j \right| \pm 2r_{water} \right) \right) \right) \quad (6.23)$$

where r_i denotes the position vector of the ith polymer bead, $i=1 \ldots N_{Beads,polymer}$. $N_{Beads,polymer}$ is the total number of polymer beads (HPMC, PVP or MCC in our case), r_j denotes the position vector of the jth SA bead, r_o is the position vector of the bead at the geometric center of the HPMC-SA agglomerate, r_{water} is the radius of a water bead which is roughly equal to the radius of the other beads (see Table 6.2), and Δ is the Dirac function. The developed script for the calculation of the percentage $N_{beads,polymer}^{outside}$ is given in appendix I.
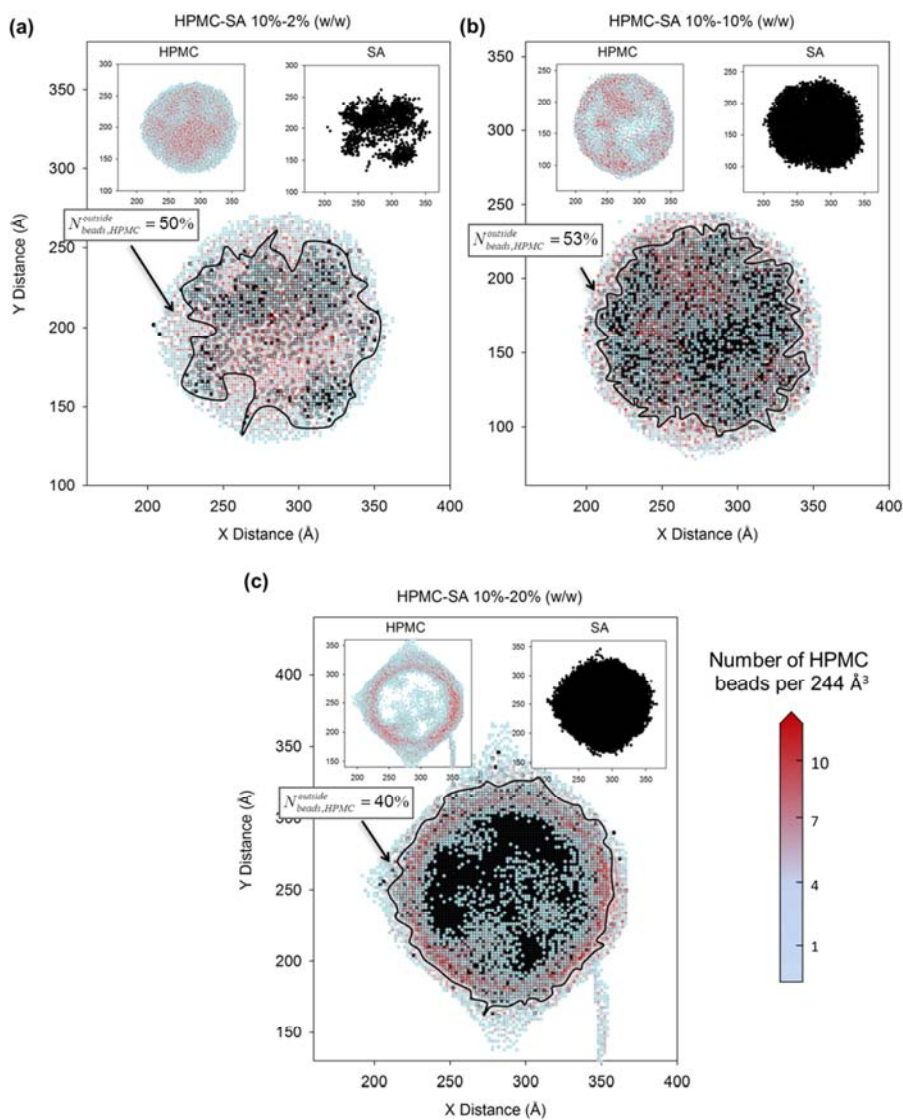
Fig. 6.5 – Distribution of HPMC beads around and through SA agglomerate under different amounts of SA, HPMC: Hydroxypropyl-methylcellulose, SA: Stearic acid.

In Fig. 6.5 (a), the agglomerate structure with 2% SA (w/w) is like an assembly of small patches of SA embedded in a matrix of HPMC that globally forms a spherical agglomerate. The percentage of HPMC beads outside all SA beads is equal to 50%.

In Fig. 6.5 (b), SA beads form a large spherical cluster surrounded by $N_{beads,\,polymer}^{outside}$ = 53% of HPMC. Therefore 47% of HPMC beads have diffused inside the SA inner core. The colored HPMC density scale indicates that HPMC is well distributed inside the SA inner core.

In Fig. 6.4 (c) and (d), the increase of the SA concentration to 20% (w/w) for the same HMPC content changed the stable structure of the system. From a spherical shape of SA cluster obtained for lower SA concentration at 2 and 10% (w/w), we ended up with a tubular shape at 20% (w/w) of SA. Laboulfie et al. (2013) also noticed in their experiments that an increase of SA concentration in HPMC-water solution destabilized the suspension and favored the formation of large SA agglomerate. From our simulations in Fig. 6.5 (c), with the increase of SA beads, we notice that the density of HPMC beads that covers the SA cluster decreases to $N_{beads,\,polymer}^{outside}$ = 40%. We also observe a denser SA core and that less HPMC molecules are able to diffuse deeply in the SA core. This hints that HPMC polymer would be less likely to get through the SA agglomerate as SA concentration reaches 20% (w/w). In summary, at large SA concentration, the SA molecules tend to cluster together and push at the fringes the HPMC molecules.

Fig. 6.5 shows a distribution function $\Gamma(r,dr)$ that represents the percentage of beads of HPMC as a function of the radial distance starting from the HPMC-SA agglomerate geometric center. The cumulative concentration is also shown. $\Gamma(r,dr)$ gives insights about the uniformity of the HPMC polymer distribution inside SA agglomerate and the size of the SA agglomerate (see also Fig. 6.7). $\Gamma(r,dr)$ is obtained by applying the following equation:

$$\Gamma(r,dr) = \frac{100}{N_{Beads,\,polymer}} \sum_{i} \Delta(H(|r - r_o| - |r_i - r_o|) + H(|r_i - r_o| - |r + dr - r_o|)) \tag{6.24}$$

where H is the Heaviside function. The script for the calculation of $\Gamma(r,dr)$ is given in appendix H.

The higher the distribution curve $\Gamma(r,dr)$ peak at a given radial distance, the more polymer beads are at that distance. The narrower $\Gamma(r,dr)$, the denser the polymer shell outside the SA agglomerate. The vertical lines in Fig. 6.6 separate the percentage of HPMC that are inside the SA agglomerate from the outside ones. The percentages at which the vertical lines are drawn are taken from $N_{beads,\,polymer}^{outside}$ values calculated before using equation (6.23). They enable us to estimate an equivalent SA core radius given

by the intersection between the cumulative distribution curve and the corresponding vertical line (see Fig. 6.7).
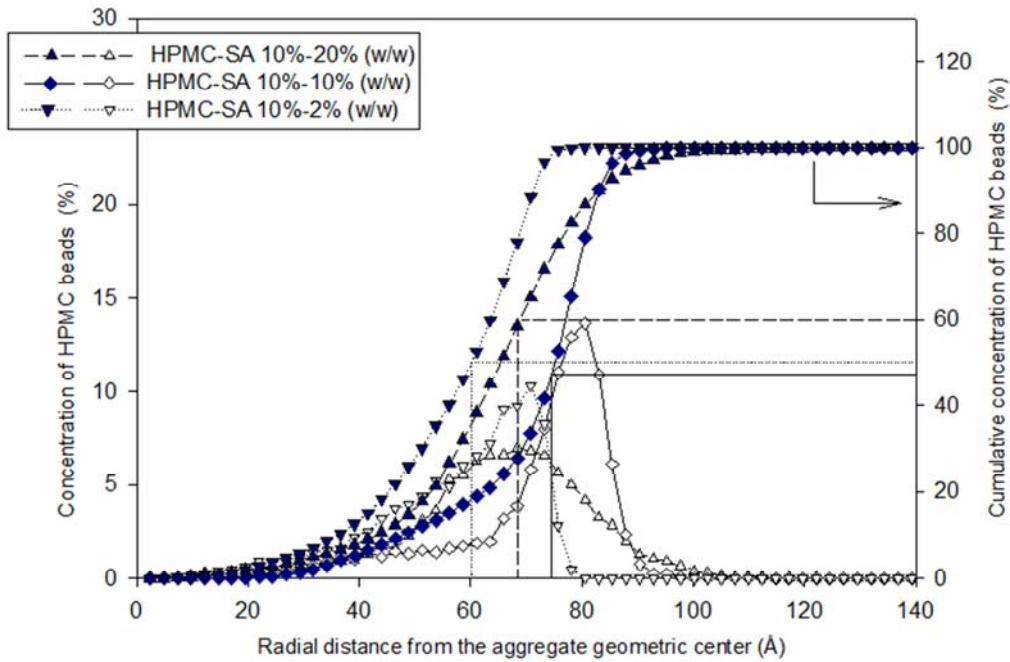
Fig. 6.6 – Concentration of HPMC beads $\Gamma(r, dr)$ as a function of the radial distance from SA agglomerate geometric origin. HPMC: Hydroxypropyl-methylcellulose and SA: Stearic acid.
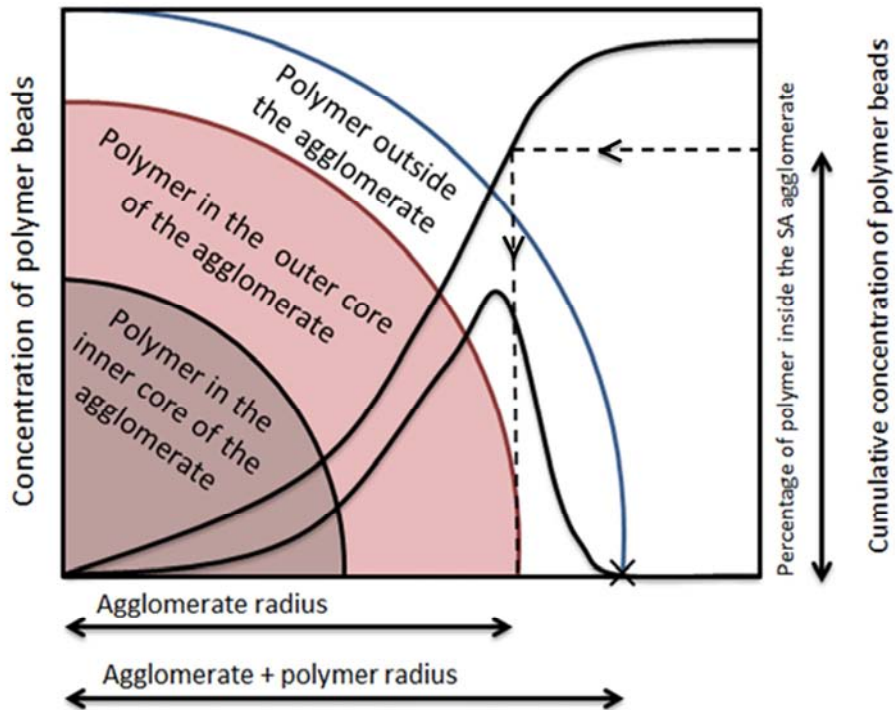
Fig. 6.7 – Schematic representation of the distribution function $\Gamma(r, dr)$ in relation to the agglomerate structure and size.

From Fig. 6.6, we obtain: $R_{equivalent}$. We obtain $R_{equivalent}^{sphere}$ = 60 Å for 2% (w/w) of SA, $R_{equivalent}^{sphere}$ = 74 Å for 10% (w/w) of SA, and $R_{equivalent}^{tubular}$ = 69 Å for the tubular structure obtained for 20% (w/w) of SA.

In Fig. 6.6, HPMC-SA 10%-2% (w/w) displays a wider spread distribution than HPMC-SA 10%-10% (w/w) indicating that more HPMC beads have diffused inside the SA agglomerate at 2% of SA. This confirms the conclusion obtained from Fig. 6.5 (a) and (b). HPMC-SA 10%-2% (w/w) shows lower peak and lower $R_{equivalent}^{sphere}$ than HPMC-SA 10%-10% (w/w) because there is only 2% (w/w) of SA interacting with 10% (w/w) of HPMC.

Both HPMC-SA 10%-2% (w/w) and HPMC-SA 10%-10% (w/w) show a sharp distribution that peaks at a radial distance greater than the corresponding $R_{equivalent}^{sphere}$ value for the SA inner core (Fig. 6.6). This means that high percentage of HPMC beads are distributed on the outer surface of SA cluster. This is the best case scenario where there are enough HPMC beads inside SA agglomerate to hold the SA agglomerate in position, and enough of them outside to cover the SA agglomerate.

As the percentage of SA increases to 20% (w/w), the peak shifts to a lower value below the corresponding $R_{equivalent}^{sphere}$. This is correlated with the increase of HPMC percentage beads inside SA agglomerate to 1- $N_{beads,polymer}^{outside}$ = 60%. Additionally, the increasing number of beads of HPMC inside the SA matrix makes the layer that covers SA agglomerate less thick.

From these three simulations at various SA concentrations for the same HPMC content, we may infer that HPMC can stabilize an aqueous SA suspension provided that the proportion of HMPC vs SA is high enough and that a network of HPMC molecules is diffused in depth in the SA core. This was achieved for the 2% and 10% (w/w) of SA cases. At higher SA load, the tubular structure of SA, with a lower surface area than the spherical structure, becomes energetically more favorable. A similar conclusion was reached in the experimental part (see chapter 3) where we showed that HPMC-SA mixtures with low SA amount (below 10% (w/w)) produces stable particles.

4.3. Influence of the polymer nature on the SA based coating

To study the behavior of each polymer in the presence of SA hydrophobic filler in aqueous systems, we ran DPD simulations of polymer-SA 10%-10% (w/w) where the polymers are PVP, HPMC and MCC.

Fig. 6.8 shows the final structure of the different binary mixtures, HPMC-SA, PVP-SA and MCC-SA, in water when equilibrium state is reached. Regarding the PVP-SA mixture (Fig. 6.8 (a)), PVP polymer tends to surround SA molecules in an aqueous environment. However, a tubular structure is obtained unlike the spherical structure in the case of HPMC-SA 10%-10% (w/w) blend (Fig. 6.8 (b)). Fig. 6.9 shows the percentage of beads of each polymer as a function of the radial distance starting from the SA agglomerate geometric origin. PVP polymers diffuse in the SA agglomerate as shown in Fig. 6.9 by the curve of concentration of PVP polymer that is broader than that of HPMC and has a lower peak than the other curves.

(a) PVP ⬤-SA⬤　　　(b) HPMC ⬤-SA⬤　　　(c) MCC ⬤-SA⬤
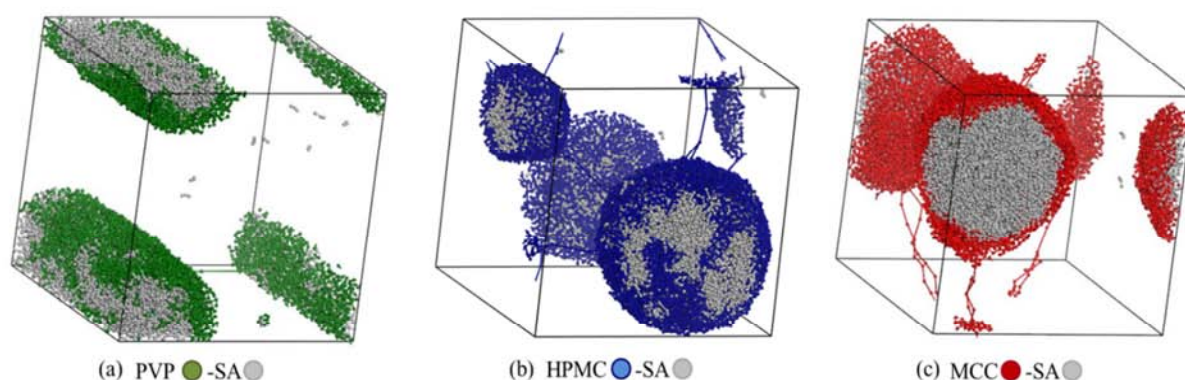
Fig. 6.8 – Snapshots of DPD simulation of PVP-SA, HPMC-SA and MCC-SA in water 10%-10% (w/w) when equilibrium state is reached. PVP: Polyvinylpyrrolidone, MCC: Microcrystalline cellulose, HPMC: Hydroxypropyl-methylcellulose, SA: Stearic acid.

In Fig. 6.8 (b), MCC interposes on the surface of SA without diffusing and forms a spherical shape. The peaked MCC curve in Fig. 6.9 implies that MCC beads tend to gather exclusively outside SA cluster and form a thick layer. Moreover, the radius of the SA inner core $R_{equivalent}^{sphere}$ = 71.76 Å is at the bottom of the MCC distribution curve. This indicates that the layer of MCC made by the beads which are in the outer core of SA agglomerate is very thin.
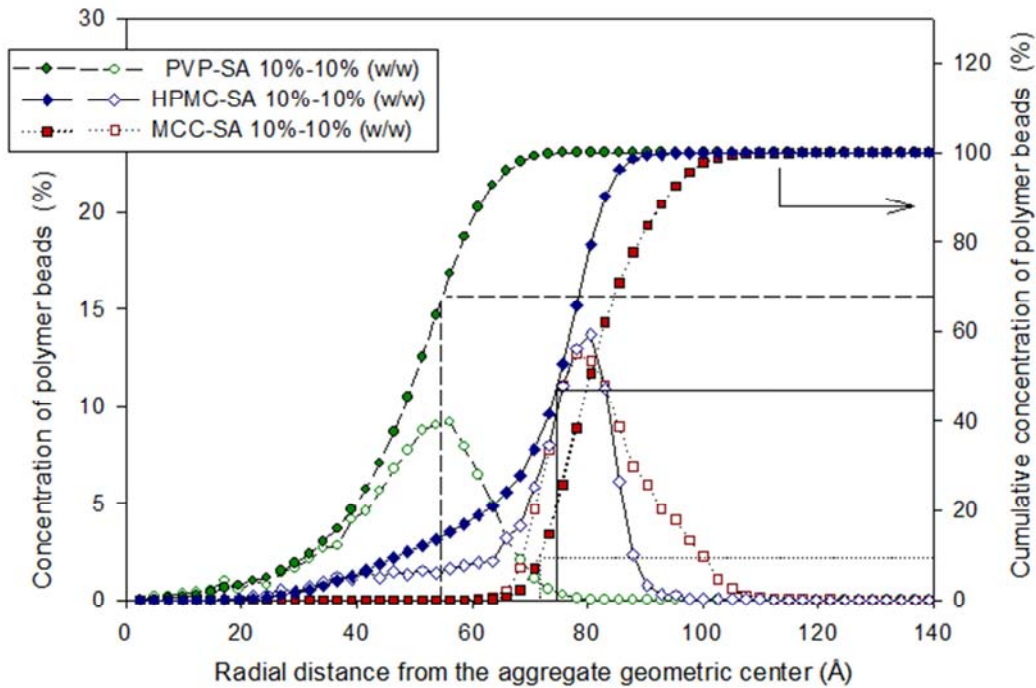
Fig. 6.9 – Concentration of polymer beads $\Gamma(r, dr)$ as a function of radial distance from polymer-SA agglomerate geometric center. PVP: Polyvinylpyrrolidone, MCC: Microcrystalline cellulose, HPMC: Hydroxypropyl-methylcellulose and SA: Stearic acid.

Fig. 6.10 shows the distribution of polymer beads (PVP and MCC) around and through SA. We have also computed $N_{beads, polymer}^{outside}$ by using equation (6.23). As shown in Fig. 6.10 (a) the percentage of beads of PVP inside SA agglomerate is high, about 67%, which leaves 33% that surrounds SA agglomerate, thus, the layer of PVP outside SA agglomerate is thin compared to the one formed by HPMC in the HPMC-SA 10%-10% (w/w) mixture. The colored PVP density scale in Fig. 6.11 shows that the majority of PVP beads which are inside the SA agglomerate are distributed in the outer core of SA agglomerate.

In Fig. 6.10 (b), the percentage of MCC that diffuses inside SA agglomerate is 9%. MCC are mainly distributed in the outer area of the SA agglomerate. The amount of MCC inside SA agglomerate is significantly low compared to HPMC (Fig. 6.5 (b)) and PVP (Fig. 6.10 (a)). Consequently, since colloidal dispersions always show Brownian motion and hence collide with each other frequently (Napper, 1983), the physical bond between SA and MCC is susceptible to detach, and SA particles could escape the MCC layer, and therefore, form large agglomerate.

By comparing the previous simulation results on the effect of 10% (w/w) of PVP, HPMC and MCC on 10% (w/w) of SA, we may deduce that PVP is able to stabilize SA particle but it's not as effective as HPMC. The percentage of MCC beads which are in the core of SA agglomerate is very low

compared to HPMC and PVP. This tells us that MCC may be a good dispersant but not a good stabilizer for SA.
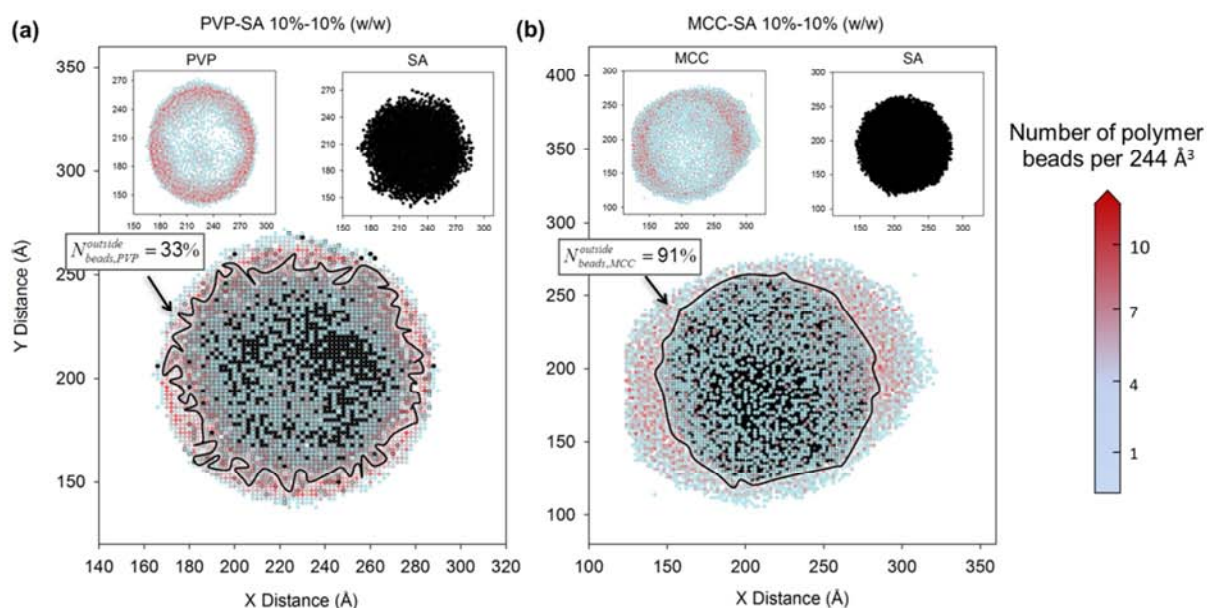
Fig. 6.10 – Distribution of polymer beads (PVP and MCC) around and through SA agglomerate. PVP: Polyvinylpyrrolidone, MCC: Microcrystalline cellulose and SA: Stearic acid.

Overall, even though DPD simulations are in a smaller scale, experimental (see chapter 3) and DPD results share the same tendencies. Low percentage of PVP inside the SA agglomerate and the thin layer formed by PVP around SA agglomerate explain the partial stability of SA when mixed with PVP seen in chapter 3. The inability of MCC to diffuse inside the SA agglomerate despite the complete coverage of SA by MCC explains why MCC is unable to produce small SA particles, but able to prevent the formation of big SA agglomerates (see chapter 3).

4.4. Effect of plasticizer (PEG400) on aqueous polymeric dispersions structure

In this section, we examine the structure of PVP, HPMC and MCC in the presence of a plasticizer (PEG400) using our DPD model. Polymer and plasticizer content in each mixture is fixed to 10% (w/w).

For a compound to be effective as a plasticizer, it must be able to diffuse into the polymer. The plasticizer will diffuse into the colloidal polymer dispersion with the rate and extent of diffusion being dependent on its water solubility and affinity for the polymer phase (McGinity and Felton, 2008).

129

Plasticizers molecules act by inserting themselves between the polymer chains thereby extending and softening the polymer. This will improve the mechanical properties of the final film (McGinity and Felton, 2008).

In Fig. 6.11 (a) and (b), PVP and PEG as well as HPMC and PEG are well mixed, and PVP-PEG forms a tubular structure. In Fig. 6.11 (c), MCC and PEG does not mix and MCC surrounds PEG beads.

(a) PVP ●-PEG ●   (b) HPMC ●-PEG ●   (c) MCC ●-PEG ●
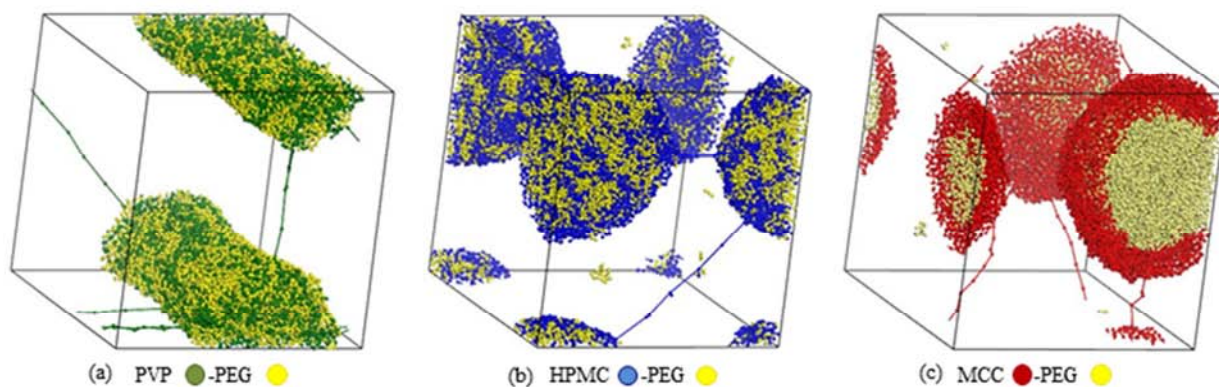
Fig. 6.11 – Images of DPD simulation of PVP-PEG400, HPMC-PEG400 and MCC-PEG400 10%-10% (w/w) in water when equilibrium state is reached. PVP: Polyvinylpyrrolidone, MCC: Microcrystalline cellulose, HPMC: Hydroxypropyl-methylcellulose, PEG: Polyethylene glycol.

Fig. 6.12 shows the distribution of polymer beads (PVP, HPMC and MCC) around and through PEG plasticizer. In Fig. 6.12 (b), PVP shows the highest percentage of beads inside PEG (98% of PVP), meaning that PEG is a suitable plasticizer for PVP. PEG also mixes well with HPMC (Fig. 6.12 (b)) with 82% of HPMC beads that diffuses through PEG and 18% of HPMC that surround PEG beads. MCC however, completely surrounds PEG with 84% of MCC beads outside PEG (see Fig. 6.12 (c)). This suggests that MCC is not compatible with PEG as a plasticizer.

Radial distance distribution in Fig. 6.13 show similar trends; we have a wide PVP distribution curve and the vertical dotted line intersect with the cumulative PVP-PEG curve at high percentage of PVP, confirming that PVP beads mix with PEG plasticizer. It can also be seen that MCC curve has the highest and the narrowest peak. MCC always surrounds the other compounds (SA and PEG), forming a thicker external layer compared to the layers formed in all the other mixtures. We infer that low cohesion force of MCC yields to the agglomeration of the second compound (PEG or SA), preventing MCC polymer from forming a cluster.
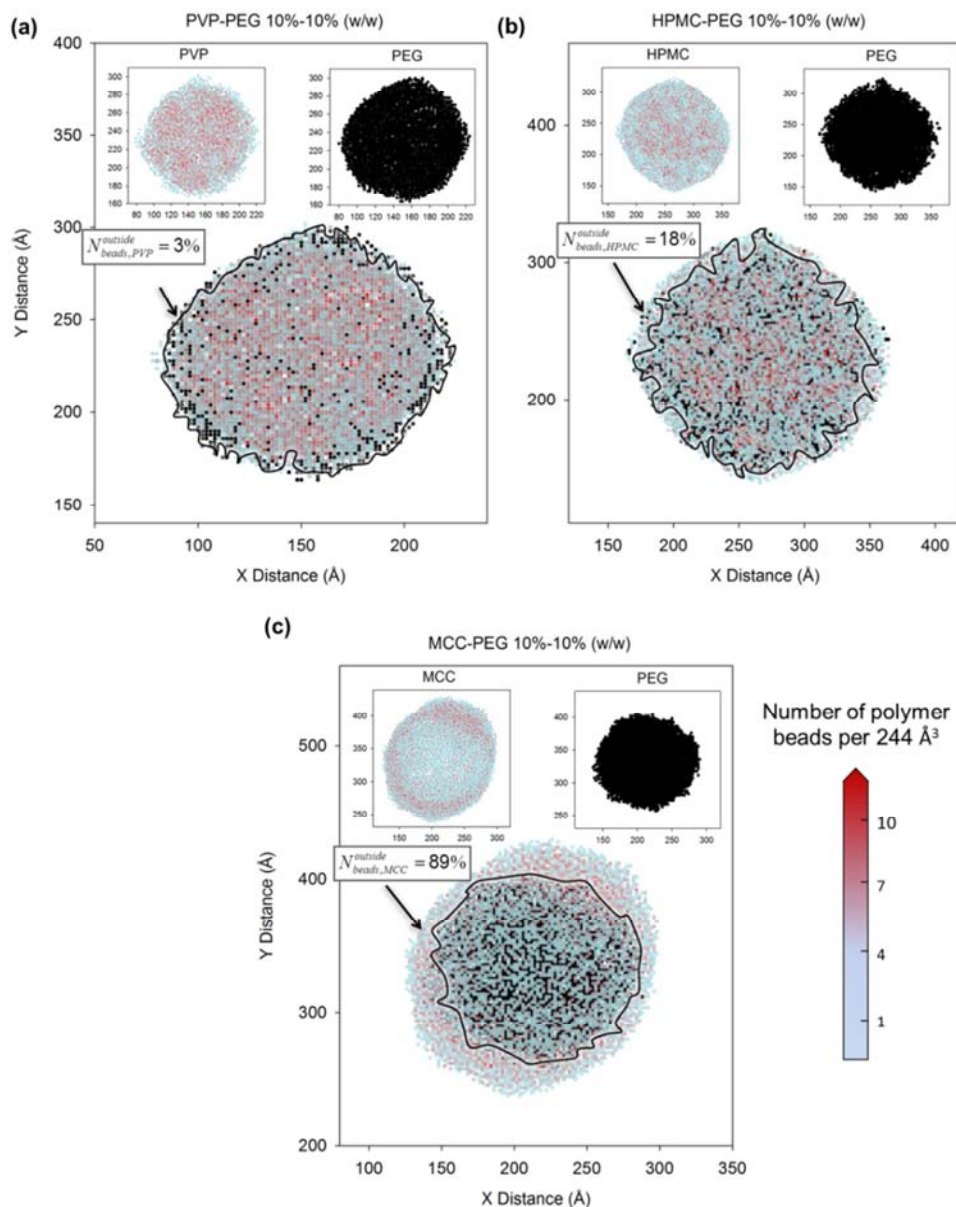
Fig. 6.12 – Distribution of polymer beads (PVP, HPMC and MCC) around and through PEG. PVP: Polyvinylpyrrolidone, MCC: Microcrystalline cellulose and PEG: Polyethylene glycol.

DPD conclusions are similar to DSC results obtained in chapter 3. DSC analysis showed that HPMC and MCC have double melting peaks indicating partial miscibility but HPMC interacts better with PEG than MCC. Also, from DSC, we concluded that PVP and PEG are more miscible and compatible than HPMC and MCC. This also was confirmed by the Flory formula (See chapter 3).
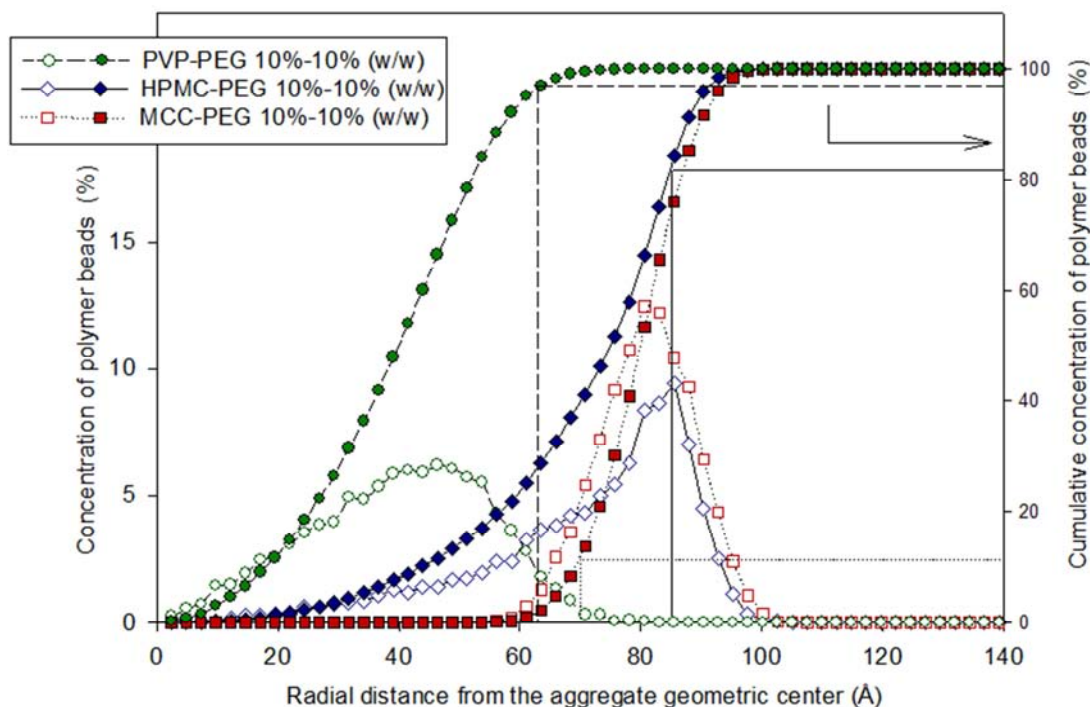
Fig. 6.13 – Concentration of polymer beads $\Gamma(r, dr)$ diffused inside PEG agglomerate as a function of radial distance from SA agglomerate geometric center. PVP: Polyvinylpyrrolidone, MCC: Microcrystalline cellulose, HPMC: Hydroxypropyl-methylcellulose and PEG: Polyethylen glycole.

4.5. Structure factor, diffusivity coefficient and end-to-end distance

4.5.1. Structure factor

The structure factor *S(Q)* describes the distribution of scattering material in real space and thus, accounts of the degree of a particle packing structure inside a colloidal dispersion (Mittal, 2002). *Q* here is the scattering vector. *S(Q)* is derived by the Fourier transformation of the radial distribution of the DPD simulation results *g(r)* (Allen and Tildesley, 1987). In order to include all possible pair interactions and to increases the resolution of the spectrum, DPD analysis of the structure factor was done with a large cut-off distance equal to 314 Å.

Fig. 6.14 shows the evolution of the structure factor *S(Q)* of SA beads in the HPMC-SA mixture when the SA fraction is increased. Each curve was averaged over the last 50 DPD time units (i.e. 268.7 ps) of simulation. A pronounced first peak of the structure factor translates into a higher sized agglomerate formation and more organized structure. The peak of the structure factor at 2% (w/w) of SA is very low, thus, the SA beads are unorganized and tend to scatter (Fig. 6.14). This corresponds to the small patches of SA trapped inside the HPMC matrix obtained in Fig. 6.4 (a). The

curve sharpens for higher SA fractions which indicate that the SA beads are more ordered. This behaviour is reminiscent of an agglomerate size growth.
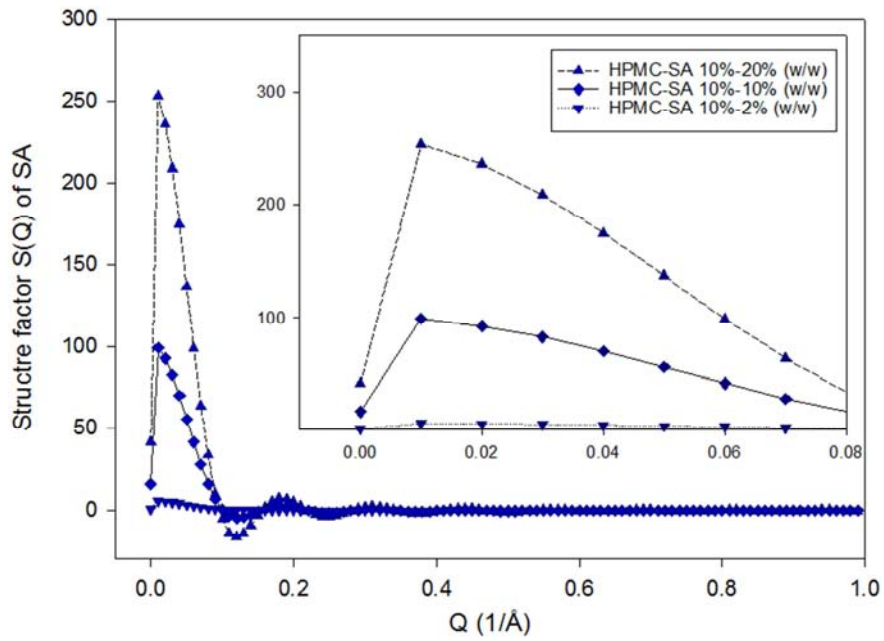
Fig. 6.14 – Average structure factor $S(Q)$ of HPMC-SA under different percentages of SA. HPMC: Hydroxypropyl-methylcellulose, SA: Stearic acid.
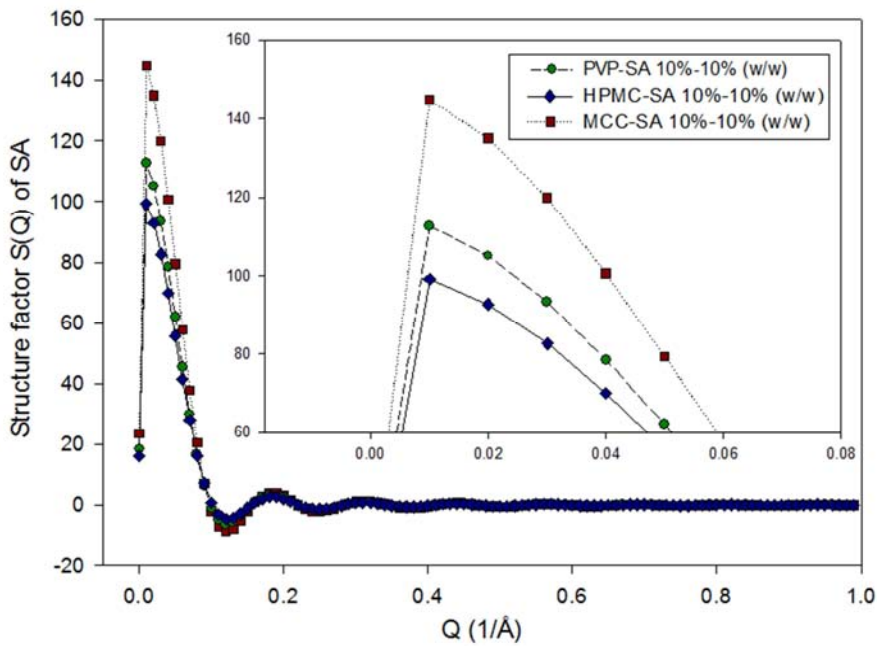
Fig. 6.15 – Average structure factor S(Q) of stearic acid (SA) agglomerates formed when using different polymeric compounds, PVP: Polyvinylpyrrolidone, MCC: Microcrystalline cellulose, HPMC: Hydroxypropyl-methylcellulose

The average structure factor curves of SA in PVP-SA, HPMC-SA and MCC-SA are shown in Fig. 6.15. MCC-SA mixture demonstrates the highest first peak, indicating formation of large SA agglomerate limited by the neat MCC spherical shell. The SA agglomerate structure is also better organized in the case of MCC-SA than in the cases of PVP-SA and HPMC-SA.

4.5.2. Diffusivity coefficient

The diffusivity coefficient D in DPD simulations is anticipated from Einstein's mean square displacement relation (Allen and Tildesley, 1987; Einstein, 1905). The equation that we used to calculate D is given by the following formula:

$$D = \frac{1}{6} \lim_{t \to \infty} \frac{d}{dt} < \left| r_i(t) - r_i(0) \right|^2 >$$

(6.25)

Note that the original equation given by Einstein in 1905, $< x^2 >=< y^2 >=< z^2 >= 2Dt$, is in one dimensional Cartesian coordinates and for quiescent fluid.
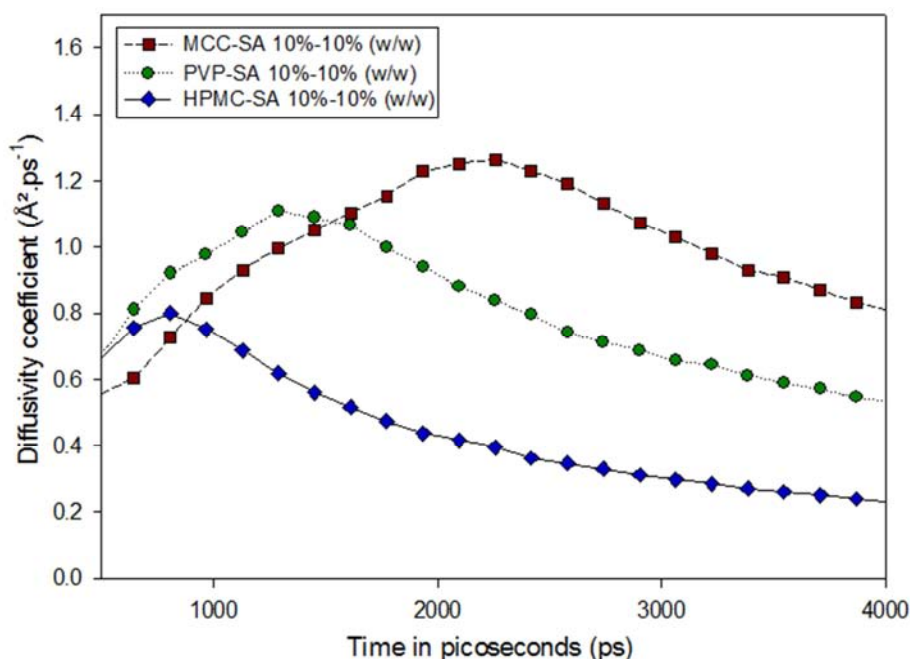
Fig. 6.16 – Evolution of the diffusivity of HPMC, PVP and MCC in the mixtures HPMC-AS, PVP-AS and MCC-AS (10%-10% (w/w) in water) respectively, as a function of time in DPD units. HPMC: Hydroxypropyl-methylcellulose, PVP: Polyvinylpyrrolidone, MCC: Microcrystalline cellulose, SA: Stearic acid.

Ideally, adsorption of polymer should occur relatively quickly during the stabilization (Vincent, 1974). Fig. 6.16 shows the evolution of the coefficient of diffusivity over DPD time of HPMC, PVP and MCC when mixed with SA in aqueous environment. We notice that the diffusion coefficient comes

134

out higher than for a typical fluid, when expressed in physical units. As follows from Groot and Warren (1997), it is possible to increase the dissipation strength to achieve exact agreement with the experiments. Unfortunately, this requires a much smaller time step to be able to integrate the higher friction forces. Furthermore, since we are mainly looking for qualitative results and considering that the structure of the materials in the DPD simulation is not affected by the dissipation strength, we chose to keep the default values of the dissipation strength proposed by Groot and Warren (1997).

According to equation (6.25), a steeper slope in the diffusion curve indicates fast diffusion. HPMC reaches steady state faster than MCC and PVP and have lower first peak (Fig. 6.16), meaning that trapping SA molecules by HPMC polymer is easier than by the other polymers. This suggests that HPMC is a better stabilizing agent for SA than MCC and PVP.

4.5.3. End-to-end distance

In Fig. 6.17 (a), we present the end-to-end distance distribution curve at equilibrium state (last simulation step) of HPMC polymer and we compare it to the end-to-end distance of SA. This parameter is the distance between one end of a polymer chain (or long molecule) to the other end, and thus describes the coiling degree of a polymer chain. Because of their low chain length compared to HPMC, SA end-to-end distribution curve show a pronounced peak and a narrower curve than HPMC. The curves are spread between 2 and 60 Å for HPMC and between 2 and 20 Å for SA. HPMC polymer chains that surround SA agglomerate have higher end-to-end distance and thus, are less coiled. It appears that SA agglomerate forces the surrounding HPMC chains to straighten-up.
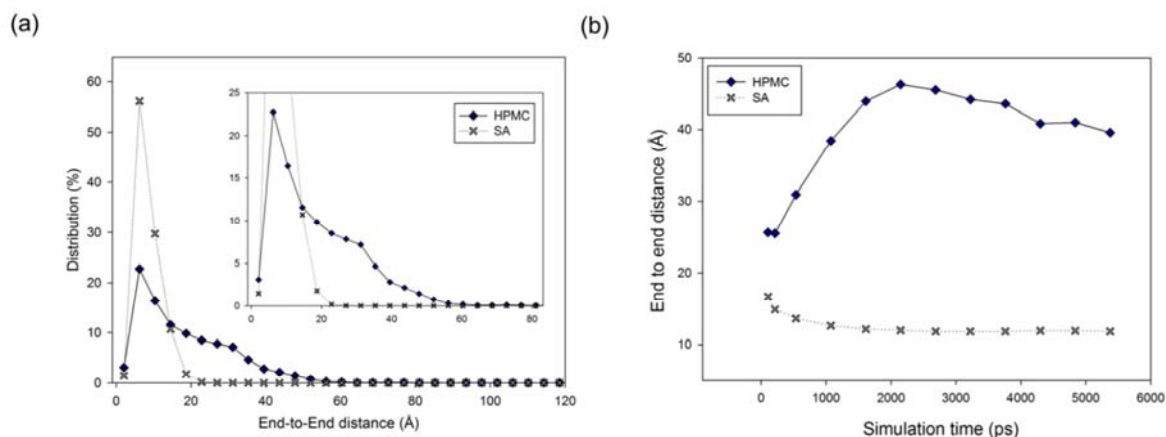
Fig. 6.17 – End-to-end distance of HPMC and SA in HPMC-SA mixture. (a) End-to-end distance of the last step of the DPD simulation, (b) Average end-to-end distance as a function of simulation time, each point is averaged over 10 successive steps.

Fig. 6.17 (b) shows the evolution of the average end-to-end distance as a function of simulation time, each value is averaged over 10 simulation steps. We notice that the end-to-end distance of SA

decreases until the simulation time is 1000 ps, and then remains constant. This means that SA is aggregating and the distance between joined beads of SA molecules decreases under the action of the strong repulsive forces of the water beads and HPMC beads. On the other hand, HPMC end-to-end distance starts increasing rapidly until the 2200th time unit. This is the time before which the spherical SA agglomerate was formed and the HPMC polymer starts covering the formed agglomerate. The small decrease in the end-to-end distance of HPMC polymer chains at the end of simulation is due to the compression and stretching of the spherical agglomerate before reaching the equilibrium state.

MCC's end-to-end distance curve shown in Fig. 6.18 (a) shows a wide distribution between 2 and 70 Å, the majority of the MCC chains have an end-to-end distance between 5 and 20 Å. The high end-to-end distance of MCC chains can also be explained by the absence of MCC beads inside the SA agglomerate; because the less polymer beads that diffuse inside the SA agglomerate, the less coiled the polymer chain. Most of the MCC chains extend themselves to surround the SA agglomerate, and the high repulsion between SA and MCC beads prevent their mixing. In addition, MCC presents wider distribution than HPMC, indicating less coiled chains. To make sure that the end-to-end distance became stationary, we run longer simulations for MCC and HPMC (see appendix K).
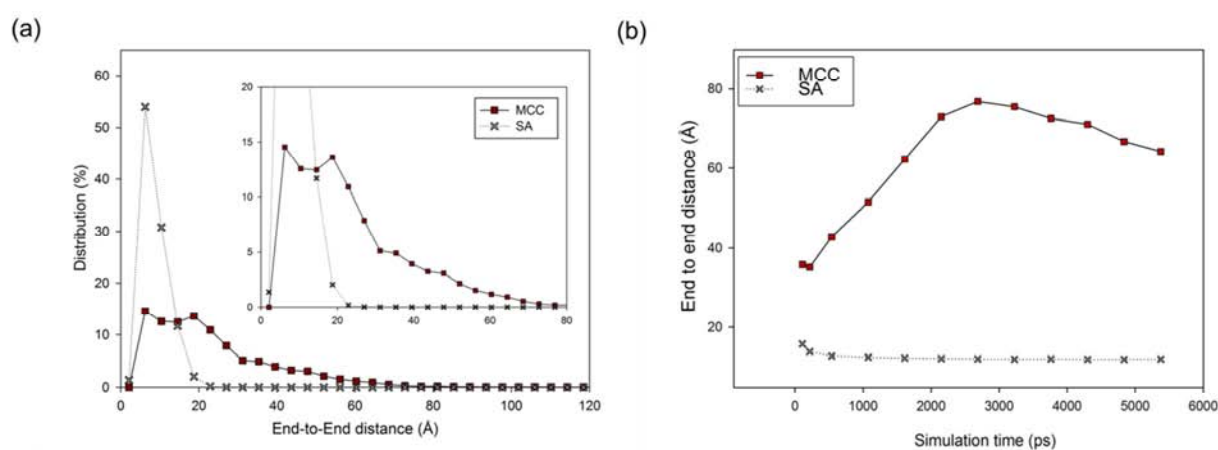
Fig. 6.18 – End-to-end distance of MCC and SA in MCC-SA mixture. (a) End-to-end distance of the last step of the DPD simulation, (b) Average end-to-end distance as a function of simulation time, each point is averaged over 10 successive steps.

Fig. 6.19 (b) and (b) show the evolution of the end-to-end distance of PVP in the PVP-SA mixture along the x coordinate and through simulation time respectively. PVP has a shorter number of beads per polymer chain than MCC and HPMC, resulting in a lower end-to-end distance than HPMC and MCC. In Fig. 6.19 (b) PVP's average end-to-end distance increases until 1500 ps to 27 Å than decreases to 23 Å. At the beginning of the simulation PVP chains extend, then, when the tubular structure begins to form PVP chains begin to coil.
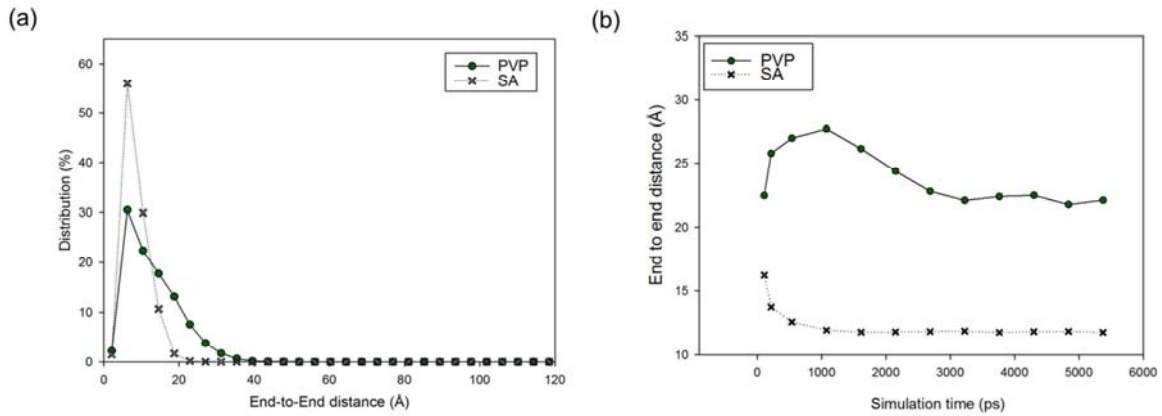
Fig. 6.19 – End-to-end distance of PVP and SA in PVP-SA mixture. (a) End-to-end distance of the last step of the DPD simulation, (b) Average end-to-end distance as a function of simulation time, each point is averaged over 10 successive steps.

4.6. Affinity predictions obtained from DPD simulations

The adherence of a material on the surface of a second material requires good affinity between them. Strong affinity between two materials in an aqueous system translates into thicker layer on the surface of the stronger cohesive material (Jarray et al., 2015). In chapter 5, we extended the work of adhesion and the tensile strength equations originally formalized by Gardon (1976) to ternary systems, and then predicted the affinity between different compounds in aqueous systems. Table 6.7 shows the affinity between the materials predicted using the DPD simulation results, and compares them with our previous model (see chapter 5) based on the work of adhesion $W_{Adhesion}$ and tensile strength $\sigma_{tensile}$.

In Table 6.7, the letter "O" means compound A surrounds compound B in water, the letter "X" means compound B surrounds compound A in water, and the letter "M" means compound A and B are mixed in water.

Table 6.7 – Affinity predicted with PVP, MCC and HPMC in water using different approaches.

A	B								
	PVP			MCC			HPMC		
	DPD	$W_{Adhesion}$	$\sigma_{tensile}$	DPD	$W_{Adhesion}$	$\sigma_{tensile}$	DPD	$W_{Adhesion}$	$\sigma_{tensile}$
SA	X	O	O	X	X	X	X	X	X
PEG400	M	M	X	X	X	X	X	X	X

PVP: Polyvinylpyrrolidone, MCC: Microcrystalline cellulose, HPMC: Hydroxypropyl-methylcellulose, SA: Stearic acid, PEG: Polyethylene glycol.
O: A surrounds B, X: B surrounds A, M: A and B are mixed in water

From Table 6.7, we can see that the DPD simulations and the work of adhesion approach tend to give similar predictions. All approaches predict that MCC adheres on the surface of the other

compounds (SA and PEG) when they are dispersed in water, and that HPMC tend to surround SA and PEG. Also, in the case of PVP-PEG in water, DPD simulations and the work of adhesion approach agree and show that PVP tend to mix with PEG. The difference between the approaches occurs for PVP-SA. The reason could be that the cohesion work of SA in water is underestimated when using Gardon's correlation in the case of the work of adhesion approach (see chapter 5).

5. Conclusion

In this chapter, we proposed a mesoscale "coarse-grain" model for hydroxypropyl-methylcellulose (HPMC), polyvinylpyrrolidone (PVP), microcrystalline cellulose (MCC), polyethylene glycol (PEG) and stearic acid (SA). DPD method was applied to the coarse grain model and dynamic simulations were launched, allowing to describe the structure of colloidal suspensions composed of the aforementioned polymers. Interfacial energy of polymers obtained from DPD simulations are close to the experimental values. We have examined polymer-SA interactions with particular emphasis on the percentage of polymer that diffuses inside SA agglomerate. DPD simulation results were further analyzed using the structure factor, end-to-end distance and the diffusion coefficient. The results show that our "coarse grain" model is able de reproduce some structural features of aqueous colloidal formulations and to give some explanations on the experimental results obtained in chapter 3.

According to DPD results, at low percentages of SA (below 10% (w/w)), HPMC completely covers SA and forms a network that diffuses deeply through SA. At higher SA load a tubular structure is obtained and there is not enough HPMC to cover the SA core and to penetrate inside it. Low HPMC polymer inside the SA agglomerate core weakens the attachment between SA crystal and HPMC and may result in agglomeration. MCC interposes in the outer surface of SA agglomerate without diffusing inside them. PVP shows an opposite behavior comparing to MCC and high amount of PVP beads diffuses through SA particles and a tubular structure is obtained. HPMC diffuses faster through water than PVP and MCC, indicating better stabilization performance of HPMC. In addition, DPD simulations showed that PEG plasticizer mix well with PVP indicating good compatibility between them. Partial diffusion of PEG through HPMC is obtained showing that there is partial miscibility between HPMC and PEG. However, PEG and MCC are not miscible, and MCC tend to cover PEG in water.

The affinity results between the materials obtained through DPD simulation are similar to those obtained by the predictive models based on the work of adhesion and the tensile strength (see chapter 5).

General conclusion and perspectives

In coating and agglomeration processes, the properties of the final product, such as solubility, size distribution, permeability and mechanical resistance depend on the process parameters and the binder (or coating) solution properties. These properties include the type of solvent used, the binder composition and the affinity between its constituents. This latter controls also the stability of the colloidal formulations. While previous PhD works at Laboratoire de Génie Chimique (PhD of Benali, 2006 and of Laboulfie 2013) confirmed experimentaly these statements and hypothesized some explanations, we have attempted in this work to confirm these hypotheses by using both experimental, theoretical model and molecular simulation approaches.

In the first chapter, we presented the context of the study, as well as the issues and problems encountered in granulation and coating formulation. We described the granulation process and the process by which agglomeration and coating mechanisms occur. In a second part of chapter one, we addressed the issues of colloid stability and plasticizer-polymer compatibility often encountered during binder or coating formulation. Finally, we presented the objectives of this work.

In the second chapter, we presented the materials used throughout this thesis and the experimental instruments including Cryogenic-SEM instruments, Malvern Mastersizer 2000, Differential scanning calorimetry, Ultra-Turrax disperser and CAMAG manual handcoater.

In the third chapter, experimental results were presented and discussed; particle size distribution analysis showed that for low percentage of SA (below 10% w/w) and in the presence of HPMC, the majority of SA particles are below 1 µm in diameter. However, PVP is not as effective stabilizer as HPMC and exhibits partial stability. We also found that MCC is also able to prevent the formation of big SA agglomerates and may be a better stabilizing agent than HPMC. SEM images revealed that HPMC surrounds SA agglomerates with a hatching textured film and anchors on their surface. In addition, better SEM images are obtained when using High pressure freezing (HPM100). SEM images also showed that MCC covers SA agglomerate but it's not able to diffuse inside its inner core. DSC analysis showed that PEG is a good and compatible plasticizer for PVP. HPMC and MCC are not as compatible as PVP, but HPMC shows higher degree of miscibility and more attraction to PEG molecules than MCC.

In the fourth chapter, σ-profiles of the materials were generated using Dmol3-COSMO. We have found that HPMC, PVP and PEG have similar σ-profile, indicating similar behavior in water. MCC and SA σ-profiles indicated low solubility in water. Also, we used molecular simulation and group

contribution methods to calculate the solubility parameter (δ). The obtained values were close to the experimental ones and were used in chapter five for the prediction of solid-binder interactions.

In the fifth chapter, we compared two approaches to predict the binder-substrate affinity in dry and in aqueous media, one based on the work of adhesion and the other based on the ideal tensile strength (Rowe, 1988). The novelties in this chapter are four folds. First, the equations used in both approaches are generalized and rewritten as a function of the Hildebrand solubility parameter δ. δ is obtained from molecular simulations or predicted from HSPiP group contribution method. Secondly, a correlation between δ and the experimental surface tension γ is established for cellulose derivative (such as HPMC and Ethyl cellulose). Thirdly, the concept of ideal tensile strength, originally formalized by Gardon (1967) for binary systems, is extended to ternary systems and applied for granulation in aqueous media. Fourthly, the approaches are tested for various systems and compared to experimental observations. For dry binary systems, predicted adhesive and cohesive properties agree with literature experimental observations, but the work of adhesion approach performs better than the ideal tensile strength approach. Both approaches predict that HPMC is a good binder for MCC. The results also indicate that PEG400 has a good affinity with HPMC and Stearic acid.

In aqueous systems, the predictions fully agree with the observations of Laboulfie et al. (2013). We noticed that the work of adhesion is positive for all the materials. Following Israelachvili's (2010) conclusions, this implied that all the compounds should agglomerate in water. The model also predicted that MCC has the lowest work of adhesion and cohesion in water, meaning that for all the mixtures, MCC will most likely adhere on the surface of the other compounds when they are dispersed in water. In addition, whereas no interactions are observed between SA and HPMC in dry system, we found that HPMC adhere on the surface of SA when they are placed in water.

In the sixth chapter we used mesoscale simulations to investigate the structure of agglomerates formed in aqueous colloidal formulations used in coating and granulation processes. For the simulations, dissipative particle dynamics (DPD) and a coarse-grained approach were used. In the DPD method, the materials are described as a set of soft beads interacting according to the Flory-Huggins model. The repulsive interactions between the beads were evaluated using the solubility parameter (δ) as input, where, δ was calculated by all-atom molecular dynamics.

To prevent colloidal agglomeration of SA, the stabilizing agent has to be adsorbed strongly enough on the surface of the particle and should form a thick adsorbed layer around it. DPD simulation results showed that the HPMC polymer is able to adsorb in depth into the inner core of SA agglomerate and covers it with a thick layer. We also observed that the structure of HPMC-SA mixture varies under different amounts of SA. For high amounts of SA, HPMC becomes unable to fully stabilize SA. However, MCC interposes in the outer surface of SA agglomerate without diffusing

inside them. PVP shows an opposite behavior comparing to MCC and high amount of PVP beads diffuses through SA particles and a tubular structure is obtained. This indicated a susceptibility to SA particle agglomeration in the case of MCC-SA and PVP-SA. Diffusivity coefficient showed that HPMC diffuses faster than MCC and PVP in water. Structure factor indicates the formation of a better organized structure in the case of MCC-SA and PVP-SA mixtures.

For a compound to be effective as a plasticizer, it must be able to diffuse into the polymer, and they must be miscible. DPD simulations showed that PEG plasticizer does not diffuse between the MCC polymer chains and MCC covers PEG with a spherical shell. On the other hand, PEG diffuses inside PVP and HPMC and mix with it, indicating good miscibility. PEG polymer diffuses inside HPMC chains thereby extending and softening the composite polymer. Overall, the experimental results obtained in chapter 3 are similar to the DPD simulation results. The affinity predictions obtained by the predictive models based on the work of adhesion and the tensile strength are similar to those obtained using DPD simulation.

The following table summarizes the experimental results and compares them with the results obtained by the different models and simulation methods:

Results summery Table

Mixture	Experiments	The different models
SA in water	▪ Phase separation [a], ▪ SA has the form of crystalline needles that form large agglomerate in water and their size is around 50 μm [b, c],	▪ SA is not soluble in water [e].
HPMC in water	▪ Transparent and soluble in water [a], ▪ HPMC forms an amorphous structure in water [c], ▪ HPMC form more ordered crystal structure with fewer impurities than MCC and PVP [d].	▪ HPMC is soluble in water [e], ▪ PVP, HPMC and PEG have similar behavior in water (i.e. possible miscibility in each other) [e].
PVP in water	▪ Transparent and soluble in water [a].	▪ PVP is soluble in water [e].
MCC in water	▪ Forms a white mixture [a] ▪ MCC has a very low solubility in water [b].	▪ MCC has low solubility in water [e].

a: Solution appearances, b: Particle size distribution, c: Cryogenic-SEM, d: DSC, e: COSMO,f: molecular simulation, g: work of adhesion model, h: tensile strength model, i: DPD., j: Hamaker model.

Results summery Table (continuation)

Mixture	Experiments	The different models
HPMC-SA	▪ The agglomerates are monodisperse at 2% (w/w) of SA [b] ▪ At 2% (w/w) of SA, HPMC fully stabilizes SA giving rise to the smallest particles [b] ▪ HPMC surrounds SA crystals with a gel network which prevent their agglomeration [c] ▪ The stabilization of SA by HPMC is limited to SA percentages below 20% (w/w) [b, c].	▪ HPMC mix with SA in dry systems [g, h, j] ▪ HPMC surrounds SA in aqueous systems [g, h, i] ▪ SA particles are stabilized by HPMC particles in water [i] ▪ HPMC becomes unable to stabilize SA at high percentages of SA (above 20%) [i] ▪ HPMC is a better stabilizing agent for SA than MCC and PVP [i].
PVP-SA	▪ PVP is able to partially stabilize SA but it is not as effective as HPMC [b] ▪ Large SA agglomerates as well as some small SA agglomerates can be seen by SEM [c].	▪ SA surrounds PVP in dry systems [g, h, j] ▪ PVP tend to mix with SA in aqueous systems [i] ▪ PVP is able to stabilize SA particle but it's not as effective as HPMC [i].
MCC-SA	▪ MCC can prevent the formation of big SA particles even at 20% (w/w) of SA [b] ▪ At low percentages of SA, HPMC is better stabilizing agent than MCC [b,c] ▪ The MCC network in MCC-SA is like a crossing net and MCC does not adsorb in the surface of SA crystals [c].	▪ MCC surround SA in aqueous systems [g, h, i], but mix with SA in dry systems [g] ▪ MCC does not diffuse inside SA agglomerates [i] ▪ MCC may be a good dispersing agent but not a good stabilizer [i].
HPMC-PEG	▪ Transparent solution [a] ▪ HPMC form more ordered crystal structure with fewer impurities than MCC [d] ▪ Partial miscibility between PEG and HPMC [d].	▪ HPMC and PVP are more compatible with PEG400 as a plasticizer than MCC [f] ▪ HPMC surrounds PEG particles in dry systems [g, h] and in aqueous systems [g, h, i] ▪ Partial miscibility between PEG and HPMC [i].

a: Solution appearances, b: Particle size distribution, c: Cryogenic-SEM, d: DSC, e: COSMO, f: molecular simulation, g: work of adhesion model, h: tensile strength model, i: DPD, j: Hamaker model.

Results summery Table (continuation)

Mixture	Experiments	The different models
PVP-PEG	▪ PEG is a good plasticizer for PVP [d].	▪ PVP is miscible with PEG in water [e] ▪ PVP mix with PEG in dry systems [g] ▪ PVP mix with PEG in aqueous systems [g, i].
MCC-PEG	▪ MCC and PEG molecules show repulsion [d] ▪ MCC is less compatible with PEG than PVP and HPMC [d].	▪ MCC surrounds PEG in aqueous systems [g, i] ▪ MCC mix with PEG in dry systems [g] ▪ MCC is not compatible with PEG as a plasticizer [i].

a: Solution appearances, b: Particle size distribution, c: Cryogenic-SEM, d: DSC, e: COSMO, f: molecular simulation, g: work of adhesion model, h: tensile strength model, i: DPD, j: Hamaker model.

Perspectives

The results presented in this thesis showed the dominant effect of the solvent during coating formulation. In this context, it would be interesting to try solvents other than water and to investigate their effect on the affinity and the stability of the coating formulation.

From a mesoscopic modelisation point of view, it would be desirable to compare the DPD simulation results to those obtained from a mesoscopic model developed based on the Boltzmann inversion method. Also, it would be interesting to improve the DPD model by adjusting the dissipation strength to achieve agreement with experiment in order to obtain more quantitative results.

Another perspective is to produce a description of macroscale particle processes from information at the micro and meso scale. Depending on which type of phenomena that is of importance for the wet granulation process, macroscopic properties of interest can be identified and a compartment model is afterward constructed accordingly (based on the information already obtained at particle level), which is able to describe large scale processes under different flow conditions. Then, macroscopic simulation can be launched using simulation techniques such as DEM and FEM.

References

A

Ash M. and Ash I., Handbook of Green Chemicals, first ed., Endicott, NY, 1998.

Albers W. and Overbeek J.Th.G., Stability of emulsions of water in oil. III. Flocculation and redispersion of water droplets covered by amphipolar monolayers, J. Colloid Sci. 15 (1960), 489–502.

Allen M. P. and Tildesley D. J., Computer Simulation of Liquids, Oxford Science Publications, Clarendon Press, 1987.

Amighi K. and Moes A. Influence of plasticizer concentration and storage conditions on the drug release rate from Eudragit RS 30 D film-coated sustained-release theophylline pellets. Eur. J. Pharm. Biopharm. 42 (1) (1996), 29–35.

Arwidsson H., Hjelstuen O., Ingason D. and affner C.Gr., Properties of ethyl cellulose films for extended release. Part 2. Influence of plasticizer content and coalescence conditions when using aqueous dispersions, Acta Pharmaceutica Nordica 3 (2) (1991), 65–70.

Autumn K., Sitti M., Liang Y. A., Peattie A.M., Hansen W. R., Sponberg S., Kenny T. W., Fearing R., Israelachvili J.N., and Full R. J., Evidence for van der Waals adhesion in gecko setae, Proc. Natl. Acad. Sci. USA99 (2002), 12252 –12256.

B

Baghbanzadeh M., Rana D., Matsuura T., Lan C. Q., Effects of hydrophilic CuO nanoparticles on properties and performance of PVDF VMD membranesn, Desalination 369 (2015), 75–84.

Barton A.F.M., CRC Handbook of Solubility Parameters and Other Cohesion Parameters, 1991.

Barnett J., Chow J., Ives D. et al. Purification, characterization and selective inhibition of human prostaglandin G/H synthase 1 and 2 expressed in the baculovirus system. Biochim. Biophys. Acta 1209 (2) (1994), 130–139.

Barra J., Falson-Rieg F. and Doelker E., Influence of the organization of binary mixes on their compactibility, Pharm. Res. 16 (1999), 1449-1455.

Barra J., Lescure F., Falson-Rieg F. and Doelker E., Can the organization of a binary mix be predicted from the surface energy, cohesion parameter and particle size of its components?, Pharm. Res. 15 (1998), 1727–1736.

Barton A.F.M., CRC Handbook of Solubility Parameters and Other Cohesion Parameters, 1991.

Becke, A. D., A multicenter numerical integration scheme for polyatomic molecules, J. Chem. Phys. 88 (1988), 2547–2551.

Becker D., Rigassi T., Bauer Brandi A., Effectiveness of binders in wet granulation: comparison using model formulations of different tablet ability, Drug. Dev. Ind. Pharm. 23(8) (1997), 791–808.

Becker O.M. and Watanabe M., Dynamics methods in computational biochemistry and biophysics, 2001.

Beerbower A., Surface free energy: a new relationship to bulk energies, J. Colloid Interface Sci., 35 (1971), 126–132.

Belmares M., Blanco M., Goddard W.A. 3rd, Ross R.B., Caldwell G., Chou S.H., J. Pham, P.M. Olofson and C. Thomas, Hildebrand and Hansen solubility parameters from molecular dynamics with applications to electronic nose polymer sensors. J. Comput. Chem. 25 (2004) 1814–1826.

Benali M., Prédiction des interactions substrat-liant lors de la granulation : Etude expérimentale dans un mélangeur à fort taux de cisaillement, approches thermodynamiques par simulation moléculaire, thesis 2006, INPT.

Benali M., Gerbaud V. and Hemati M., Effect of operating conditions and physico-chemical properties on the wet granulation kinetics in high shear mixer, Powder Technol.190 (1-2) (2009), 160-169.

Bhushan, B., Israelachvili J.N., Landman U, Nanotribology-Friction, wear and lubrication at the atomic-scale. Nature 374 (1995), 607–616.

Bicerano J., Prediction of Polymer Properties (CRC Press), 2002.

Biovia, Material Studio Suite release 7, 2013, http://accelrys.com/products/materials-studio/index.html

Bodmeier R. and Paeratakul O., The distribution of plasticizers between aqueous and polymer phases in aqueous colloidal polymer dispersions. Int. J. Pharm. 103(1) (1994), 47–54.

Bodmeier R. and Paeratakul O. Plasticizer uptake by aqueous colloidal polymer dispersions used for the coating of solid dosage forms. Int. J. Pharm. 152(1) (1997), 17–26.

Boek E.S., Coveney P.V., Lekkerkerker H.N.W., Computer simulation of rheological phenomena in dense colloidal suspensions with dissipative particle dynamics, J. Phys: Condens. Matter 8 (47) (1996), 9509-9512.

Boek E.S., Coveney P.V., Lekkerkerker H.N.W., and van der Schoot P., Simulating the rheology of dense colloidal suspensions using dissipative particle dynamics, Physical Review E, 55(3) (1997), 3124-3133.

Bonn R. and van Aartsen J.J., Solubility of polymers in relation to surface tension and index of refraction, Eur. Polym. J. 8 (1972), 1055-1066.

Borsacchi S., Martini F., Geppi M., Pilati F., Toselli M., Structure, dynamics and interactions of complex solegel hybrid materials through SSNMR and DSC: Part II, ternary systems based on PEePEG block copolymer, PHS and silica, Polymer 52 (2011), 4545-4552.

Bouillot B., Approches Thermodynamiques pour la Prédiction de la Solubilité de Molécules d'Intérêt Pharmaceutique, thesis 2011, INPT.

Bustamante P., Martin A., and Gonzalez-Guisandez M.A., Partial solubility parameters and solvatochromic parameters for predicting the solubility of single and multiple drugs in individual solvents, J Pharm Sci 82 (1993), 635-640.

Brock T., Groteklaes M. and Mischke P., European Coatings Handbook, 2nd revised edition, 2010.

Brogly M., Fahs A. and Bistac A., Surface properties of new-cellulose based polymer, coatings for oral drug delivery systems, Polymer Preprints 52(2) (2011) 1055–1056.

Grulke E.A., Solubility Parameter Values in Polymer Handbook (eds Brandrup & Immergut), J. Wiley, (1998).

C

Calvo F., Benali M., Gerbaud V., and Hemati M., Close-packing transitions in clusters of Lennard-Jones spheres. Computing Letters, vol. 1 (4) (2005), 183-191.

Cameron I.T., Wanga F.Y., Immanuel C.D. , Stepanek F. , Process systems modelling and applications in granulation:Areview, Chem. Eng. Sci. 60 (2005), 3723–3750

Cao X., Xu G., Li Y. and Zhang Z., Aggregation of poly(ethylene oxide)-poly(propylene oxide) block copolymers in aqueous solution: DPD simulation study, J. Phys. Chem A. 109(45) (2005), 10418-10423.

Cao J., Leroy F., Depression of the melting temperature by moisture for alpha-form crystallites in human hair keratin, Biopolymers 77 (2005), 38-43.

Capes C.E. and Danckwerts P.V., Granule formation by the agglomeration of damp powders, Part 1- The mechanism of granulate growth, Trans. Instn. Chem. Engr. 43 (1965), 116–124.

Cheremisinoff N.P., (1989). Handbook of Polymer Science and Technology. Boca Raton, FL: CRC Press.

Choi P., Kavassalis T.A., and Rudin A., Estimation of the three-dimensional solubility parameters of alkyl phenol ethoxylates using molecular dynamics. J. Colloid Interface Sci. 150 (1992) 386-393.

Choi P., Kavassalis T.A. and Rudin A., Measurement of Three-Dimensional Solubility Parameters of Nonyl Phenol Ethoxylates Using Inverse Gas Chromatography, J. Colloid Interface Sci. 180 (1996), 1-8.

Chipot C., Les méthodes numériques de la dynamique moléculaire, CNRS, Université Henri Poincaré, 2003.

Chitu M.T.M, Granulation humide des poudres cohésives: rhéologie, mécanismes de croissance et tenue mécanique des granules, Thèse de Doctorat, Université de Toulouse, 2009.

Chowhan Z.T., Role of binders in moisture-induced hardness increase in compressed tablets and its effect on in vitro disintegration and dissolution. J. Pharm. Sci. 69 (1980), 1–4.

Cole G., Hogan J. and Aulton M.E., Pharmaceutical coating technology. Informa Health Care, 1995.

Cotts D.B., and Reyes Z., Electrically conductive organic polymers for advanced applications, Noyes Data Corp, Park Ridge, NJ, 1986.

Crowl V.T. and Malati M.A., Adsorption of polymers and the stability of pigment dispersions, Discuss. Faraday Soc. 42 (1966), 301–312.

D

Debye P., Die van der waalsschen kohäsionskräfte. Physikalische Zeitschrift 21 (1920), 178–187.

Delley B., Ground-State Enthalpies: Evaluation of Electronic Structure Approaches with Emphasis on the Density Functional Method, J. Phys. Chem. A, 110 (2006), 13632–13639.

Demajo L.P., Rimai D.S. and Sharpe L.H., Fundamentals of Adhesion and Interfaces (CRC Press), 2000.

Derjaguin B.V. and Landau L.D., A theory of the stability of strongly charged lyophobic sols and of the adhesion of strongly charged particles in solutions of electrolytes, Acta Physiochim. USSR 14 (1941), 633–662.

Diu B., Guthmann C., Lederer D. andRoulet B., 1989, Physique statistique, Hermann, Paris, 1989.

Dupre A., Theorie Mecanique de La Chaleur, Gauthier-Villan, Paris, France 1869.

Duris J, Kachrimanis K., Nikolakakis I., Đurić Z., Ibrić S., Preparation and characterization of carbamazepine-Soluplus® Hot-Melt Extruded solid dispersions. 8th World Meeting on Pharmaceutics, Pharm. Biopharm. Tech. (2012),19- 22

E

Einstein A., Über Die von der Molekularkinetischen Theorie der Wärme Geforderte Bewegung von in Ruhen-den Flüssigkeiten Suspendi, Physik 322 (8) (1905) 549–560.

Einstein A., Investigations on the Theory of the Brownian Movement, edited with notes by R. Fürth, Dover publications, New-York, 1956.

Eliasen H., Schaefer T., Gjelstrup K.H., Effects of binder rheology on melt agglomeration in a high shear mixer, Int. J. Pharm. 176 (1) (1998), 78–83.

Ellison J., Wykoff G., Paul A., Mohseni R. and Vasiliev A.,Efficient dispersion of coated silver nanoparticles in the polymer matrix, Colloids Surf., A 447 (2014), 67–70.

Enézian G.M., La compression directe des comprimés à láide de la cellulose microcrystalline, Pharm. Acta. Helv. 47 (1972), 321–363.

Ennis B.J., Li J., Tardos G., Pfeffer R., The Influence of Viscosity on the Strength of an Axially Strained Pendular Liquid Bridge, Chem. Eng. Sci. 45(10) (1990), 3071–3088.

Ennis B.J., Tardos G.I and Pfeffer R., A microlevel-based characterization of granulation phenomena, Powder Technol. 65 (1991), 257-272.

Español P., Serrano M. and Zuniga I., Coarse-graining of a fluid and its relation to dissipative particle dynamics and smoothed particle dynamics. Int. J. Mod. Phys. C 8 (1997) 899–908.

Español P., Dissipative particle dynamics revisited, SIMU Newsletter 4 (2002) 59–77.

F

Flekkoy E.G., Wagner G., Feder J., Hybrid model for combined particle and continuum dynamics. Europhys Lett 52(3) (2000) 271–276.

Flory P.J., Thermodynamics of high polymer solutions, J. Chem. Phys. 10 (1942) 51–61.

Flyvbjerg H. and H.G. Petersen, Error estimates on averages of correlated data, J. Chem. Phys. 91 (1989), 461-467.

Flory P. J., Theromdynamics of crystallization in high polymers. IV. A theory of crystalline states and fusion in polymers, copolymers, and their mixtures with diluents, J. Chem. Phys. 17 (1949), 223-240.

Fowkes F. M., Dispersion force contributions to surface and interfacial tensions, contact angles, and heats of immersion. Adv. Chem. Ser. 43(1964), 99–111.

Frenkel D. and Smit B., Understanding Molecular Simulation: from Algorithms to Applications, Academic Press, San Diego, 1996.

Fritz G., Schädler V., Willenbacher N. and Wagner N.J., Electrosteric Stabilization of Colloidal Dispersions, Langmuir 18 (2002), 6381–6390.

Fu J., Adams M.J., Reynolds G. K., Salman AD., Hounslow M.J., Impact deformation and rebound of wet granules, Powder. Technol. 140 (3) (2004), 248-257.

G

Gama Goicochea A.; Adsorption and Disjoining Pressure Isotherms of Confined Polymers using Dissipative Particle Dynamics, Langmuir 23 (2007), 11656-11663.

Gardon J.L., Variables and interpretation of some destructives cohesion and adhesion tests. In Treatise on Adhesion and Adhesives (1967), 269-324.

Gardon J.L., Critical Review of Concepts Common to Cohesive Energy Surface Tension, Tensile Strength, Heat of Mixing, Interracial Tension, and Butt Joint Strength, J. Colloid Interface Sci. (1977), 582-596.

Gerstner W., Crystal form and particle size of organic pigments in printing inks and paints, J. Oil. Col. Chem. Assoc. 49 (1966), 954–973.

Gee G., Thermodynamic of rubber solutions and gels in advances in colloid science (New York), 1946.

Girifalco L.A. and Good R.J., A Theory for the Estimation of Surface and Interfacial Energies. I. Derivation and Application to Interfacial Tension, J. Phys. Chem. 61 (1957), 904-909.

Girifalco L. A. and Hodak M., Van der Waals binding energies in graphitic structures, Phys. Rev. B65 (2002), 125404.

Glicksman M. E., Diffusion in solids. Field Theory, Solid-State Principles, and Applications. Wiley-Interscience, 2000.

Greenwood J.A., Adhesion of elastic spheres, Math. Phys. Eng. Sci. 453 (1961) (2001), 1277-1297.

Green D. W., Perry R. H., Perry's Chemical Engineers' Handbook, Eighth Edition, McGraw-Hill, 2008.

Gregory P., Chambers Science and Technology Dictionary. Chambers Harrap Publishers: New Penderel House, 283-288, London, UK, 1988.

Groot R.D., Electrostatic interactions in dissipative particle dynamics—simulation of polyelectrolytes and anionic surfactants, J. Chem. Phys. 118 (2003), 11265–11277.

Groot R.D. and Warren P.B., Dissipative particle dynamics: bridging the gap between atomistic and mesoscopic simulation, J. Chem. Phys. 107 (1997) 4423–4435.

Groot R. D. and Rabone K. L., Mesoscopic Simulation of Cell Membrane Damage, Morphology Change and Rupture by Nonionic Surfactants, Biophys. J. 81 (2001) 725–736.

Grulke E. A., Solubility Parameter Values. In Polymer Handbook, 4th Ed., Brandrup J., Immergut E. H., Grulke E. A., Eds. Wiley, John & Sons, Incorporated: 1999, 675-627.

Guo H., Qiu X. and Zhou J., Self-assembled core-shell and Janus microphase separated structures of polymer blends in aqueous solution, J. Chem. Phys 139 (2013), 084907.

Guskova O.A., Pal S., and Seidel C., Organization of nanoparticles at the polymer brush-solvent interface, Europhys. Lett. 88 (3) (2009), 38006.

H

Halász K. and L.Csóka, Plasticized Biodegradable Poly(lactic acid) Based Composites Containing Cellulose in Micro- and Nanosize, Journal of Engineering 23 (2013), 1-9.

Hamaker H.C., The London—van der Waals attraction between spherical particles, Physica (4), 10, (1937), 1058–1072.

Hansen C. M., In Hansen Solubility Parameters: A User's Handbook, Second Edition CRC Press: New York, 2007.

Hansen C.M., The three-dimensional solubility parameter - key to paint component affinities: I. solvents, plasticizers, polymers, and resins, J. Coat. Technol. 39 (1967) 505–510.

Hansen J.-P. and Verlet L., Phase transitions of the Lennard-Jones system, Phys. Rev. 84 (1969) 151–161.

Hansen J.-P. and Schiff D., Influence of interatomic repulsion on the structure of liquids at melting, Mol. Phys. 25 (6) (1973) 1281–1290.

Hapgood K., Khanmohammadi B., Granulation of hydrophobic powders, Powder Technol. 189 (2009), P. 253–262.

Heinämäki J.T., Lehtolab V.-M., Nikupaavoa P. and Yliruusia J.K., The mechanical and moisture permeability properties of aqueous-based hydroxypropyl methylcellulose coating systems plasticized with polyethylene glycol, International Journal of Pharmaceutics 112 (1994), 191-196.

Hennet L., Krishnan S., Pozdnyakova I., Cristiglio V., Cuello G. J., Fischer H. E., Bytchkov A., Albergamo F., Zanghi D., Brun1 J.F., Brassamin S., Saboungi M.L., and Price D.L., Structure and dynamics of levitated liquid materials, Pure Appl. Chem. 79 (10) (2007) , 1643-1652.

Hildebrand J.H., and Scott R.L.,The solubility of nonelectrolytes, third edition, Reinhold Pub. Corp., New York, 1950.

Hermana D., Walz J. Y., Adsorption and stabilizing effects of highly-charged latex nanoparticles in dispersions of weakly-charged silica colloids, J. Colloid Interface. Sci. 449 (2015), 143–151.

Hemati M., Benali M., Product Design and Engineering: Best Practices, Vol.1, chapter 8, Edited by Ulrich Bröckel, Willi Meier and Gerhard Wagner, Weinheim, 2007.

Hohenberg P. and Kohn W., Inhomogeneous Electron Gas, Phys. Rev. 136 (1964), B864-B871.

Holm P., High shear mixer granulators, in: Dilip M. Parikh: Handbook of pharmaceutical granulation technology, 81 (1997) 151-204.

Hoogerbrugge P.J., Koelman J.M.V.A, Simulating microscopic hydrodynamic phenomena with dissipative particle dynamics. Europhysics Letters 30(4) (1992) 191–196.

Hoy K.L , New values of the solubility parameters from vapor pressure data, J. Coat. Technol. 42 (1970) 76-118.

HSPiP V.3.1 Software (2010), http://www.hansen-solubility.com/HSPiP.html

I

Iley W.J., Effect of Particle Size and Porosity on Particle Film Coatings, Powder Technol. 65 (1991) 441–445.

Rasband W. S., ImageJ, National Institutes of Health, Maryland, USA, 1997. <http://imagej.nih.gov/ij/> (accessed 2013).

Iranloye T.A. and Parrott E.L., Effects of compression force, particle size, and lubricants on dissolution rate, J. Pharm. Sci. 67 (1978), 535–539.

Irisa H. and Yokomine T., Determination of DPD Model Aiming Biomedical Application, Int. J. Soft. Comput. Biomed. Hum. Sci. 15, No.2 (2010), 27–32.

Irving J.H. and Kirkwood J.G., The statistical mechanical theory of transport processes. IV. The equations of hydrodynamics. J.Chem.Phys. 18 (6) (1950) 817–829.

Israelachvili J.N, Intermolecular and Surface Forces (Academic Press), 2010.

Iveson, S.M., Litster, J.D., Hapgood, K., Ennis, B.J. Nucleation, growth and breakage phenomena in agitated wet granulation processes: a review. Powder Technol. 2001a, 117 (1), 3–39.

Iveson S. M. and Litster J.D., Fundamental Studies of granule consolidation, Part 2: Quantifying the effects of particle and binder properties, Powder Technol. 99 (1998), 243–250.

J

Jarray A., Gerbaud V. and Hemati M., Prediction of solid - binder affinity in dry and aqueous systems: Work of adhesion approach vs. ideal tensile strength approach, Powder. Technol. 271 (2015) 61–75.

Johnson J.L., Wimsatt J., Buckel S.D., et al. Purification and characterization of prostaglandin H synthase-2 from sheep placental cotyledons. Arch. Biochem. Biophys. 324 (1995), 26–34.

Jaiyeoba K.T. and Spring M.S., The granulation of ternary mixtures: The effect of the solubility of the excipients, J. Pharm. Pharmacol. 32 (1980a), 1-5.

Jaiyeoba K.T. and Spring M.S., The granulation of ternary mixtures: The effect of the wettability of the powders, J. Pharm. Pharmacol. 32 (1980b), 386-388.

Jiménez A., Fabra M.J., Talens P. and Chiralt A., Effect of lipid self-association on the microstructure and physical properties of hydroxypropyl-methylcellulose edible films containing fatty acids, Carbohydr. Polym. 82 (2010) 585-593.

Gregory J., Effects of Polymers on Colloid Stability in "The Scientific Basis of Flocculation", Vol. 27, 1978.

Johansen A., Schaefer T., Effects of interactions between powder particle size and binder viscosity on agglomerate growth mechanisms in a high shear mixer, Eur. J. Pharm. Sci. 12 (3) (2001), 297–309.

K

Keddie J.L., Meredith P., Jones R.A.L. and Donald A.M., Kinetics of film formation in acrylic latexes studied with multiple-angle-of-incidence ellipsometry and environmental SEM, Macro-molecules 28 (8) (1995), 2673–2682.

Keesom W.H., The second virial coefficient for rigid spherical molecules whose mutual attraction is equivalent to that of a quadruplet placed at its center. Proc. R. Acad. Sci. 18 (1915), 636–646.

Keningley S.T., Knight P.C., Marson A.D., An investigation into the effects of binder viscosity on agglomeration behavior, Powder Technol. 91 (2) (*1997*), 95–103.

Keddie J.L., Meredith P., Jones R.A.L. and Donald A.M., Rate-limiting steps in film formation of acrylic latexes as elucidated with ellipsometry and environmental scanning electron microscopy, Ch. 21 in:

Khoufech A., Benali M. and Saleh K. , Influence of liquid formulation and impact conditions on the coating of hydrophobic surfaces, Powder Technol. 270 (B), 2015, 599–611

Kim D.I., Grobelny J., Pradeep N., Cook R.F, Origin of adhesion in humid air, Langmuir 24 (2008) 1873–1877.

King J.W., Determination of the solubility parameter of soybean oil by inverse gas chromatography, LWT-Food Sci. Technol. 28 (2) (1995), 190–195.

Kinloch A. J., Adhesion and Adhesives: Science and Technology, Chapman and Hall, 1994.

Klamt A., COSMO-RS: From quantum chemistry to fluid phase thermodynamics and drug design, Elsevier Science Ltd., Amsterdam, The Netherlands, 2005.

Klamt A. and Schüürmann G., COSMO: A new approach to dielectric screening in solvents with explicit expressions for the screening energy and its gradient, J. Chem. Soc., Perkin Trans. 2 (1993), 799-805.

Kleinebudde P., Roll compaction/dry granulation: pharmaceutical applications. Eur. J. Pharm. Biopharm. 58 (2004), 317–326.

Kleis J. and Schröder E., Van der Waals interaction of simple, parallel polymers, J. Chem. Phys.122 (2005), 164902.

Knight P.C., Instone T., Pearson J. M. K., Hounslow M.J., Powder Technol. 97 (3) (1998), 246–257.

Koehnen D. M., Smolders C. A., The determination of solubility parameters of solvents and polymers by means of correlations with other physical quantities, J. Appl. Polym. Sci. 19 (1975), 1163–1179.

Koelman J.M.V.A. and Hoogerbrugge P.J., Dynamic simulation of hard-sphere suspensions under steady shear. Europhys. Lett. 21 (1993), 363-368.

Koelmans H. and Overbeek J.Th.C., Discussions of the Faraday Society, 18, 1954.

Kohn W. and Sham. L. J., Self-Consistent Equations Including Exchange and Correlation Effects, Phys. Rev. 140 (1965), A1133–A1138.

Kundu J., Patra C. and Kundu S.C., Design, fabrication and characterization of silk fibroin-HPMC-PEG blended films as vehicle for transmucosal delivery, Mater. Sci. Eng. C 28 (2008), 1376-1380.

L

Laboulfie F., Depôt en couche mince d'un multi-materiau à la surface de particules solides : application à l'enrobage de particules alimentaires (Toulouse, INPT), 2013.

Laboulfie F., Hemati M., Lamure A. and Diguet S., Effect of the plasticizer on permeability, mechanical resistance and thermal behaviour of composite coating films, Powder Technol. 238 (2013) 14-19.

Lehmann K., The application and processing of acrylic coatings in form of aqueous dispersions compared with organic solutions, Acta Pharm. Fenn. 91 (1982), 225–238.

Lerk C.F., Bolhuis GK. Comparative evaluation of excipients for direct compression, I. Pharm. Weekbl. 108 (1973), 469–481.

Lipkowitz K.B. and Boyd D.B., Reviews in Computational Chemistry, Wiley, volume 27, 2010.

Liu M., Meakin P., and Huang H., Dissipative particle dynamics simulation of pore-scale multiphase fluid flow, Water Resour. Res., 43(4) (2007), W04411.

Lister J.D., Ennis B.J. , Iveson S.M. and Hapgood K., Nucleation, growth and breakage phenomena in agitated wet granulation processes: a review, Powder Technol. 117 (2001), 3-39.

London, F. Zur theorie und systematik der molekularkräfte. Zeitschrift für Physik A Hadrons Nuclei 63 (1930), 245–279

Lovorka Z. and Graham B., The use of surface energy values to predict optimum binder selection for granulations, Int. J. Pharm. 59 (1990), 155-164.

Lucio I., Capillary flow of dense colloidal suspensions, University of Edinburgh, 2007.

Lyngaae-Jorgensen J., Melting point of crystallites in dilute solutions of polymers. Poly(vinyl chloride) in tetrahydrofuran, J. Phys. Chem. 80 (1976), 824-828.

M

Mahato R.I. and A.S. Narang, Pharmaceutical Dosage Forms and Drug Delivery, Second Edition (CRC Press), 2011.

Maiti A. and McGrother S., Bead–bead interaction parameters in dissipative particle dynamics: Relation to bead-size, solubility parameter, and surface tension, J. Chem. Phys. 120 (2004) 1594–1601.

Mark J.E., Polymer Data Handbook, Ed.; Oxford University Press: New York, 1998.

Martinez-Salazar J., Alizadeh A., Jimenez J. J. and Plans J., On the melting behavior of polymer single crystals in a mixture with a compatible oligomer: 2. polyethylene/paraffin, Polymer 37 (1996), 2367-2371

Marsac P.J., Li T.L., Taylor L.S., Estimation of drug–polymer miscibility and solubility in amorphous solid dispersions using experimentally determined interaction parameters. Pharm. Res. 26 (2009), 139–151.

Marsac P.J., Shamblin S.L., Taylor L.S., Theoretical and practical approachesfor prediction of drug–polymer miscibility and solubility. Pharm. Res. 23 (2006), 2417–2426.

Mayoral E. ,and Nahmad-Achar E. ,Study of interfacial tension between an organic solvent and aqueous electrolyte solutions using electrostatic dissipative particle dynamics simulations, J. Chem. Phys. 137 (2012), 194701.

McGinity J.W. and Felton L.A., Aqueous Polymeric Coatings for Pharmaceutical Dosage Forms, third ed., Marcel Dekker Inc., 2008.

Milani J. and Maleki G., Hydrocolloids in Food Industry in Food Industrial Processes - Methods and Equipment, book edited by Benjamin Valdez, 2012.

Moor H. and Riehle U., Snap-freezing under high pressure: a new fixation technique for freeze-etching. proc. 4th European Reg. Conf. Electron Microscopy. 2 (1968), 33-34.

Miller R.W., Roller Compaction Technology. In: Handbook of Pharmaceutical Granulation Technology, 2nd edition, Parikh, D. (Ed.), Taylor & Francis, Florida, USA, 2005.

Miralles M.J., McGinity J.W. and Martin A., Combined water-soluble carriers for coprecipitates of tolbutamide. J. Pharm. Sci. 71 (1982), 302–304.

Mitrevej K.T., Augsburger L.L., Adhesion of tablets in a rotary tablet press II: effects of blending time, running time, and lubricant concentration. Drug. Dev. Ind. Pharm. 8 (1982), 237–282.

Mittal K.L., Promod Kumar, Emulsions, Foams, and Thin Films, Taylor & Francis Inc, 2000.

N

Napper D.H., Polymeric Stabilization of Colloidal Dispersions. Academic Press, London, 1983.

Newitt D.M. and Conway-Jones .J.M., A contribution to the theory and practice of granulation. Trans. Inst. Chem.Eng., 36 (1958), 422–442.

Nichols G., Byard S., Bloxham M. J., Botterill J., Dawson N. J., Dennis A., Diart V., North N.C., Sherwood J. D., A Review of the Terms Agglomerate and Aggregate with a Recommendation for Nomenclature Used in Powder and Particle Characterization, J. Pharm. Sci. 91 (10) (2002), 2103–2190.

Nishi T., Wang T.T., Melting Point Depression and Kinetic Effects of Cooling on Crystallization in Poly(vinylidene fluoride)-Poly(methyl methacrylate), Macromolecules 8 (6) (1975), 909–915.

Novik K.E. and Coveney P.V., Using dissipative particle dynamics to model binary immis-cible fluids, Int. J. Mod. Phys. C, 8(4) (1997), 909–918.

Novik K.E. and Coveney P.V., Finite-difference methods for simulation models incorporat-ing nonconservative forces, J. Chem. Phys., 109(18) (1998), 7667–7677.

O

Oelmeier S.A., Dismer F. and J. Hubbuch, Molecular dynamics simulations on aqueous two-phase systems - Single PEG-molecules in solution, BMC Biophys. 5 (2012), 14.

Oh E. , Luner P.E., Surface free energy of ethylcellulose films and the influence of plasticizers, Int. J. Pharm. 188 (1999) 203 – 219.

Onions A., Films from water-based colloidal dispersions, Manuf. Chem. 12 (1986), 55–59.

Ould-Chikh S., Elaboration, mise en forme et résistance mécanique de bi matériaux sphériques : application en catalyse, Thèse université de Lyon, Ecole Normale supérieure de Lyon, Lyon, 2008.

Owens D. K. and Wendt R. C., Estimation of the surface free energy of polymers, J. Appl. Polym. Sci. 3 (1969), 1741–1747.

Ozturk A.G., Ozturk S.S., Palsson B.O., Wheatley T.A. and Dressman J.B., Mechanism of release from pellets coated with an ethylcellulose-based film, J. Control. Release 14 (1990), 203–213.

P

Patel D., Chaudhary P., Mohan S., Khatri H., Enhancement of glipizide dissolution rate through nanoparticles: Formulation and In vitro evaluation, e-J. of Sci. & Tech. Vol. 7 (4) (2012), 19-31.

Pracella M., Dainelli D., Galli G., Chiellini E., Polymer blends based on mesomorphic components .1. properties of poly(tetramethylene terephthalate) poly(decamethylene 4,4' terephthaloyldioxydibenzoate) blends   makromolekulare chemie-macromolecular chemistry and physics 187, 10 (1986), 2387–2400.

Parks G. S., Huffman H. M, The free energies of some organic compounds. American Chemical Society Monograph Series no. 60, The Chemical Catalog Company Inc., New York, 1932.

Paruta A. N., Sciarrone B. J., Lordi N.G., Correlation between solubility parameters and dielectric constants, 51 (7) (1962), 704–705.

Perdew JP, Wang Y, Accurate and simple analytic representation of the electron-gas correlation energy Phys. Rev. B 45 (23), 13244–13249.

Perrin J., Les atomes. Constable, London, 1913.

Phillips G. O., Williams P. A., Handbook of Hydrocolloids, Second Edition, 2009.

Pivkin I.V., Karniadakis G.E., Controlling density fluctuations in wall bounded dissipative particle dynamics Systems, Phys. Rev. Lett. 96 (2006) 206001.

Pirika, site web, 2010, http://pirika.com/NewHP/Y-MB/Y-MB.html.

Planinšeka O., Pišekb R., Trojaka A. and Srčiča S., The utilization of surface free-energy parameters for the selection of a suitable binder in fluidized bed granulation, Int. J. Pharm. 207 (2000) 77–88.

Prausnitz J.M., Lichtenthaler R.N. and Azevedo E.G., Molecular Thermodynamics of Fluid Phase Equilibrium. 3rd edition. Prentice Hall International, Upper Saddle River. 1999.

Provder, Winnik and Urban (Eds)., ACS (Division of Polymeric Materials, Science and Engineering) International Symposium Series No. 648, Film Formation in Waterborne Coatings (1996), 332–348.

Q

R

Rekvig L., Hafskjold B., and Smit B., "Molecular Simulations of Surface Forces and Film Rupture in Oil/Water/Surfactant Systems", Langmuir 20 (26) (2004), 11583–11593.

Renouf S., Etude d'un procédé d'émulsification. Suivi rhéologique in situ dans un rhéo-émulseur et formation de goutte sprimaires dans un champ d'écoulement. Thèse de Doctorat, Institut National Polytechnique de Lorraine, Nancy, France, 2000.

Rowe R.C., The adhesion of film coatings to tablet surfaces – the effect of some direct compression excipients and lubricants. J. Pharm. Pharmacol. 29 (1977), 723–726.

Rowe R.C., Adhesion of film coating to tablet surfaces - a theoretical approach based on solubility parameters, Int. J. Pharm (1988), 219-222.

Rowe R.C., Interactions in coloured powders and tablet formulations: a theoretical approach based on solubility parameters, Int. J. Pharm. 53 (1989a), 47-51.

Rowe R.C., Polar/non-polar interactions in the granulation of organic substrates with polymer binding agents, Int. J. Pharm. 56 (1989b), 117-124.

Rowe R.C., Sheskey P.J. and Quinn M.E., Handbook of Pharmaceutical Excipients, 6th Edition (Pharmaceutical Press), 2009.

Rumpf H., The strength of granules and agglomerates. In: Knepper, W.A. (Ed.), Agglomeration. John Wiley and Sons, New York, NY, 1962.

Rumpf H., Methoden des Granulieren, Chem. Eng. Technol., 30 (1958), 144–158.

S

Sadeghi F., Ford J.L., Rubinstein M.H. and Rajabi-Siahboomi A.R., Study of drug release from pellets coated with surelease containing hydroxypropyl methyl cellulose. Drug. Dev. Ind. Pharm. 27(5) (2001), 419–430.

Saleh K., Steinmetz D., Hemati M., Experimental study and modeling of fluidized bed coating and agglomeration, Powder Technol. 130 (1–3) (19) (2003), 116–123.

Salman A.D., Hounslow M.J and Seville J.P.K, ELSEVIER, Handbook of Powder Technology, Granulation, Volume 11, 2007.

Schaefer T., Mathiesen C., Melt pelletization in a high shear mixer. 9. Effects of binder particle size. Int. J. Pharm 139 (1996), 139–148.

Schlijper A.G., Hoogerbrugge P.J., and Manke C.W., Computer simulations of dilute polymer solutions with the dissipative particle dynamics method, J. Rheol. 39(3) (1995), 567–579.

Schulz S.G., Frieske U., Kuhn H., Schmid G., Müller F., Mund C., and Venzmer J., The self-assembly of an amphiphilic block copolymer: A dissipative particle dynamics study, Tenside Surfact. Det., 42(3) (2005), 180-183.

Schulz S.G., Kuhn H., Schmid G., Mund C. and Venzmer J., Phase behavior of amphiphilic polymers: A dissipative particles dynamics study, Colloid. Polym. Sci. 283(3) (2004), 284-290.

Schubert H., Herrmann W., and Rumpf H., Deformation behaviour of agglomerates under tensile stress, Powder Technol.11 (1975), 121–131.

Schubert H., Principles of agglomeration, Intl. Chem. Eng. 21(3) (1981), 363–377.

Scott G.D., Packing of Spheres: Packing of Equal Spheres, Nature, 199 (1960), 908-909.

Scott R. L., The thermodynamics of high polymer solutions. V. Phase equilibria in the ternary system: polymer 1 - polymer 2 - solvent, J. Chem. Phys. 17 (1949), 279-284.

Sheldon T.J., Adjiman C.S., and Cordiner J.L., Pure component properties from group contribution: Hydrogen-bond basicity, hydrogen-bond acidity, Hildebrand solubility parameter, macroscopic surface tension, dipole moment, refractive index and dielectric constant, Fluid. Phase. Equilib. 231 (2005), 27-37.

Simons S.J.R., Rossetti D., Pagliai P., Ward R., Fitzpatrick S., The relationship between surface properties and binder performance in granulation, Chem. Eng Sci 60 (2005), 4055–4060.

Simpson J.A., Weiner E.S.C., The Oxford English Dictionary, 2nd ed., Oxford, England: Clarendon Press. 1989.

Sistla Y.S., Jain L. and Khanna A., Validation and prediction of solubility parameters of ionic liquids for CO_2 capture. Sep. Purif. Technol., 97 (2012) 51-64.

Small P.A. , Some factors affecting the solubility of polymers, J. Appl. Chem. 3 (1953), 71-80.

Smith P.G. and Nienow A.W., On Atomizing a Liquid Into Gas Fluidized Bed., Chem. Engng. Sci. 37 (1982), 950–954.

Sphael J., Kinget R., Influence of solvent composition upon film-coating, Pharm. Acta Helv. 55 (6) (1980), 157-160.

Steward P.A., Hearn J., Wilkinson M.C., An overview of polymer latex film formation and properties, Adv. Colloid Interface Sci. 86 (2000), 195–267.

Stubberud L., Arwidsson H.G., Hjortsberg V. and Graffner C., Water–solid interactions. Part 3. Effect of glass transition temperature, Tg and processing on tensile strength of compacts of lactose and lactose/polyvinyl pyrrolidone, Pharm. Dev. Technol. 1(2) (1996), 195–204.

Sun W., Li Y., Xuc W. and Maia Y.-W, Interactions between crystalline nanospheres: comparisons between molecular dynamics simulations and continuum models, RSC Adv., 4 (2014), 34500–34509.

Sun W., Interaction forces between a spherical nanoparticle and a flat surface, Phys. Chem. Chem. Phys., 16 (2014), 5846-5854

Sun H. and Rigby D., Polysiloxanes: ab initio force field and structural conformational and thermophysical properties, Spectrochim.Acta A 53 (1997), 1301-1323.

Sun H., COMPASS: An ab initio force-field optimized for condensed-phase applications overview with details on alkane and benzene compounds, J. Phys. Chem. B 102 (1998), 7338–7364.

Sutmann G., Molecular Dynamics - Extending the Scale from Microscopic to Mesoscopic, Institute for Advanced Simulation, 2009.

T

Thielmann F., Naderi M., Ansari M. A. and Stepanek F., The effect of primary particle surface energy on agglomeration rate in fluidised bed wet granulation, Powder Technol. 181 (2008), 160–168

Tijssen R., Billiet H.A.H., Schoenmakers P.J., Use of solubility parameter for predicting selectivity and retention in chromatography, J. Chromatogr. 122 (1976), 185-203.

Tomasini M.D., Tomassone M.S., Dissipative particle dynamics simulation of poly(ethylene oxide)-pol(ethylethylene) block copolymer properties for enhancement of cell membrane rupture under stress, Chem. Eng. Sci. 71 (2012), 400–408.

Travis K.P., Bankhead M., Good K. and Owens S.L., New parametrization method for dissipative particle dynamics, J. Chem. Phys. 127 (2007) 014109.

Trofimov S., Ph.D. thesis, Thermodynamic consistency in dissipative particle dynamics, Technische Universiteit Eindhoven, 2003.

U

V

Van Krevelen D.W., Chemical structure and properties of coal, XXVII-coal constitution and solvent extraction, Fuel (1965) 229-242.

Van Olphen H., An Introduction to Clay Colloid Chemistry, John Wiley and Sons, New York, 1963.

Venturoli M. and Smit B., Simulating the self-assembly of model membranes, Phys.Chem. Comm. 2(10) (1999), 45–49.

Verwey E.J.W., Overbeek J.Th.G., Theory of the stability of lyophilic colloids, Elsevier, Amsterdam, 1948

Vincent B., The effect of adsorbed polymers on dispersion stability, Adv. Colloid Interface Sci. 4 (1974), 193–277.

Visser J., Particle adhesion and removal: a review, Particul. Sci. Technol. 13 (1995), 169–196.

Vosko S. H., Wilk L. and Nusair M., Accurate spin-dependent electron liquid correlation energies for local spin density calculations: a critical analysis. Can. J. Phys. 58 (8) 1980), 1200–1211.

W

Walbridge D-J. and Waters J.A., Rheology of Sterically Stabilized Dispersions of Polymethyl methacrylate) in Aliphatic Hydrocarbons, Discuss. Faraday Soc. 42 (1966), 294–300.

Wu S., Polar and nonpolar interactions in adhesion, J. Adhesion 5(1973), 39–55.

Wypych G., Handbook of Antiblocking, Release, and Slip Additives, third edition, ChemTec Publishing, 2014.

X

Y

Yalkowsky, S. H. and Dannenfelser R. M. (1992). Aquasol Database of Aqueous Solubility, Version 5, PC Version, College of Pharmacy, Univ. of Arizona – Tucson.

Yalkowsky S.H. and He Y., Handbook of Solubility Data. Boca Raton, FL: CRC Press, 2003.

Young T., An Essay on the Cohesion of Fluids, Philos. Trans. R. Soc. 95 (1805), 65–87.

Z

Zajic L. and Buckton G., The use of surface energy values to predict selection for granulations optimum binder, Int. J. Pharm. 59 (1990), 155-164.

Zhanga D., Floryb J.H. , Panmaia S., Batraa U., Kaufmana M.J., Wettability of pharmaceutical solids: its measurement and influence on wet granulation, Colloids and Surfaces A: Physicochemical and Engineering Aspects 206 (2002), 547–554.

Zimon A.D., Adhesion, molecular interaction and surface roughness. In: ZIMON, A.D. (ed.), Adhesion of Dust and Powder, 2nd ed., London, 1982.

Appendixes

Appendix A – Basis sets examples

The table below summarizes the basis sets used in Biovia Material studio (Biovia, 2013). The triple-numerical (TNP) set which we have used in our calculations has been recently generated and validated by Delley (2006).

Table A.1 - Basis sets used in Biovia Material studio (Biovia, 2013)

Basis Name	Description	Examples
MIN	Minimal basis. One AO for each occupied atomic orbital. Yields low accuracy but fast computation.	H: 1s C: 1s 2s 2p Si: 1s 2s 2p 3s 3p
DN	Double Numerical. MIN + a second set of valence AOs. Improved accuracy over MIN.	H: 1s 1s' C: 1s 2s 2p 2s' 2p' Si: 1s 2s 2p 3s 3p 3s' 3p'
DND	Double Numerical plus d-functions. Like DN with a polarization d-function on all non-hydrogen atoms. The default basis set, providing reasonable accuracy for modest computational cost.	H: 1s 1s' C: 1s 2s 2p 2s' 2p' 3d Si: 1s 2s 2p 3s 3p 3s' 3p' 3d
DNP	Double Numerical plus polarization. Like DND including a polarization p-function on all hydrogen atoms. Best accuracy, highest cost. Important for hydrogen bonding.	H: 1s 1s' 2p C: 1s 2s 2p 2s' 2p' 3d Si: 1s 2s 2p 3s 3p 3s' 3p' 3d
TNP	Triple Numerical plus polarization. Like DNP including additional polarization functions on all atoms. Available only for H to Cl except He and Ne. Best accuracy, highest cost.	H: 1s 1s' 2p 1s" 2p' 3d O: 1s 2s 2p 2s' 2p' 3d 2s" 2p" 3p 4d S: 1s 2s 2p 2s' 2p' 3s 3p 3s' 3p' 3d 3s" 3p" 3d' 4d
DNP+	Double Numerical plus polarization, with addition of diffuse functions. Good accuracy for cases requiring diffuse functions, very high cost coming mostly from very large atomic cutoffs required for this set. Important for anions, excited state calculations and for cases where long-range effects are non-negligible. The bold components are the additional diffuse functions.	H: 1s 1s' 2p 1s" **2p'** C: 1s 2s 2p 2s' 2p' 3d **1s' 2p" 3d'** Si: 1s 2s 2p 3s 3p 3s' 3p' 3d **1s' 2p' 3d'**

Appendix B – Block average method

The method involves repeated "blocking" of data. To see how it works, let's consider a set of N data; $x_1, x_2...., x_n$. The data set is then transformed into a new data set $x'_1, x'_2...., x'_{n'}$ which has half the size of the original set:

$$x'_i = 0.5(x_{2i-1} + x_{2i})$$

$$n' = 0.5n$$

(B.1)

We then define $\overline{x}'$ the average of the n' "new" data. The variance is given by:

$$\Omega^2(x') = < x'^2 > - < x'>^2 = \frac{1}{n'}\sum x'^2 - \overline{x}'^2$$

(B.2)

We continue performing the procedure of the same "blocking" transformation until the averages x'_i becomes uncorrelated and a plateau is reached (See Fig. B.1). If it's the case the following equation which gives the variance of the data set should hold:

$$\Omega^2(x) = \frac{\Omega^2(x')}{n'-1}(\pm\sqrt{\frac{2\Omega^2(x')}{(n'-1)^2}}) \approx \text{Constant}$$

(B.3)
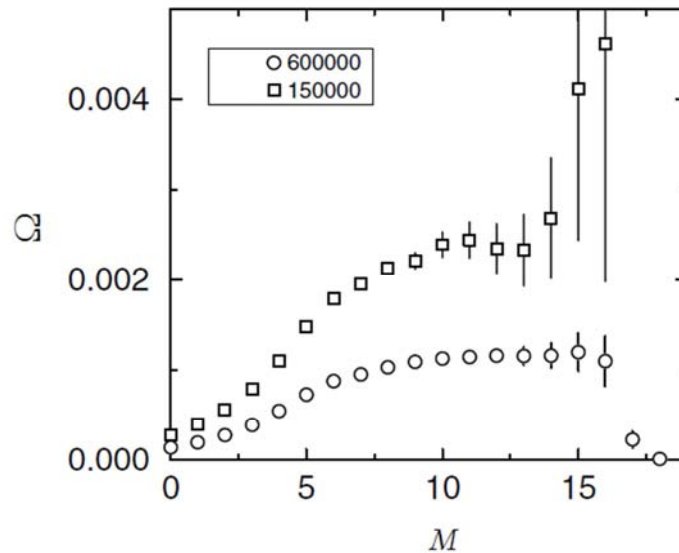
Fig. B.1 – The standard deviation Ω of the potential energy as a function of the number of block operations M for a simulation of 150.000 and 600.000 time steps. Adapted from Frenkel and Smit (2002).

The number of times we perform the blocking operation is noted *M*. Fig. B.1 shows a plot of the variance Ω of the potential energy plot of Lennard-jones fluid versus the number of blocking operations. The error increases until a plateau is reached for high values of *M*. In this plateau, the values of the potential energy become completely uncorrelated.

In our calculation, we run the simulation for a long time (500 000 time steps), but we did not reach a plateau:
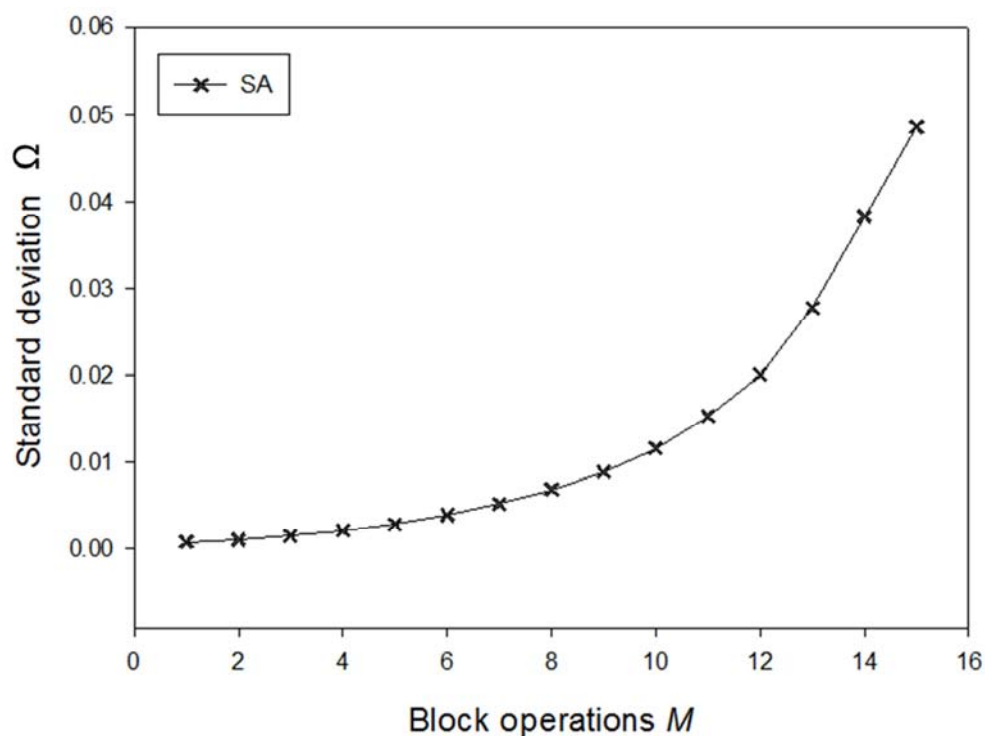
Fig. B.2 – The standard deviation Ω of the potential energy of HPMC and SA as a function of the number of block operations *M*.

Appendix C – Sigma profiles

Fig. C.1 shows the σ-profile of water with and without correction factor and compares them to sigma profile calculated using ADF software under the same parametrization described in chapter 4. Fig. C.1 shows the σ-profiles of water taken from (Klamt, 2005). It's clear from both figure that Dmol3 gives squeezed σ-profiles compared to the ones obtained from the literature and with ADF. Dmol3 also gives large amounts of segments compared to ADF and Klamt (2005). After using the correctif factor, the σ-profile becomes similar to those from the literature and ADF, with the same maxima and minima.
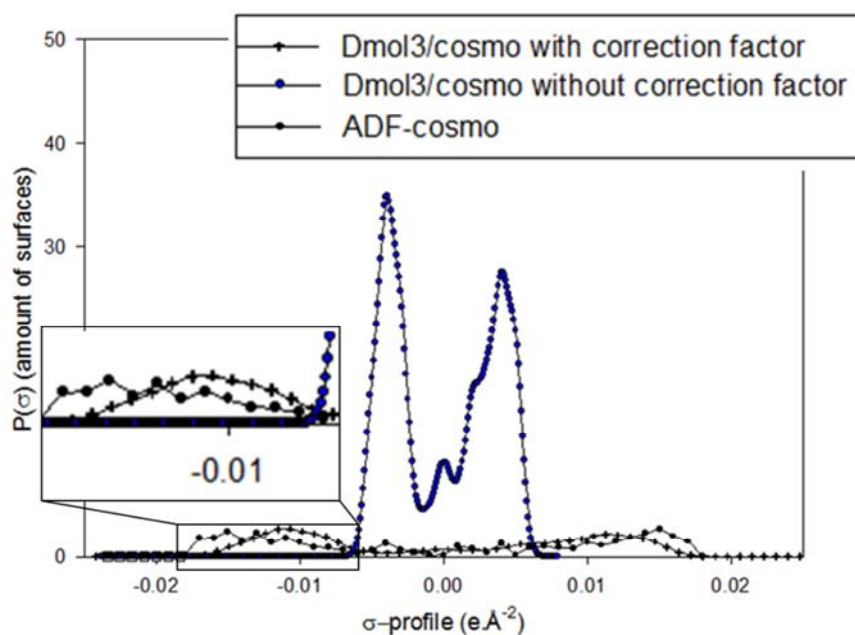
Fig. C.1 – σ-profile of water with and without correction factor compared to ADF results
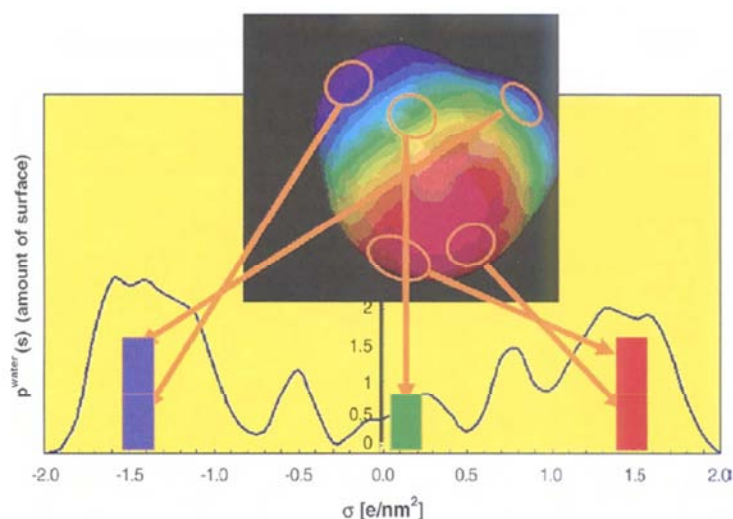
Fig. C.2 – σ-profile of water (Klamt, 2005)

164

Appendix D – work of adhesion equations

The full expressions of the work of adhesion given by Girifalco and Good (1957) and Wu (1973) are shown in the following table:

Table D.1- Work of adhesion equations proposed by by Girifalco and Good (1957) and Wu (1973).

Girifalco and Good	Wu
$W_{AB} = 2\Phi_I \Phi_V (\gamma_A \gamma_B)^{0.5}$ $\Phi_I = \dfrac{\varepsilon_{AB}}{(\varepsilon_A \varepsilon_B)^{0.5}}$ $\Phi_V = \dfrac{4(v_A v_B)^{1/3}}{(v_A^{1/3} + v_B^{1/3})^2}$	$W_{AB} = 2\varphi_{AB}(\gamma_A \gamma_B)^{0.5}$ $\varphi_{AB} = 2\left[\dfrac{x_A^d x_B^d}{g_A x_A^d + g_B x_B^d} + \dfrac{x_A^p x_B^p}{g_A x_A^p + g_B x_B^p}\right]$ $x_i^p = \dfrac{\gamma_i^p}{\gamma_i}$ and $x_i^d = \dfrac{\gamma_i^d}{\gamma_i}$ $g_A = \dfrac{\gamma_A}{\gamma_B}$ and $g_B = \dfrac{\gamma_B}{\gamma_A}$

Here, in table D.1, in Girifalco and Good expression, the ε's are the repulsive potential constants, v_A and v_B the molar volumes of material A and B respectively, γ_A and γ_B are the surface free energy of A and B respectively. For polymer molecules, it's better to interpret v as the molar volume of the polymer segment or the repeat unit (Barton, 2010).

In the expression of the work of adhesion proposed by Wu, x_i^p and x_i^d are the polar and the nonpolar fraction of phase i, and the ratios g_A and g_B are defined by the ratio of the surface free energy.

Appendix E – Surface free energy calculation using the molar Parachor

The surface free energy is the thermodynamic work to be done per unit area of surface extension and as such is a manifestation of the intermolecular forces. Its value can be obtained indirectly from contact angle measurement of two liquids of known polarity or from empirical correlations to estimate the surface free energy. For polymers we have used the correlation with the molar parachor P (Bicerano, 2002):

$$\gamma = (\frac{P}{v})^4 \qquad\qquad (E.1)$$

Here, γ is the surface free energy and v is the molar volume.

$$P = 3.989792\, V_W + N_{ps}\, 0.502094 \qquad\qquad (E.2)$$

where V_W is the Van der Waals volume and N_{ps} is a correction term:

$$N_{ps} = -3N_{(carbon\ atoms\ with\ \Omega=\Omega^v)} + 6N_{(carbonyls\ groups)} + 16N_{(-S-)} + 6N_{Br} - 6N_F \qquad (E.3)$$

Here, $N_{(carbon\ atoms\ with\ \Omega=\Omega^v)}$ equals to the number of carbon atoms which are singly bonded to all of their neighbors, $N_{(carbonyl\ groups)}$ is the total number of carbonyl (-C=O), $N_{(-s-)}$, N_{Br} and N_F are the numbers of sulfur atoms in the lowest (divalent) oxidation state, bromine atoms, and fluorine atoms, respectively, in the repeat unit. For non-polymer compounds; acids and water we used the structural contribution method of Sugden found in Bicerano Book (2002).

Appendix F – The ideal tensile strength in third medium

In the general case of two different bodies A and B interacting in a third medium C, the relationship between the adhesive tensile strength and the work of adhesion is given by the following expression:

$$W_{ACB}(h) = \int_{h}^{\infty} \sigma(x)_{ACB} dx \qquad \text{(F.1)}$$

$W_{ACB}(h)$ is the work required to move to infinity the surface of a body A separated from another body B by a distance h and both placed in a third medium C, the previous equation can be converted to:

$$\sigma(x)_{ACB} = \frac{dW_{ACB}(h)}{dh}\bigg|_{h=\infty} - \frac{dW_{ACB}(h)}{dh}\bigg|_{h=x} = -\frac{dW_{ACB}(h)}{dh}\bigg|_{h=x} \qquad \text{(F.2)}$$

Then, using the relationship (5.8) , proposed by Israelachivili (2010), we obtain the following equation:

$$\sigma(x)_{ACB} = -\frac{dW_{ACB}(h)}{dh}\bigg|_{h=x} = -\frac{dW_{AB}(h)}{dh}\bigg|_{h=x} - \frac{dW_{CC}(h)}{dh}\bigg|_{h=x} + \frac{dW_{AC}(h)}{dh}\bigg|_{h=x} + \frac{dW_{CB}(h)}{dh}\bigg|_{h=x} \qquad \text{(F.3)}$$

Now, let's follow the same route of resolution made by Gardon (1967), he began by assuming a law of force between surfaces of particles instead of whole particles, then, he divided the surface of each particle into interacting sites. Under those assumptions, for two particles A and B in vacuum, he proposed the following equation of the tensile strength:

$$\sigma(x)_{AB} = -\frac{dW_{AB}(h)}{dh}\bigg|_{h=x} = \pi N_A N_B \left(\frac{\varepsilon_{AB}}{6x^3} - \frac{\lambda_{AB}}{90x^9} \right) \qquad \text{(F.4)}$$

Where ε_{AB} and λ_{AB} are the attractive and repulsive potential constants between A and B respectively, N_A and N_B are the number of sites interacting between A and B. Equation (F.3) becomes:

$$\sigma(x)_{ACB} = \pi N_A N_B \left(\frac{\varepsilon_{AB}}{6x^3} - \frac{\lambda_{AB}}{90x^9} \right) + \pi N_C^2 \left(\frac{\varepsilon_{CC}}{6x^3} - \frac{\lambda_{CC}}{90x^9} \right) - \pi N_C N_B \left(\frac{\varepsilon_{AC}}{6x^3} - \frac{\lambda_{AC}}{90x^9} \right) - \pi N_A N_C \left(\frac{\varepsilon_{BC}}{6x^3} - \frac{\lambda_{BC}}{90x^9} \right) \qquad \text{(F.5)}$$

When two particles in a liquid are in equilibrium, $\sigma_{ACB} = 0$ and $x = d^0_{ACB}$:

$$d^0_{ACB} = (\frac{N_A N_B \lambda_{AB} + N_C^2 \lambda_{CC} - N_A N_C \lambda_{AC} - N_B N_C \lambda_{BC}}{15(N_A N_B \varepsilon_{AB} + N_C^2 \varepsilon_{CC} - N_A N_C \varepsilon_{AC} - N_B N_C \varepsilon_{BC})})^{(1/6)}$$ (F.6)

This distance can be rewritten using the following relationships (Gardon, 1967):

$$W_{AB} = 0.0625\pi N_A N_B \varepsilon_{AB} / d^0_{AB}{}^2$$

$$d^0_{AB} = (\frac{\lambda_{AB}}{15\varepsilon_{AB}})^{1/6}$$ (F.7)

with d^0_{AB} is the distance where A and B in vacuum are in equilibrium and W_{AB} is the total adhesion work in binary mixture. Equation (F.6) becomes:

$$d^0_{ACB} = (\frac{W_{AB}d^0_{AB}{}^8 + W_{CC}d^0_{CC}{}^8 - W_{AC}d^0_{AC}{}^8 - W_{BC}d^0_{BC}{}^8}{W_{AB}d^0_{AB}{}^2 + W_{CC}d^0_{CC}{}^2 - W_{AC}d^0_{AC}{}^2 - W_{BC}d^0_{BC}{}^2})^{(1/6)}$$ (F.8)

Using equation (5.13), d^0_{ACB} becomes:

$$d^0_{ACB} = (\frac{\sigma^{max}_{AB}d^0_{AB}{}^9 + \sigma^{max}_{CC}d^0_{CC}{}^9 - \sigma^{max}_{AC}d^0_{AC}{}^9 - \sigma^{max}_{BC}d^0_{BC}{}^9}{\sigma^{max}_{AB}d^0_{AB}{}^3 + \sigma^{max}_{CC}d^0_{CC}{}^3 - \sigma^{max}_{AC}d^0_{AC}{}^3 - \sigma^{max}_{BC}d^0_{BC}{}^3})^{(1/6)}$$ (F.9)

If the sites are in contact, spherical and identical, d^0_{AB} is the distance between the center of the neighboring sites of the particle A and the particle B. Henceforth, as Gardon suggested, we can write:

$$d^0_{AB} = (0.63\frac{6}{\pi N_{av}})^{1/3}\frac{(v_A^{1/3} + v_B^{1/3})}{2} = 0.629\times 10^{-8}(v_A^{1/3} + v_B^{1/3})$$ (F.10)

where v is the molar volume, N_{av} is the Avogadro number and 0.63 takes into account close random packing of the sites (Scott, 1960), equation (F.9) becomes:

$$d^0_{ACB} = 0.629*10^{-8}(\frac{\sigma^{max}_{AB}(v_A^{1/3} + v_B^{1/3})^9 + \sigma^{max}_{CC}(2v_C^{1/3})^9 - \sigma^{max}_{AC}(v_A^{1/3} + v_C^{1/3})^9 - \sigma^{max}_{BC}(v_A^{1/3} + v_C^{1/3})^9}{\sigma^{max}_{AB}(v_A^{1/3} + v_B^{1/3})^3 + \sigma^{max}_{CC}(2v_C^{1/3})^3 - \sigma^{max}_{AC}(v_A^{1/3} + v_C^{1/3})^3 - \sigma^{max}_{BC}(v_B^{1/3} + v_C^{1/3})^3})^{(1/6)}$$ (F.11)

Given that the sites are spherical, d^0_{ACB} should be equal or higher than d^0_{AB}.

By integrating the tensile strength $\sigma(x)_{ACB}$ in equation (F.5) from d^0_{ACB} to infinity, we obtain the total adhesive work in a medium C:

$$W_{ACB} = \frac{\pi N_A N_B \varepsilon_{AB} + \pi N_C^2 \varepsilon_{CC} + \pi N_A N_C \varepsilon_{AC} + \pi N_B N_C \varepsilon_{BC}}{16 d^0_{ACB}{}^2}$$

(F.12)

The maximum tensile strength σ^{max}_{ACB} between compounds A and B placed in a third medium is obtained by solving:

$$\frac{d\sigma(x)_{ACB}}{dx} = 0$$

(F.13)

Thus, we obtain the distance d^{max}_{ACB} between A and B where the stress is maximum:

$$d^{max}_{ACB} = \left(\frac{N_A N_B \lambda_{AB} + N_C^2 \lambda_{CC} - N_A N_C \lambda_{AC} - N_B N_C \lambda_{BC}}{5(N_A N_B \varepsilon_{AB} + N_C^2 \varepsilon_{CC} - N_A N_C \varepsilon_{AC} - N_B N_C \varepsilon_{BC})}\right)^{(1/6)} = 3^{(1/6)} d^0_{ACB}$$

(F.14)

Hence, replacing x by d^{max}_{ACB} in (F.5) gives:

$$\sigma^{max}_{ACB} = \frac{\pi N_A N_B \varepsilon_{AB} + \pi N_C \varepsilon_{CC} + \pi N_A N_C \varepsilon_{AC} + \pi N_B N_C \varepsilon_{BC}}{9 d^{max}_{ACB}{}^3} = \frac{\pi N_A N_B \varepsilon_{AB} + \pi N_C \varepsilon_{CC} + \pi N_A N_C \varepsilon_{AC} + \pi N_B N_C \varepsilon_{BC}}{15.59 d^0_{ACB}{}^3}$$

(F.15)

Substitution from (F.12), we obtain the relationship between the total work of adhesion and the ideal tensile strength:

$$\sigma^{max}_{ACB} = \frac{1.0263 \, W_{ACB}}{d^0_{ACB}}$$

(F.16)

An almost identical result can be obtained if, instead of using the Gardon's equation (5.13), we start with adhesive tensile strength formula based on Lennard-Jones law of force (Greenwood, 2001):

$$\sigma_{AB}(x) = \frac{8 W_{AB}}{3 \upsilon_{AB}} \left(\left(\frac{\upsilon_{AB}}{x}\right)^3 - \left(\frac{\upsilon_{AB}}{x}\right)^9\right)$$

(F.17)

If we envisage the atomic spacing υ_{AB} to be the potential equilibrium distance between A and B, after using the same previous method of computation, we will obtain:

$$\sigma_{AB}^{\max} = \frac{1.243 W_{AB}}{d_{AB}^0} \text{ and } \sigma_{ACB}^{\max} = \frac{1.243 W_{ACB}}{d_{ABC}^0} \tag{F.18}$$

$$\sigma_{AB}^{\max} = \frac{1.243 W_{AB}}{d_{AB}^0} \text{ and } \sigma_{ACB}^{\max} = \frac{1.243 W_{ACB}}{d_{ABC}^0}$$

Appendix G – Solubility parameter calculation (perl script)

```perl
#!perl
use strict;
use Getopt::Long;
use MaterialsScript qw(:all);
# Title: Cohesive energy, intermolecular energy and solubility calculation
in a mesoscopic level/molecular level
# Author: JARRAY Ahmed
# Version: 1.0
# MS Version: 7
# Modules: Materials Visualizer/Forcite
######################################################################
# Editable settings and inputs
my $doc = $Documents{"AS0.xtd"};
my $forcefield_name= "COMPASSII";
my $in= 99;
#######Calculations#########################################
my $beads = $doc->UnitCell->Molecules;
$beads->Beads->Count;
my $coh_energy=0;
my $coh_energyd=0;
my $coh_energyp=0;
my $coh_energyh=0;
my $fenergy=0;
my $fenergyd=0;
my $fenergyp=0;
my $fenergyh=0;
my $solt=0; my $sold=0; my $solp=0; my $solh=0;
#We Create our study table in order to store our final results
my $studyTable = Documents->New("Energie.std");
$studyTable->InsertColumn(0, "Non bond Energy tot(kcal/mol)");
 $studyTable->InsertColumn(1, "Non bond Energy polymer (kcal/mol)");
 $studyTable->InsertColumn(2, "Non bond Energy interaction(kcal/mol)");
 $studyTable->InsertColumn(3, "Cohesive Energy (J/cm3)");
 $studyTable->InsertColumn(4, "Solubility parm (J/cm3)^0.5");
 $studyTable->InsertColumn(5, "Solubility parm d (J/cm3)^0.5");
 $studyTable->InsertColumn(6, "Solubility parm p (J/cm3)^0.5");
 $studyTable->InsertColumn(7, "Solubility parm h (J/cm3)^0.5");
#Total number of frames in the trajectory
my $numFrames = $doc->Trajectory->NumFrames;
#We copy the cell in a temporary xsd file
#And eliminate all the unattached beads in every frame of the trajectory
file
for ( my $j=$in; $j<=$numFrames; $j++) {
my $nobnd=0; my $nobndd=0; my $nobndp=0; my $nobndh=0;
$doc->Trajectory->CurrentFrame = $j;
my $ac = Documents->New("all.xsd");
$ac->CopyFrom($doc);
my $beads = $ac->UnitCell->Molecules;
Modules->Forcite->ChangeSettings([CurrentForcefield =>
"$forcefield_name"]);
Modules->Forcite->ChangeSettings(["3DPeriodicElectrostaticSummationMethod"
=> "Ewald"]);
```

```perl
Modules->Forcite->Energy->Run($ac);
my $toen=$ac->NonBondEnergy;
my $toend=$ac->VanDerWaalsEnergy;
my $toenp=$ac->ElectrostaticEnergy;
my $toenh=$ac->HydrogenBondEnergy;
#We create a temporary file of the first temporary file already created
#we store each molecule (just one molecule)
for (my $i=0; $i<$beads->Count; ++$i) {
my $ac2 = Documents->New("all2.xsd");
$ac2->CopyFrom($ac);
my $beads2 = $ac2->UnitCell->Molecules;
my $beadss2 = $ac2->UnitCell;
#delete all the other Molecule/monomer/polymer in the cell
my  $mol=$beadss2->Molecules($i)->Center->X;
 foreach my $bead2 (@$beads2) {
 if ($bead2->Center->X != $mol){
     $bead2->Delete;} }
#we run the energy calculations using mesocite
Modules->Forcite->ChangeSettings([CurrentForcefield =>
"$forcefield_name"]);
Modules->Forcite->ChangeSettings(["3DPeriodicElectrostaticSummationMethod"
=> "Ewald"]);
Modules->Forcite->Energy->Run($ac2);
$nobnd=$nobnd+$ac2->NonBondEnergy;
$nobndd=$nobndd+$ac2->VanDerWaalsEnergy;
$nobndp=$nobndp+$ac2->ElectrostaticEnergy;
$nobndh=$nobndh+$ac2->HydrogenBondEnergy;
$ac2->Discard;}
#we extract the results
$fenergy=-$toen+$nobnd;
$fenergyd=-$toend+$nobndd;
$fenergyp=-$toenp+$nobndp;
$fenergyh=-$toenh+$nobndh;
my $lat_volume=$doc->Lattice3D->CellVolume;
my $coh_enrgy=($fenergy/$lat_volume)*(4.1858/0.6022)*10**3;
my $coh_enrgyd=($fenergyd/$lat_volume)*(4.1858/0.6022)*10**3;
my $coh_enrgyp=($fenergyp/$lat_volume)*(4.1858/0.6022)*10**3;
my $coh_enrgyh=($fenergyh/$lat_volume)*(4.1858/0.6022)*10**3;
$solt=$solt+$coh_enrgy**(1/2);
$sold=$sold+$coh_enrgyd**(1/2);
$solp=$solp+$coh_enrgyp**(1/2);
$solh=$solh+$coh_enrgyh**(1/2);
$studyTable->Cell($j-1,0)=$toen;
$studyTable->Cell($j-1,1)=$nobnd;
$studyTable->Cell($j-1,2)=$fenergy;
$studyTable->Cell($j-1,3)=$coh_enrgy;
$studyTable->Cell($j-1,4)=$coh_enrgy**(1/2);
$studyTable->Cell($j-1,5)=$coh_enrgyd**(1/2);
$studyTable->Cell($j-1,6)=$coh_enrgyp**(1/2);
$studyTable->Cell($j-1,7)=$coh_enrgyh**(1/2);
$studyTable->InsertRow();
$ac->Discard;}
$studyTable->Cell($numFrames,4)=$solt/($numFrames-$in+1);
$studyTable->Cell($numFrames,5)=$sold/($numFrames-$in+1);
$studyTable->Cell($numFrames,6)=$solp/($numFrames-$in+1);
$studyTable->Cell($numFrames,7)=$solh/($numFrames-$in+1);
```

Appendix H – Radial distribution of agglomerates

```perl
#!perl

use strict;
use Getopt::Long;
use MaterialsScript qw(:all);
# Title: Radial distance of agglomerates
# Author: JARRAY Ahmed
# Version: 1.0
# MS Version: 7
# Modules: Materials Visualizer/Mecocite
###########################################################################
#Inputs
my $docname = "PEG.xsd";my $water = "HPMC";
#Table creation
my $studyTable2 = Documents->New("W.std");
$studyTable2->InsertColumn(0, "distance");
$studyTable2->InsertColumn(1, "Concentartion");
$studyTable2->InsertColumn(2, "Number");
#We create a new doc
my $doc = $Documents{$docname};
my $lattice = $doc->SymmetryDefinition;
my $lx=$lattice->LengthA;
my $molecule = $doc->UnitCell->Sets("set1")->Beads;
my $beads2 = $doc->UnitCell->Sets($water);
my $numB=$beads2->Beads->Count-1;
my $numA=$doc->UnitCell->Sets("set1")->Count-1;
   my $centroid = $doc->CreateCentroid($molecule);
   my $center = $centroid->CentroidXYZ;
 #We fix the number of bins
 my $bins=100;
  my @arr;
  my $dist1;
  my $inc=$lx/$bins;
   #We apply the equation
  for ( my $j=0; $j<=$bins; $j++) {
  $arr[$j]=0;
  }
 foreach my $atom (@$molecule){
   my $x1=$atom->XYZ->X-$center->X;
   my $y1=$atom->XYZ->Y-$center->Y;
   my $z1=$atom->XYZ->Z-$center->Z;
   $dist1 = sqrt ($x1*$x1 + $y1*$y1 + $z1*$z1);
   for ( my $j=1; $j<=$bins; $j++) {
   if ($dist1>($j-1)*$inc and $dist1<$j*$inc ){
   $arr[$j]=$arr[$j]+1;
   ;}
    $studyTable2->Cell($j,0)=$j*$inc;
    $studyTable2->Cell($j,1)=$arr[$j]/$numB;
    $studyTable2->Cell($j,2)=$arr[$j];
}      ;
}
print $numA/$numB;
```

Appendix I – Percentages of polymers

```perl
#!perl

use strict;
use Getopt::Long;
use MaterialsScript qw(:all);
# Title: Percentages of polymers (Npolymer) in the agglomerates
# Author: JARRAY Ahmed
# Version: 1.0
# MS Version: 7
# Modules: Materials Visualizer/Mecocite
####################################################################
#inputs
my $docname = "SA.xsd";
my $dropletset = "SA";
my $water = "MCC";
my $r=8.14;
my $density=0.965;
use constant PI => 4 * atan2(1, 1);
################################################################
my $doc = $Documents{$docname};
#round function
sub round {
 my $number = shift || 0;
 my $dec = 10 ** (shift || 0);
 return int( $dec * $number + .5 * ($number <=> 0)) / $dec;
}
my $beads1 = $doc->UnitCell->Sets($dropletset);
my $beads2 = $doc->UnitCell->Sets($water);
my $studyTable2 = Documents->New("W.std");
$studyTable2->InsertColumn(0, "x");
$studyTable2->InsertColumn(1, "y");
$studyTable2->InsertColumn(2, "z");
my $x1;
my $y1;
my $z1;
my $Bille1= $beads1->Beads;
my $Bille2= $beads2->Beads;
my $box1=0; my $box2=0; my $boy1=0; my $boy2=0; my $boz1=0; my $boz2=0; my
$bxy1=0; my $bxy2=0; my $bxy3=0; my $bxy4=0; my $bxz1=0; my $bxz2=0; my
$bxz3=0; my $bxz4=0; my $bzy1=0; my $bzy2=0; my $bzy3=0; my $bzy4=0; my
$num=0; my @bille; my $w=0; my $u=0; my @bix;
foreach my $bi2 (@$Bille2) {
foreach my $bi1 (@$Bille1) {
$w=$w+1;
$x1=$bi2->X-$bi1->X;
$y1=$bi2->Y-$bi1->Y;
$z1=$bi2->Z-$bi1->Z;
if ($x1>0){$box1=$box1+1;}
if ($x1<0){$box2=$box2+1;}
if ($y1>0){$boy1=$boy1+1;}
if ($y1<0){$boy2=$boy2+1;}
if ($z1>0){$boz1=$boz1+1;}
if ($z1<0){$boz2=$boz2+1;}
if ($x1<0 and $y1<0){$bxy1=$bxy1+1;}
```

```perl
if ($x1>0 and $y1>0){$bxy2=$bxy2+1;}
if ($x1<0 and $y1>0){$bxy3=$bxy3+1;}
if ($x1>0 and $y1<0){$bxy4=$bxy4+1;}
if ($x1<0 and $z1<0){$bxz1=$bxz1+1;}
if ($x1>0 and $z1>0){$bxz2=$bxz2+1;}
if ($x1<0 and $z1>0){$bxz3=$bxz3+1;}
if ($x1>0 and $z1<0){$bxz4=$bxz4+1;}
if ($z1<0 and $y1<0){$bzy1=$bzy1+1;}
if ($z1>0 and $y1>0){$bzy2=$bzy2+1;}
if ($z1<0 and $y1>0){$bzy3=$bzy3+1;}
if ($z1>0 and $y1<0){$bzy4=$bzy4+1;}
}
if ($boy1 >0 and  $boy2 >0 and $boz1 >0 and $boz2 >0  and $box1 >0 and
$box2 >0 and $bxy1 >0 and  $bxy2 >0 and $bxz1 >0 and $bxz2 >0  and $bzy1 >0
and $bzy2 >0  and $bxy3 >0 and  $bxy4 >0 and $bxz3 >0 and $bxz4 >0  and
$bzy3 >0 and $bzy4 >0){;
$bille[$num]=$bi2;
    $num=$num+1;
    print " xxx ", $num;
}
$box1=0; $box2=0; $boy1=0; $boy2=0; $boz1=0; $boz2=0; $bxy1=0;$bxy2=0;
$bxy3=0; $bxy4=0; $bxz1=0; $bxz2=0; $bxz3=0; $bxz4=0; $bzy1=0; $bzy2=0;
$bzy3=0; $bzy4=0;
}
$doc->CreateSet("set1", \@bille);
print $num;
```

Appendix J – Functional categories of pharmaceutical products

In this appendix, we show functional categories of several pharmaceutical excipients. All the data are collected and organized from Rowe (2009):

	Coating agent;	Binder	Viscosity increasing agent	stabilizing agent	Solubilizing agent	plastiziers	Emulsifiying agent	Suspending agent	Dispersing agent	Wetting agent	Solubility in water	toxicity
Acacia		x	x	x			x	x			-	relatively nontoxic
Acetyltributyl Citrate						x					insoluble	relatively nontoxic
Agar		x	x	x			x	x			Soluble in boiling water	relatively nontoxic
Albumin				x							soluble	nontoxic
Alginic Acid		x		x				x			-	nontoxic
Aluminum Monostearate				x							insoluble	relatively nontoxic
Aluminum Oxide									x		insoluble	relatively nontoxic
Ammonium Alginate				x			x				-	nontoxic
Bentonite			x	x				x			insoluble	
Benzyl Benzoate					x	x					insoluble	toxic
Calcium Carbonate	x	x									Insoluble (95%)	nontoxic
Carboxymethyl-cellulose Calcium	x		x	x			x	x			Insoluble	nontoxic
Carrageenan			x	x			x	x			Soluble (at 80°C)	relatively nontoxic

	Coating agent;	Binder	Viscosity increasing agent	stabilizing agent	Solubilizing agent	plastiziers	Emulsifiying agent	Suspending agent	Dispersing agent	Wetting agent	Solubility in water	toxicity
Carboxymethyl-cellulose Sodium				x				x	x		Partially soluble	Low toxicity
Cellulose Acetate	x										soluble	nontoxic
Ceratonia		x	x	x				x			soluble	
Ceresin	x			x							insoluble	Low toxicity
Cetyl Alcohol	x						x				insoluble	Low toxicity
Cetylpyridinium Chloride				x						x	soluble	relatively nontoxic
Chitosan	x	x	x								Sparingly soluble	nontoxic
Chlorobutanol						x					Freely soluble in hot water	toxic
Cyclodextrins				x	x						Soluble (1/7 at 20C)	toxic
Dibutyl Phthalate						x					Practicly Insoluble (1/2500)	relatively nontoxic
Dibutyl Sebacate						x					insoluble	nontoxic
Ethylcellulose	x	x	x								insoluble	nontoxic
Ethylene Glycol Stearates				x			x				insoluble	relatively nontoxic
Gelatin	x	x	x					x			Soluble (40C)	nontoxic
Glucose	x	x									soluble	nontoxic
Glyceryl Monostearate				x	x		x				insoluble	nontoxic
Guar Gum		x	x					x			insoluble	nontoxic

	Coating agent;	Binder	Viscosity increasing agent	stabilizing agent	Solubilizing agent	plastiziers	Emulsifiying agent	Suspending agent	Dispersing agent	Wetting agent	Solubility in water	toxicity
Hydroxyethyl Cellulose	x	x	x					x			soluble	nontoxic
Hydroxyethylmethyl Cellulose	x	x	x					x			insoluble in hot water	nontoxic
Hydroxypropyl Cellulose	x	x	x	x			x	x			Soluble (1/2)	nontoxic
Hydroxypropyl Starch		x	x				x				insoluble	nontoxic
hydroxypropyl methylcellulose (Hypromellose)	x	x	x	x	x		x	x	x		Soluble in cold water	nontoxic
Hypromellose Phthalate	x										insoluble	nontoxic
Lecithin					x		x				insoluble	-
Macrogol 15 Hydroxystearate				x	x						Soluble	relatively nontoxic
Magnesium Aluminum Silicate		x	x	x				x			insoluble	nontoxic
Maltodextrin	x	x	x								soluble	nontoxic
Methylcellulose	x	x	x				x	x			Insoluble in hot water	nontoxic
Pectin				x			x				Soluble	nontoxic
Phospholipids					x		x	x	x	x	soluble	Low toxicity
Poloxamer					x		x		x	x	soluble	nontoxic
Polycarbophil		x					x	x			insoluble	nontoxic
Polyethylene Glycol						x					soluble	nontoxic
Polyethylene Oxide	x	x									soluble	Low toxicity

178

	Coating agent;	Binder	Viscosity increasing agent	stabilizing agent	Solubilizing agent	plastiziers	Emulsifiying agent	Suspending agent	Dispersing agent	Wetting agent	Solubility in water	toxicity
Polyoxyethylene Stearates					x		x			x	soluble	nontoxic
Polyvinyl Alcohol	x		x	x							insoluble	nontoxic
Povidone		x						x			soluble	nontoxic
Propylene Glycol				x		x					soluble	relatively nontoxic
Propylene Glycol Alginate			x	x			x	x			soluble	nontoxic
Povidone	x	x	x	x							soluble	nontoxic
Pyrrolidone					x	x					soluble	toxic by ingestion
Saponite			x				x				-	nontoxic
Sodium Alginate		x	x	x				x			insoluble	nontoxic
Sorbitan Esters					x		x	x	x	x	insoluble	nontoxic
Sorbitol			x			x					soluble	-
Stearic Acid					x		x				insoluble	nontoxic
Sucrose	x	x	x					x			Soluble 1in 0.5	toxic by ingestion
Tragacanth			x					x			insoluble	nontoxic
Vitamin E Polyethylene Glycol Succinate		x			x		x	x			miscible	-
Xanthan Gum			x	x				x			soluble	nontoxic
Zein	x	x									insoluble	nontoxic

Appendix K – MCC and HPMC End-to-end distance for longer simulation time.

Fig. K.1 shows the average end-to-end distance as a function of simulation time. We run simulations of MCC and HPMC for long simulation time (8061 ps) to make sure that the end-to-end distance of MCC and HPMC became stable.
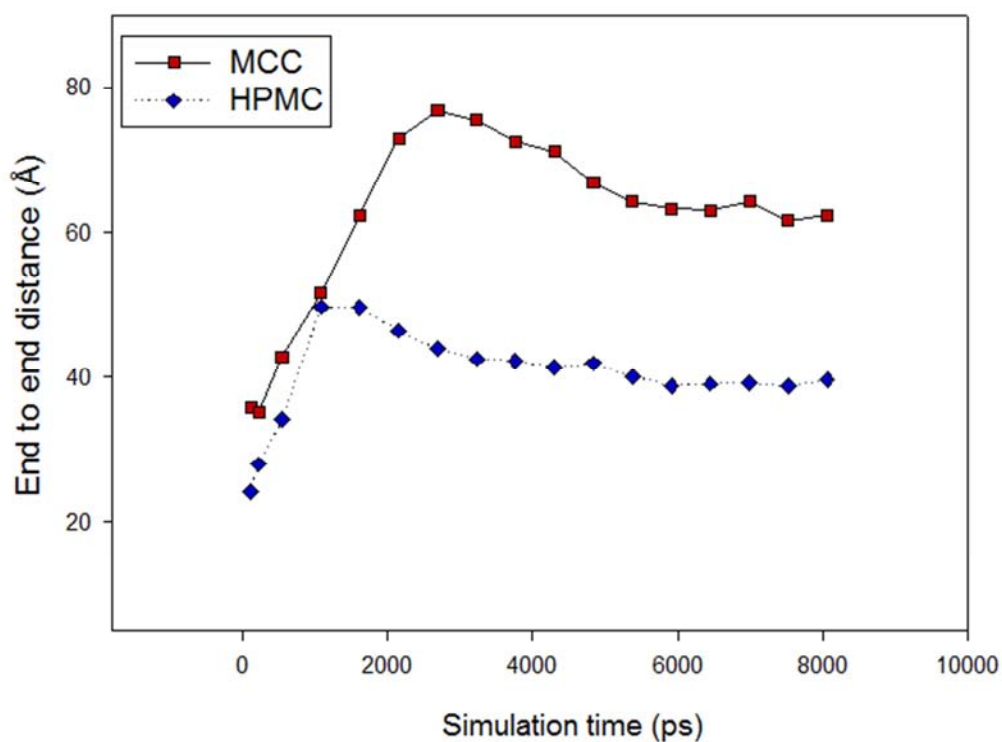

Fig. K.1 - Average end-to-end distance as a function of simulation time, each point is averaged over 10 successive steps.

Appendix L – a_{ii} calculation based on the water compressibility

By combining the compressibility of the DPD model with that of the real system, Groot and Warren (1997) were able to relate the compressibility factor $\varkappa^{-1}$ to the parameter of repulsion a_{ii} between the same type of beads:

$$(\varkappa^{-1}) = (\overline{\varrho}_{molecule} k_B T \varkappa_T)^{-1} = \frac{1}{k_B T}(\frac{\partial P}{\partial \varrho_{molecule}})_T = \frac{r_c^3}{k_B T}(\frac{\partial P}{\partial \overline{\varrho}_{molecule}})_T \tag{L. 19}$$

$$(\overline{\varkappa}^{-1}) = 1 + \frac{2\varsigma a_{ii} \varrho r_c^4}{k_B T} = (\frac{\partial \overline{P}}{\partial \overline{\varrho}})_T = \frac{r_c^3}{k_B T}(\frac{\partial P}{\partial \overline{\varrho}})_T \tag{L. 20}$$

Where P is the pressure, T the temperature, a is an adjustment parameter equal to 0.101 ($\pm$ 0.001), and $\varkappa_T$ the isothermal compressibility of the compound. At the same time, we must keep in mind that this compressibility factor varies linearly with the coarse-grain number N_m, a detail originally passed over by Groot and Warren (1997), and recently rectified by Groot and Rabone (2001). In the DPD simulations, the compressibility must be equal to that of the real system:

$$(\overline{\varkappa}^{-1}) = \frac{r_c^3}{k_B T}(\frac{\partial P}{\partial \overline{\varrho}})_T = (\varkappa^{-1}) = \frac{r_c^3}{k_B T}(\frac{\partial P}{\partial \overline{\varrho}_{molecule}})_T \tag{L. 21}$$

Substitution from:

$$r_c = (\frac{\overline{\varrho}}{\varrho})^{1/3} = (N_m V_{molecule} \overline{\varrho})^{1/3}$$

We obtain:

$$\frac{1}{k_B T}(\frac{\partial P}{\partial \overline{\varrho}})_T = \frac{1}{k_B T}(\frac{\partial \overline{\varrho}_{molecule}}{\partial \overline{\varrho}})_T (\frac{\partial P}{\partial \overline{\varrho}_{molecule}})_T = \frac{N_m}{k_B T}(\frac{\partial P}{\partial \overline{\varrho}_{molecule}})_T \tag{L. 22}$$

Combination with equation (L.2) gives:

$$(\varkappa^{-1}) = \frac{(\overline{\varkappa}^{-1})}{N_m} = \frac{1}{N_m} + \frac{2\varsigma a_{ii} \varrho r_c^4}{k_B T N_m}$$

Under standard conditions, the dimensionless compressibility of water is $(\varkappa^1)$ =15.9835≈16, hence, it

becomes possible to determine the repulsion parameter a_{ii}:

$$a_{ii} = (16 N_m - 1) \frac{k_B T}{2\varsigma \varrho r_c^4}$$

Appendix M - Particle size effect on particles interactions in dry systems

1. Introduction

Agglomerate structure and particle-particle affinity strongly depend on the size of the particles. Benali (2007) as well as Barra (1998) confirmed this statement and found that small particles surround coarser particles. Calvo et al. (2005) investigated structures of clusters of spherical particles bound by elementary Lennard-Jones forces by assuming that the particles were homogenously filled. They found that the as the diameter increases, the potential becomes very sharp and the cluster become more and more compact. The work of adhesion model and the tensile strength model developed in chapter 5 consider only the interactions between particles with the same size.

In this appendix, first, a model based on the work of Benali (2006) and Israchivili (2010) to predict the affinity between particles of different sizes was developed. This model gives insights about the influence of the size of the particles on the affinity and organization between particles in dry systems. The obtained predictions are compared to the experimental observation obtained by Barra (1998) for different ranges of particles sizes. Then, a second approach was developed based on the Lenard-Jones potential that also takes into account the particle size. In this approach, we use the Hamaker constant for the calculation of the equilibrium well depth ε_{ij} of the Lennard-Jones potential specific to each material. Then, using only the Lennard-jones potential, we run mesoscale simulations to predict the affinity between the particles.

2. Van der Waals attractive forces in relation to the Hamaker constant

In 1873, the Dutch physicist J.D. van der Waals proposed the idea of the existence of non-covalent and non-electrostatic forces that govern the interactions between all atoms and molecules. These forces are responsible for the cohesion between many liquids and molecular crystals, but also are present in the polymerization phenomena (Kleis and Schröder, 2005), and ensure the cohesion of graphitic material (Girifalco and Hodak, 2002) and other lamellar systems. Recently, their importance in adhesion phenomena has also been shown (Autumn et al., 2002). These forces also cause the flocculation phenomenon in colloidal systems which results in agglomeration of the particles.

Van der Waals force originated from three distinct interactions, polar forces translated by the term Debye V_D (Debye, 1920), Dipole forces corresponding to the end of Keesom V_K (Keesom, 1915), and the dispersion forces expressed by the term of London V_L (London, 1930). All of them are proportional to r^{-6}, where r is the distance between the atoms or molecules.

$$U = U_D + U_K + U_L$$

$$U = -\frac{1}{(4\pi\varepsilon_0)^2}(2a_e\mu^2 + \frac{2}{3}\frac{\mu^4}{k_BT} + \frac{3}{4}hva_e^2)r^{-6} = -\frac{C}{r^6}$$

(M.1)

Where C is the constant of van der Waals, ε_0 is the vacuum permittivity, a_e is the electronic polarizability, μ is the dipolar moment, h is the Plank constant, v is the vibration frequency, k_B the Boltzmann constant and T the temperature.

From equation (M.1), it is possible to calculate the interaction energy of van der Waals between two macroscopic bodies separated by a distance r:

$$E_{VDW} = \int\limits_{V1}\int\limits_{V2} U_{VDW}\, \varrho_1\varrho_2\, dV_1 dV_2$$

(M.2)

where ϱ_1 and ϱ_2 are the number density of body 1 and body 2 respectively, V_1 and V_2 are the volume of each body. To integer equation (M.2), Hamaker considered the interaction between two particles and derived the following general equation for the van der Waals interaction energy valuable for cases where the sizes of the particles are comparable to their separation (Israelachvili's, 2010).

$$E_{VDW} = -\frac{A}{6}K \tag{M.3}$$

with

$$K = (\frac{2R_A R_B}{D^2 + 2R_A D + 2R_B D} + \frac{2R_A R_B}{D^2 + 2R_A D + 2R_B D + 4R_A R_B} + \ln(\frac{D^2 + 2R_A D + 2R_B D}{D^2 + 2R_A D + 2R_B D + 4R_A R_B}))$$

where A is the Hamaker (1937) constant, expressed in joules. This parameter takes into account the molecular properties of the interacting bodies. A is given by the following expression:

$$A = \pi^2 C \varrho_1 \varrho_1 \tag{M.4}$$

Typical values of the Hamaker constants of condensed phases, whether solid or liquid, are about 10^{-19} J for interactions in a vacuum (Israchivili, 2010),

Benali (2006) also arrived at the same equation (M.3) by integration of the potential of Lennard-Jones over the surface of two sphere separated by a distance D. Using this equation, he found that for the same equilibrium well depth, and the same equilibrium distance in the potential of Lennard-Jones, small particles will surround bigger particles.

If we consider two flat surfaces at a very close distance (i.e. $D << R_A$ and R_B), the interaction energy becomes:

$$E_{VDW} = -\frac{A}{12\pi D^2} \tag{M.5}$$

For two spherical particles with the same consideration ($D << R_A$ and R_B), we obtain the following equation:

$$E_{VDW} = -\frac{A}{6D}(\frac{R_1 R_2}{R_1 + R_2}) \tag{M.6}$$

Fig M.1 taken from Israelachvili's (2010) book shows the van der Waals interactions for different geometries of the interacting bodies:
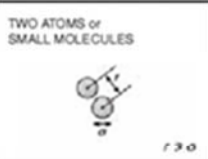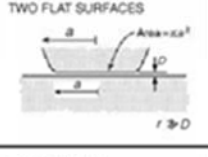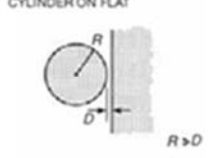
Geometry of bodies with surfaces *D* apart (*D«R*)		Van der Waals Interaction*	
		Energy, E_{vdw}	Force, $F = -dW/dD$
Two atoms or small molecules	TWO ATOMS or SMALL MOLECULES	$-C/r^6$	$-6C/r^7$
Two flat surfaces (per unit area)	TWO FLAT SURFACES	$W_{flat} = -A/12\pi D^2$	$-A/6\pi D^3$
Two spheres or macromolecules of radii R_1 and R_2	TWO SPHERES	$\dfrac{-A}{6D}\left(\dfrac{R_1 R_2}{R_1+R_2}\right)$	$\dfrac{-A}{6D^2}\left(\dfrac{R_1 R_2}{R_1+R_2}\right)$ Also $F = 2\pi\left(\dfrac{R_1 R_2}{R_1+R_2}\right)W_{flat}$
Cylinder of radius *R* near a flat surface (per unit length)	CYLINDER ON FLAT	$\dfrac{-A\sqrt{R}}{12\sqrt{2}D^{3/2}}$	$\dfrac{-A\sqrt{R}}{8\sqrt{2}D^{5/2}}$

Fig. M.1 – Van der Waals interaction energy E_{VDW} and force F between macroscopic bodies of different geometries in terms of their Hamaker constant. Adapted from Israelachvili (2010).

3. Model development

3.1. Approach 1: Interaction energy in dry systems

The adhesive contact interaction between two bodies originates from the interaction of individual atoms belonging to the bodies (Sauer and Shaofan, 2007). These molecular interactions are at a very short distance that any two macroscopic bodies A and B which are in contact can be considered planar. The total energy of two planar surfaces at a distance *D* apart (see Figure M.1) is derived from equation (M.5) and given by Israelachvili's (2010):

$$E_{VDW} = -\frac{A}{12\pi}\left(\frac{1}{D_0^2} - \frac{1}{D^2}\right) \tag{M.7}$$

where D_0 is the distance between two neighboring atoms. Israelachvili (2010) proposed a value of D_0 equal to 0.165 nm which is equal to the interatomic distance divided by 2.5. This value yields results for surface energy in good agreement with experimental data except for some strongly H-bonding liquids.

At $D = D_0$ (two surfaces in contact), $E_{VDW} = 0$, while for $D = \infty$ (two isolated surfaces) E_{VDW} becomes:

$$E_{VDW}(\infty) = -\frac{A}{12\pi D_0^2} = -2\gamma = -W$$

or
$$\qquad\qquad\qquad\qquad\qquad\qquad\qquad\qquad\qquad\qquad\qquad\text{(M.8)}$$

$$W = \frac{A}{12\pi D_0^2}$$

Hence, equation (M.3) becomes:

$$E_{VDW} = -2\pi K D_0^2 W_{AB} \qquad\qquad\qquad\qquad\qquad\qquad\text{(M.9)}$$

By using the work of adhesion values, calculated in chapter 5, in equation (M.9), it becomes possible to calculate the energy of interaction between two bodies and take into consideration their size. The affinity and organization between the particles that composes the compounds can be determined using E_{VDW} following the same approach proposed in chapter 5. By analogy to chapter 5, we can state that for two material A and B:

- If E_{VDW} (A-B) > E_{VDW} (A-A) > E_{VDW} (B-B): both compounds tend to mix.

- If E_{VDW} (A-A) > E_{VDW} (A-B) > E_{VDW} (B-B): compound A will surround compound B in vacuum.

- If E_{VDW} (B-B) > E_{VDW} (A-B) > E_{VDW} (A-A): compound B will surround compound A in vacuum.

3.2. Approach 2: Mapping the Hamaker equation to the Lennard-Jones Potential

In this subsection, we will map the interaction between two spherical to a van der Waals potential using the Hamaker constant in equation (M.8). The van der Waals interaction is typically modelled by the Lennard-Jones potential which has the following form:

$$\qquad\qquad\qquad\qquad\qquad\qquad\qquad\qquad\qquad\qquad\qquad\text{(M.10)}$$

$$U(r) = \varepsilon_{ij}\left(\frac{r_{ij}}{r}\right)^{12} - 2\varepsilon_{ij}\left(\frac{r_{ij}}{r}\right)^{6}$$

This potential represents the interaction between two neutral atoms (or molecules) separated by a distance r. ε_{ij} corresponds to the energy well at $r = r_{ij}$ with r_{ij} is the equilibrium distance where the force $F(r)$ between particle i and particle j vanishes:

$$F(r) = \frac{\partial\, U(r)}{\partial\, r} \tag{M.11}$$

For $r > r_{ij}$, the Lennard-Jones potential is usually approximated by the 1/r6 term:

$$U(r) = -\frac{C}{r^6} \quad \text{with} \quad C = 2\varepsilon_{ij} r_{ij}^6 \tag{M.12}$$

Combining equation (M.4) and (M.12), we get the following expression of the energy well ε_{ij} between particle i and particle j, in terms of the Hamaker constant:

$$\varepsilon_{ij} = \frac{A_{ij}}{2(r_{ij})^6 \varrho_i \varrho_j \pi^2} \tag{M.13}$$

The density ϱ_i is the number of atoms i in a volume V_i. One atom i occupy therefore the volume given by:

$$V_i = \frac{4}{3}\pi (r_i / 2)^3 \tag{M.14}$$

Sun (2014) and Sun et al. (2014) also used this formula for the interactions between nanospheres.

For the equilibrium distance between dissimilar non-bonded atoms, we will adopt the Good-Hope rule:

$$r_{ij} = \sqrt{r_i r_j} \tag{M.15}$$

Using equations (M.14) and (M.15) in equations (M.16), we get:

$$\varepsilon_{ij} = 0.185\, A_{ij} \text{ (in joule)} \tag{M.16}$$

Considering the lack of an explicit formula that gives r_{ij}, we took $r_{ij} = 3.5$ Å which is equal to the equilibrium distance between carbon atoms taken from COMPASSII forcefield (Sun, 1998). By taking such consideration, only ε_{ij} between the particles will affect the simulation outcome.

To consider the size of the particles in the simulation, we may express equation M.3 as:

$$E_{VDW} = -\frac{A}{6}K'H = \frac{A'}{6}K' \tag{M.17}$$

where $K = K'H$ and $A' = AH$, with K' is the constant K when R_1 equal to R_2 (i.e. $K' = K(R_1 = R_2)$).

188

By taking *A'* as the Hamaker constant in equation (M.16), we get an equilibrium well depth ε_{ij} that takes into accounts the particles size.

4. Results and discussions

4.1. Application of approach 1: Interaction energy

In order to study the effect of particle size on the interaction and organization of the agglomerated particles, we will apply equation (M.9), that take into account the size of the particles, to our materials; PVP, MCC, HPMC, EC, NA and SA. The prediction will be compared to Barra's (1998) observations. The Hamaker constant *Aij* values calculated using equation (M.8) are shown in Table M.1:

Table M.1 – Hamaker constants calculated using equation (M.8).

Aij (10^{-20} j)	PVP	MCC	HPMC	EC	NA	SA
PVP	8.538	-	-	-	-	-
MCC	7.477	10.954	-	-	-	-
HPMC	6.863	7.122	6.903	-	-	-
EC	6.666	5.787	6.265	6.600	-	-
NA	9.296	9.341	7.00	6.480	1.118	-
SA	7.833	7.264	6.785	6.466	8.313	7.378

PVP: Polyvinylpyrrolidone, MCC: Microcrystalline cellulose, HPMC: Hydroxypropyl-methylcellulose, EC: Ethyl cellulose, NA: Niflumic acid, SA: Stearic acid.

Table M.2 and M.3 show the affinity, predicted using our model, between HPMC and NA, and between EC and NA respectively. Small particles of EC tend to surround bigger particles of NA. Only after increasing the size of NA particles to 300 μm, that NA becomes able to surround EC. HPMC also surrounds NA, but, NA becomes able to surround HPMC at lower particle sizes (around 100 μm) comparing to the case of NA-EC couple. Benali (2006) also concluded that smaller particles tend to surround bigger particles.

Tables M.4 and M.5 present the affinity of EC-NA and HPMC-NA couples observed by Barra (1998). The obtained predictions have the same tendency as the observation of Barra (1998). For particles with the same size, EC mixes with NA and HPMC surrounds NA. The difference between the model and the observations of Barra is mainly in the size of the particle at which smaller particles starts to surround the bigger particles. Our model predicts that 20 μm NA particles adhere on EC's and HPMC's when their particle size is around 300 μm and 100 μm respectively. However, Barra (1998) observations are at particle size of 32-45 μm for HPMC and 45-63 μm for EC, he also

observed that for higher particle size of NA, HPMC and EC surrounds NA. This may imply the use of a corrector factor to ajust the model to the observation.

Table M.2 – Interactions between HPMC and NA for different particle sizes.

HPMC-NA		HPMC				
		20 μm	50 μm	100 μm	300 μm	1000 μm
NA	20 μm	HPMC/NA	M	NA/HPMC	NA/HPMC	NA/HPMC
	50 μm	HPMC/NA	HPMC/NA	M	NA/HPMC	NA/HPMC
	100 μm	HPMC/NA	HPMC/NA	HPMC/NA	M	NA/HPMC
	300 μm	HPMC/NA	HPMC/NA	HPMC/NA	HPMC/NA	M
	1000 μm	HPMC/NA	HPMC/NA	HPMC/NA	HPMC/NA	HPMC/NA

HPMC: Hydroxypropyl-methylcellulose, NA: Niflumic acid.
M: Bad affinity.

Table M.3 – Interactions between EC and NA for different particle sizes.

EC-NA		EC				
		20 μm	50 μm	100 μm	300 μm	1000 μm
NA	20 μm	M	M	M	NA/EC	NA/EC
	50 μm	EC/NA	M	M	M	NA/EC
	100 μm	EC/NA	EC/NA	M	M	NA/EC
	300 μm	EC/NA	EC/NA	EC/NA	M	M
	1000 μm	EC/NA	EC/NA	EC/NA	EC/NA	M

EC: Ethyl cellulose, NA: Niflumic acid.
M: Bad affinity.

Table M.4 – Interactions between HPMC and NA observed by Barra (1998).

HPMC-NA		HPMC			
		20-32 μm	32-45 μm	45-63 μm	63-125 μm
NA	20-32 μm	NA/HPMC	NA/HPMC	NA/HPMC	NA/HPMC
	32-45 μm	HPMC/NA	HPMC/NA	NA/HPMC	NA/HPMC
	45-63 μm	HPMC/NA	HPMC/NA	HPMC/NA	NA/HPMC
	63-125 μm	HPMC/NA	HPMC/NA	HPMC/NA	M

HPMC: Hydroxypropyl-methylcellulose, NA: Niflumic acid.
M: Bad affinity.

Table M.5 – Interactions between EC and NA observed by Barra (1998).

EC-NA		EC			
		20-32 μm	32-45 μm	45-63 μm	63-125 μm
NA	20-32 μm	M	M	NA/EC	NA/EC
	32-45 μm	EC/NA	EC/NA	M	NA/EC
	45-63 μm	EC/NA	EC/NA	M	NA/EC
	63-125 μm	EC/NA	EC/NA	EC/NA	M

EC: Ethyl cellulose, NA: Niflumic acid.

M: Bad affinity.

Tables M.6, M.7 and M.8 present the affinity predictions of HPMC-SA, MCC-NA and PVP.SA respectively. When SA and HPMC have the same particle size, they tend to mix. For HPMC's size above 50 μm, small SA particles adhere on HPMC's in vacuum. As SA particle size increases, HPMC particules adhere on the big SA particles.

Table M.6 – Interactions between HPMC and SA for different particle sizes.

HPMC-SA		HPMC				
		20 μm	50 μm	100 μm	300 μm	1000 μm
SA	20 μm	M	SA/HPMC	SA/HPMC	SA/HPMC	SA/HPMC
	50 μm	HPMC/SA	M	SA/HPMC	SA/HPMC	SA/HPMC
	100 μm	HPMC/SA	M	M	SA/HPMC	SA/HPMC
	300 μm	HPMC/SA	HPMC/SA	M	M	SA/HPMC
	1000 μm	HPMC/SA	HPMC/SA	HPMC/SA	HPMC/SA	M

HPMC: Hydroxypropyl-methylcellulose, SA: Stearic acid.

M: Bad affinity.

Table M.7 – Interactions between MCC and SA for different particle sizes.

MCC-SA		MCC				
		20 μm	50 μm	100 μm	300 μm	1000 μm
SA	20 μm	M	SA/MCC	SA/MCC	SA/MCC	SA/MCC
	50 μm	M	M	SA/MCC	SA/MCC	SA/MCC
	100 μm	MCC/SA	M	M	SA/MCC	SA/MCC
	300 μm	MCC/SA	M	M	M	SA/MCC
	1000 μm	MCC/SA	M	M	M	M

MCC: Microcrystalline cellulose, SA: Stearic acid.

M: Bad affinity.

Table M.8 – Interactions between PVP and SA for different particle sizes.

PVP-SA		PVP				
		20 μm	50 μm	100 μm	300 μm	1000 μm
SA	20 μm	SA/PVP	SA/PVP	SA/PVP	SA/PVP	SA/PVP
	50 μm	PVP/SA	SA/PVP	SA/PVP	SA/PVP	SA/PVP
	100 μm	PVP/SA	M	SA/PVP	SA/PVP	SA/PVP
	300 μm	PVP/SA	PVP/SA	M	SA/PVP	SA/PVP
	1000 μm	PVP/SA	PVP/SA	PVP/SA	PVP/SA	SA/PVP

PVP: Polyvinylpyrrolidone, SA: Stearic acid.
M: Bad affinity.

MCC-SA couple shows higher mixing tendencies than HPMC-SA, and MCC is less likely to surround SA particles (Table M.7). Regardless of the PVP particle size, SA particles always surround PVP particles in vacuum when their size is equal to 20 μm (Table M.8).

4.2. Application of approach 2: Lennard-Jones

To apply the model developed in the approach 2, we run simulation using mesocite module in Biovia (2013). The interactions parameters of Lennard-Jones potential between the different materials constitute the forcefield applied on the system. Lennard-Jones interactions between particles with the same size are presented in table M.9. The simulation runs over 1000 ps with a time step of 10 fs.

Table M.9 – Lenard-jones interactions parameter for particles with the same size

Mixture	r_{ij} (Å)	ε_{ij} (kcal.mol^{-1})
HPMC-HPMC	3.5	1.824
HPMC-MCC	3.5	1.886
HPMC-PVP	3.5	1.817
HPMC-PEG	3.5	1.951
HPMC-SA	3.5	1.797
MCC-MCC	3.5	2.901
MCC-PVP	3.5	1.98
MCC-PEG	3.5	2.025
MCC-SA	3.5	1.923
PVP-PVP	3.5	2.261
PVP-PEG	3.5	2.161
PVP-SA	3.5	2.074
PEG-PEG	3.5	2.202
PVP-SA	3.5	2.074
SA-SA	3.5	1.954
NA-NA	3.5	2.961
NA-HPMC	3.5	1.854
EC-EC	3.5	1.748
EC-NA	3.5	1.716

Figures M.2 and M.3 show the affinity and organization of HPMC-NA and EC-NA obtained for different particles sizes. When the particles have the same size, HPMC surrounds NA. Upon increasing the particle size HPMC, NA becomes able to adhere on HPMC particles. The same conclusions are obtained for EC-NA mixture. EC surrounds NA when R_{EC} = R_{NA}, and if the particles size of one of the material increases, the small particles surrounds the big ones. This is in adequacy with the finding of Barra (1998) (see tables M.3 and M.4) and with the conclusions of Benali (2006).
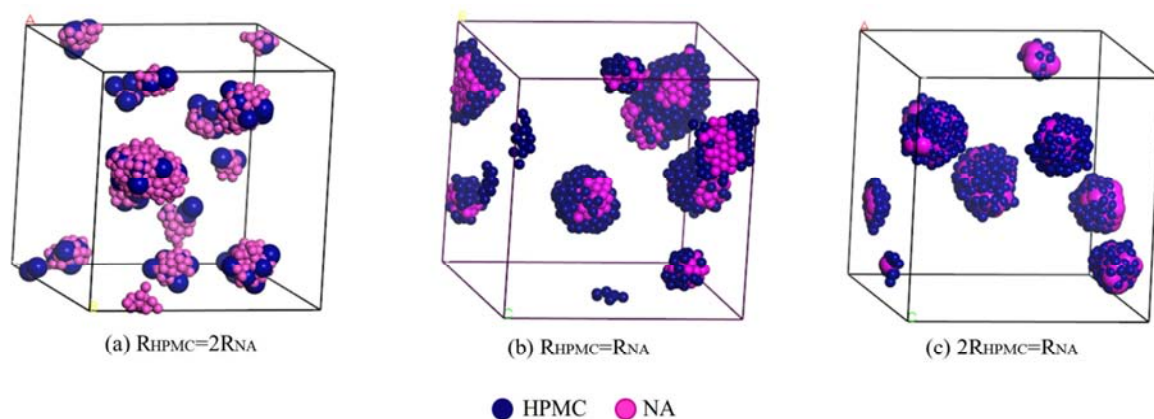

(a) $R_{HPMC}=2R_{NA}$ (b) $R_{HPMC}=R_{NA}$ (c) $2R_{HPMC}=R_{NA}$

● HPMC   ● NA

Fig. M.2 – Snapshots of the organization between HPMC and NA, HPMC: Hydroxypropyl-methylcellulose, NA: Niflumic acid.

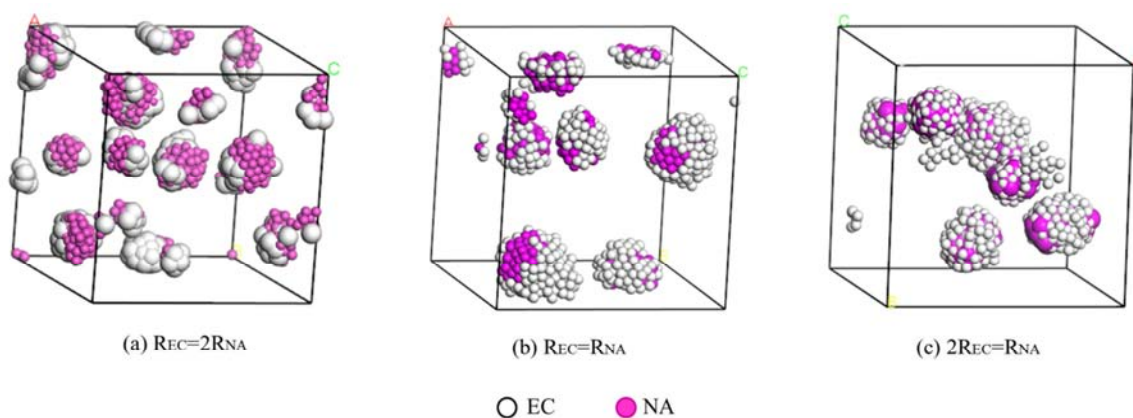(a) $R_{EC}=2R_{NA}$ (b) $R_{EC}=R_{NA}$ (c) $2R_{EC}=R_{NA}$

○ EC   ● NA

Fig. M.3 – Snapshots of the organization between EC and NA, EC: Ethyl cellulose, NA: Niflumic acid.

Figures M.4, M.5 and M.6 show snapshots of the particles affinity in vacuum of HPMC-SA, MCC-SA and PVP-SA. At the same particle size, HPMC and SA particles tend to mix, which corresponds to the affinity predictions obtained with the work of adhesion model (see chapter 5, Table 5.7). If we double the particle size of HPMC, SA adheres on the big HPMC particles, and inversely, if we double the particle size of SA, HPMC surrounds SA particles.

Regarding MCC-SA (Fig M.5), when the particles are at the same size, MCC and SA particles are mixed with a slight tendency of SA particles to surround MCC. Upon increasing the size of MCC particles, SA surrounds MCC particles. When $R_{SA}=2R_{MCC}$, MCC partially surrounds SA particles (i.e. bad coverage of SA by MCC). In Fig. M.6, SA tend to surround PVP when $R_{PVP}=R_{SA}$, when doubling the size of PVP particles, SA cover better PVP particles, but, PVP surrounds SA upon increasing SA particle size. Overall, by comparing the predictions obtained using approach 1 to those obtained using approach 2, we find similar predictions.
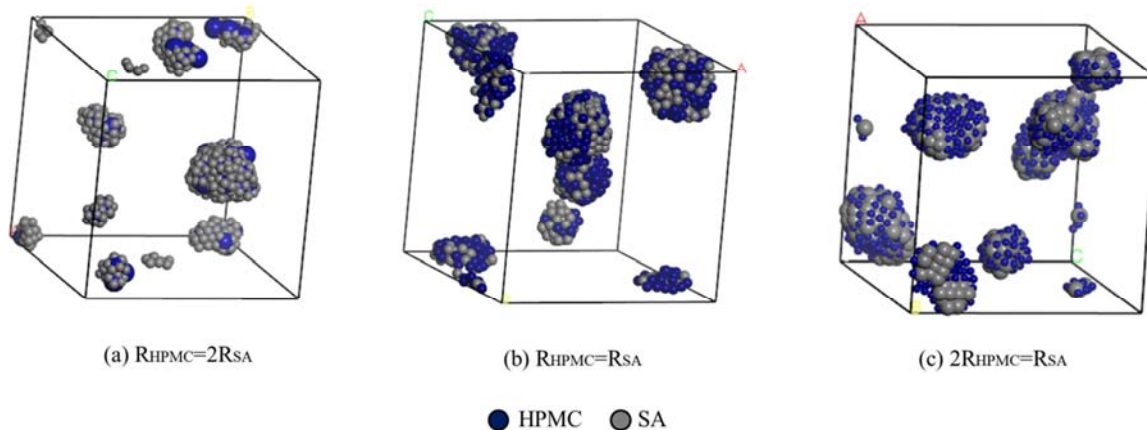

(a) $R_{HPMC}=2R_{SA}$ (b) $R_{HPMC}=R_{SA}$ (c) $2R_{HPMC}=R_{SA}$

● HPMC   ○ SA

Fig. M.4 – Snapshots of the organization between HPMC and SA, HPMC: Hydroxypropyl-methylcellulose, SA: Stearic acid.

(a) $R_{MCC}=2R_{SA}$ (b) $R_{MCC}=R_{SA}$ (c) $2R_{MCC}=R_{SA}$

● MCC   ○ SA
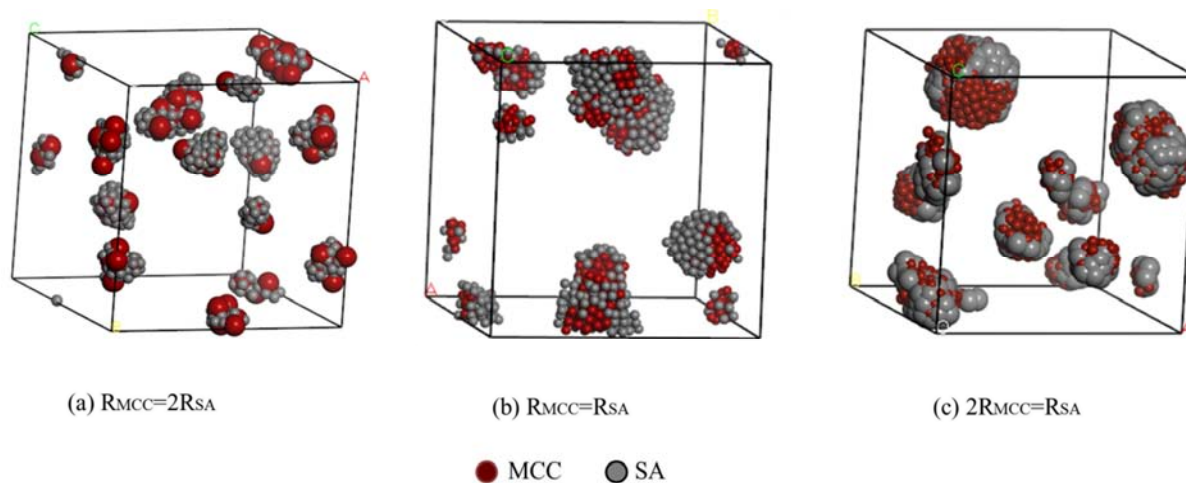
Fig. M.5 – Snapshots of the organization between HPMC and SA, HPMC: Hydroxypropyl-methylcellulose, SA: Stearic acid.

(a) R$_{PVP}$=2R$_{SA}$ (b) R$_{PVP}$=R$_{SA}$ (c) 2R$_{PVP}$=R$_{SA}$
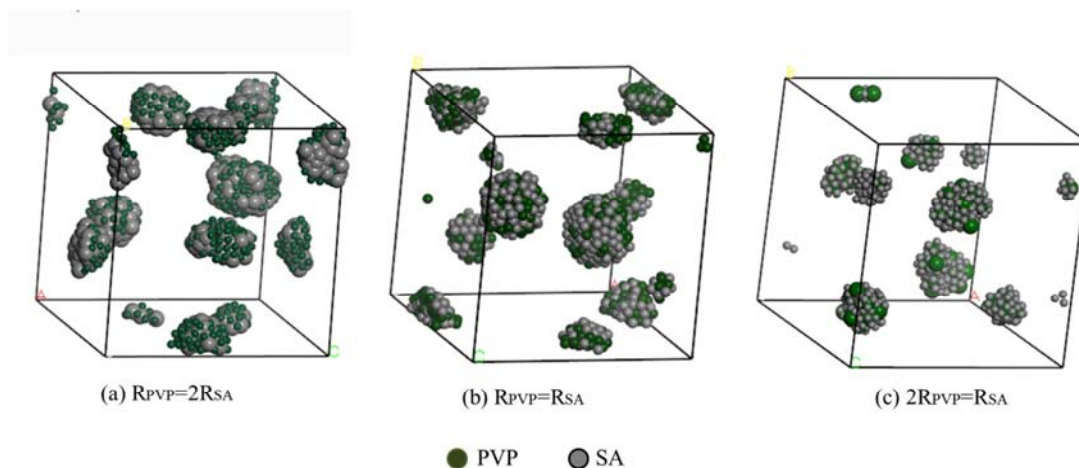
● PVP   ○ SA

Fig. M.6 – Snapshots of the organization between PVP and SA, HPMC: Hydroxypropyl-methylcellulose, SA: Stearic acid.

5. Conclusion

In this appendix, a model was proposed to predict the affinity between particles of different sizes. The model combines the work of adhesion equation and the Hamaker constant to calculate the interactions between the particles. The obtained results are similar to Barra's (1998) observations; small particles of NA adhere on the coarser particles of HPMC, similar particles size of HPMC and NA produces random homogeneity. Similarly, Small particles of NA adhere on the coarser particles of EC.

In a second part of this appendix, we used the Hamaker constant to calculate the equilibrium well depth ε_{ij} of the Lennard-Jones potential. We are aware that this approach was based on several assumptions such as the fact that the interactions between the particles are described by the $1/r^6$ term of Lennard-jones, and also, the choice of r_{ij} = 3.5 Å for all the materials, nevertheless, the affinity predictions obtained by this approach were similar to those obtained by approach 1 (i.e. interaction energy approach), and also similar to the observation of Barra (1998).

Ph.D. Thesis abstract

Wet granulation process requires the addition of a coating agent or binder, typically composed of surfactants, water, plasticizers and fillers. This work has two objectives; a) to investigate the particles behaviour and agglomeration mechanism in dry and aqueous systems, and b) to develop predictive methodologies and theoretical tools of investigation allowing to choose the adequate binder and to formulate the right coating solution.

In order to predict the binder-substrate affinity in dry and in aqueous media, two approaches were compared; one based on the work of adhesion and the other based on the ideal tensile strength. Both approaches yielded results in good agreement with the experimental observations. Then, we used experimental techniques and mesoscale simulations to investigate the structure of agglomerates formed in aqueous colloidal formulations used in coating and granulation processes. The obtained results show that HPMC polymer is a better stabilizing agent for Stearic acid than PVP and MCC. In addition, HPMC is able to cover the SA germ with a thick layer and to adsorb in depth into its inner core, preventing further agglomeration and crystal growth of SA. For high amounts of SA (above 10% (w/w)), HPMC is unable to fully stabilize SA.

Keywords

Agglomeration, binder, molecular simulation, DPD, colloid, pharmaceutical products, coating.

Résumé de thèse

Le procédé de granulation en voie humide nécessite l'ajout d'un agent d'enrobage ou liant, typiquement composé d'agents tensioactifs, d'eau, de plastifiant et de charge hydrophobe. L'objectif de ce travail est double; a) examiner le comportement des particules et le mécanisme d'agglomération dans les systèmes secs et aqueux aux échelles microscopique et mésoscopique, et b) développer des méthodologies prédictives permettant de choisir le liant adéquat et formuler la bonne solution d'enrobage. Afin de prédire l'affinité liant-substrat en milieu sec et en milieu aqueux, nous avons comparé deux approches; la première est basée sur le travail de l'adhésion alors que la seconde s'appuie sur le concept de résistance à la traction idéale. Les approches développées ont été ensuite confrontées aux données expérimentales.

Pour étudier la structure des agglomérats formés dans les formulations colloïdales utilisées dans les procédés d'enrobage. Nous nous sommes appuyés sur des techniques de caractérisation expérimentales et des simulations mésoscopiques. Les résultats montrent que le polymère HPMC est un meilleur agent stabilisant pour le SA que le PVP et le MCC. En outre, HPMC est capable de recouvrir la germe de SA d'une couche épaisse et d'y pénétrer en profondeur, empêchant ainsi l'agglomération et la croissance des cristaux de SA. Néanmoins, HPMC est incapable de stabiliser les particules de SA lorsque celles-ci sont en quantités élevées (supérieurs à 10% (w/w)).

Mots clés

Agglomération, liant, simulation moléculaire, DPD, colloïdes, produits pharmaceutiques, enrobage.